Anion-Tuning of Supramolecular Gel Properties

LLOYD, GARETH,OWEN

Anion-Tuning of Supramolecular Gel Properties

A thesis submitted for the fulfillment of the requirements for the degree of

Doctor of Philosophy

In the faculty of Science of Durham University

by

Gareth Owen Lloyd

Department of Chemistry

Durham University

South Road

Durham

2009

Abstract

Low molecular weight gelators (LMWGs) are a class of compounds that has garnered great interest from material, synthetic, supramolecular and biological chemists. Anion tuning of these supramolecular gels is a burgeoning field of study. Two classes of compounds, chiral bisureas and urea derivatised pyrazoles are studied.

The synthesized chiral bisurea compounds act as gelators in a variety of solvents. Addition of anions in the form of tetrabutyl ammonium salts was found to afford break up of the gels. Studies reveal that the rheological characteristics of these materials can be tuned using the simple addition of sub-stoichiometric amounts of anion. Variation in the length of the alkyl chain of the spacer separating the chiral and bisurea moieties affects the gel formation of a series of related compounds. Compounds with even numbered spaced alkyl chains were found to gel, whereas the odd numbered spaced alkyl chain compounds did not. Crystal growth within the gel matrix influences the crystallization processes and the use of anion induced break down of the LMWGs allows for easy recovery of the grown crystals. Drug compounds, bound upon gelation of a solution containing the drugs, were found to be released in a controlled manner from the gel matrix.

Urea functionalised pyrazoles were synthesized. Crystallographic determination of the hydrogen bonding of the compounds as well as the coordination chemistry of these compounds was obtained. Anion binding studies, in addition to the crystallographic results, reveal that the urea or thiourea groups form an intramolecular hydrogen bond with the pyrazole group resulting in an *anti* conformation. This prevents formation of gels except in one case. The gelation of 1-(3-methyl-1*H*-pyrazol-5-yl)-3-(3-nitrophenyl)urea in acidic water overcomes this problem by protonation of the pyrazole group resulting in a *syn* conformation of the urea group. Anion tuning of the gel properties is revealed where nitrate and chloride result in precipitation of gels and the rheological characteristics can be tuned by changing the anion's identity.

Acknowledgements

Thanks must go most of all to the Commonwealth Scholarship Commission for providing me with a Scholarship to bring me half the way around the world to study at the most amazing university. Thank you.

Thank you Prof. Jon Steed and the JWS group. You guys have taught me more than I could imagine and the last three years have passed too quickly as there is still so much to learn. To the gel boys, do I need say anymore?

To my athletics family, thank you for keeping me sane, although everyone has to agree some of us are just a little insane. I will never forget that medal.

To my parents, thank you for supporting me and giving me the drive to accomplish all that I have dreamed of. It has been wonderful to have you within travelling distance and getting to know you again. The family has been too far apart.

To Jacqueline, you have added that icing to the carrot cake that this time in Durham has been. Thank you.

Contents

Abbreviations

1D	One Dimensional
2D	Two Dimensional
3D	Three Dimensional
A	Absorbance
AIEE	Aggregation-Induced Enhanced Emission
Asp	Aspirin
ASU	Asymmetric Unit
BOC	*tert*-Butyloxycarbonyl
CBZ	Carbamazepine
CGC	Critical Gelation Concentration
$CHCl_3$	Chloroform
$(CH_3)_2CO$	Acetone
cm	centimeter
conc	Concentration
CSD	Cambridge Crystallographic database
DME	1,2-Dimethyl ether
DMF	Dimethyl formamide
DMSO	Dimethyl sulfoxide
ε	Extinction coefficient
EELS	Electron energy-loss spectroscopy
E_s	Young's modulus of a gel strut
EtOAc	Ethyl Acetate
EtOH	Ethanol
G'	Storage or elastic shear modulus
G''	Loss or viscous modulus
Hz	Hertz
IBU	Ibuprofen
IR	InfraRed
l	Pathlength travelled by light through sample
LMW	Low Molecular Weight

LMWG	Low Molecular Weight Gelator
log	Logarithm
m	metre
MeCN	Acetonitrile
MeOH	Methanol
MG	Methoxyglycol anion
MPLA	least-squares plane instruction in Shelxl
N	Newton
NMR	Nuclear Magnetic Resonance
NPU	1,3-bis(*m*-nitrophenyl)urea
Osc.	Oscillation
ρ_s	density of the struts
Pa	Pascal
PFP	Pentafluorophenyl ligand
PXRD	Powder X-Ray Diffracion
RMS	Root Mean Square
SEM	Scanning Electron Microscopy
t	Time
TBA^+	tetrabutylammonium
TBP	3,5-Di-*t*-butylpyrazolate
TBPH	3,5-Di-*t*-butylpyrazole
TEM	Transmission Electron Microscopy
T_{gel}	Gel transition temperature from gel to solution
THF	Tetrahydrofuran
Tol	Toluene
T_{sg}	Gel transition temperature from solution to gel

Figure captions

Figure 1.1. a, b) Photographs of the reversible phase transition between the gel and sol states of **1.6** in 1,2-dichloroethane (neutral gel **(a)** and protonated sol **(b)**). **c, d)** Fluorescence images and **e, f)** SEM images of the neutral gel and the protonated sol, respectively. (Reproduced with permission from ref.[122])

Figure 1.2. **a)** Hydrogel of **1.7-Na** containing 0.1 mM of crystal violet. **b)** Toluene added to the hydrogel of **1.7-Na** containing the dye. **c)** Status of hydrogel after the addition of 1.1 equiv of HCl. **d)** Subsequent heating results in selective gelation of the toluene phase containing crystal violet, leaving the aqueous layer clear within a few minutes of addition. (Reproduced with permission from ref.[80])

Figure 1.3 a) Gel films of **1.18** in cyclohexane. **b)** reversible gel-sol transitions by a variety of stimuli. Top left represents the redox controlled transition between the gel and sol states. Top right and bottom left is the thixotropic character of the gel. (Reproduced with permission from ref.[160])

Figure 1.4 a) gelation of cyclohexane by free **1.20**, **b)** of cyclohexane by the [Fe(**1.20**)$_2$](ClO_4)$_2$ complex **c)** precipitation of the analogous ruthenium complex, and d) a gel of **1.20** doped with Fe(II). (Reproduced with permission from ref.[164])

Figure 1.5. Ca^{2+} responsiveness of hydrogelator **1.26**. **a)** Phase diagram of the gel-sol transition, revealing the number of equivalents of Ca^{2+} required to induce gelation at each gelator concentration. **b)** Photographs of the Ca^{2+}-induced sol-to-gel transition ([**1.26**] = 0.30 wt %; [Ca^{2+}]/[**1.26**] = 1.0; [Na_2EDTA]/[Ca^{2+}] = 10). **c)** Corresponding dynamic viscoelastic properties before and after the addition of Ca^{2+}. (Reproduced with permission from ref.[11])

Figure 1.6. Rheological detection of **a)** light- and **b)** temperature-triggered gelation of **1.27**/liposome precursor fluid (12 vol % $CaCl_2$-loaded liposomes in a sucrose solution of **1.27** (30 mg/mL)). (Reproduced with permission from ref.[173])

Figure 1.7. SEM images showing morpholgy of xerogels of **1.28** in **a)** water – spongy globules (gel forms instantaneously), **b)** 1 mM $CaCl_2$ – fused globules (gel takes 15 mins to form), **c)** 1 mM

$MgCl_2$ – fused globules (gel takes 15 mins to form), and **d)** 1 mM NaCl – aggregated spheres (gel takes 7 mins to form). (Reproduced with permission from ref.[79])

Figure 1.8. The acetone gel of **1.29**, showing the transitions between the gel state and liquid states upon addition of chemical stimuli (X = F^-, Cl^- or BF_4^-). **a)** Acetone gel of **1.29** (2.0 wt %). **b)** Acetone gel of **1.29** (2.0 wt %) containing (from left) 1.1 equiv of TBA^+ F^-, 1.7 equiv of TBA^+ Cl^-, and 10 equiv of TBA^+ BF_4^-. **c)** BF3·OEt_2 (1.0 equiv for TBA^+ salt) mixture after sonication of **1.29** and TBA^+ F^- (left) or TBA^+ Cl^- (right) in acetone. **d)** $ZnBr_2$ (1.0 equiv for TBA^+ salt) mixture after sonication of **1.29** and TBA^+ F^- (left) or TBA^+ Cl^- (right) in acetone. (Reproduced with permission from ref.[184])

Figure 1.9. Transition of the supramolecular gel of **1.31c** in octane (10 mg/ml) to a solution upon addition of 10 equivalents of TBA^+ Cl^- added as a solid to the top surface of the gel. The highly emissive solution generated by the decomposition of the gel has fluorescence emission at 524 and 574 nm (λ_{ex} = 470 nm) indicating that the bound Cl^- by **1.31c** is soluble in the octane explaining the breakdown of the gel. (Reproduced with permission from ref.[189])

Figure 1.10. a) The **1.34** p-xylene gel; **b)** addition of 10 equivalents of TBAF to the hot p-xylene solution of **1.34** followed by cooling to RT; **c) 1.34** EtOH gel; **d)** reddish **1.34** EtOH gel after addition of 10 equivalents of F^-. **e)** Diffusion of F^- from a concentrated p-xylene solution (50 equiv.) through the **1.34** p-xylene gel. From left to right: **1.34** p-xylene gel; immediately after addition of TBA^+ F^- solution; after 2, 3 and 4 h; and overnight standing. (Reproduced with permission from ref.[193])

Figure 1.11. Schematic representation of the reversible polymerisation and the reversible conversion between folded and unfolded conformations of a coordination chain upon counteranion exchange of **1.37** resulting in gelation to solution, and vice versa, state changes. **a)** Depolymerisation of the coordination polymers due to strong binding of the F^- to the Ag^+ metal centres resulting in the breakdown of the gel. Repolymerisation and reformation of the gel by the addition of 1.2 equivalents of TBA^+ BF_4^-. **b)** Transition from gel to sol caused by the conformational change in **1.37** induced by the addition of $C_2F_5CO_2^-$. The reformation of gel is accomplished by addition of TBA^+ BF_4^-. (Reproduced with permission from ref.[202])

Figure 1.12. Gels of **1.38** (11 wt % in acetonitrile) exhibit multi-responsive behaviour including the chemo-response to formic acid and TBA^+ ClO_4^-. **a)** Sonication induced toughening of the gel of **1.38**. **b)** Chemo-responsive break down of the gel by the addition of formic acid or TBA^+ ClO_4^- caused by the osmotic deswelling of the gel or salting out of the organic phase. **c)** Thixotropic

(recovery of gel after gel is sheared to breaking point, *i.e.* mechano-responsive) character of the gel. **d)** Thermotropic (temperature sensitive) character of the gel. (Reproduced with permission from ref.[207])

Figure 1.13. Diagram showing the luminescence profiles of Au(I) pyrazolate complex **1.40** in hexane as solutions and gels, and the schematics of the self-assembling structures. Anion tuning by the use of Cl^- between the red and blue gel states occurs due to the removal of the intercalated Ag^+ **a)** Sol of complex **1.40** that shows barely any visible luminescence (λ_{ext} = 254 nm). **b)** Gel of **1.40** that contain stacks of complexes resulting in bright red luminescence (λ_{ext} = 254 nm). **c)** Sol containing AgOTf (0.01 equivalents) that shows green luminescence (λ_{ext} = 365 nm) due to intercalation of silver between sets of **1.40**. **d)** Gel containing AgOTf (0.01 equivalents) showing blue luminescence (λ_{ext} = 365 nm) due to intercalation of Ag^+ into the stacks of **1.40**. (Reproduced with permission from ref.[212])

Figure 1.14. Chiral bisurea compounds for the study of anion tunable LMWGs.

Figure 1.15. Urea and thiourea functionalised pyrazoles for the formation of metal and salt LMWGs that can be tuned using anions.

Figure 2.1. A time sweep of the rheological character of a gel of **2.1a** at 0.3% by weight in MeCN. It shows how even though a gel has formed instantaneously upon cooing the gel continues to 'mature'. The strengthening is highlighted by the increase in the G' value (Light grey filled ○) while the G'' value (Grey filled ◇) stays relatively the same. **a)** Inset showing a micrograph image of air trapped in a clear gel as seen upon brief sonication of a gel solution. **b)** Inset shows the branching by growing fibres resulting spherulitic networks in a gel as it matures.

Figure 2.2. DMSO:Water gels formed by the addition of water to a solution of **2.1a** in DMSO. From left to right the solvents are: pure water, ratios 1:9; 2:8; 3:7; 4:6; 5:5; 6:4; 7:3; 8:2; 9:1; pure DMSO. Note that the more aqueous samples, 1:9; 2:8; 3:7, are precipitated and/or form weak gels. Note the 8:2; 9:1 and pure DMSO samples are clear solutions.

Figure 2.3. Image of the same samples as in Figure 2.2 but after heating to dissolution followed by cooling to room temperature. Homogenous gels were obtained for the more aqueous solutions. Only pure water and ratios 7:3; 8:2; 9:1 DMSO:H_2O and pure DMSO did not form gels. Compound **2.1a** is partially soluble in water but does not form a gel. Note that the vial containing the 7:3 solution contains small crystals which were used for the determination of the compound's crystal structure.

Figure 2.4. Rheology of **2.1a** showing a frequency sweep performed on a gel of **2.1a** at 0.3% by weight MeCN gel. Typically the consistency of the *G′* (Light grey filled ◇) and *G″* (Dark grey filled ○) values over the frequency range indicates the solid-like nature of the gel material. The greater than a magnitude value of *G′* over the *G″* value demonstrates the elastic behaviour of the gel. Both axis values are shown as a logarithmic (log) scale.

Figure 2.5. Rheology of **2.1a** showing a stress sweep, as a function of oscillation (osc.) torque, on a gel of **2.1a** at 0.3% by weight MeCN gel. The stress sweep shows the rigidity and strength of the gel which breaks at a relatively high shear strength. *G′* value (Light grey filled ◇) stays constant until the torque begins to become too strong and the struts start to break under the strain. Eventually *G′* for the samples drops to below the *G″* value (Dark grey filled □) and the sample is said to be flowing, coloured guide lines show blue (*G′*) passing red (*G″*). This transition point were the *G″* value becomes greater the *G′* value gives the "yield stress". Both axis values are shown on a log scale.

Figure 2.6. The G′ dependence on the concentration (indication of strength of gel) of compound **2.1a** in MeCN. The plateau point, at around 0.45 % by weight, is used as the cut off point for the determination of the $G' \propto [\text{conc}]^n$ relationship. Errors bars on all points represent standard deviation for ten determinations of *G′* values for a given sample. An example of the deviation in results for different samples at the same weight percent is represented by the two measurements on samples at 0.35% by weight. Lines are for a power law and a linear relation of best fits.

Figure 2.7. a) Crystalline material seen upon drying a gel sample of **2.1a** in MeCN using SEM. **b)** Crystalline material seen upon drying a gel sample of **2.1a** in $CHCl_3$ using SEM. **c)** SEM image of compound **2.1a** xerogel formed from a gel made in a DMSO:H_2O mixture at 6:4. This image is a better representation of the gel structure than images seen in parts a and b. Note how the gel fibres are rod-shaped and show no indication of the chirallity of the gelator. **d)** Higher resolution image of the fibre connections of the DMSO:H_2O gel. There are large fibres/crystals that are bound to the smaller gel fibres.

Figure 2.8. a) TEM image of compound **2.1a** gel formed in a $CHCl_3$ at 0.5% by weight. **b)** Cryo-SEM image of a $CHCl_3$ gel of **2.1a** showing the fibrous gelatinous morphology as seen in the TEM image, which is in strong contrast to the dried crystalline SEM samples of Figure 7a and 7b. To the top right of the image can be seen the edge of crystalline structure similar in morphology to the dried gel.

Figure 2.9. a) Ellipsoid plot of **2.1a**. Atoms shown as 50% ellipsoids with labels for atoms involved in the hydrogen bonding. **b)** Anti-parrallel urea-urea tapes formed within the structure of **2.1a**. Molecules shown in capped-stick representation. $R_2^1(6)$ hydrogen bonding shown by dashed red lines. Selected hydrogen bond distances: N1–H1N···O1 2.875(6) Å, N2–H2N···O1 2.956(6) Å, N3–H3N···O2 2.871(6) Å and N4–H4N···O2 2.939(6) Å.

Figure 2.10. PXRD patterns of the xerogel of compound **2.1a** formed from the drying of the $CHCl_3$ gel (Blue line), drying of MeCN gel (Red line) and the simulated PXRD of the single crystal data of compound **2.1a** (Black line). The first three characteristic peaks match for all the samples. There is a systematic drift to lower 2θ values of the powder sample peaks compared to the simulated pattern due to the single crystal structure being obtained at 120K compared to the powder samples which were obtained are room temperature. Intensities have been normalised to the same scale.

Figure 2.11. Influence of different anions (0.1 equivalents of anion added as their TBA^+ salts) on the storage modulus (G') at a frequency of 1 Hz and a temperature of 20 °C, as a function of osc. torque of the 0.3% by weight gel of compound **2.1a** in MeCN. The anions added are BF_4^- (Orange △); Br^- (Blue ◇); NO_3^- (Pink □); Cl^- (Yellow △) and $MeCO_2^-$ (Black ◇). The pure gel is represented as brown ○. F^- is not shown as it forms a liquid. G' and G'' axis values are shown in log scale.

Figure 2.12. The effect of adding anion in form of TBA^+ Cl^- on G', G'' and T_{sg} for a gel of **2.1a** at 0.3% by weight and in MeCN, as measured by varying the temperature from 70°C to 25°C. The △ symbols (G' open; G'' filled) represent 0.1 equivalents of anion added and the □ symbols (G' open; G'' filled) represent 0.2 equivalents added. Arrows indicate T_{sg} points. G' and G'' axis values are shown in log scale.

Figure 2.13. The effect of adding the anion TBA^+ NO_3^- on the storage moduli for a gel of **2.1a** at 0.3% by weight and in MeCN measured by varying the osc. torque from 10 micro N.m to 1000 micro N.m, at a fixed frequency of 1 Hz. The ◇ symbols represent 0.1 equivalents of anion added; the ○ symbols represent 0.2 equivalents added and the □ symbols represent 0.5 equivalents added. G' decreases as more anion is added to the gel. G' and G'' axis are values shown in log scale.

Figure 2.14. The change in chemical shift of one of the NH protons of compound **2.1a** during the titration of TBA^+ $MeCO_2^-$ done in MeCN at 50 °C from which the binding strengths of **2.1a** for the anion is determined.

Figure 2.15. Figure showing the results of a Job Plot analysis for the binding of TBA^+ $MeCO_2^-$ by compound **2.1a** giving a 1:1 binding ratio (0.5 mole fraction of host). The two NMR signals, represented by the ◇ and □ symbols, are those assigned to the NH protons of the urea groups.

Figure 2.16. Figure showing the results of a Job Plot analysis for the binding of TBA^+ Cl^- by compound **2.1a** giving a 1:1 binding ratio (0.5 mole fraction of host). The two NMR signals, represented by the ◇ and □ symbols, are those assigned to the NH protons of the urea groups.

Figure 2.17. Alternation of gel (even *n*) and sol (odd *n*) formation in $CHCl_3$ by compounds **2.1a** – **2.1g**. All vials are at 1 % by weight in 2 ml of solvent.

Figure 2.18. a) SEM image of the xerogel of **2.1a** gel from MeCN (solvent) showing the rod-shaped nature of the dried gel sample due to crystallisation. **b)** SEM image of the xerogel of **2.1c** gel from MeCN showing the thread-like nature of the gel fibres and the helical twist induced by the chiral gelator. **c)** SEM image of the xerogel of a MeCN gel of **2.1e** showing the brittle (more crystalline) fibrous nature of the gel fibres. **d)** SEM image of the xerogel of a MeCN gel of **2.1g**.

Figure 2.19. PXRD pattern of the xerogel of compound **2.1c** at room temperature formed from the drying of a $CHCl_3$ gel (Black line) and the simulated PXRD pattern from the single crystal determination (performed at 120K) (Red line). Intensity of the simulated PXRD has been normalised to that of the xerogel.

Figure 2.20. PXRD patterns at room temperature of a powder sample of the as synthesised **2.1e** from the precipitation/gel formation in the synthesis solvent $CHCl_3$ (Black line) and the xerogel of **2.1g** formed from the drying of the $CHCl_3$ gel (Grey line). Intensity of **2.1g** PXRD normalised to that of **2.1e**.

Figure 2.21. Crystal packing diagrams showing the urea tape motif of compounds **2.1a** (**a**), **2.1c** (**b**). Note how the urea tape motifs are anti-parallel and the phenylethyl groups are in a *gauche* arrangement. Selected hydrogen bond for **2.1c**: N1–H1N···O1 2.944(4) Å, N2–H2N···O1 2.923(4) Å, N3–H3N···O2 2.930(4) Å, N4–H4N···O2 2.905(4) Å.

Figure 2.22. Crystal packing diagrams showing the urea tape motif of compounds **2.1d** (**a**), **2.1f** (**b**). Note how the urea tape motifs are parallel and the phenylethyl groups are in an *anti* arrangement. Selected hydrogen bonds: **2.1d** N1–H1N···O1 2.869(4) Å, N2–H2N···O1 2.939(4) Å, N3–H3N···O2 2.895(4) Å, N4–H4N···O2 2.866(4) Å and **2.1f** N1–H1N···O1 2.915(2) Å, N2–H2N···O1 2.881(2) Å, N3–H3N···O2 2.949(2) Å, N4–H4N···O2 2.886(2) Å.

Figure 2.23. Molecular structure of **2.1c** in form II. Atoms are shown as ellipsoids at 50% probability. Selected hydrogen bonds: N1···O1^{i} = 2.8859(15) Å; ∠ N1–H1N···O1^{i} = 145.0°, N2···O1^{i} = 2.8565(15) Å; ∠ N2–H2N···O1^{i} = 143.8°, N3···O2^{ii} = 2.9111(15) Å; ∠ N3–H3N···O2^{ii} = 147.0°, N4···O2^{ii} = 2.8172(15) Å; ∠ N4–H4N···O2^{ii} = 154.8°, (*i* = 1+x, y, z and *ii* = x-1, y, z)

Figure 2.24. Packing arrangements of **2.1c** in **a)** form I and **b)** form II.

Figure 2.25. Fibrous strands of the gels formed by **2.2**. **a)** SEM image of a MeCN 0.06 % by weight gel and **b)** is of a DMSO:H_2O 0.3 % by weight gel. Note how the fibres are larger for the more concentrated gel (i.e. higher weight %) and how the fibres are joined together through both weaving and inter-growth of fibres.

Figure 2.26. Helical fibres found within gels of compound **2.2**. **a)** is of a 0.1 % by weight $CHCl_3$ gel and **b)** is of a 0.06 % by weight MeCN gel. Note how the two images show two different sets of direction for the helical twist of the fibres. This indicates that the helicity direction is not determined by the chirality of compound **2.2**.

Figure 2.27. Rheology of **2.2** showing a time sweep performed on a gel of **2.2** at 0.1% by weight MeCN gel. Typically the gel's strength increases over time as shown by the increase in *G′* (Dark grey filled ◇) with time while *G″* (Light grey filled □) does not change.

Figure 2.28. Rheology of **2.2** showing a frequency sweep performed on a gel of **2.2** at 0.1% by weight MeCN gel. Typically the consistency of the *G′* (Dark grey filled ◇) and *G″* (Light grey filled □) values over the frequency range indicates the solid-like nature of the gel material. The fact that the *G′* value is a magnitude of order larger than *G″* value, demonstrates the elastic behaviour of the gel.

Figure 2.29. Rheology of **2.2** showing a stress sweep on a 0.1% by weight MeCN gel. The stress sweep shows the rigidity and strength of the gel, which breaks at a relatively high shear strength. *G′* value (Grey filled ◇) stayed relatively constant until the torque begins to become too strong

and the struts start to break under the strain. Eventually *G′* for the samples dropped to below the *G″* value (Light grey filled □) and the sample is said to be flowing. *G′* and *G″* axis values shown on a log scale.

Figure 2.30. PXRD pattern of **2.2** from the as-synthesised materials.

Figure 2.31. A gel of **2.2** at 0.6% by weight in a DMSO:H_2O 5:5 solvent mixture was shown to reform after being sheared to breaking point. The gel was allowed to set for 25mins upon which a stress sweep was performed from a range of 10 micro N.m to 15 000 micro N.m (Time 25.2 min to 57.4 min). The gel started to flow at around 10 000 micro N.m. Upon removal of this shear force the measurements were continued at a low frequency and stress value. As can be seen the gel reforms over time, the *G′* value reached ~ 55% of its original value. *G′* shown as grey filled ◇ and *G″* as grey filled ○. *G′* and *G″* axis values shown on a log scale.

Figure 2.32. SEM images of the dried thixotopic gel formed by **2.2** in a DMSO:H_2O mixture after shearing and "self-repair". **a)** Note that the ends of fibres that join the fibres together are thinned. **b)** Close up SEM image of the areas that join the gel fibres of the thixotropic gel together. Note how the fibres join together and can be easily be broken and re-grown. The small fragile connections result in a weaker gel.

Figure 2.33. Fluorescence spectra of a gel of **2.2** at 0.06% by weight in DMSO:H_2O. The dark blue spectrum (lowest intensity spectrum) is of the hot solution. The general increase of the intensity, as indicated by the arrow, is seen as the temperature decreased. This decrease in temperature also resulted in gelation. There is also a small red shift in the band.

Figure 2.34. Fluorescence spectra of a gel of **2.2** at 0.003% by weight in DMSO:H_2O. The spectra do not change by much as the solution cooled. When the solution is given a shake, gel formation starts to occur and the band intensity increased (as shown by the arrow).

Figure 2.35. Rheological study of the tuning of gels of **2.2** using the addition of anion in the form of TBA^+ $MeCO_2^-$. Time sweep measurements were performed on gels of **2.2** at 0.1% by weight in MeCN with varied amounts of TBA^+ $MeCO_2^-$ added. *G′* represented as dark filled symbols and *G″* as light filled symbols. △ symbols are for the pure gel, □ symbols are for 0.05 equivalents of TBA^+ $MeCO_2^-$ added, ◇ symbols are for 0.2 equivalents of TBA^+ $MeCO_2^-$ added and ○ symbols are for 0. 5 equivalents of TBA^+ $MeCO_2^-$ added.

Figure 2.36. Rheological study of the tuning of gels of **2.2** using the addition of anion in the form of TBA^+ $MeCO_2^-$. Frequency sweep measurements were performed on gels of **2.2** at 0.1% by weight in MeCN with varied amounts of TBA^+ $MeCO_2^-$ added. *G′* represented as dark filled symbols and *G″* as light filled symbols. △ symbols are for the pure gel, □ symbols are for 0.05 equivalents of TBA^+ $MeCO_2^-$ added, ◇ symbols are for 0.2 equivalents of TBA^+ $MeCO_2^-$ added and ○ symbols are for 0. 5 equivalents of TBA^+ $MeCO_2^-$ added.

Figure 2.37. Rheological study of the tuning of gels of **2.2** using the addition of anion in the form of TBA^+ $MeCO_2^-$. Stress sweep measurements were performed on gels of **2.2** at 0.1% by weight in MeCN with varied amounts of TBA^+ $MeCO_2^-$ added. *G′* represented as dark filled symbols and *G″* as light filled symbols. △ symbols (blue guide line) are for the pure gel, □ symbols (green guide line) are for 0.05 equivalents of TBA^+ $MeCO_2^-$ added, ◇ (red guide line) symbols are for 0.2 equivalents of TBA^+ $MeCO_2^-$ added and ○ symbols (purple guide line) are for 0. 5 equivalents of TBA^+ $MeCO_2^-$ added. The "yield stress", as represented by the swapping of the *G′* being larger than *G″*, decreases with increasing equivalents of anion added (shown with an arrow). "Yield stress" values are estimated to be where the eye-guiding colour lines (linear plot between two points) intersect.

Figure 2.38. Molecular structure of **2.3**. Note how the urea groups are in an anti-parallel orientation. Atoms are shown at 50% probability ellipsoids.

Figure 2.39. The urea tape motif of **2.3** in which each molecule is hydrogen bonded to four other molecules. C-H hydrogen atoms are omitted for clarity. Selected hydrogen bond distances: N1–H1N···O4 = 2.793(4) Å, N2–H2N···O4 = 3.056(4) Å, N3–H3N···O3 = 2.973(4) Å and N4–H4N···O3 2.933(3) Å

Figure 2.40. The two dimensional hydrogen bonded layer of the molecules of **2.3**. Structure viewed looking down [100]. C-H hydrogen atoms are omitted for clarity.

Figure 2.41. The overall packing of **2.3** as viewed looking down [100]. C-H hydrogen atoms are omitted for clarity.

Figure 2.42. Photograph of the Asp crystals grown from a 0.3% gel by weight of **2.1a** in MeCN through a microscope at x40 magnification. Note the visible gel fibres that have been broken by smearing some of the gel that contains the crystals on a microscope.

Figure 2.43. Pictures showing the result of crystallisation of CBZ from the gel state from acetone as a solvent resulting in a large single crystal of the acetone solvate of CBZ and its isolation from the gel by using the reversibility of the LMW gel. **a)** A photograph under UV irradiation of the vial containing the gel to highlight the crystal from the gel as the crystal was luminescent and the gel was not. **b)** The large single crystal forms within the gel which stays intact when anion in the form of TBA^+ $MeCO_2^-$ was added to dissolve the gel to form a clear solution. **c)** The crystal was then easily separated for use.

Figure 2.44. Release of ibuprofen (10mg) from a gel of **2.1a** at 0.5% by weight 7:3 H_2O:EtOH into pure water over time.

Figure 2.45. IBU release (30mg in sample gel) over time from a 0.3% gel of **2.1a** in EtOH:H_2O 3:7 into pure water followed using UV spectroscopy.

Figure 2.46. The initial release of IBU from the gel appears to follow the one-dimensional diffusion law $c \propto kt^{1/2}$ (Abscissa is $t^{1/2}$ and ordinate is the normalised concentration). However, after approximately two hours the rate has greatly slowed down and a second mechanism was evident.

Figure 2.47. Local Avrami plot of the kinetics of drug release (IBU) from a gel of **2.1a** at 0.3% by weight of EtOH:H_2O 3:7 mixture into pure water. Note how the initial negative slope is linear but then deviates once approximately 0.45 α of the drug has been released compared to the equilibrium level of drug release. This shows a second mechanism of diffusion is occurring during the release of IBU from the gel.

Figure 2.48. The effect to pH on the release of IBU (10 mg in sample of gel) from a 0.3% gel of **2.1a** in EtOH:H_2O 3:7 into water. The black points are the release into pure water, the dark grey points are the release into basic, pH 10, water and the light points are the release into acidic, pH 2, water.

Figure 3.1. Molecular structures of **3.1** and **3.2**. **a)** Compound **3.2**. **b)** Compound **3.2** chloroform solvate. **c)** Compound **3.1**. Atoms are shown as ellipsoids at 50% probability. Selected hydrogen bonds: **3.2** N3···O1 = 2.736(2) Å; ∠ N3–H3B···O1 = 126.4°, N4···N1 = 2.681(2) Å; ∠ N4–H4···N1 = 107.5°, **3.2**·2$CHCl_3$ N3···O1 = 2.743(3) Å; ∠ N3–H3A···O1 = 126.0°, N4···N1 = 2.667(3) Å; ∠ N4–H4···N1 = 108.3°, **3.1** N3···O1 = 2.768(2) Å; ∠ N3–H3A···O1 = 126.1° and N4···N1 = 2.627(2) Å; ∠ N4–H4···N1 = 111.7°.

Figure 3.2. The crystal structure of **3.3**. **a)** Molecular structure of **3.3**. Atoms are shown as ellipsoids at 50% probability. **b)** Dimer formation through the hydrogen bonding of the thiourea groups. **c)** Herringbone-like packing of the dimers. Hydrogen bonds from the N–H of the pyrazole to the S1 are shown as dashed red lines. Hydrogen bonds between dimers shown as dashed yellow lines. Selected hydrogen bonds: N4⋯N2 = 2.687(2) Å; ∠ N4–H4N⋯N2 = 140.6°, N3⋯S1^{i} = 3.345(1) Å; ∠ N3–H3N⋯S1^{i} = 148.3° and N1⋯S1^{ii} = 3.285(2) Å; ∠ N1–H1N⋯S1^{ii} = 152.4° (*i* = 2-x, 1-y, -z and *ii* = x-½, ½-y, z-½).

Figure 3.3. a) ASU of **3.3**.$CHCl_3$. Atoms are shown as ellipsoids at 50% probability. **b)** Packing of the dimers of **3.3** to form a 2D hydrogen bonded sheet. Hydrogen bonds between dimers are shown as yellow dashed lines. Hydrogen bonds involving the pyrazole N–H group are shown as red dashed lines. **c)** Packing of these sheets one on top of each other results in channels. **d)** These channels are occupied by the $CHCl_3$. Selected hydrogen bonds: N4⋯N2 = 2.684(3) Å; ∠ N4–H4N⋯N2 = 141.1°, N8⋯N6 = 2.703(3) Å; ∠ N8–H8N⋯N6 = 140.7°, N3⋯S1^{i} = 3.367(2) Å; ∠ N3–H3N⋯S1^{i} = 162.0°, N7⋯S2^{ii} = 3.328(2) Å; ∠ N7–H7N⋯S2^{ii} = 162.1°, N1⋯S1^{ii} = 3.296(2) Å; ∠ N1–H1N⋯S1^{ii} = 169.5° and N5⋯S2^{ii} = 3.346(2) Å; ∠ N5–H5N⋯S2^{ii} = 166.3° (*i* = -x, 1-y, 1-z, *ii* = 1-x, 1-y, 1-z).

Figure 3.4. Molecular structures of **3.4**, **3.5** and **3.6**. **a)** BOC protected 3-amino-5-methylpyrazole, **3.5**. **b)** BOC protected 3-aminopyrazole, **3.4**. **c)** BOC protected 3-amino-5-phenylpyrazole, **3.6**. Selected hydrogen bonds: **3.5** N3⋯O1 = 2.7812(16) Å; ∠ N3–H3N⋯O1 = 119.8°, **3.4** N3⋯O1 = 2.735(2) Å; ∠ N3–H3N⋯O1 = 128.1° and **3.6** N3⋯O2 = 2.6918(11) Å; ∠ N3–H3N⋯O2 = 121.6°. Atoms are shown as ellipsoids at 50% probability.

Figure 3.5. The two molecular structures of the two molecules of the ASU of the crystal structure of **3.8.** Atoms are shown as ellipsoids at 50% probability. Selected hydrogen bonds: N3⋯O2 = 2.7338(18) Å; ∠ N3–H3N⋯O2 = 120.5° and N7⋯O5 = 2.7049(17) Å; ∠ N7–H7N⋯O5 = 125.9°.

Figure 3.6. a) Simplified diagram showing the donor and acceptor groups. b) Helix formed by **3.8**. Selected hydrogen bonds: N4⋯N5 = 3.0243(19) Å; ∠ N4–H4N⋯N2 = 173.0° and N8⋯N1^{i} = 2.9437(19) Å; ∠ N8–H8N⋯N1^{i} = 150.1° (*i* = -x, y, -z).

Figure 3.7. Molecular structure of **3.10**. Atoms are shown as ellipsoids at 50% probability. Selected hydrogen bond: N4⋯N2 = 2.6651(17) Å; ∠ N4–H4N⋯N2 = 139.4°.

Figure 3.8. Hydrogen bonding of the dimers of **3.10** to form a hydrogen bond chain. Selected hydrogen bonds: N3⋯O1^{i} = 2.8153(15) Å; ∠ N3–H3N⋯O1^{i} = 166.3° and N1⋯O3^{ii} = 2.9703(16) Å; ∠ N1–H1N⋯O3^{ii} = 171.1° (*i* = -x, 1-y, -z and *ii* = 1-x, -y-1, -z)

Figure 3.9. Perpendicular inter-chain packing of **3.10**.

Figure 3.10. Molecular structure of **3.11a** in form I. Atoms are shown as ellipsoids at 50% probability. Selected hydrogen bonds: N4⋯N2 = 2.7328(18) Å; ∠ N4–H4N⋯N2 = 139.0° and N5⋯N2 = 2.6153(17) Å; ∠ N5–H5N⋯N2 = 112.7°.

Figure 3.11. Dimer formation by **3.11a** in form I. Selected hydrogen bonds: N3⋯O1^{i} = 2.7859(16) Å; ∠ N3–H3N⋯O1^{i} = 166.0° (*i* = -x, y, -z).

Figure 3.12. Molecular structure of **3.11a** in form II. Atoms are shown as ellipsoids at 50% probability. Selected hydrogen bond: N5⋯N2 = 2.660(12) Å; ∠ N4–H4N⋯N2 = 112.0°.

Figure 3.13. Formation of a urea tape by **3.11a**, form II. Selected hydrogen bonds: N3⋯O1^{i} = 2.902(11) Å; ∠ N3–H3N⋯O1^{i} = 151.3° and N4⋯O1^{i} = 2.822(11) Å; ∠ N4–H4N⋯O1^{i} = 156.5° (*i* = x-1, y, z).

Figure 3.14. X-ray molecular structure of [$Zn_2Cl_2(\mu$-$Cl)_2(\kappa$-*N,O*-**3.10**$)_2$] (50 % ellipsoids). Selected bond distances: Zn1⋯N2 = 2.013(5) Å, Zn1⋯O1 = 2.093(4) Å, Zn1⋯Cl2 = 2.5845(17) Å, Zn1⋯Cl1 = 2.2492(17) Å and Zn1⋯Cl2^{i} = 2.3289(18) Å (*i* = -x, 2-y, -z).

Figure 3.15. Hydrogen bonding of complexes [$Zn_2Cl_2(\mu$-$Cl)_2(\kappa$-*N,O*-**3.10**$)_2$] into columns **(a)** which are stacked next to each other **(b)**. Selected hydrogen bonds: N1⋯Cl2 = 3.126(4) Å; ∠ N1–H1⋯Cl2 = 120.7°, N1⋯Cl1^{ii} = 3.314(4) Å; ∠ N1–H1⋯Cl1^{ii} = 128.3°, C7⋯O1 = 2.813(4) Å; ∠ C7–H7⋯O1 = 120.9°, C7⋯O2 = 2.705(4) Å; ∠ C7–H7⋯O2 = 97.6°, N4⋯Cl1^{iii} = 3.257(4) Å; ∠ N4–H4⋯Cl1^{iii} = 152.3° and N3⋯Cl1^{iii} = 3.292(4) Å; ∠ N3–H3⋯Cl1^{iii} = 146.1° (*ii* = -x, y, ½ - z and *iii* = x, y-1, z).

Figure 3.16. The ASU of [CuBr(κ-*N,O*-**3.10**$)_2$]Br.2H_2O showing the chelating coordination of compound **3.10** to copper and the hydrogen bonding to the anion by the urea group of **3.10**. Atoms shown as ellipsoids at 50 % probability. Selected coordination bonds: Cu1⋯O1 = 2.034(2) Å; Cu1⋯O4 = 2.025(2) Å; Cu1⋯N2 = 1.923(2) Å; Cu1⋯N2 = 1.923(2) Å; Cu–Br 2.693(1) Å with angles of ∠ N2–Cu1–N7 = 176.7(1)° and ∠ O1–Cu1–O4 = 144.5(1)°. Selected hydrogen bonds:

N8···Br2 = 3.370(2) Å; ∠ N8–H8N···Br2 = 149.6°, N9···Br2 = 3.370(2) Å; ∠ N9–H9N···Br2 = 149.6°, O7W···Br2 = 3.481(2) Å; ∠ O7W –H7W···Br2 = 165.6°, O8W···Br2 = 3.706(2) Å; ∠ O8W –H8W ···Br2 = 154.7°, C7···O1 = 2.854(3) Å; ∠ C7–H7···O1 = 119.8°, C7···O2 = 2.711(4) Å; ∠ C7–H7···O2 = 96.5°, C18···O4 = 2.984(3) Å; ∠ C18–H18···O4 = 116.2° and C18···O5 = 2.721(3) Å; ∠ C18–H18···O5 = 96.6°.

Figure 3.17. Extensive hydrogen bonding of [CuBr(*κ*-*N,O*-**3.10**)$_2$]Br.2H_2O. Selected hydrogen bonds: N1···Br2^{i} = 3.370(2) Å; ∠ N1–H1···Br2^{i} = 149.6°, N6···O7W^{ii} = 2.806(3) Å; ∠ N6–H6N···O7W^{ii} = 152.2°, N3···Br1^{iii} = 3.304(2) Å; ∠ N3–H3N···Br1^{iii} = 158.7°; N4···Br1^{iii} = 3.371(2) Å; ∠ N4–H4N···Br1^{iii} = 157.2°, O7W···O8W^{iv} = 2.885(4) Å; ∠ O7W –H7W···O8W^{iv} = 164.9° and O8W···Br1^{v} = 3.293(2) Å; ∠ O8W –H8W···Br1^{v} = 162.9° (*i* = 1-x, 1-y , -z; *ii* = 1-x, ½+y , ½-z; *iii* = -x, 1-y , -z; *iv* = x, ½-y, z-½ and *v* = 1-x, y-½, ½-z).

Figure 3.18. The complex of [Cu(*κ*-*N,O*-**3.10**)$_2$(MeOH)$_2$](BF$_4$)$_2$ showing the chelating coordination of compound **3.10** to copper and the hydrogen bonding to the anion by the urea group of **3.10**. Atoms shown as ellipsoids at 50 % probability and labelled atoms represent the asymmetric unit. Selected bond distances: Cu1···N2 = 1.9209(15) and Cu1···O1 = 1.9706(11) Cu1···O4 = 2.5243(13). Selected hydrogen bonds: N1···O1^{i} = 2.898(2); ∠ N1-H1N···O1^{i} = 111.4° (*i* = -x, -y, -z).

Figure 3.19. Packing of [Cu(*κ*-*N,O*-**3.10**)$_2$(MeOH)$_2$](BF$_4$)$_2$. Selected hydrogen bonds: N3···O4^{ii} = 2.968(2); ∠ N3-H3N···O4^{ii} = 155.5°, N3···F4 = 2.802(2); ∠ N3-H3N···F4 = 139.5° and O4···O3^{iii} = 2.868(2); ∠ O4-H4···O3^{iii} = 162.8° (*ii* = 1+x, y, z and *iii* = -x, -y, 1-z).

Figure 3.20. ASU of [{Cu(*μ*-*κ*-*O,O,N,N*-**3.11a**)(MeOH)}$_6$](MeCO$_2$)$_6$·6MeOH. Atoms are shown as ellipsoids at 30% probability. Selected bond lengths: N5···Cu1 = 2.001(4) Å, N2···Cu1 = 1.882(5) Å, O1···Cu1 = 2.004(3) Å, O6···Cu1 = 2.216(4) Å and O2^{i}···Cu1 = 1.939(3) Å. Selected hydrogen bonds: N3···O3 = 2.730(6); ∠ N3-H3N···O3 = 165.3° and N4···O4 = 2.765(6); ∠ N4-H4N···O4 = 169.9°, O5···O3 = 2.824(6); ∠ O5-H5···O3 = 164.9° and O6···O4^{ii} = 2.679(5); ∠ O6-H6···O4^{ii} = 173.4° (*i* = 1+y, 1-x+y, -z and *ii* = $^{5}/_{3}$-x, ⅓-y, ⅓-z).

Figure 3.21. Hexamer ring of [{Cu(*μ*-*κ*-*O,O,N,N*-**3.11a**)(MeOH)}$_6$](MeCO$_2$)$_6$·6MeOH. Non-coordinated MeOH has been removed for clarity.

Figure 3.22. Overall packing of stacks of [{Cu(*μ*-*κ*-*O,O,N,N*-**3.11a**)(MeOH)}$_6$]$^{6+}$. Hydrogens and hydrogen bonds are not shown for clarity.

Figure 3.23. Molecular structures of [*mer*-Cd(κ-*O,N,N*-**3.11a**)$_2$]. Water and hydrogen atoms bound to carbon atoms are not shown for clarity. Atoms are shown as ellipsoids at 50% probability. Selected bond distances: Cd2···O1 = 2.393(9), Cd2···N2 = 2.234(7), Cd2···N5 = 2.304(8); Cd2···O3 = 2.398(9), Cd2···N7 2.251(9) and Cd2···N10 = 2.312(8)

Figure 3.24. Packing of *mer*-[Cd(κ-*O,N,N*-**3.11a**)$_2$] through hydrogen bonds between the urea groups and included methanol resulting in interstitial spaces filled by disordered water, N4···O5 = 2.892(13); ∠ N4-H4N···O5 = 157.4^o, N3···O2^i = 2.850(10); ∠ N3-H3N···O5^i = 152.4^o, O5···O2^i = 2.721(11); ∠ O5-H5···O2^i = 150.2^o, N9···O6 = 2.729(14); ∠ N9-H9N···O6 = 159.9^o, N8···O4^{ii} = 2.821(10); ∠ N8-H8N···O4^{ii} = 150.5^o and O6···O4^{ii} = 2.729(11); ∠ O6-H6···O4^{ii} = 169.6^o (*i* = -x, ½-y, 1-z and *ii* = -x, y-½, 2-z).

Figure 3.25. Ellipsoid plot of compound **3.13** showing the η^2 and η^1 coordination by TBP and THF to the aluminium centre. Hydrogen atoms and the interstitial THF have been removed for clarity. Ellipsoids are shown at 50% probability.

Figure 3.26. Ellipsoid plot of compound **3.14** showing the ligation of aluminium by PFB, TBP and a methoxyglycol anion in a bimetallic complex. Hydrogen atoms and the interstitial DME have been removed for clarity. *t*-butyl groups on the TBP ligands have been removed for clarity and the disordered groups as well. Ellipsoids are shown at 30% probability.

Figure 3.27. a) Crystal packing in the homoleptic compound Al(TBP)$_3$ channel structure of the hexane solvate of **3.12**. **b)** High Z' structure (Z' = 4) of the homoleptic compound Al(TBP)$_3$, **3.12**.

Figure 3.28. Job plot of binding by **3.3** with $MeCO_2^-$ showing the 2:1 host to guest ratio. Only the N3–H3N resonance which shows the maximum amount of shift during the titration is plotted for clarity.

Figure 3.29. Molecular structure of (**3.3**)(TBA^+)($MeCO_2^-$)·H_2O with the TBA^+ removed for clarity. Atoms are shown as ellipsoids at 50% probability. Selected hydrogen bonds: N4···N2 = 2.660(3) Å; ∠ N4–H4N···N2 = 143.3^o, N3···O1 = 2.856(3) Å; ∠ N3–H3N···O1 = 143.3^o, O3W···O2 = 2.777(3) Å; ∠ O3W–H3A···O2 = 163.5^o and O3W···S1 = 3.315(3) Å; ∠ N3–H3N···O1 = 175.1^o.

Figure 3.30. Packing of (**3.3**)(TBA^+)($MeCO_2^-$)·H_2O. **a)** 1D hydrogen bonded stacking of **3.3** hydrogen bonded to $MeCO_2^-$ and the H_2O as viewed down [001]. **b)** Layer pattern of the packing with negatively charged layers of **3.3** $MeCO_2^-$ H_2O (shown in capped stick representation)

alternating with positively charged TBA^+ layers (shown in space-filled representation). Selected hydrogen bond: $N1\cdots O2^i = 2.687(3)$ Å; $\angle$ $N1–H1N\cdots O2^i = 175.1^{\circ}$ (i = -x, y-½, ½-z).

Figure 3.31. Photograph of the gels of compound **3.10** at 1% by weight in water acidified with, from left to right, H_3PO_4; H_2SO_4; HPF_6 and HBF_4.

Figure 3.32. Gels formed by compound **3.10** in water at pH 1.0 acidified with H_2SO_4. From left to right the concentrations are 1.3%, 0.6%, 0.15% and 0.1% by weight in 5ml of solution. The 0.1% by weight solution only partially gels and therefore does not survive the inversion test.

Figure 3.33. Rheology of gelation by **3.10** showing a frequency sweep performed on a gel of **3.10** at 0.1% by weight in water acidified with H_2SO_4 to a pH of 1.0. Typically the consistency of the G' (Dark grey filled ◇) and G'' (Light grey filled ○) values over the frequency range indicates the solid-like nature of the gel material. The value of G' is typically five times greater than the G'' value and constant with respect to the frequency demonstrating the elastic behaviour of the gel. The G' and G'' axis is shown as a log scale.

Figure 3.34. Rheology of the gelation by **3.10** showing a stress sweep on a gel of **3.10** at 0.1% by weight in water acidified with H_2SO_4 to a pH of 1.0. The stress sweep shows the rigidity and strength of the gel which breaks at a relatively high shear strength. G' value (Dark grey filled ◇ with brown line) stays constant until the torque begins to become too strong and the struts start to break under the strain where upon G' becomes less than G'' (Light grey filled □ with green line). Lines are there to help aid the eye. The G' and G'' axis is shown as a log scale.

Figure 3.35. Study in the variation in G' with change in concentration for gels of **3.10** in acidified water at pH 1.0 using H_2SO_4 (y = G' (Pa) and x = concentration in mg in 5 ml). $G' \propto [\text{conc}]^n$ relationship is confirmed with n = 2.2. Errors on data points, determined as standard deviations of ten measurements on a sample, are smaller than symbol size used. Both the G' axis and concentration axis are shown on a log scale.

Figure 3.36. Study in the variation in “yield stress” with change in concentration for gels of **3.10** in acidified water at pH 1.0 using H_2SO_4 (y = “Yield Stress” (micro Nm) and x = concentration in mg in 5ml). “Yield stress” $\propto [\text{conc}]^n$ relationship is confirmed with n = 1.5. Errors on plotted points are determined as the standard deviation for the point determined by taking the average of the measured points either side of the “yield stress” (see Figure3.34 for example). Both the “yield stress” axis and concentration axis are shown on a log scale.

Figure 3.37. a) SEM image of dried gels of **3.10** in water acidified with H_2SO_4 to a pH of 1.0 that has been covered with a thin layer of Pt. b) TEM image of a gel of **3.10** in water acidified with H_2SO_4 to a pH of 1.0.

Figure 3.38. EELS data from the gel sample of **3.10** in water acidified to pH 1.0 with H_2SO_4. The collected spectra (Filled blue area) is baseline corrected (Red line) to give the EELS data (Green line). This reveals peaks at 164 eV (S), 284 eV (C), 401 eV (N) and 532 eV (O).

Figure 3.39. ASU of (**3.10H$^+$**)$_2$(SO_4^{2-})·7H_2O. Atoms are shown as ellipsoids at 50% probability. Selected hydrogen bonds: N2···O8 = 2.575(2) Å; ∠ N2–H2N···O8 = 118.4°, C7···O8 = 2.750(2) Å; ∠ C7–H7···O8 = 121.5°, N7···O11 = 2.663(2) Å; ∠ N7–H7N···O11 = 118.3° and C18···O11 = 2.836(2) Å; ∠ C18–H18···O11 = 121.1°, N8···O14 = 2.8184(19) Å; ∠ N8–H8N···O14 = 169.4°, N9···O15 = 2.9459(18) Å; ∠ N9–H9N···O15 = 168.2° and N1···O17^{i} = 2.7439(18) Å; ∠ N1–H1N···O17^{i} = 171.9° (*i* = x, y-1, z).

Figure 3.40. Packing diagram of (**3.10H$^+$**)$_2$(SO_4^{2-})·7H_2O showing the stacking of **3.10H$^+$** one on top of each other resulting in a column in which the SO_4^{2-} and water are located. Packing viewed down [100].

Figure 3.41. Rheology by frequency sweep of the HBF_4 (△) and HPF_6 (□) acidified gels.

Figure 3.42. TEM images of gels of **3.10** acidified with **a,b)** HBF_4, **c,d)** HPF_6.

Figure 3.43. Electron diffraction images of gels of **3.10** acidified with HBF_4 (top) and HPF_6 (bottom). Top diffraction *d*–spacing for the HBF_4 acidified gels are 2.46 Å; 2.11 Å; 1.86 Å; 1.55 Å; 1.32 Å and 1.12 Å. Bottom diffraction *d*–spacing for the HPF_6 acidified gels are 2.07 Å; 1.81 Å; 1.31 Å and 1.10 Å.

Figure 3.44. SEM images of dried gels of **3.10** acidified with **a)** HBF_4 and **b)** HPF_6..

Figure 3.45. Molecular structure of (**3.10H$^+$**)(BF_4^-)·H_2O. Atoms are shown as ellipsoids at 50% probability. Selected hydrogen bonds: BF_4^- are N3···F3 = 2.965(2) Å; ∠ N3–H3N··· F3 = 148.4°, N3···F1 = 3.069(2) Å; ∠ N3–H3N··· F1 = 145.9°, N4···F1 = 2.9275(19) Å; ∠ N4–H4N··· F1 = 149.4°, O4···O1 = 2.814(2) Å; ∠ O4–H4W··· O1 = 177.3°, N1···O4^{i} = 2.653(2) Å; ∠ N1–H1N··· O4^{i} = 170.5°, O4···F3^{ii} = 2.981(2) Å; ∠ O4–H4W··· F3^{ii} = 149.4° and N2···F2^{iii} = 2.7539(19) Å; ∠ N2–H2N··· F2^{iii} = 140.9° (*i* = -x, 1-y, 1-z and *ii* = x, y-1, z and *iii* = x-1, y-1, z).

Figure 3.46. a) Structure of **$3.10H^+$** BF_4^- H_2O as viewed down (100). **b)** Structure of **$3.10H^+$** BF_4^- H_2O as viewed down (010). Hydrogen bonds not shown for clarity.

Figure 3.47. Molecular structure of (**$3.10H^+$**)(BF_4^-)·**3.10**. Atoms are shown as ellipsoids at 50% probability. **a)** Disordered proton on N1. Selected hydrogen bonds: N1···O4 = 2.722(3) Å; ∠ N1–H1N··· O4 = 113.2°, N2··· O4 = 2.743(3) Å; ∠ N2–H2N··· O4 = 111.7°, N2···O1 = 2.685(3) Å; ∠ N2–H2N··· O1 = 119.3°, C7···O1 = 2.930(3) Å; ∠ C7–H7··· O1 = 118.9° N1···N7 = 2.843(3) Å; ∠ N1–H1N···N7 = 162.5° or N7···N1 = 2.843(3) Å; ∠ N7–H7N···N1 = 167.6° N7···O4 = 2.838(3) Å; ∠ N7–H7N··· O4 = 114.7° C22···O4 = 2.905(3) Å; ∠ C22–H22··· O4 = 118.3°. **b)** Disordered proton on N7. Selected hydrogen bonds: N3···F1 = 2.935(3) Å; ∠ N3–H3N···F1 = 155.6° and N4···F2 = 2.897(3) Å; ∠ N4–H4N···F2 = 160.9° N8···F4^{i} = 2.908 (3) Å; ∠ N8–H8N···F4^{i} = 145.9°, N9···F4^{ii} = 2.958(3) Å; ∠ N9–H9N···F4^{ii} = 157.4° and N6···O3^{iii} = 3.192(3) Å; ∠ N6–H6N··· O3^{iii} = 164.8° (*i* = 1-x, 1-y, 2-z; *ii* = 1+x, 1+y, z and *iii* = 1+x, y, 1+z).

Figure 3.48. Packing diagram of (**$3.10H^+$**)(BF_4^-)·**3.10** showing the stacking of 1D hydrogen bonded **$3.10H^+$ 3.10** threads alternating with the layers of BF_4^-. Hydrogen bonds are not shown for clarity.

Figure 3.49. PXRD pattern for dried **3.10** gel acidified with HPF_6. Selected *d*-spacings: 2.08 Å; 1.85 Å; 1.70 Å; 1.21 Å and 1.13 Å.

Figure 3.50. PXRD pattern for dried **3.10** gels acidified with HBF_4. Selected *d*-spacings: 2.15 Å; 1.95 Å; 1.81 Å; 1.77 Å; 1.75 Å; 1.60 Å and 1.46 Å.

Figure 3.51. Frequency sweep rheometry of **3.10** gels acidified with H_3PO_4 (○) and $MePO_4H_2$ (◇). Dark grey filled symbols are of *G′* and light grey filled symbols are of *G″*.

Figure 3.52. TEM image of **3.10** gel acidified with H_3PO_4 at room temperature.

Figure 3.53. PXRD pattern for dried **3.10** gel acidified with $MePO_3H_2$.

Figure 3.54. PXRD pattern for dried **3.10** gels acidified with $EtPO_3H_2$.

Figure 3.55. TEM images of the gels from acidification of a water solution of **3.10** with HNO_3. **a)** and **b)** are from a **3.10** with HNO_3 gel sample. **c)** and **d)** are from a **3.10** with HNO_3 gel that has started to break down to a precipitate.

Figure 3.56. Molecular structure of (**3.10H**$^+$)(NO_3^-)·MeOH. Atoms are shown as ellipsoids at 50% probability. Selected hydrogen bonds for intra-molecular bonds: N2···O1 = 2.598(2) Å; ∠ N2–H2N···O1 = 120.3°, C7···O1 = 2.855(3) Å; ∠ C7–H7···O1 = 120.4°, N7···O4 = 2.667(2) Å; ∠ N7–H7N···O4 = 118.3° and C18···O4 = 2.884(3) Å; ∠ C18–H18···O4 = 120.2°. Selected hydrogen bonds for chelated nitrate: N3···O7 = 2.982(3) Å; ∠ N3–H3N···O7 = 170.7°, N4···O8 = 2.785(2) Å; ∠ N4–H4N···O8 = 165.9°, N8···O7 = 3.318(3) Å; ∠ N8–H8N···O7 = 161.8°, N8···O9 = 3.040(3) Å; ∠ N8–H8N···O9 = 144.4° and N9···O9 = 2.778(3) Å; ∠ N9–H9N···O9 = 157.5°. Selected hydrogen bonds for methanol and methanol hydrogen bonded nitrate: N1···O11 = 2.687(3) Å; ∠ N1–H1N···O11 = 172.9°, N1···O10 = 3.080(3) Å; ∠ N1–H1N···O10 = 117.2° and N2···O10 = 3.097(3) Å; ∠ N2–H2N···O10 = 115.3°, O14···O12 = 2.835(3) Å; ∠ O14–H14W···O12 = 171.5°, O13···O10 = 2.969(2) Å; ∠ O13–H13W···O10 = 150.1°, N6···O14 = 2.645(3) Å; ∠ N6–H6N···O14 = 169.6° and N7···O13 = 2.803(2) Å; ∠ N7–H7N···O13 = 146.5° (*i* = 1-x, 1-y, 1-z and *ii* = 1+x, y, 1+z).

Figure 3.57. Overall crystal packing of (**3.10H**$^+$)(NO_3^-)·MeOH. Hydrogen bonds are not shown for clarity.

Figure 3.58. Molecular structure of 2[(**3.10H**$^+$)(Cl^-)]·MeOH·H_2O. Atoms are shown as ellipsoids at 20% probability. Selected hydrogen bonds for intra-molecular hydrogen bond: N2···O1 = 2.716(19) Å; ∠ N2–H2N···O1 = 121.0°, C7···O1 = 2.906(18) Å; ∠ C7–H7···O1 = 123.2°, N7···O4 = 2.657(17) Å; ∠ N7–H7N···O4 = 118.5° and C18···O4 = 2.805(18) Å; ∠ C18–H18···O4 = 119.9°. Selected hydrogen bonds for Cl1: N3···Cl1 = 3.258(16) Å; ∠ N3–H3N··· Cl1 = 159.0°, N4··· Cl1 = 3.230(16) Å; ∠ N4–H4N··· Cl1 = 165.4°, N8··· Cl1 = 3.172(16) Å; ∠ N8–H8N··· Cl1 = 160.9° and N9··· Cl1 = 3.281(15) Å; ∠ N9–H9N··· Cl1 = 156.9°. Selected hydrogen bonds for Cl2 and methanol: N1···Cl1 = 2.956(18) Å; ∠ N1–H1N··· Cl1 = 174.1°, N6···O8 = 3.330(16) Å; ∠ N6–H6N··· O8 = 163.3°, N7···O7 = 2.775(15) Å; ∠ N7–H7N··· O7 = 145.2° and Cl1, O7···Cl1^i = 3.009(16) Å; ∠ O7–H7A··· Cl1^i = 156.6° (*i* = 1-x, 2-y, 1-z).

Figure 3.59. Overall packing of 2(**3.10H**$^+$) 2Cl^- MeOH H_2O. Atoms are shown in capped stick representation except for the Cl^- and water oxygen which are shown as small spheres.

Figure 3.60. PXRD pattern for dried **3.10** gel acidified with HNO_3.

Figure 3.61. PXRD pattern for dried **3.10** gel acidified with HCl.

Figure 3.62. Photograph of gels of **3.10** at 1% by weight in water acidified with, from left to right, $EtPO_4H_2$; $MePO_4H_2$, H_3PO_4; H_2SO_4; HPF_6 and HBF_4. The samples for the acids H_3PO_4; H_2SO_4; HPF_6 and HBF_4 are the same as those shown in Figure 3.31.

Figure 3.63. Anion tuning of the rheometric characterisations of **3.10** gels shown by stress sweep rheometry of the hydrogels of **3.10** at 1% by weight acidified with H_2SO_4 (Blue ◇), H_3PO_4[3] (Orange □), $MePO_3H_2$ (Green ◇), HBF_4 (Light blue △), HPF_6 (Brown ○) and $EtPO_3H_2$ (Light green □).

Scheme captions

Scheme 3.1 Possible products from the reaction of 3-amino-5-methylpyrazole with an isocyanate to give, from left to right, desired urea, 2-carboxamide, 1-carboxamide.

Scheme 3.2 Possible reaction products from the reaction of 3-amino-5-methylpyrazole with di-*tert*-butylpyrocarbonate, the BOC-protection reaction.

Scheme 3.3 Reaction products, **3.7**, **3.8** and **3.9**, of the pyrazole urea synthesis by reacting **3.5** with three different isocyanates.

Scheme 3.4 The synthetic route to the synthesis of **3.10** from 3-amino-5-methylpyrazole via a BOC-protection of the pyrazole ring.

Scheme 3.5 The two possible isomers from the reaction of two equivalents of *p*-tolylisocyanate with 3-amino-5-methylpyrazole. **3.11a** 1-carboxamide-3-urea isomer and **3.11b** 2-carboxamide-3-urea isomer.

Scheme 3.6. Redox transmetallation ligand exchange reaction between Aluminium metal and 3,5-*t*-butylpyrazole (TBPH) and dipentaflourophenylmercury.

Table captions

Chapter 1
Introduction

1.1 What is a gel?

By definition, gels are solid, jelly-like materials formed from colloidal mixtures. They are colloidal in nature due to the dispersion of the gelator (the solid continuous phase) within a solvent (the liquid dispersed phase). What makes gels so interesting is that by weight and volume they are mostly liquid, yet they behave like a solid. Many applications of gels have been envisaged and discovered because of the gels' abilities to trap and immobilize large volumes of liquid (and sometimes active guest molecules) using relatively low masses of gelator. Gels have been applied in the photographic, food, cosmetic and petroleum industries, and have additional potential uses in drug delivery,[1-12] lithography,[13-15] catalysis (as supports),[16-21] scaffolds (such as in tissue engineering and materials synthesis)[22-31] and as separation materials,[32-37] to name but a few.[27,38-68]

The set of compounds that act as gelators is surprisingly diverse, and virtually all liquids can be immobilised within a gel. Gelators such as polymers, proteins and inorganic substances - like clays and silica - have been studied extensively. Although low molecular weight gelators (LMWGs) have been known for a long time, it is only recently that they have become a focused area of supramolecular chemistry and materials science.[27,38-68] This increased interest has occurred because of the high versatility of such compounds towards synthetic modification. In practice, this 'molecular tunability' allows for greater control of the properties of the gel-phase assemblies.

The macroscopic properties of a gel - in particularly its rheological properties - are determined by the three-dimensional (3D) entangled networks of the micro/nanostructured supramolecular fibres.[38-65] In the case of LMWGs, the structure of these fibres is determined by supramolecular interactions such as hydrogen bonding, π-π stacking, hydrophobic effects, metal coordination and van der Waals interactions.

Often these interactions are divergent and orientated in one or two dimensions such that the small molecules preferentially self-assemble into 1D fibrils, resulting in fibre formation. The association of these fibres into larger bundles (which branch further through mechanisms such as crystallographic mismatch branching)[44] and the eventual physical knotting of these fibres, results in a 3D network that retards the movement of the liquid by capillary force alone. The reversibility of these supramolecular interactions means that LMWGs are easily manipulated by external stimuli, allowing for the tuning of the physical properties of the gel. This has been accomplished by using mechanical stimuli (in the form of thixotropy and sonication-aided gelation) as well as thermal, electrochemical, electromagnetic and chemical stimuli.[38-65] Chemical stimuli, as additives, have also been reported to change the characteristics of the gel, for example, variation of pH,[7,8,11,12,15,18,69-84] the addition/response to biologically relevant compounds such as vancomycin, insulin and enzymes,[4-6,8,20,38,56,84-95] the incorporation of metals (metallogels)[51,96] and the addition and incorporation of anions.[52,97]

1.2 Tuning of LMWGs

LMWGs can be divided into compounds that gel water (hydrogels) and those that gel organic solvents (organogels) and there are examples that are capable of both. Except for a few examples, the majority of LWMGs were only discovered and reported in the last couple of decades.[38,39,48] Even so, there is a surprisingly large variation in the structures of compounds that are LMWGs. There are compounds that contain natural product based moieties such as amino acids, saccharides, bile salts, nucleosides and nucleotides. There are compounds with diverse sets of functional groups and structures such as amines, carboxylic acids, amides, ureas, hydrophobic groups like long alkyl chains, dendrimers, metal sites, metal binding sites, azobenzenes, perfluoronated alkyl chains and dye-systems, to name but a few.[27,38-68] As there is such a large variability in the structure of LMWGs, a recognisable advantage for the use of these compounds over the other known gelators, there has been as large a development of ways to tune the gel properties of LMWGs.[54] This tuning ability has led to many ideas for applications of LMWGs.[27,38,68] The following paragraphs describe some of the methods used to tune

LMWGs' properties and some of the applications that have arisen from them. We will then focus on the tuning of gel properties by anion binding in particular.

The thermal reversibility of most LMWGs is one of the key advantages of these types of materials. Thermally reversible gels are termed physical gelators, i.e. their physical state can be changed, and the majority of LMWGs undergo thermally reversible gel to sol transformations, unlike most polymers and biopolymer gels (though not all).[45] The reversibility allows for hot solutions to be gelled by cooling and the gel to be broken down by heating, therefore, increasing the LMWG's solubility. There are even a few interesting examples of the opposite effect on gel formation, that is, gel formation on heating, and the breaking down of the gel upon cooling of a LMWG.[98,99] An example of this increase in temperature gel setting involves a two component gelator of a chiral amine-functionalised calix[4]arene (**1.1**) and 2,3-dibenzoyltartaric acid in cyclohexane.[98] The mixture with the L enantiomer of 2,3-dibenzoyltartaric acid behaves 'normally' in that the solution gels upon cooling. The D enantiomer of 2,3-dibenzoyltartaric acid enantiomer does the opposite and gels upon heating a solution to 60 °C.

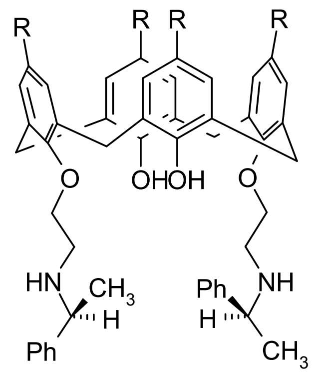

R = $C(CH_3)_2(CH_2)_{13}CH_3$

1.1

The dissolving and/or melting temperature point of a gel discovered when increasing the temperature is referred to as its T_{gel}.[48] There are several methods to measure this point but all generally use a shearing mechanism and temperature variation to disturb the gel. These methods include the dropping ball method, the inverted tube method and rheological shearing during a temperature sweep using a rheometer.[48] In the cases where there is a measurable energy change due to the sudden phase change event a differential scanning calorimetry (DSC) measurement can be used.[48]

LWMGs can be physically sheared. In most cases this causes the gel to break down and the resultant flow become permanent. However, in a few special cases the phenomenon of thixotropy occurs.[69,100-104] This is when the gel has an inbuilt repair mechanism and therefore the gel reforms after it has been made to flow after shearing. This occurrence within gels is not the only way in which a gel can be tuned by physical means. Sonication of solutions or suspensions of LMWGs has become a focused area of interest.[54,65,105-108] The use of "sound" in some cases is the only way to form these LMW gels.[65,108]

Chemical reactions are by far the most utilised means to tune a LMWG.[54] One such example is when chemical moieties are capable of light-induced conformational and/or chemical changes. This process has been harnessed by designers of LMWGs to create gels that can be tuned to either their solution or gel states.[1,14,16,54,88,109-118] Azobenzene moieties are one of the more commonly used groups.[110,112-114] The UV induced change from the *trans* conformation to the *cis* conformation often results in disruption of the gel state resulting in a solution. Shinkai was one of first to use this principle although many others have followed this work up with many applications, such as drug delivery,[1] and insightful studies such as the cooperative effects of this transformation within the self-assembled fibres.[112]

Shinkai used an azocholesterol derived LMWG, compound **1.2**, to show that the *trans*-*cis* photoisomerisation of the azobenzene moiety was the cause of the sol-gel phase transition.[113] The transition was reversible by using the appropriate wavelength to cause the *cis*-*trans* photoisomerisation. Carbon-carbon double bonds also undergo a *trans*-to-*cis* transformation under UV irradiation and this has also been utilized in the formation of gels that can be transformed to sols upon exposure to UV radiation.[1,111,115] Light-induced chemical transformations are also a popular means of transforming the gel state.[14,116]

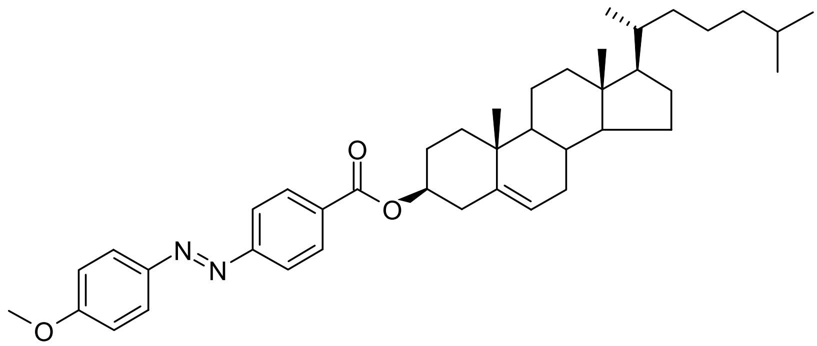

1.2

Bisthienylethene LMWGs have been shown to undergo the transformation from an open to a closed state without degradation of the gel.[14,116] This results in a tunable gel, the use of which has been envisioned in fields of opto- and electronic smart materials, logic gate, fluorescence sensors and other molecular photonic devices.[14,88] The integration of the photo-sensitive spiropyran group into a LMWG has resulted in a gel that can be transformed from the gel state to the sol state through exposure to UV light.[88] The photodimerization (which can be reversible) and polymerization of unsaturated hydrocarbons has also been investigated within the gel state of LMWGs.[16,117-121]

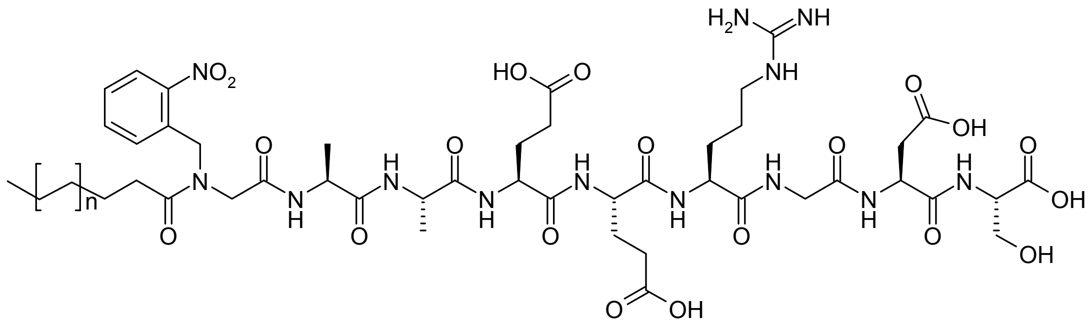

1.3 *n* = 11

An interesting method of inducing gel formation is to use photo-induced cleavage reactive groups that results in a product that acts as a LMWG.[109] Stupp *et al.* have done this using compound **1.3** (a peptide) and have induced the formation of the gel by irradiation of **1.3**. The gel has been used as a medium for testing biological activity of living cells.[109] Compound **1.3** contains the photolabile 2–nitrobenzyl group.

Upon exposure of an aqueous solution of **1.3** and $CaCl_2$ to UV light (λ_{max} = 350nm) for 45 mins the solution turns to a hydrogel.

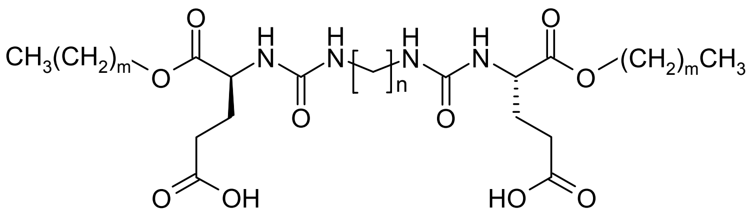

1.4 *m* = 0;3;5;7;11;14 *n* = 4;8;6;12

Many LMWG contain functional groups that are sensitive to the pH of their environment.[7,8,11,12,15,18,69-84] These groups can be deprotonated or protonated according to the pH of the solution and this may remove or create important interactions vital to the gel tuning and/or formation resulting in a gel that can be tuned by changing the pH. Estroff and Hamilton were some of the first to actively show this process of pH tuning of a LMWG.[75] Using compounds **1.4** they showed that the compounds gel at different pHs and salt conditions (ionic strength). The number of carbon atoms within the spacer and alkyl esters also have a great effect on the gel ability with some compounds not gelling at all. The pH at which the compounds do gel is also tuned by the number of carbon atoms.

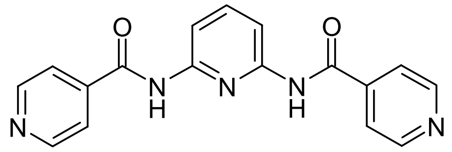

1.5

Jung *et al.* showed that the pH can be used to tune the emissive properties of a gel of compound **1.5**.[76] Compound **1.5** gels over the entire pH range but shows a higher T_{gel} at neutral pH 7. This thermally more stable gel at pH 7 also shows a stronger emission of blue light and weaker emission is noted at pH 13 and pH 2. The authors explain this observation in light of the fact that at low acidic pH **1.5** is protonated and under highly basic conditions the retardation of the gel process prevents significant aggregation of **1.5** to give strong fluorescence, besides the fact that gel formation still occurs at both low and high pH. Park *et al.* also showed similar production of emissive gels of compound **1.6** that can be tuned by pH variation.[122]

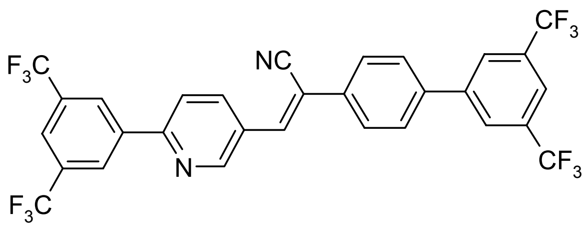

1.6

The protonation of a pyridyl group is once again the mechanism by which the gel is tuned by the decrease in pH. However as **1.6** forms organogels the authors use the photo-induced release of protons to induce the gel-to-sol transition. This was accomplished by using the photoacid generator triphenylsulfonium trifluoromethane sulfonate (PAG) which releases protons (H^+) and counter ions ($CF_3SO_3^-$) upon UV light exposure. This is illustrated by Figure 1.1.

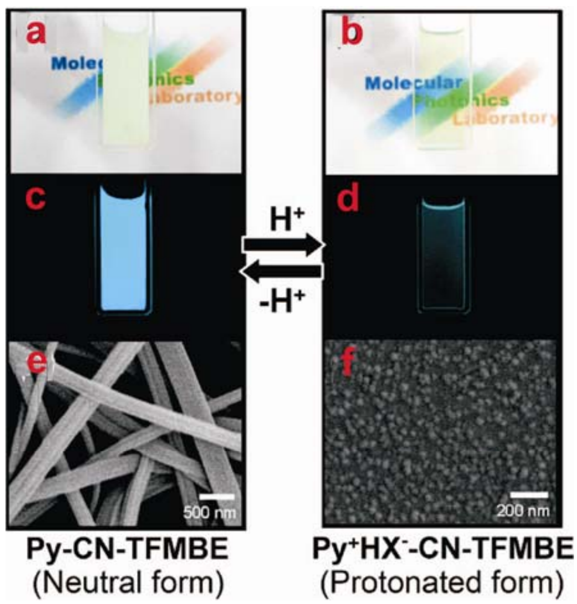

Figure 1.1. a, b) Photographs of the reversible phase transition between the gel and sol states of **1.6** in 1,2-dichloroethane (neutral gel **(a)** and protonated sol **(b)**). **c, d)** Fluorescence images and **e, f)** SEM images of the neutral gel and the protonated sol, respectively. (Reproduced with permission from ref.[122])

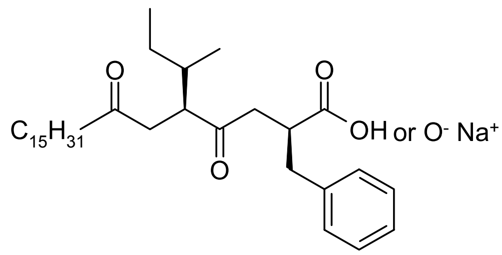

1.7

Das *et al.* showed how pH control of gelation of compound **1.7** (as well as other related compounds), a dipeptide based LMWG, can be used effectively to entrap compounds such as dyes.[80] The sodium salt of **1.7** (**1.7-Na**) is a rare case of a LMWG of both organic solvents and water. Interestingly, the conversion to the sodium salt improves the gelation ability of **1.7** as the compound gels organic solvents with a critical gelation concentration, CGC, of approximately 0.8% by weight whereas **1.7-Na** gels them at a CGC of approximately 0.35% by weight. As **1.7** does not gel water, the lowering of the pH by the addition of HCl resulted in the breakdown of the gel due to protonation of the carboxylate group. The authors use this understanding of pH controlled gelation to target removal of a dye (crystal violet) from water by varying gelation through changes in pH (Figure 1.2). By gelling the dye-containing aqueous solution with **1.7-Na** a hydrogel is formed. By adding toluene to the surface (which has no effect) and then adding HCl they were able to remove the dye from the water phase. Heating this mixture gently and then cooling resulted in the toluene phase becoming a gel that contains the dye. This sequence of experiments showed how the assembled gel fibres were interacting strongly with the dye and were able to transport it between two very different phases.

Host:guest interactions can be used to tune the properties of a gel.[54,61,77,78,88,93,98,123-135] There have been some classical host:guest systems developed that can be used as LWMGs. An interesting host:guest system of cucurbit[7]uril (**1.8**) in acidic water was shown by Kim *et al.* **1.8** to only gel in aqueous solutions at pH values below its pK_a, which was determined to be 2.2 by a simple titration method.[77] At, and above, this pH, the hydronium ion bound to the carbonyl portal groups can be displaced by Na^+ or K^+ resulting in the break-down of the gel to give a solution. In addition Kim *et al.* showed how a small amount of added guest 4,4′-diaminostilbene dihydrochloride

(**1.9**) was used to tune the gel properties of this system. A solution containing just 0.1 equivalents of **1.9** compared to **1.8** results in a gel. Upon exposure to UV light compound **1.9** undergoes a *trans-cis* isomerisation resulting in it being bound much more strongly by the cucurbit[7]uril host. This prevents the binding of the water/hydronium ions breaking the hydrogen bonding network of the gel therefore resulting in sol formation.

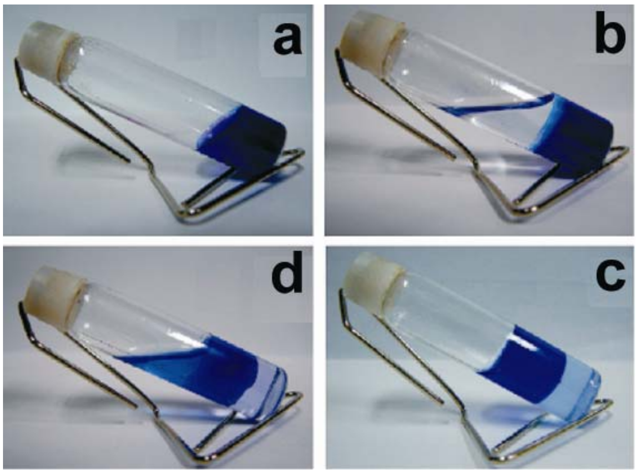

Figure 1.2. **a)** Hydrogel of **1.7-Na** containing 0.1 mM of crystal violet. **b)** Toluene added to the hydrogel of **1.7-Na** containing the dye. **c)** Status of hydrogel after the addition of 1.1 equiv of HCl. **d)** Subsequent heating results in selective gelation of the toluene phase containing crystal violet, leaving the aqueous layer clear within a few minutes of addition. (Reproduced with permission from ref.[80])

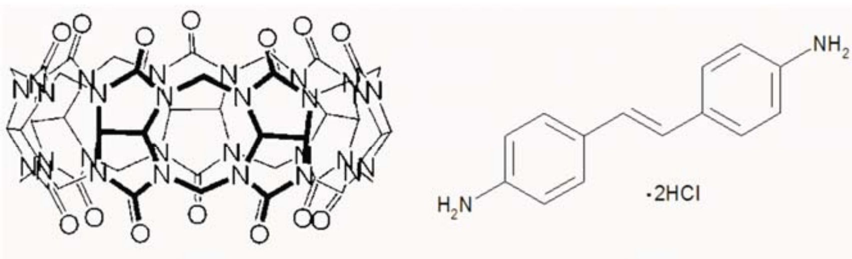

1.8 **1.9**

Calixarenes are well known in the field of host-guest chemistry and the interaction between this class of hosts and chiral amine guests has been exploited by

Zheng and coworkers to make LMWGs.[98,124,125] The calixarenes such as compound **1.1** reported by this group are able to form gels with several chiral amines, *i.e.* the systems are two–component gels. Fascinating properties have been described such as the selective gelation of a single enantiomer and gelation at elevated temperatures (60 ^{o}C) by the D-2,3-dibenzoyltartaric acid whereas L-2,3-dibenzoyltartaric acid shows "normal" behaviour and gels at a lower temperature.[98]

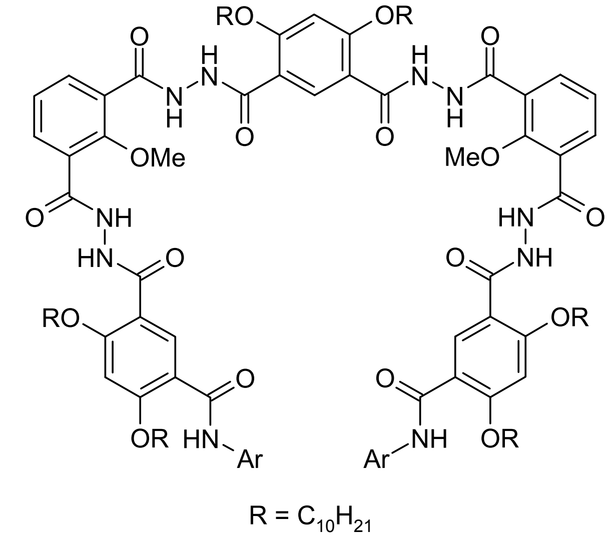

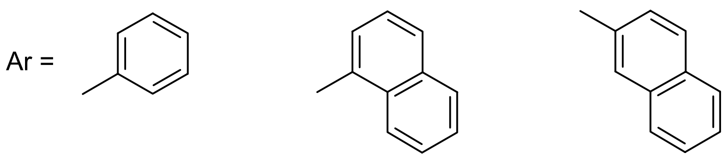

1.10a **1.10b** **1.10c**

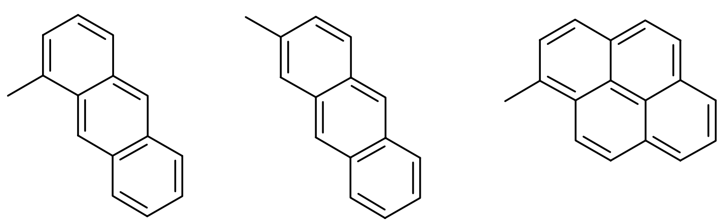

1.10d **1.10e** **1.10f**

Using a mixture of two or more components is becoming a common means of tuning gels.[16,59,61,71,78,99,125,129,130,136-147] Smith reviewed this concept in 2005.[61] A range of chemical additives can be used to tune many characteristics of the LMWGs such as their structural, physical and electromagnetic properties.[131-134] Fluorescent compounds like 8-anilinonaphthalene-1-sulfonic acid, propyldansylamide and pyrene are all environment-sensitive fluorescent probes.[132-134] This allows the investigator to probe the hydrophobicity of the gel interiors where the probes are immobilised. Other additives can be used to tune the properties of the gels. Examples include the use of polymers to strengthen LMWGs[131] and the interaction between [60]fullerene and a LMWG porphyrin has also been utilised by Shinkai *et al.* to strengthen the gels.[127] A foldamer based LMWG (**1.10**) reported by Li *et al.* shows chirality induced comformational properties due to the interaction with added glucose.[126]

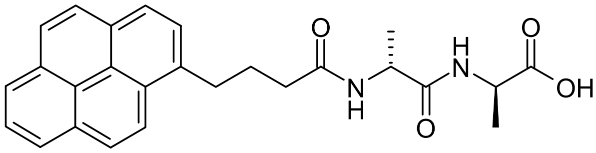

1.11

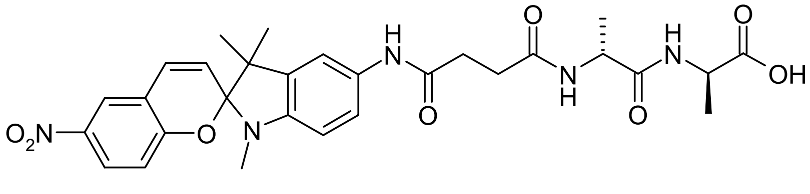

1.12

Some additives can be used to break down the gel due to the strong interaction of the additive with the LWMG. Vancomycin, an antibiotic, has been used to both strengthen a gel and cause a transformation from gel to sol.[88,93] With compound **1.11**, the interaction with vancomycin causes an improvement in the gelation ability.[93] In contrast compound **1.12** breaks down from a gel to a sol upon the addition of vancomycin.[88] In both these cases the interaction between the D-ala-D-ala residues and the vancomycin are important for these tuning abilities. Indeed, with compound **1.12**, replacement of the D-ala-D-ala residue with L-ala-L-ala results in no tuning by the addition of vancomycin. This biologically inspired gel tuning has been further expanded using other gelators.[4-6,8,20,26,32,38,56,84,86,87,89-92,94,95,148-152] When an enzyme cleavable moiety is incorporated into the LMWG the gel can be tuned using the catalytic properties of enzymes. The group of Xu and co-workers is one of the groups investigating LMWG with biological aspects in mind.[20,56,87,90,91,93,148,149] Compound **1.13** is an example of their work. This phosphate compound does not gel water. But when the phosphate group is enzymatically converted to the hydroxyl group the new compound (**1.14**) does gel water. Therefore compound **1.13** can be used to cause gelation in the presence of a phosphatase enzyme.[90]

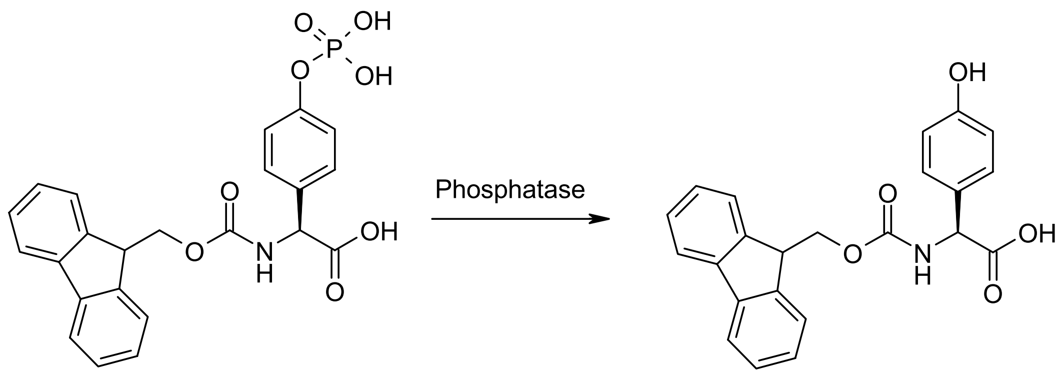

1.13 **1.14**

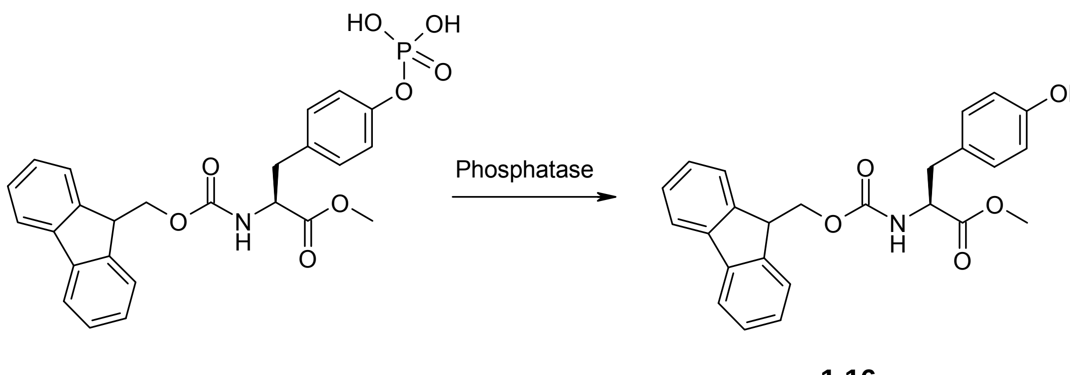

1.15 **1.16**

Work by Yang, Wang, Kong *et al.* with a very similar compound to **1.13**, compound **1.15**, also shows how an enzymatic process can be used to form a gel.[94] Compound **1.15** does not form a gel under any circumstances, nor does the dephosphorylated compound **1.16**. However, when a low concentration of phosphatase enzyme is used an opaque gel is formed. This gel contains a mixture of compounds **1.15** and **1.16**. Mixtures of the two compounds could also not be induced to gel therefore showing that the enzymatic action of converting **1.16** to **1.15** assists the supramolecular fibrillar assembly and therefore gel formation. The use of an enzyme catalysed reaction to degrade a gel has also been studied. This idea is highlighted by the work of John *et al.* who used a LMWG consisting of a sugar and fatty acid.[6] The cleavage of the fatty acid moiety using a hydrolase enzyme resulted in the destruction of the gel.

1.3 Metal-based tuning of LMWGs

The example of the industrially important lithium greases, such as the Li^+ salt of 12-hydroxyoctadecanoic acid,[153] shows that it has long been known that metals can be incorporated into gel systems. The use of metal ions as a factor in designing an effective gelator allows for a vast range of diverse properties.[96] These properties include catalytic activity, magnetism, different coordination geometries, labile coordination interactions, redox reactions and the absorption and emission of light offered by the metallic elements to enhance the tunability of the gel, to name but a few. As a result, *metallogels*, LMWG gels that in some way incorporate a metallic element, have recently become highly topical.[51,96] The manipulation of metal sites within a LMWG to tune the gel characteristics or the use of a metal interaction with a LMWG to tune gel behaviour have developed as interesting ways of fine tuning gel properties. The use of porphyrins, with their bound metals, as components of LMWGs has led to tunable gels. These compounds are representative of LWMGs which have metal binding sites, are discrete compounds (i.e. non-polymeric in nature) and can be manipulated at the metal site to tune the gel properties. Work by Shinkai *et al.*

expanded on the idea of achieving control of the stacking mode of porphyrin compounds as a means of self assembly and gelation.[154-158]

The symmetrical 4-substituted compounds **1.17a-e** are versatile gelators, for example **1.17a** gels 14 (for *n* = 3) and 10 (for *n* = 11) out of the 23 solvents tested.[154] Interestingly the Zn(II) complex of urea gelator **1.17c** (**Zn·1.17c**) does not gel benzene, toluene, and *p*-xylene. However, addition of piperazine, which is able to link the metalloporphyrin units together *via* axial coordination to the Zn(II) ion, results in an H-aggregate type structure and the formation of stable gels in those solvents.[154] The stoichiometry of the **Zn·1.17c** piperazine complexes was found to have a great impact on the gelling behavior, with a 2:1 ratio affording gels with a one-dimensional fibrillar network at much lower concentrations, and with a thixotropic character. In the 1:1 complexes the critical gelator concentration is around one order of magnitude higher and leads to a two-dimensional sheet-like morphology of the aggregates. Addition of DABCO only allows partial gelation and results in 2D sheet-like aggregate morphologies, whereas ethylenediamine and *N.N'*-dimethylethylenediamine disrupt gel formation completely.

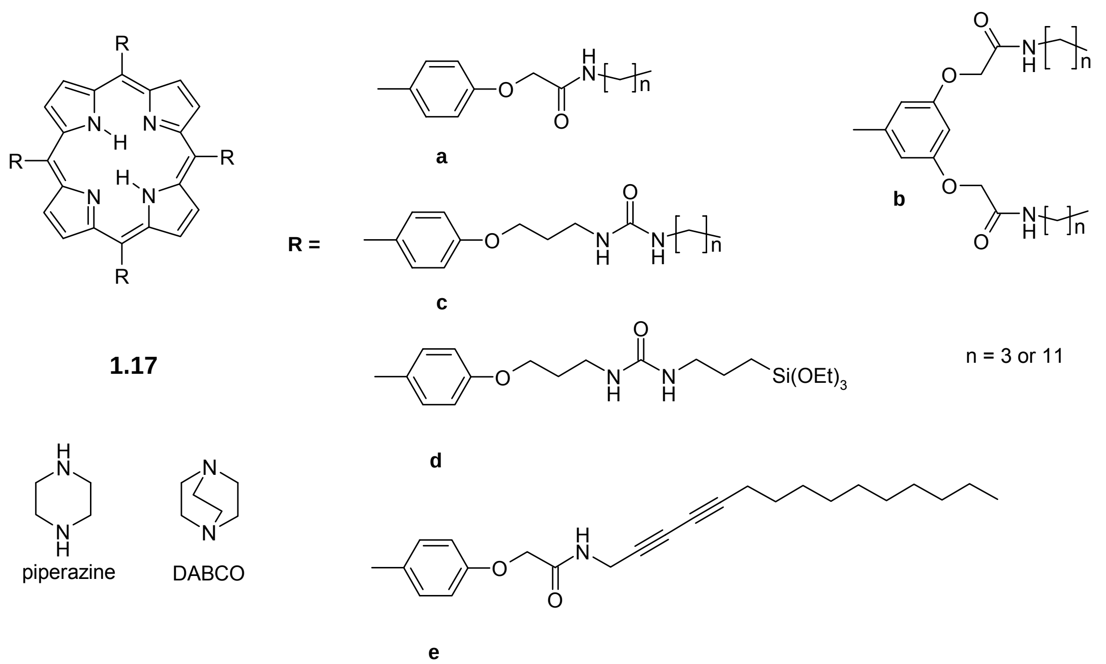

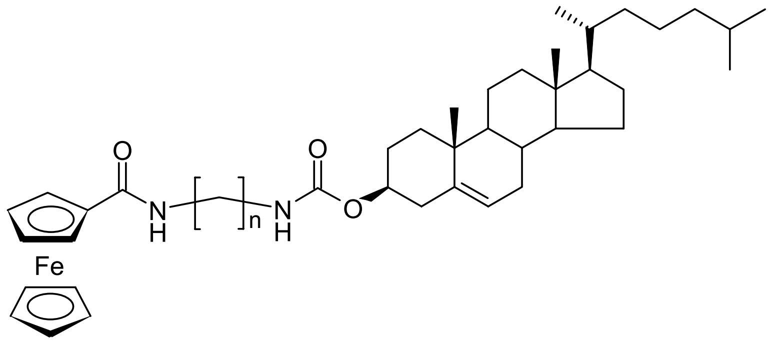

1.18 n = 0,2,3,4

The above example represents tuning of a gel characteristic by binding of a ligand to the metal within the LMWG. The metal oxidation state (redox active organic systems have been shown to undergo similar processes)[159] can be changed using redox reactions thus providing a means to tune a gel. The cholesterol appended ferrocene, compound **1.18** shows gelling behaviour depending on the chain length of the linker.[160,161] The gelator with n = 0 rigidifies cyclohexane and CCl_4 at concentrations as low as 0.09 percent by weight. With n = 2, compound **1.18** also gels but at a higher concentration, whereas for longer lengths of the spacer chain gelling ability is lost altogether. FT-IR and ^1H NMR spectroscopic studies suggest that not only the ferrocene and cholesterol unit, but also the hydrogen bonds between the adjacent spacer groups are essential for the assembly of the gel network. The gel is rigid enough to be molded into films that support themselves in the wet state and is responsive to a wide range of stimuli, both chemical and mechanical (Figure 1.3a). As well as being broken up and formed reversibly upon shaking, sonication and heating, **1.18** shows redox switching. In this case oxidation was carried out using $(NH_4)_2Ce(NO_3)_6$ and the gel network was destroyed. Subsequent reduction by NH_2NH_2 re-established the gel network and the redox process could be confirmed by UV-vis spectroscopy (Figure 1.3b).

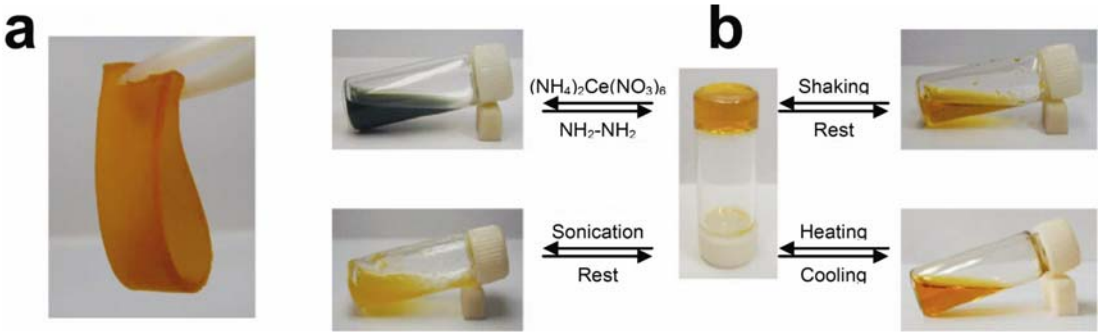

Figure 1.3 a) Gel films of **1.18** in cyclohexane. **b)** reversible gel-sol transitions by a variety of stimuli. Top left represents the redox controlled transition between the gel and sol states. Top right and bottom left is the thixotropic character of the gel. (Reproduced with permission from ref.[160])

Another way to tune a gel's properties is use of a different metal within the LWMG. Platinum complexes have been prepared and studied because of their interesting luminescent behaviour. The group of Shinkai reported the 8-quinolinol based organogelator **Pt·1.19a** and its non-gelating reference **Pt·1.19b** in a study into possible ways of protecting the excited state from O_2-quenching by "insulating" the phosphorescent group in a gel fiber with peripheral alkoxy groups.[30,101,162] Compound **Pt·1.19a** gels 18 organic solvents out of 25 tested, some of these, like *p*-xylene, cyclohexane and other alkanes, gel at critical gelation concentrations as low as 0.01% by weight. UV-vis spectral analysis reveals a red shift in the ligand centered π-π transition and the singlet intraligand charge transfer when going from sol to gel. This was interpreted as a J-aggregation mode of the 8-quinolinol platinum(II) chelate groups, which led to thermo- and solvatochromic behaviour exhibited in the absorption and emission spectra. The sol of **Pt·1.19a** appears yellow and emits at 460 nm when excited at 365 nm, the gel was orange and emits at 490 nm. Interestingly, the luminescence intensity in the gel phase was clearly less susceptible to O_2-quenching, thus demonstrating the insulating effect aspired to in the gel design.[162] Incidentally, compounds **1.19a** and **1.19b** can also be complexed by copper(II) and palladium(II) without compromising any of the gelation capacity of these systems, with gel fiber aggregation being attributed to strong π-π stacking and hydrogen bonding interactions between the amide groups. The different metallogels exhibit field emission performances, with the turn-on field depending on the type of metal in the complex. Although these fields are higher than for other organic field emission substances, the ease of preparation makes these gels interesting for photo- and electrochemical materials.[30]

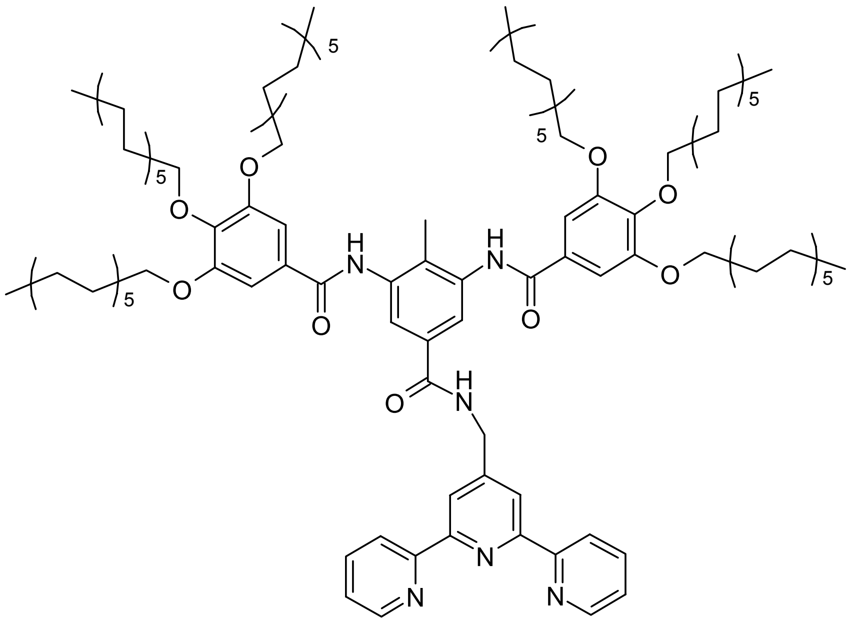

1.20

Addition of metals to a compound that already gels can be used to tune the gel.[163] The terpyridine appended 3,5-diacylamino toluene derivative **1.20** and its binding to iron(II) and ruthenium(II) reported by the group of Ziessel highlights how this technique of tuning using the addition of metals can be used.[164] The free ligand aggregated as a transparent organogel from cyclohexane at 2.6 weight% (Figure 1.4a). The iron complex also gelled the same solvent at a slightly higher critical gel concentration (3% by weight), whereas the ruthenium equivalent does not form a gel under the same conditions (Figure 1.4a–c). Both the iron-gel and the ruthenium complex exhibited strong coloration stemming from metal-to-ligand charge transfer expected in the presence of terpyridine.

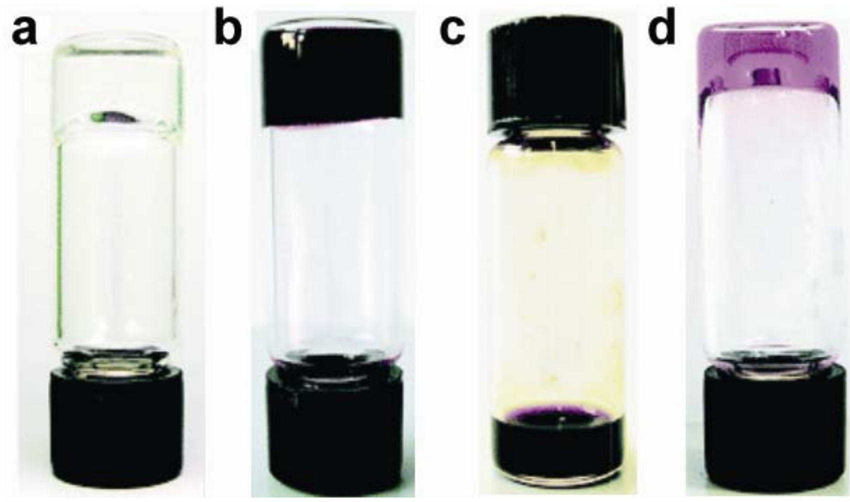

Figure 1.4 a) gelation of cyclohexane by free **1.20**, **b)** of cyclohexane by the [Fe(**1.20**)$_2$](ClO_4)$_2$ complex **c)** precipitation of the analogous ruthenium complex, and d) a gel of **1.20** doped with Fe(II). (Reproduced with permission from ref.[164])

All organogels in this system are thermoreversible and showed a tight hydrogen bonding network, involving the amide groups, by FT-IR spectroscopy. The failure of the ruthenium derivative to form stable gels might be related to the chloride counter ions, which could be responsible for interfering with the hydrogen bonding. A small amount of $Fe(ClO_4)_2$ in solution layered on top of a gel of free **1.20** led to absorption of the metal cation accompanied by the characteristic colour of the complex developing inside the gel. Sprinkling an excess of the metal salt on the gel resulted in complete breakage of the assembly over a few days.

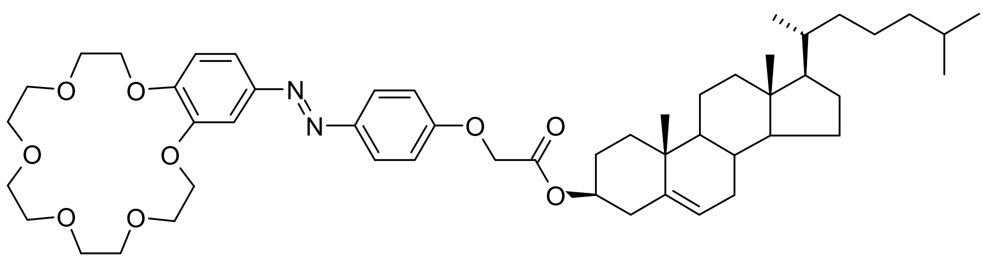

1.21

One very early gelator for which cation binding was reported to have an influence on the rheology is the cholesterol derivative **1.21** containing a benzocrown moiety and an azobenzene linker.[165] Without any metal binding this ligand was found to gel a selection of hydrocarbons and alcohols. The gel-sol transition temperature was found to be influenced by the addition of cations, which can bind to the crown ether fragment, and in the presence of Li^+, Na^+, K^+, Rb^+, and NH_4^+, the T_{gel} rose with increasing cation concentration by up to 20 °C and then gradually decreased. On the other hand, Cs^+ lowered the transition temperature systematically, and inhibited gelation completely at higher concentrations. This behaviour was thought to be caused by a 1:2 metal-crown sandwich complex that may disrupt the order in the helical stacking usually observed in these cholesterol systems.[165] Complexation of a group I metal leading to gel tuning has been reported by Ghoussoub and Lehn who investigated the effect of sequential binding and release of K^+ by a [2.2.2]cryptand in the presence of the bis-guanine monomer **1.22**.[166]

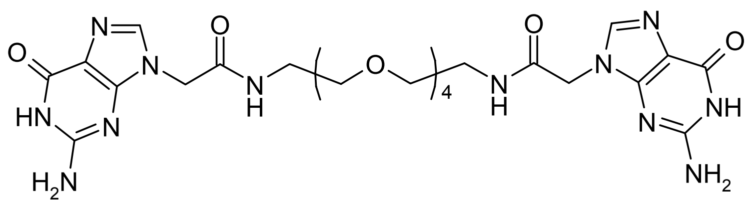

1.22

Compound **1.22** is a gelator by itself in aqueous media, but introduction of the potassium affords an increase in T_{gel} that plateaus at high concentrations. The gelation properties of **1.22** were attributed to the formation of an extended polymeric assembly driven by hydrogen bonding involving four guanine units organized in a macrocycle stabilized by the K^+ cations (a G-quartet motif). Interestingly reversible gel-sol interconversion was achieved by the addition of [2.2.2]cryptand, which resulted in loss of the gel network, as a result of the removal of the potassium from the coordination matrix by the cryptand to form [$K^+ \subset$ 2.2.2]. Subsequent addition of HCl led to protonation of the cryptand and K^+ release with reformation of the gel. Further acidification and neutralization allowed for reversibly tunable gels.

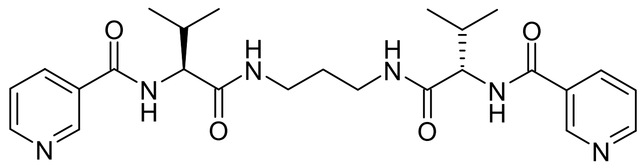

1.23a

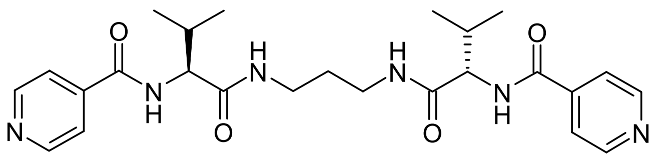

1.23b

The dipyridine ligands **1.23a** and **1.23b** incorporate amide linkages and form pH responsive gels when a solution of them in aqueous HCl is exposed to ammonia vapour.[167] They also gel a range of organic solvents with hydrogen bonding as a driving force in the fibre creation. $Pd(AcO)_2$ in toluene was layered on top and the gels and allowed to diffuse into them overnight. This resulted in orange coloration of the gel phase and TEM suggested that palladium had indeed been incorporated into the fibrils. Interestingly, attempts to complex the ligands to Pd(II) outside the gel phase were unsuccessful and led to decomposition to palladium black. The metal doped gels were found to act as effective catalysts in the aerobic oxidation of benzyl alcohol with about 10 turnovers. The low turnover indicates some deactivation process, although the palladium inside the gel was stable towards decomposition.

There is a remarkable number of LMWG that are salts. Of these compounds there are the important examples that contain metals as the cationic species, e.g. Na^+, Al^{3+} and Ca^{2+}.[8,11,12,38,39,48,50,51,57,59,61,63,70,72,79-81,83,129,168-178] This metal can be used to tune and induce gelation. Good illustrations of the use of LMWG salts include industrially important compounds like the Li^+ salt of 12-hydroxyoctadecanoic acid[153] and the gelators (most of which are hydrogelators) based on fatty acids and their derivatives that have been used in a biological context.[50,56,57] Often amino acid based gelators with carboxylic acid functionalities only gel as the appropriate salt leading to tuning capabilities. This tuning of the gel properties has led to pH reversible gels in many cases, an important means of tuning the gelation properties of certain materials.[7,8,11,12,15,18,69-84] There have been some excellent examples of the use of specific metals and/or their salts to tune gel properties as illustrated by the following cases.

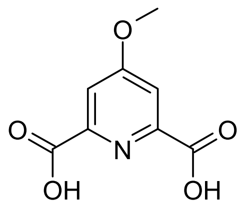

1.24

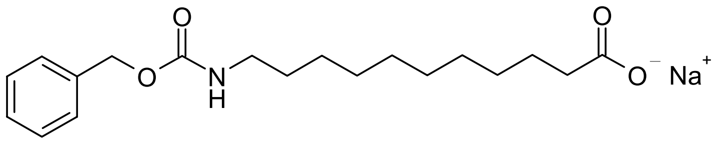

1.25

Variation of the metal ion in a salt LMWG can be used to tune a gel.[70,172] In the case of compound **1.24** a gel is formed when NaOH is added to a DMSO mixture. KOH and RbOH still give gels but these gels are less stable. In the cases of LiOH, NH_4^+ OH^- and tetrabutylammonium hydroxide (TBA^+ OH^-) no gel was formed showing how important the metal ion is for the production of a gel.[70] A similar trend was shown by compound **1.25** which gelled with Na^+ and Rb^+ (once again a weak gel) but not with Li^+ and K^+.[172] The importance of the Na^+ to gelation is cleverly shown by the addition of [2.1.1]cryptand which selectively binds to Na^+ preventing the gelation of a hot solution.

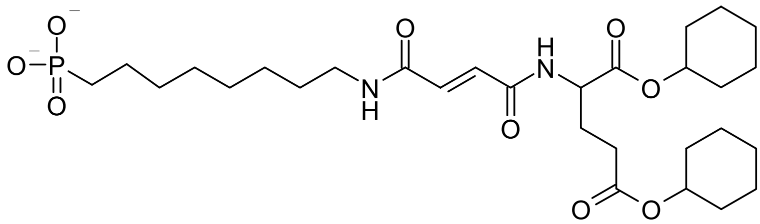

1.26

Ca^{2+} ions are very important physiologically and have therefore been used in testing gelation of some hydrogels.[11,173,174] Hamachi and coworkers synthesized the hydrogelator compound **1.26**.[11] One of the chemical stimuli allowing for formation of the gel state was found to be Ca^{2+} (Figure 1.5). The reversibility of gelation can be accomplished by using EDTA (or OH^{-}) to bind the Ca^{2+} and the authors cleverly use this process to release model drugs from the gel state.

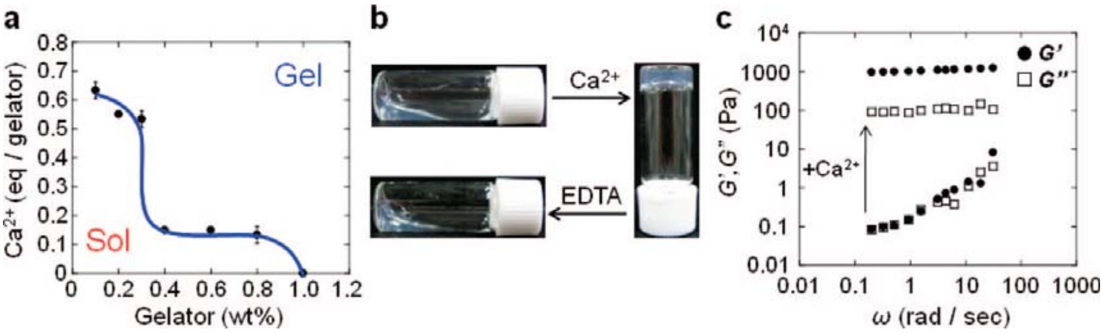

Figure 1.5. Ca^{2+} responsiveness of hydrogelator **1.26**. **a)** Phase diagram of the gel-sol transition, revealing the number of equivalents of Ca^{2+} required to induce gelation at each gelator concentration. **b)** Photographs of the Ca^{2+}-induced sol-to-gel transition ([**1.26**] = 0.30 wt %; [Ca^{2+}]/[**1.26**] = 1.0; [Na_2EDTA]/[Ca^{2+}] = 10). **c)** Corresponding dynamic viscoelastic properties before and after the addition of Ca^{2+}. (Reproduced with permission from ref.[11])

Messersmith *et al.* ingeniously use light and/or temperature induced release of Ca^{2+} from loaded liposomes to induce gelation of a short peptide which consists of 16 amino acids with alternating hydrophobic and hydrophilic residues, compound **1.27**.[173] Compound **1.27** by itself is highly soluble in pure water but in the presence of millimolar concentrations of NaCl, KCl or $CaCl_2$ a gel is formed. The authors show how they use trapped Ca^{2+} within liposomes that can be broken down by light or heat to induce gelation upon simulation of a solution of **1.27** and these liposomes (Figure 1.6).

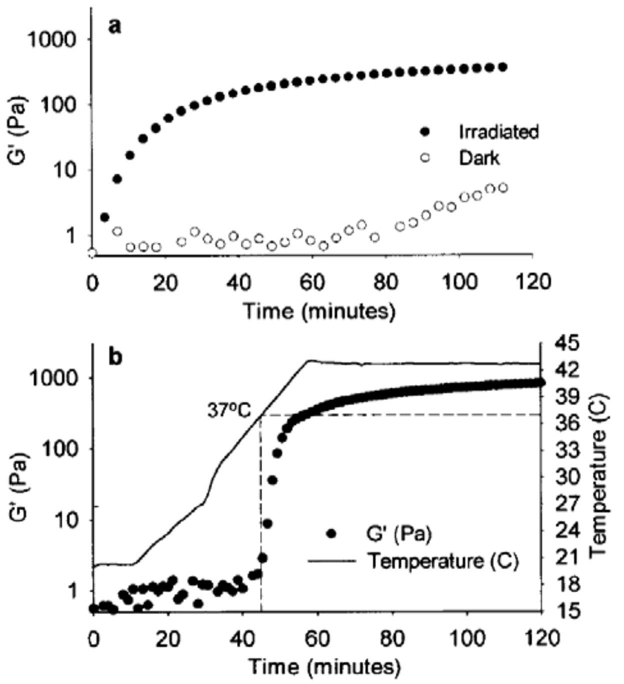

Figure 1.6. Rheological detection of **a)** light- and **b)** temperature-triggered gelation of **1.27**/liposome precursor fluid (12 vol % $CaCl_2$-loaded liposomes in a sucrose solution of **1.27** (30 mg/mL)). (Reproduced with permission from ref.[173])

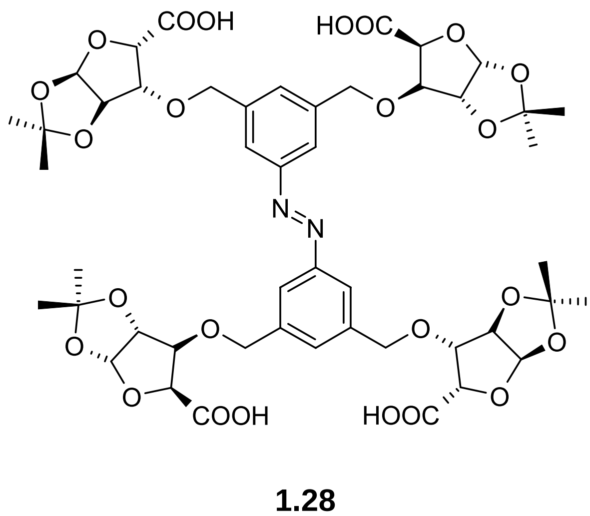

1.28

The type of metal cation within a LMWG can also have an effect on the morphology and kinetics of gelation. With compound **1.28** the cationic species has a drastic influence on the gel formed.[79] The presence of the salts NaCl, KCl, $CaCl_2$ or $MgCl_2$ at 1 mM concentrations in water causes **1.28** to gel at a different rate and morphology. NaCl slows the gelation period from instantaneously in pure water to approximately seven mins and the morphology changes from spongy globules to aggregated spheres (Figure 1.7). KCl slows the gel formation down a little more and a wrinkled cloth morphology results. $MgCl_2$ and $CaCl_2$ slow the gelation down to 15 mins and a fused globular morphology results. The use of $BaCl_2$ results in precipitation and no gelation. These results clearly show how a gel can be tuned by the metal species.

These many and varied ways of tuning the properties of LMWGs show how important the tuning of LMWGs is for the development of practical uses.

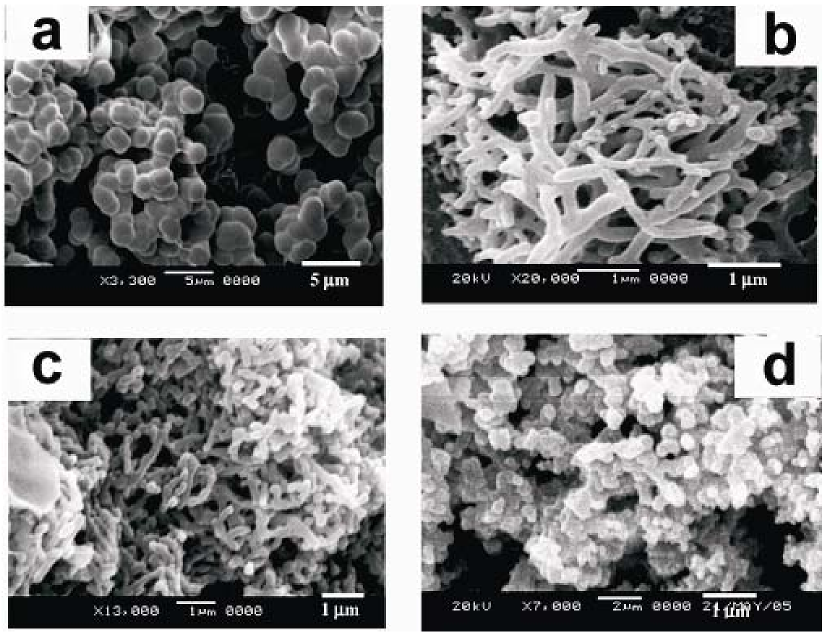

Figure 1.7. SEM images showing morpholgy of xerogels of **1.28** in **a)** water – spongy globules (gel forms instantaneously), **b)** 1 mM $CaCl_2$ – fused globules (gel takes 15 mins to form), **c)** 1 mM $MgCl_2$ – fused globules (gel takes 15 mins to form), and **d)** 1 mM NaCl – aggregated spheres (gel takes 7 mins to form). (Reproduced with permission from ref.[79])

1.4 Anion tuning of LMWGs

The principle of using anions in the tuning of gel properties has developed into a recognizable subfield of LWMG chemistry.[52,97] The field of anion binding by supramolecular hosts is well established and reasonably well understood.[179-183] Several host designs have been developed, with the majority using hydrogen bonding functionalities to bind anions. Owing to the commonality of hydrogen bonding between LMWGs and anion-binding supramolecular hosts, it is unsurprising that some researchers have begun to investigate the combination of these properties. An excellent example is of the use of compound **1.29** as a LWMG that is affected by the addition and removal of anions.[184]

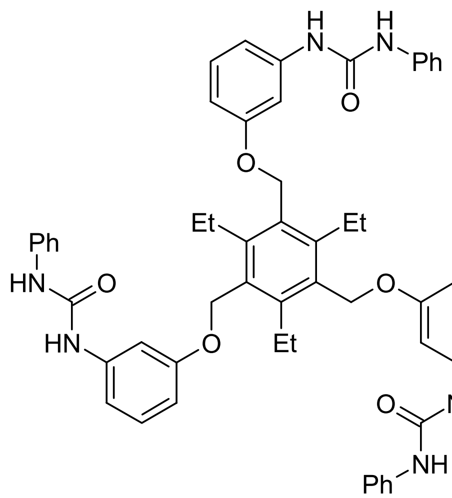

1.29

Compound **1.29** contains the preorganizing triethyl benzene core[180,185,186] and multiple urea-derived anion binding moieties.[184] Compound **1.29** is a LWMG, and forms gels in polar solvents such as acetone (CGC 1.5 wt %), methanol (CGC 2.0 wt %) and tetrahydrofuran (CGC 5 wt %), on brief sonication of the solution. The acetone gels of **1.29** respond to chemical stimuli in the form of anions, resulting in homogeneous solutions (Figure 1.8). The anion is added as a tetrabutylammonium salt, the cation being chosen for its inert properties. There is a linear correlation between the binding constants for the formation of the 3:1 complex (log β_{13}) - determined using standard solution nuclear magnetic resonance (NMR) spectroscopic titration experiments - and the minimum amount of anion required for the complete gel-sol transition (indeed the very weakly bound BF_4^- does not influence the gel properties of **1.29** at all). The entire process is reversible and repeatable, and can also be used as a method of detecting or identifying fluoride. Reversibility of the dissolution of the gel is demonstrated by addition of the Lewis acid $BF_3{\cdot}OEt_2$ to a solution of **1.29** containing tetrabutylammonium fluoride (TBA^+ F^-). This reverses the effect of the fluoride anion, and a gel reforms upon sonication, whereas the same is not observed for the other anions. However, $ZnBr_2$ acts as a non-specific chemical stimulus for re-gelation by binding to the added anions much more strongly than **1.29** does (Figure 1.8).

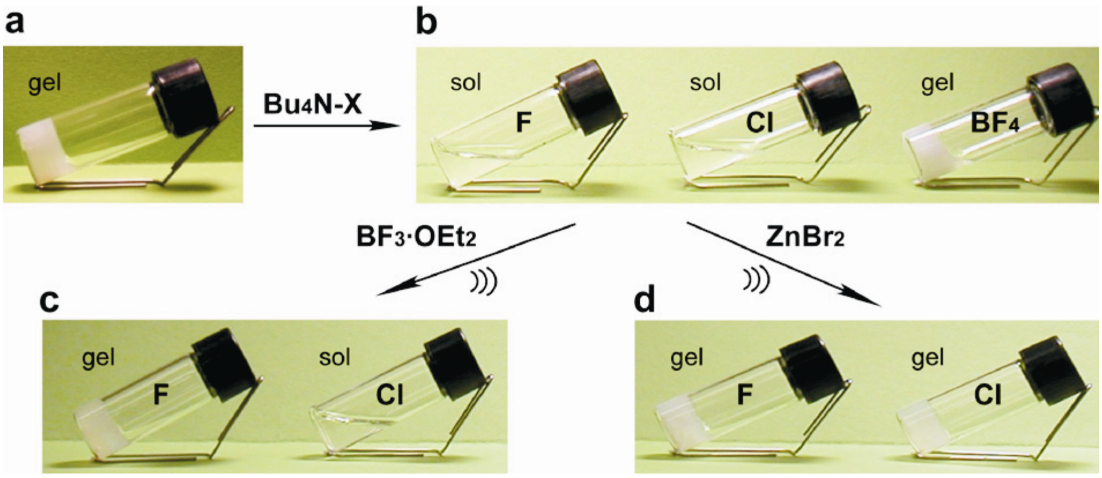

Figure 1.8. The acetone gel of **1.29**, showing the transitions between the gel state and liquid states upon addition of chemical stimuli (X = F^-, Cl^- or BF_4^-). **a)** Acetone gel of **1.29** (2.0 wt %). **b)** Acetone gel of **1.29** (2.0 wt %) containing (from left) 1.1 equiv of TBA^+ F^-, 1.7 equiv of TBA^+ Cl^-, and 10 equiv of TBA^+ BF_4^-. **c)** BF3·OEt_2 (1.0 equiv for TBA^+ salt) mixture after sonication of **1.29** and TBA^+ F^- (left) or TBA^+ Cl^- (right) in acetone. **d)** $ZnBr_2$ (1.0 equiv for TBA^+ salt) mixture after sonication of **1.29** and TBA^+ F^- (left) or TBA^+ Cl^- (right) in acetone. (Reproduced with permission from ref.[184])

Another example of the influence of anion binding on gel formation is exemplified by the bis(urea) functionalized binaphthalene derived compound, **1.30**.[187]

This study, primarily based around the circular dichroism (CD) of **1.30** shows that the gel in cyclohexane (CGC = 6 mg/ml) can be destroyed by the addition of $TBA^+ F^-$.

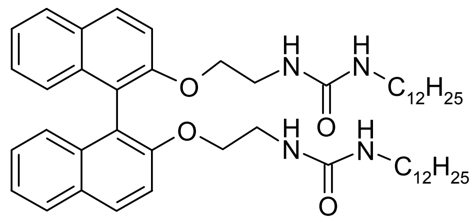

1.30

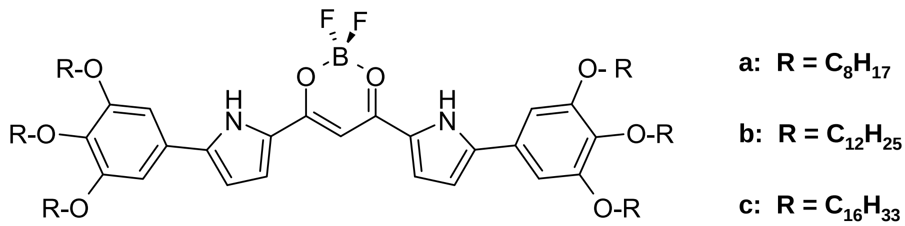

1.31

Maeda *et al.* have produced some notable results working with the anion binding and gel formation of C_3-bridged oligopyrroles.[188,189] A long alkyl substituted derivative of the C_3-bridged oligopyrroles, **1.31**, affords a transparent emissive gel in hydrocarbon solvents such as octane (CGC = 10 mg/ml). The addition of anions causes the gel to break down. This is exemplified by the breakdown of a **1.31c** gel in octane upon the addition of ten equivalents of solid $TBA^+ Cl^-$ to the upper surface of the gel resulting in the gel becoming a solution. Additionally, both the UV-Vis and the fluorescence spectra are notably changed (Figure 1.9). The addition of different solid TBA^+ salts show how the rate of breakdown is dependent on the anion (time required for F^- is minutes, Cl^- is 2 hours, CH_3COO^- is 3 hours and Ph_4B^- does not perturb the gel).

The phenomenon of gelation can be described as a form of arrested or partial crystallisation.[39] In this context, the hydrogels of **1.32** show an interesting transformation from gel to crystalline material when exposed to NaCl.[190] As Cl^- binds to **1.32** (K_{11} = 1114 M^{-1} by NMR spectroscopic titration), chloride complexation inhibits fibre growth along the fibre axis (and long axis of the needle shaped crystal) allowing growth in the other two dimensions.

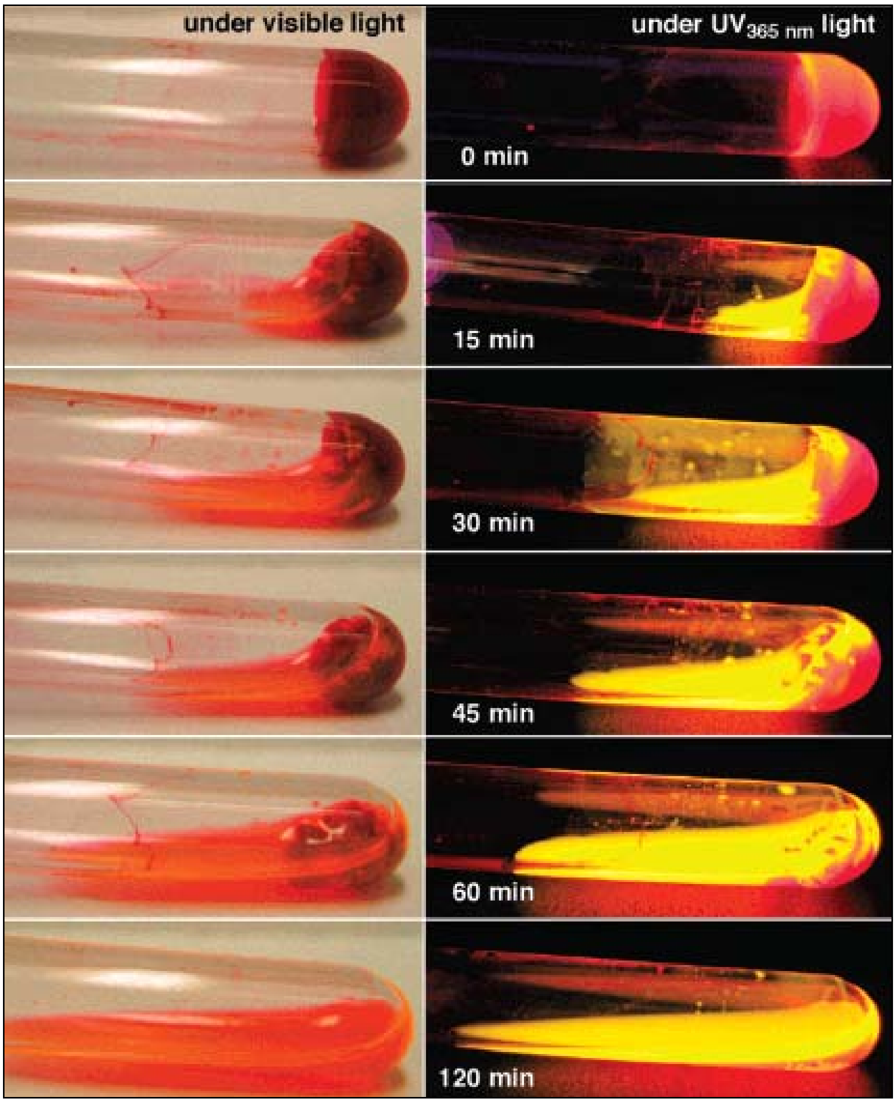

Figure 1.9. Transition of the supramolecular gel of **1.31c** in octane (10 mg/ml) to a solution upon addition of 10 equivalents of TBA^+ Cl^- added as a solid to the top surface of the gel. The highly emissive solution generated by the decomposition of the gel has fluorescence emission at 524 and 574 nm (λ_{ex} = 470 nm) indicating that the bound Cl^- by **1.31c** is soluble in the octane explaining the breakdown of the gel. (Reproduced with permission from ref.[189])

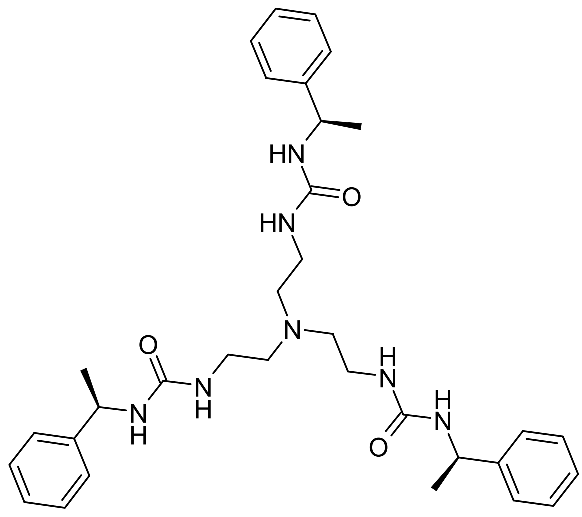

1.32

The strong binding of F^- by anion binding hosts has its origin in the high basicity of the anion, and this is manifested when sometimes the hydrogen bonding moiety in some hosts is deprotonated. Owing to the strong binding of F^- by hydrogen-bonding hosts, there have now been a number of studies on how F^- affects gel formation by LMWGs, and the use of F^- as a chemical switch. A good example is the behaviour of the family of compounds **1.33**.[191]

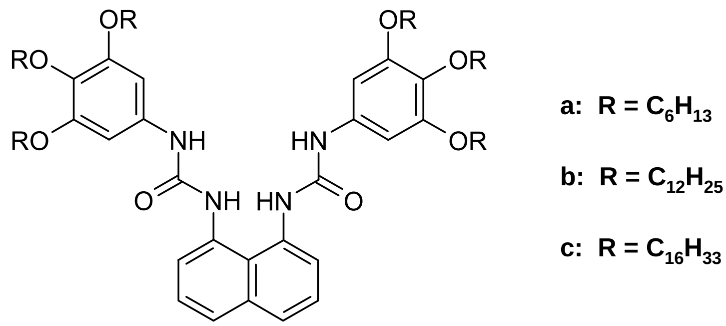

1.33

These compounds gel a variety of solvents with the R = $C_{12}H_{25}$ compound (**1.33b**) showing the greatest versatility. Addition of four equivalents of TBA^+ F^- to the 1,4-dioxane **1.33b** gel resulted in a transition from a gel to a solution state. This process is reversed by the addition of trifluoroacetic acid (TFA). The details of these processes were probed using fluorescence spectroscopy. The measured photoluminescence intensity of **1.33b** in the gel state (λ = 433 nm) is greatly increased in comparison to that in solution (λ = 359, 376 and 396 nm) and this can be attributed to the phenomenon of aggregation-induced enhanced emission. The **1.33b**·F^- aggregate in solution shows an emission band centred at 450 nm. With the addition of increasing amounts of TBA^+ F^- to a **1.33b** gel, there is a subsequent decrease in the band at 433 nm observed for the gel, and an increase in the band observed for the **1.33b**·F^- complex. Interestingly, in the solution state, **1.33b** that has been exposed first to TBA^+ F^- and then TFA has a similar emission spectrum to that of the starting **1.33b**. Surprisingly, however, addition of TBA^+ F^- followed by TFA on the reformed gel results in a blue-shift of the emission band by 70 nm. This change in the gel character (compared with the gel before addition of fluoride and TFA) is also manifested in the morphology, as shown by the scanning electron micrograph (SEM) images of the dried gels. This result highlights the continued difficulty of assigning gel structure. Are the contents of these gels identical (pure **1.33b**), or is the new gel made of a **1.33b·F^-·H^+** aggregate (as Yang *et al.* suggest)? Indeed, is the new gel some type of morphological "polymorph"?[50,108,192]

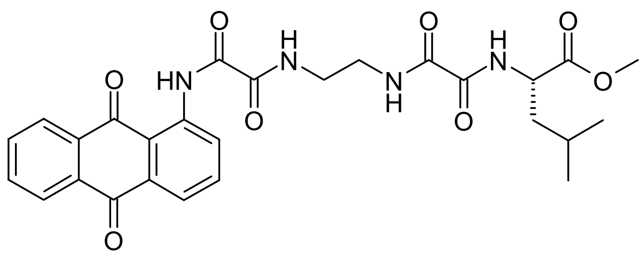

1.34

An example where the gel is influenced by the interaction between the gelator in the gel state and F^- was reported by Žinić, Mandolini, Cametti *et al.*[193] Working with oxalamide-derived anthraquinone compounds they showed that compound **1.34** forms gels in a variety of solvents and that the properties of these gels can be tuned using anions. In *p*-xylene gels the addition of TBA^+ F^- (10 equivalents) causes the gel to break down and form a reddish solution. The change in colour and prevention of gelation is caused by the basic F^- interacting with (possibly deprotonating) the NH group closest to the anthraquinone moiety in **1.34** (Figure 1.10). This effect can be prevented when the solvent used in the gel is changed. An ethanol gel does not change to a solution upon addition of TBA^+ F^- (10 equivalents) as the fluoride is better solvated by the more polar protic solvent and therefore the anion cannot compete with the NH interactions that allow gelation to occur. Addition of a concentrated TBA^+ F^- *p*-xylene solution on top of the gel results in a gradual breakdown of the gel over four hours (Figure 1.10). The fluoride ion is the only anion that behaves this way with gels of **1.34**. This has led the authors to speculate that these fluoride responsive gels may provide the basis for a non-fluid and therefore more robust gel-based system for the naked-eye detection of fluoride.

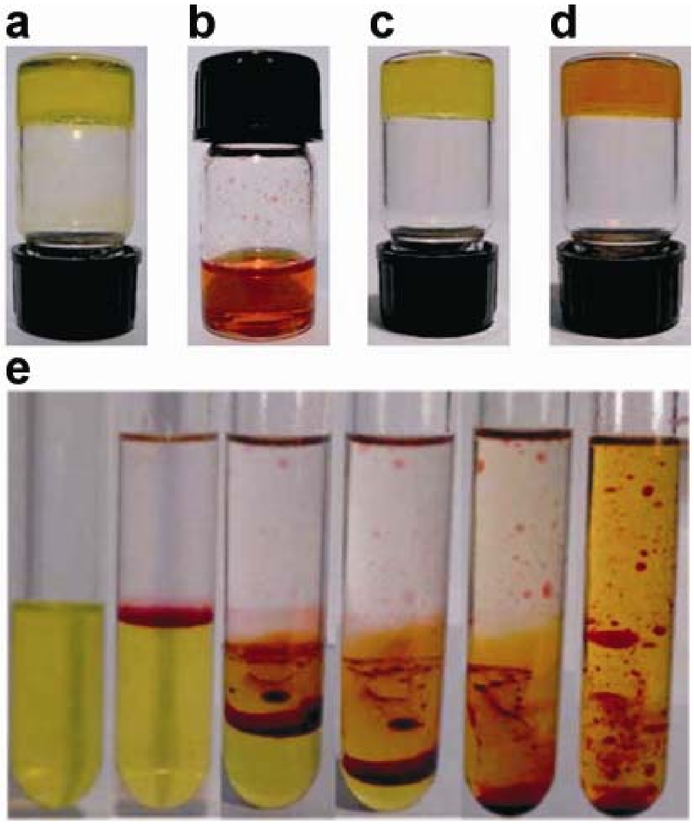

Figure 1.10. a) The **1.34** p-xylene gel; **b)** addition of 10 equivalents of TBAF to the hot p-xylene solution of **1.34** followed by cooling to RT; **c) 1.34** EtOH gel; **d)** reddish **1.34** EtOH gel after addition of 10 equivalents of F^-. **e)** Diffusion of F^- from a concentrated p-xylene solution (50 equiv.) through the **1.34** p-xylene gel. From left to right: **1.34** p-xylene gel; immediately after addition of TBA^+ F^- solution; after 2, 3 and 4 h; and overnight standing. (Reproduced with permission from ref.[193])

Due to the selective binding of F^- by **1.35**, a benzoxazole-based organogelator, Lee and coworkers show that they could also visually detect F^- using a gel-based system.[194] Deprotonation by F^- causes a colour change from colourless to green in **1.35**, so when 100 equivalents of TBA salts are added to the gel, a similar effect is seen. F^- causes breakdown of the gel and generation of the colour. Other anions cause break down of gel but do not generate the same colour change except in the case of CH_3COO^- which only gives a very pale green colour.

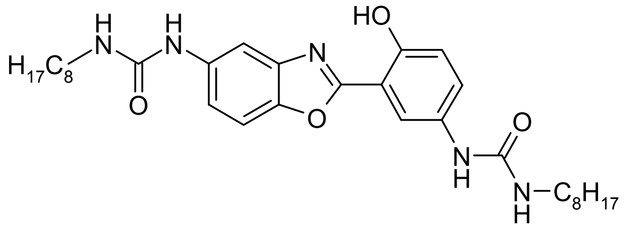

1.35

The binding of F^- (or any anion) to the hydrogen bonding moieties of a LMWG can be used to determine the importance of those functional groups in the aggregation processes of gel formation. This is most often expressed in the form of a gel-to-sol transition. An important aspect is that it is not always necessary to use stoichiometric or excess amounts of anion to disrupt the formation of the gel.[195-197] Gel-to-sol transitions are not the only resultant affects caused by the addition of anions to a gel; anions can also be used to change the strength of the gel - cases are known of both anion-induced weakening and strengthening of gels. In addition to weakening gels and causing gel-to-sol transitions, anions can be used to enhance gelation.[12,90,93,198] Addition of halide and nitrate salts to compound **1.36** results in the formation of hydrogels, whereas **1.36** by itself does not gel.[198]

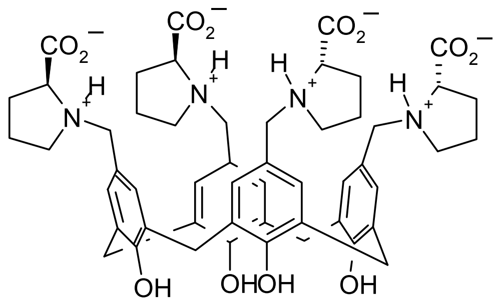

1.36

The anion-enhancement of gelation of **1.36** is suggested to be based around the Hofmeister series (specific ion effect). A typical Hofmeister series is:[199-201]

$$I^- < ClO_4^- < NO_3^- < Br^- < Cl^- < F^- < SO_4^{2-}$$

The more hydrated anions (to the right) are referred to as 'salting-out' or kosmotropic ions, and the less hydrated anions (to the left) are known as 'salting-in' or chaotropic ions. The salts containing the more chaotropic anions cause gelation of **1.36**, and salts containing kosmotropic anions cause solvation. In addition to this factor is the solubility-based trend in crystallization tendency. As a result, the most stable gels are formed when salts of NO_3^- and Br^- are added. Interestingly, it seems that the salts remain in the liquid phase and are not incorporated in the gel. The salts cause no noticeable perturbation of the ^{1}H NMR spectra of **1.36** (which might indicate solution-phase binding). Even so, the anions may be helping to preorganize **1.36**, or the Hofmeister anion effects may be the only effect.[190] Further studies will be needed to fully understand the nature of the Hofmeister anion effects as they are not greatly understood in most systems.[190,202,203]

1.5 Anion tuning of metal-based LMWGs

Studies by Lee *et al.* on gel formation by ligand **1.37** in the presence of silver(I) salts shows how the anion has an important role in templating the assembly that leads to gelation.[202-204] The silver coordinates to the pyridyl functionality in a linear fashion resulting in either a cisoid (meta groups on pyridyl groups are *cis* to each other in relation to the N□Ag□N bond) or transoid (meta groups on pyridyl groups are *trans* to each other in relation to the N□Ag□N bond) arrangement depending on the identity of the anion present in solution. Thus NO_3^-, BF_4^- and $CF_3SO_3^-$ result in the cisoid form and consequently a gel is formed when the weight percentage of **1.37** is greater than 2.5 % (Figure 1.11).[202] These anions give the cisoid isomer as they are small enough to maximise the electrostatic interactions between the cationic chains.

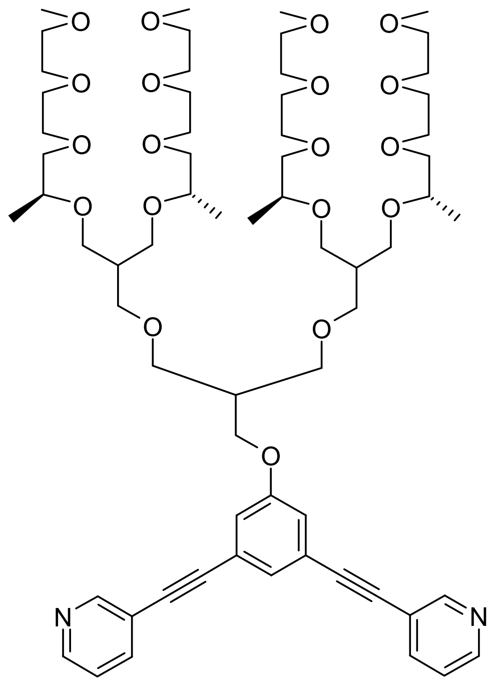

1.37

Addition of a larger anion such as $C_2F_5CO_2^-$ and $C_3F_7CO_2^-$ to the gel in the form of their TBA salts results in the disintegration of the gel. It has been shown using techniques such as circular dichroism and fluorescence spectroscopy, small-angle and wide-angle X-ray diffraction, electron microscopy (SEM and tunnelling electron microscopy (TEM)) and NMR spectroscopy how the gel-sol transformation arises from the change from the cisoid to the transoid arrangement, which in turn is caused by the anion interaction with the cationic chains.

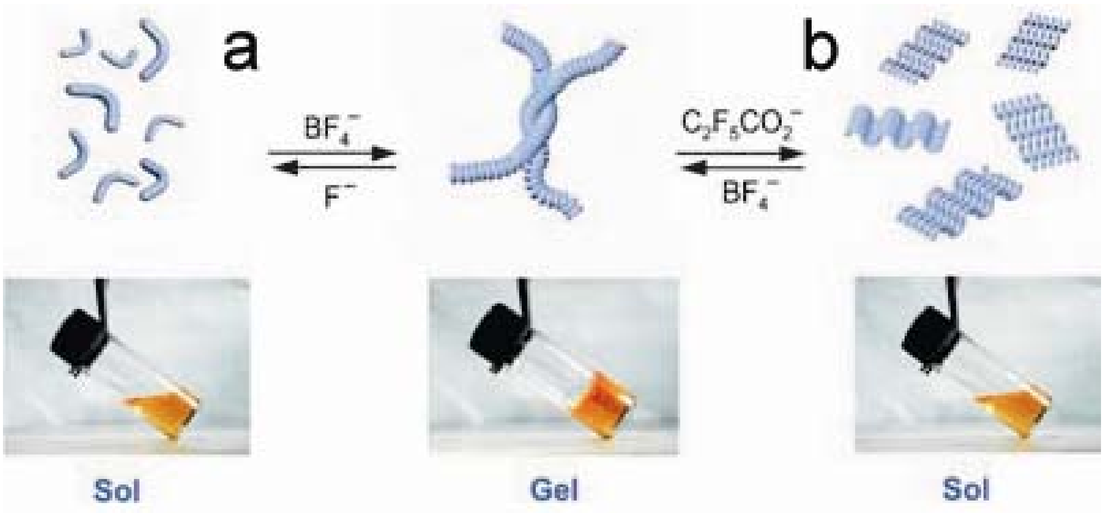

Figure 1.11. Schematic representation of the reversible polymerisation and the reversible conversion between folded and unfolded conformations of a coordination chain upon counteranion exchange of **1.37** resulting in gelation to solution, and vice versa, state changes. **a)** Depolymerisation of the coordination polymers due to strong binding of the F^- to the Ag^+ metal centres resulting in the breakdown of the gel. Repolymerisation and reformation of the gel by the addition of 1.2 equivalents of TBA^+ BF_4^-. **b)** Transition from gel to sol caused by the conformational change in **1.37** induced by the addition of $C_2F_5CO_2^-$. The reformation of gel is accomplished by addition of TBA^+ BF_4^-. (Reproduced with permission from ref.[202])

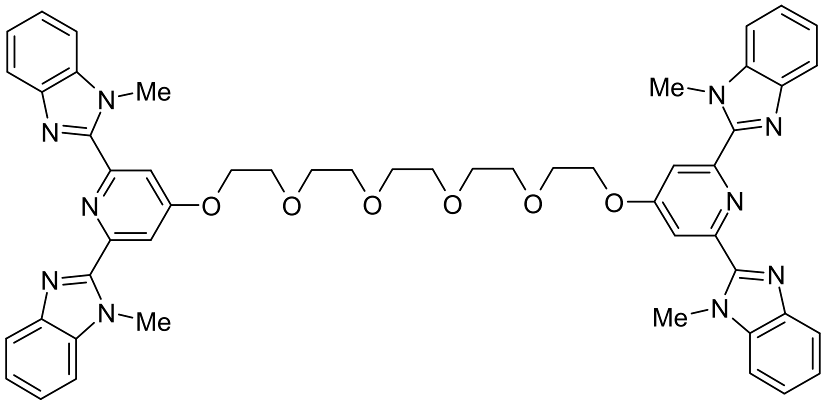

1.38

In colloidal gel chemistry the salting effect, and specifically the influence of the anion, has been studied for as long as the gels have been known – Hofmeister was studying colloidal gels when he postulated his anion series.[199-201] Recently Jamieson, Rowan and co-workers showed that a metallo-organic LMWG based around ligand **1.38** (which contains 2,6-bis(1'-methylbenzimidazolyl)-4-oxypyridine metal binding groups) and the appropriate transition metal salt forms a colloidal gel that can be influenced by the addition of anions.[104,205-209] Transition metal salt examples are $Zn(ClO_4)_2$ or $Co(ClO_4)_2$; additionally a small percentage of lanthanide ions can also be used to enhance gel formation (Figure 1.12).[207]

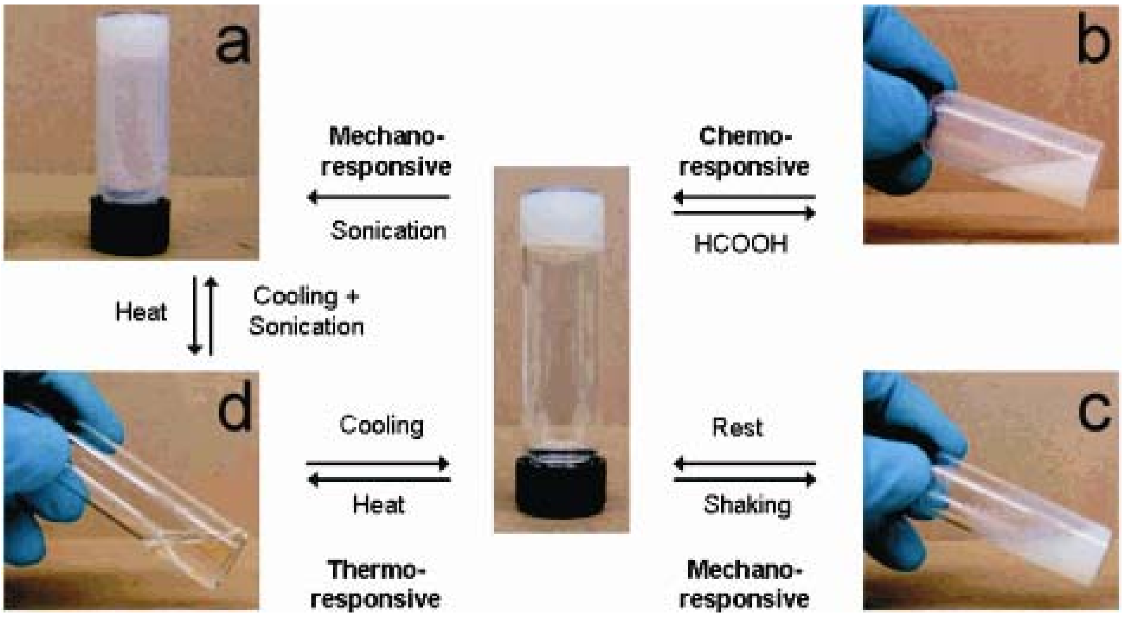

Figure 1.12. Gels of **1.38** (11 wt % in acetonitrile) exhibit multi-responsive behaviour including the chemo-response to formic acid and TBA^+ ClO_4^-. **a)** Sonication induced toughening of the gel of **1.38**. **b)** Chemo-responsive break down of the gel by the addition of formic acid or TBA^+ ClO_4^- caused by the osmotic deswelling of the gel or salting out of the organic phase. **c)** Thixotropic (recovery of gel after gel is sheared to breaking point, *i.e.* mechano-responsive) character of the gel. **d)** Thermotropic (temperature sensitive) character of the gel. (Reproduced with permission from ref.[207])

This result illustrates the difficulties that can be encountered when studying multi-component supramolecular systems. The study reveals that the addition of formic acid causes degradation of the gel. Additionally, TBA^+ ClO_4^- also degrades the gel but at a much lower concentration than formic acid. Ligand exchange is not involved in the degradation however, as demonstrated by the fact that a 20 and 60 times equivalent excess to transition metal is required to fully break down the gel for TBA^+ ClO_4^- and formic acid, respectively. The loss of gel character is inferred from the separation of the liquid phase from the gel and from the lack of ligand exchange upon addition of the salt to be due to the osmotic deswelling of the gel or salting out of the organic phase.[199-201] This work highlights the care that must be taken when establishing the causes of gel anion destabilisation in LMWG as the cause may be supramolecular in nature or physical, as shown above.

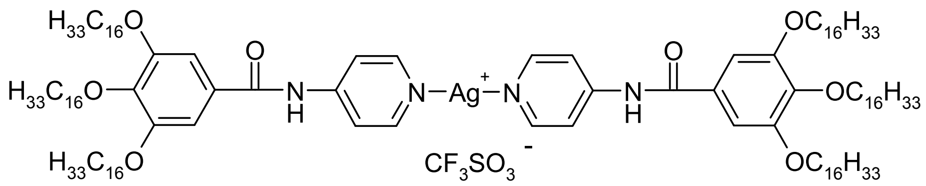

1.39

Coordination-complex-based LMWG metallogelators are an interesting group of compounds and of these, the labile silver(I) based compounds lend themselves to easy manipulation by anions.[197,202,203,210,211] A simple complex (**1.39**) with a ligand that contains the coordinating pyridyl group, the hydrogen bonding amide group and lipophilic groups for van der Waals interactions forms gels with $AgCF_3SO_3$. Silver readily reacts with halide anions to form insoluble silver halide and this process has been used to cause a gel-sol transition when potassium iodide, chloride and bromide are added to the silver(I) metallogels of **1.39** in the correct stoichiometry. Hydroxide anions can be used in a similar manner resulting in the formation of Ag_2O precipitate and the disruption of the gel. Removal of the precipitates by filtration and addition of $AgCF_3SO_3$ results in the return of the gel state showing that the response is chemo-reversible.

The ability of chloride anions to remove silver has been put into good use in the gels formed by the trinuclear Au(I) pyrozalate complex **1.40**.[212] Compound **1.40** forms a gel in hexane (CGC 5 wt%) where the hydrophobic side chains interact strongly promoting metallophilic interactions of the Au···Au type. The gel is red emissive (λ_{em} = 650 nm, λ_{ex} = 254 nm) but upon addition of 0.01 equivalents of silver(I) ions (where the silver intercalates between the stacking planes of **1.40** utilising metal-metal interactions) the gel becomes blue emissive (λ_{em} = 458 nm, λ_{ex} = 370 nm). The reversibility of this tuning of the luminescence of the gel is achieved by using chloride anions to remove the silver (Figure 1.13). This study represents the use of anions to tune the dopant characteristics that in turn cause changes in the gel features.

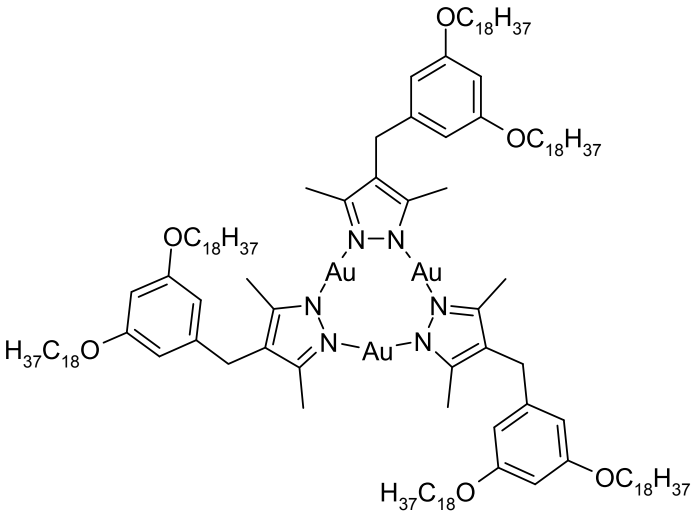

1.40

There are a large number of salts of organic anions and cations with inorganic counter ions as well as purely organic salts that have been discovered to gel a wide variety of solvents.[38,39,42,46,48-50,213-216] The characteristics of the anion intuitively play a crucial part in the gelation ability of these compounds. There have, however, been surprisingly few studies performed that directly look at the influence of the anion in LMWG salts due often to the fact that a simple change in the anion results in loss of gel character all together.[38,39,42,46,48-50,213-216] Studies by Dastidar and co-workers have gone against this trend and have studied examples where the anion is varied and therefore varies the characteristics of the gel.[59,143-145,215-217] This work looked at the importance of one-dimensional hydrogen bonding networks as a means to predict and possibly design gelation using knowledge gained through the use of crystal engineering of supramolecular synthons. A study on a family of organic salts with the dibenzylammonium cation revealed that the variation in the anion in the form of both benzoate and cinnamate derivatives allowed for the tuning of the gelation process.

[215,216] Of the 27 anions tested it was found that 19 of them showed some form of gelation and that this tendency correlates well with the formation of one-dimensional networks in the crystal structures of the salts. This insight allows the tuning of the gel characteristics, the gel strength or stability (as measured by changes in T_{gel}), and minimum gel concentration required for full gelation of a specific solvent volume, solvent type and gel fiber morphology.

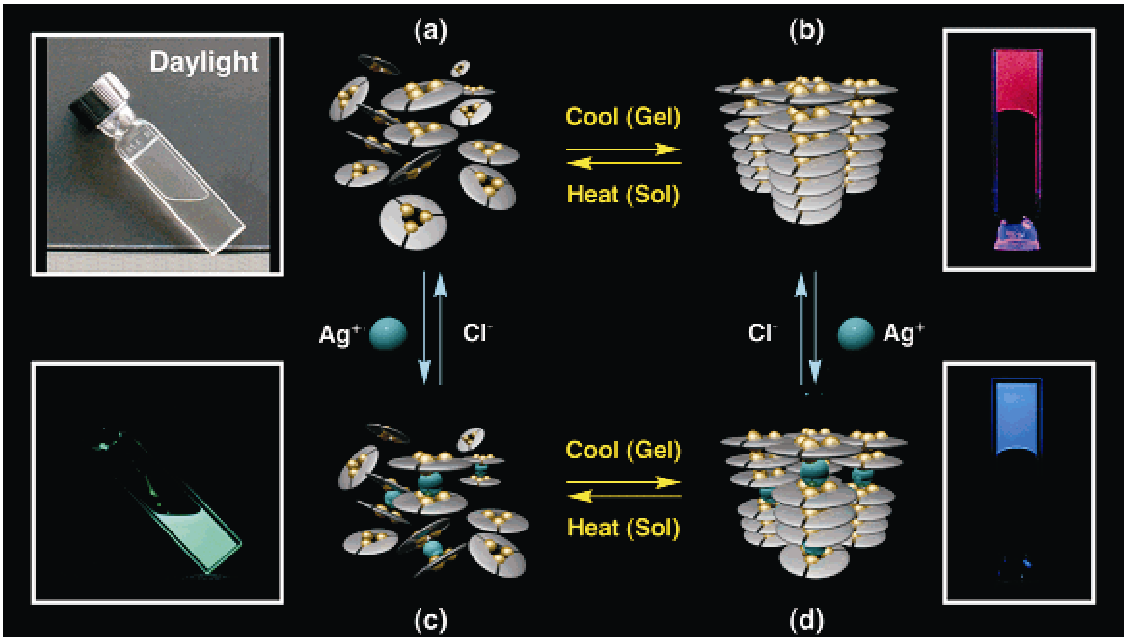

Figure 1.13. Diagram showing the luminescence profiles of Au(I) pyrazolate complex **1.40** in hexane as solutions and gels, and the schematics of the self-assembling structures. Anion tuning by the use of Cl^- between the red and blue gel states occurs due to the removal of the intercalated Ag^+ **a)** Sol of complex **1.40** that shows barely any visible luminescence (λ_{ext} = 254 nm). **b)** Gel of **1.40** that contain stacks of complexes resulting in bright red luminescence (λ_{ext} = 254 nm). **c)** Sol containing AgOTf (0.01 equivalents) that shows green luminescence (λ_{ext} = 365 nm) due to intercalation of silver between sets of **1.40**. **d)** Gel containing AgOTf (0.01 equivalents) showing blue luminescence (λ_{ext} = 365 nm) due to intercalation of Ag^+ into the stacks of **1.40**. (Reproduced with permission from ref.[212])

1.6 Aims of this work

The aim of this work is to design and synthesise LMWGs that are capable of forming anion-tunable gels.[52,97] It was also hoped that the combination of gelation and anion-binding properties of a compound could lead to the ability to tune the gel characteristics for specific 'smart' applications such as drug delivery.[38] Chiral bisurea compounds (Figure 1.14) where chosen for this task as the anion binding capabilities of the urea group is well understood,[218,219] and the gel properties of compounds that contain urea groups have also been extensively studied.[42,75,220-226] Therefore it is easy to speculate that the two can be used together within the same system.[52,97,190] The choice of the chiral group comes through reasoning that many gelators do contain chiral functionality and that chirality is a desirable property of self-assembled systems due to common use in biology, nanoassembly and functional materials.[41,53,60] In addition the presence of a single enantiomer may reduce crystallinity by preventing crystallisation in centrosymmetric space groups. The synthesised compounds are to be tested for gelation ability and their gelation properties investigated. Addition of anions will be used as a means to test if the gelation ability of the compounds is affected. If the gelation properties are changed by the addition of anions, the mechanism behind this change will be probed using such techniques as rheology and standard protocols for assessing solution equilibria, particularly NMR spectroscopic titration. Finally two potential uses of LMWGs, crystal growth control[50,75] and drug release control,[1-12] will be tested with anion tuning playing an important role in the application of these properties.

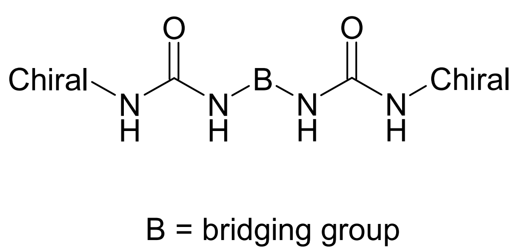

Figure 1.14. Chiral bisurea compounds for the study of anion tunable LMWGs.

The second set of aims revolves around the pyrazole group and the chemistry of this functionality.[227] Many salts (both organic and inorganic) are capable of forming gels. As the pyrazole group is capable of metal and anion coordination, as well as having the capability of being protonated, it is a useful binding group to design into a possible anion and cation tunable LMWG. Indeed, as shown by the example of Aida and co workers, pyrazoles can been incorporated into LWMGs.[212] Functionalising the pyrazole group with a urea group provides a means to bind anions in a more controlled manner (Figure 1.15). As there have been no investigations into the coordination chemistry of urea functionalised pyrazoles, simple studies into the coordination chemistry of metals and anions have also been carried out in order to increase the understanding of these compounds in the hope of designing, and, serendipitously, finding a LMWG. Using this LMWG, which contains both the pyrazole and urea groups, should result in a gel that can be tuned by varying the identity of the anion.

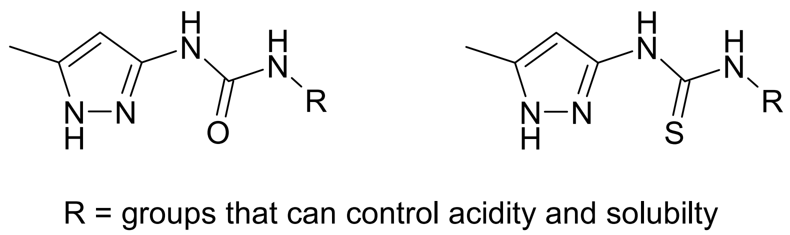

Figure 1.15. Urea and thiourea functionalised pyrazoles for the formation of metal and salt LMWGs that can be tuned using anions.

References

(1) Matsumoto, S.; Yamaguchi, S.; Ueno, S.; Komatsu, H.; Ikeda, M.; Ishizuka, K.; Iko, Y.; Tabata, K. V.; Aoki, H.; Ito, S.; Noji, H.; Hamachi, I. *Chem. Eur. J.* **2008**, *14*, 3977-3986.

(2) Liang, G. L.; Yang, Z. M.; Zhang, R. J.; Li, L. H.; Fan, Y. J.; Kuang, Y.; Gao, Y.; Wang, T.; Lu, W. W.; Xu, B. *Langmuir* **2009**, *25*, 8419-8422.

(3) Adhikari, B.; Palui, G.; Banerjee, A. *Soft Matter* **2009**, *5*, 3452-3460.

(4) van Bommel, K. J. C.; Stuart, M. C. A.; Feringa, B. L.; van Esch, J. *Org. Biomol. Chem.* **2005**, *3*, 2917-2920.

(5) Karinaga, R.; Jeong, Y.; Shinkai, S.; Kaneko, K.; Sakurai, K. *Langmuir* **2005**, *21*, 9398-9401.

(6) Vemula, P. K.; Li, J.; John, G. *J. Am. Chem. Soc.* **2006**, *128*, 8932-8938.

(7) Shome, A.; Debnath, S.; Das, P. K. *Langmuir* **2008**, *24*, 4280-4288.

(8) Panda, J. J.; Mishra, A.; Basu, A.; Chauhan, V. S. *Biomacromolecules* **2008**, *9*, 2244-2250.

(9) Feng, G. L.; Xiong, Y.; Wang, H.; Yang, Y. J. *Eur. J. Pharm. Biopharm.* **2009**, *71*, 297-302.

(10) Friggeri, A.; Feringa, B. L.; van Esch, J. *J. Control. Release* **2004**, *97*, 241-248.

(11) Komatsu, H.; Matsumoto, S.; Tamaru, S.; Kaneko, K.; Ikeda, M.; Hamachi, I. *J. Am. Chem. Soc.* **2009**, *131*, 5580-5585.

(12) Yang, Z. M.; Gu, H. W.; Zhang, Y.; Wang, L.; Xu, B. *Chem. Commun.* **2004**, 208-209.

(13) Roubeau, O.; Colin, A.; Schmitt, W.; Clérac, R. *Angew. Chem., Int. Ed.* **2004**, *43*, 3283-3286.

(14) Xiao, S. Z.; Zou, Y.; Yu, M. X.; Yi, T.; Zhou, Y. F.; Li, F. Y.; Huang, C. H. *Chem. Commun.* **2007**, 4758-4760.

(15) Chung, J. W.; An, B. K.; Park, S. Y. *Chem. Mat.* **2008**, *20*, 6750-6755.

(16) Dawn, A.; Fujita, N.; Haraguchi, S.; Sada, K.; Shinkai, S. *Chem. Commun.* **2009**, 2100-2102.

(17) Craythorne, S. J.; Anderson, K.; Lorenzini, F.; McCausland, C.; Smith, E. F.; Licence, P.; Marr, A. C.; Marr, P. C. *Chem. Eur. J.* **2009**, *15*, 7094-7100.

(18) Rodríguez-Llansola, F.; Escuder, B.; Miravet, J. F. *Org. Biomol. Chem.* **2009**, *7*, 3091-3094.

(19) Liu, Y. R.; He, L. S.; Zhang, J. Y.; Wang, X. B.; Su, C. Y. *Chem. Mater.* **2009**, *21*, 557-563.

(20) Wang, Q. G.; Yang, Z. M.; Ma, M. L.; Chang, C. K.; Xu, B. *Chem. Eur. J.* **2008**, *14*, 5073-5078.

(21) Rodríguez-Llansola, F.; Escuder, B.; Miravet, J. F. *J. Am. Chem. Soc.* **2009**, *131*, 11478-11484.

(22) Jung, J. H.; Shinkai, S. *J. Chem. Soc., Perkin Trans 2* **2000**, 2393-2398.

(23) Gundiah, G.; Mukhopadhyay, S.; Tumkurkar, U. G.; Govindaraj, A.; Maitra, U.; Rao, C. N. R. *J. Mater. Chem.* **2003**, *13*, 2118-2122.

(24) Xia, Y.; Wang, Y.; Chen, K.; Tang, L. M. *Chem. Commun.* **2008**, 5113-5115.

(25) Craythorne, S. J.; Pollock, C. L.; Blake, A. J.; Nieuwenhuyzen, M.; Marr, A. C.; Marr, P. C. *New J. Chem.* **2009**, *33*, 479-483.

(26) Godeau, G.; Bernard, J.; Staedel, C.; Barthelemy, P. *Chem. Commun.* **2009**, 5127-5129.

(27) Llusar, M.; Sanchez, C. *Chem. Mat.* **2008**, *20*, 782-820.

(28) Jung, J. H.; Ono, Y.; Shinkai, S. *Angew. Chem., Int. Ed.* **2000**, *39*, 1862-1865.

(29) Nguyen, T. T. T.; Simon, F. X.; Schmutz, M.; Mesini, P. J. *Chem. Commun.* **2009**, 3457-3459.

(30) Fujita, N.; Sakamoto, Y.; Shirakawa, M.; Ojima, M.; Fujii, A.; Ozaki, M.; Shinkai, S. *J. Am. Chem. Soc.* **2007**, *129*, 4134-4135.

(31) Wei, Q.; James, S. L. *Chem. Commun.* **2005**, 1555-1556.

(32) Mizrahi, S.; Gun, J.; Kipervaser, Z. G.; Lev, O. *Anal. Chem.* **2004**, *76*, 5399-5404.

(33) Mizrahi, S.; Rizkov, D.; Hayat, N.; Lev, O. *Chem. Commun.* **2008**, 2914-2916.

(34) Rizkov, D.; Mizrahi, S.; Gun, J.; Hoffman, R.; Melman, A.; Lev, O. *Langmuir* **2008**, *24*, 11902-11910.

(35) Gan, J. A.; El Bakkari, M.; Belin, C.; Margottin, C.; Godard, P.; Pozzo, J. L.; Vincent, J. M. *Chem. Commun.* **2009**, 5133-5134.

(36) Voss, B. A.; Bara, J. E.; Gin, D. L.; Noble, R. D. *Chem. Mat.* **2009**, *21*, 3027-3029.

(37) Loiseau, J.; Lescanne, M.; Colin, A.; Fages, F.; Verlhac, J. B.; Vincent, J. M. *Tetrahedron* **2002**, *58*, 4049-4052.

(38) Hirst, A. R.; Escuder, B.; Miravet, J. F.; Smith, D. K. *Angew. Chem., Int. Ed.* **2008**, *47*, 8002-8018.

(39) Terech, P.; Weiss, R. G. *Chem. Rev.* **1997**, *97*, 3133-3159.

(40) Araki, K.; Yoshikawa, I. In *Low Molecular Mass Gelators: Design, Self-Assembly, Function*; Springer-Verlag Berlin: Berlin, 2005; Vol. 256, p 133-165.

(41) Brizard, A.; Oda, R.; Huc, I. In *Low Molecular Mass Gelators: Design, Self-Assembly, Function*; Springer-Verlag Berlin: Berlin, 2005; Vol. 256, p 167-218.

(42) Fages, F.; Vögtle, F.; Žinić, M. *Top. Curr. Chem.* **2005**, *256*, 77-131.

(43) Kato, T.; Mizoshita, N.; Moriyama, M.; Kitamura, T. In *Low Molecular Mass Gelators: Design, Self-Assembly, Function*; Springer-Verlag Berlin: Berlin, 2005; Vol. 256, p 219-236.

(44) Liu, X. Y. In *Low Molecular Mass Gelators: Design, Self-Assembly, Function*; Springer-Verlag Berlin: Berlin, 2005; Vol. 256, p 1-37.

(45) Žinić, M.; Vögtle, F.; Fages, F. In *Low Molecular Mass Gelators: Design, Self-Assembly, Function*; Springer-Verlag Berlin: Berlin, 2005; Vol. 256, p 39-76.

(46) Ishi-i, T.; Shinkai, S. In *Supermolecular Dye Chemistry*; Springer-Verlag Berlin: Berlin, 2005; Vol. 258, p 119-160.

(47) Weiss, R. G.; Terech, P. *Molecular Gels: Materials with Self-Assembled Fibrillar Networks*; Kluwer Academic Publishers: Dordrecht, 2005.

(48) Estroff, L. A.; Hamilton, A. D. *Chem. Rev.* **2004**, *104*, 1201-1217.

(49) van Esch, J. H.; Feringa, B. L. *Angew. Chem., Int. Ed.* **2000**, *39*, 2263-2266.

(50) Sangeetha, N. M.; Maitra, U. *Chem. Soc. Rev.* **2005**, *34*, 821-836.

(51) Fages, F. *Angew. Chem., Int. Ed.* **2006**, *45*, 1680-1682.

(52) Maeda, H. *Chem. Eur. J.* **2008**, *14*, 11274-11282.

(53) Smith, D. K. *Chem. Soc. Rev.* **2009**, *38*, 684-694.

(54) Paulusse, J. M. J.; Sijbesma, R. P. *Angew. Chem., Int. Ed.* **2006**, *45*, 2334-2337.

(55) George, M.; Weiss, R. G. *Acc. Chem. Res.* **2006**, *39*, 489-497.

(56) Yang, Z.; Liang, G.; Xu, B. *Acc. Chem. Res.* **2008**, *41*, 315-326.

(57) Yang, Z.; Xu, B. *J. Mater. Chem.* **2007**, *17*, 2385-2393.

(58) Zhao, F.; Ma, M. L.; Xu, B. *Chem. Soc. Rev.* **2009**, *38*, 883-891.

(59) Dastidar, P. *Chem. Soc. Rev.* **2008**, *37*, 2699-2715.

(60) Palmans, A. R. A.; Meijer, E. W. *Angew. Chem., Int. Ed.* **2007**, *46*, 8948-8968.

(61) Hirst, A. R.; Smith, D. K. *Chem. Eur. J.* **2005**, *11*, 5496-5508.

(62) Xu, B. *Langmuir* **2009**, *25*, 8375-8377.

(63) de Loos, M.; Feringa, B. L.; van Esch, J. H. *Eur. J. Org. Chem.* **2005**, 3615-3631.

(64) Suzuki, M.; Hanabusa, K. *Chem. Soc. Rev.* **2009**, *38*, 967-975.

(65) Cravotto, G.; Cintas, P. *Chem. Soc. Rev.* **2009**, *38*, 2684-2697.

(66) Abdallah, D. J.; Weiss, R. G. *Adv. Mater.* **2000**, *12*, 1237-1247.

(67) Gronwald, O.; Snip, E.; Shinkai, S. *Curr. Opin. Colloid Interface Sci.* **2002**, *7*, 148-156.

(68) van Bommel, K. J. C.; Friggeri, A.; Shinkai, S. *Angew. Chem., Int. Ed.* **2003**, *42*, 980-999.

(69) Blow, D. M.; Rich, A. *J. Am. Chem. Soc.* **1960**, *82*, 3566-3571.

(70) Müller, W. M.; Müller, U.; Mieden-Gundert, G.; Vögtle, F.; Lescanne, M.; Heuzé, K.; D'Aléo, A.; Fages, F. *Eur. J. Org. Chem.* **2002**, 2891-2893.

(71) Kumar, D. K.; Jose, D. A.; Das, A.; Dastidar, P. *Chem. Commun.* **2005**, 4059-4061.

(72) Suzuki, M.; Yumoto, M.; Shirai, H.; Hanabusa, K. *Org. Biomol. Chem.* **2005**, *3*, 3073-3078.

(73) Lee, D. C.; McGrath, K. K.; Jang, K. *Chem. Commun.* **2008**, 3636-3638.

(74) Tsekova, D. S.; Escuder, B.; Miravet, J. F. *Cryst. Growth Des.* **2008**, *8*, 11–13.

(75) Estroff, L. A.; Hamilton, A. D. *Angew. Chem., Int. Ed.* **2000**, *39*, 3447-3450.

(76) Kim, T. H.; Seo, J.; Lee, S. J.; Lee, S. S.; Kim, J.; Jung, J. H. *Chem. Mat.* **2007**, *19*, 5815-5817.

(77) Hwang, I.; Jeon, W. S.; Kim, H. J.; Kim, D.; Kim, H.; Selvapalam, N.; Fujita, N.; Shinkai, S.; Kim, K. *Angew. Chem., Int. Ed.* **2007**, *46*, 210-213.

(78) Velázquez, D. G.; Díaz, D. D.; Ravelo, A. G.; Tellado, J. J. M. *J. Am. Chem. Soc.* **2008**, *130*, 7967-7973.

(79) Srivastava, A.; Ghorai, S.; Bhattacharjya, A.; Bhattacharya, S. *J. Org. Chem.* **2005**, *70*, 6574-6582.

(80) Kar, T.; Debnath, S.; Das, D.; Shome, A.; Das, P. K. *Langmuir* **2009**, *25*, 8639-8648.

(81) Kiyonaka, S.; Zhou, S. L.; Hamachi, I. *Supramol. Chem.* **2003**, *15*, 521-528.

(82) Zhou, S. L.; Matsumoto, S.; Tian, H. D.; Yamane, H.; Ojida, A.; Kiyonaka, S.; Hamachi, I. *Chem. Eur. J.* **2005**, *11*, 1130-1136.

(83) van Bommel, K. J. C.; van der Pol, C.; Muizebelt, I.; Friggeri, A.; Heeres, A.; Meetsma, A.; Feringa, B. L.; van Esch, J. *Angew. Chem., Int. Ed.* **2004**, *43*, 1663-1667.

(84) Kiyonaka, S.; Shinkai, S.; Hamachi, H. *Chem. Eur. J.* **2003**, *9*, 976-983.

(85) Zhang, Y.; Gu, H. W.; Yang, Z. M.; Xu, B. *J. Am. Chem. Soc.* **2003**, *125*, 13680-13681.

(86) Bhuniya, S.; Kim, B. H. *Chem. Commun.* **2006**, 1842-1844.

(87) Yang, Z. M.; Liang, G. L.; Xu, B. *Chem. Commun.* **2006**, 738-740.

(88) Qiu, Z. J.; Yu, H. T.; Li, J. B.; Wang, Y.; Zhang, Y. *Chem. Commun.* **2009**, 3342-3344.

(89) Ikeda, M.; Ueno, S.; Matsumoto, S.; Shimizu, Y.; Komatsu, H.; Kusumoto, K. I.; Hamachi, I. *Chem. Eur. J.* **2008**, *14*, 10808-10815.

(90) Yang, Z. M.; Gu, H. W.; Fu, D. G.; Gao, P.; Lam, J. K.; Xu, B. *Adv. Mater.* **2004**, *16*, 1440-1444.

(91) Yang, Z.; Liang, G.; Guo, Z.; Xu, B. *Angew. Chem., Int. Ed.* **2007**, *46*, 8216-8219.

(92) Bhuniya, S.; Seo, Y. J.; Kim, B. H. *Tetrahedron Lett.* **2006**, *47*, 7153-7156.

(93) Zhang, Y.; Yang, Z. M.; Yuan, F.; Gu, H. W.; Gao, P.; Xu, B. *J. Am. Chem. Soc.* **2004**, *126*, 15028-15029.

(94) Gao, J.; Wang, H. M.; Wang, L.; J. Y. Wang; Kong, D. L.; Yang, Z. M. *J. Am. Chem. Soc.* **2009**, *131*, 11286-11287.

(95) Kiyonaka, S.; Sada, K.; Yoshimura, I.; Shinkai, S.; Kato, N.; Hamachi, I. *Nat. Mater.* **2004**, *3*, 58-64.

(96) Piepenbrock, M. O. M.; Lloyd, G. O.; Clarke, N.; Steed, J. W. *Chem. Rev.* **2009**, in press.

(97) Lloyd, G. O.; Steed, J. W. *Nat. Chem.* **2009**, *1*, 437-442.

(98) Zhou, J. L.; Chen, X. J.; Zheng, Y. S. *Chem. Commun.* **2007**, 5200-5202.

(99) Danjo, H.; Hirata, K.; Yoshigai, S.; Azumaya, I.; Yamaguchi, K. *J. Am. Chem. Soc.* **2009**, *131*, 1638-1639.

(100) Percec, V.; Peterca, M.; Yurchenko, M. E.; Rudick, J. G.; Heiney, P. A. *Chem. Eur. J.* **2008**, *14*, 909-918.

(101) Shirakawa, M.; Fujita, N.; Shinkai, S. *J. Am. Chem. Soc.* **2005**, *127*, 4164-4165.

(102) Lescanne, M.; Grondin, P.; d'Aleo, A.; Fages, F.; Pozzo, J. L.; Monval, O. M.; Reinheimer, P.; Colin, A. *Langmuir* **2004**, *20*, 3032-3041.

(103) Terech, P.; Friol, S. *Tetrahedron* **2007**, *63*, 7366-7374.

(104) Weng, W. G.; Jamieson, A. M.; Rowan, S. J. *Tetrahedron* **2007**, *63*, 7419-7431.

(105) Naota, T.; Koori, H. *J. Am. Chem. Soc.* **2005**, *127*, 9324-9325.

(106) Bardelang, D.; Camerel, F.; Margeson, J. C.; Leek, D. M.; Schmutz, M.; Zaman, M. B.; Yu, K.; Soldatov, D. V.; Ziessel, R.; Ratcliffe, C. I.; Ripmeester, J. A. *J. Am. Chem. Soc.* **2008**, *130*, 3313-3315.

(107) Zhang, S. Y.; Yang, S. J.; Lan, J. B.; Tang, Y. R.; Xue, Y.; You, J. S. *J. Am. Chem. Soc.* **2009**, *131*, 1689-1691.

(108) Anderson, K. M.; Day, G. M.; Paterson, M. J.; Byrne, P.; Clarke, N.; Steed, J. W. *Angew. Chem., Int. Ed.* **2008**, *47*, 1058-1062.

(109) Muraoka, T.; Koh, C. Y.; Cui, H. G.; Stupp, S. I. *Angew. Chem., Int. Ed.* **2009**, *48*, 5946-5949.

(110) Ji, Y.; Kuang, G. C.; Jia, X. R.; Chen, E. Q.; Wang, B. B.; Li, W. S.; Wei, Y.; Lei, J. *Chem. Commun.* **2007**, 4233-4235.

(111) Matsumoto, S.; Yamaguchi, S.; Wada, A.; Matsui, T.; Ikeda, M.; Hamachi, I. *Chem. Commun.* **2008**, 1545-1547.

(112) Uchida, K.; Yamaguchi, S.; Yamada, H.; Akazawa, M.; Katayama, T.; Ishibashi, Y.; Miyasaka, H. *Chem. Commun.* **2009**, 4420-4422.

(113) Murata, K.; Aoki, M.; Suzuki, T.; Harada, T.; Kawabata, H.; Komori, T.; Ohseto, F.; Ueda, K.; Shinkai, S. *J. Am. Chem. Soc.* **1994**, *116*, 6664-6676.

(114) Koumura, N.; Kudo, M.; Tamaoki, N. *Langmuir* **2004**, *20*, 9897-9900.

(115) Miljanić, S.; Frkanec, L.; Meić, Z.; Žinić, M. *Eur. J. Org. Chem.* **2006**, 1323-1334.

(116) Wang, S.; Shen, W.; Feng, Y. L.; Tian, H. *Chem. Commun.* **2006**, 1497-1499.

(117) Sako, Y.; Takaguchi, Y. *Org. Biomol. Chem.* **2008**, *6*, 3843-3847.

(118) Nagasawa, J.; Kudo, M.; Hayashi, S.; Tamaoki, N. *Langmuir* **2004**, *20*, 7907-7916.

(119) Eastoe, J.; Sánchez-Domingues, M.; Wyatt, P.; Heenan, R. K. *Chem. Commun.* **2004**, 2608-2609.

(120) Moffat, J. R.; Coates, I. A.; Leng, F. J.; Smith, D. K. *Langmuir* **2009**, *25*, 8786-8793.

(121) Coates, I. A.; Smith, D. K. *Chem. Eur. J.* **2009**, *15*, 6340-6344.

(122) Chung, J. W.; An, B. K.; Park, S. Y. *Chem. Mat.* **2008**, *20*, 6750-6755.

(123) Ge, Z. S.; Hu, J. M.; Huang, F. H.; Liu, S. Y. *Angew. Chem., Int. Ed.* **2009**, *48*, 1798-1802.

(124) Zheng, Y. S.; Ji, A.; Chen, X. J.; Zhou, J. L. *Chem. Commun.* **2007**, 3398-3400.

(125) Zheng, Y. S.; Ran, S. Y.; Hu, Y. J.; Liu, X. X. *Chem. Commun.* **2009**, 1121-1123.

(126) Cai, W.; Wang, G. T.; Du, P.; Wang, R. X.; Jiang, X. K.; Li, Z. T. *J. Am. Chem. Soc.* **2008**, *130*, 13450-13459.

(127) Ishi-i, T.; Iguchi, R.; Snip, E.; Ikeda, M.; Shinkai, S. *Langmuir* **2001**, *17*, 5825-5833.

(128) Díaz, D. D.; Cid, J. J.; Vázquez, P.; Torres, T. *Chem. Eur. J.* **2008**, *14*, 9261-9273.

(129) Yang, Y.; Chen, T.; Xiang, J. F.; Yan, H. J.; Chen, C. F.; Wan, L. J. *Chem. Eur. J.* **2008**, *14*, 5742-5746.

(130) Babu, P.; Sangeetha, N. M.; Vijaykumar, P.; Maitra, U.; Rissanen, K.; Raju, A. R. *Chem. Eur. J.* **2003**, *9*, 1922-1932.

(131) Hanabusa, K.; Itoh, A.; Kimura, M.; Shirai, H. *Chem. Lett.* **1999**, 767-768.

(132) Suzuki, M.; Yumoto, M.; Kimura, M.; Shirai, H.; Hanabusa, K. *Helvetica Chimica Acta* **2003**, *86*, 2228-2238.

(133) Das, D.; Dasgupta, A.; Roy, S.; Mitra, R. N.; Debnath, S.; Das, P. K. *Chem. Eur. J.* **2006**, *12*, 5068-5074.

(134) Montalti, M.; Dolci, L. S.; Prodi, L.; Zaccheroni, N.; Stuart, M. C. A.; van Bommel, K. J. C.; Friggeri, A. *Langmuir* **2006**, *22*, 2299-2303.

(135) Inoue, K.; Ono, Y.; Kanekiyo, Y.; Ishi-i, T.; Yoshihara, K.; Shinkai, S. *J. Org. Chem.* **1999**, *64*, 2933-2937.

(136) Moffat, J. R.; Smith, D. K. *Chem. Commun.* **2008**, 2248-2250.

(137) Seo, J.; Chung, J. W.; Jo, E. H.; Park, S. Y. *Chem. Commun.* **2008**, 2794-2796.

(138) Botterhuis, N. E.; Karthikeyan, S.; Veldman, D.; Meskers, S. C. J.; Sijbesma, R. P. *Chem. Commun.* **2008**, 3915-3917.

(139) Saha, A.; Manna, S.; Nandi, A. K. *Chem. Commun.* **2008**, 3732-3734.

(140) Wang, Y. J.; Tang, L. M.; Yu, J. *Cryst. Growth Des.* **2008**, *8*, 884-889.

(141) Yagai, S.; Kinoshita, T.; Higashi, M.; Kishikawa, K.; Nakanishi, T.; Karatsu, T.; Kitamura, A. *J. Am. Chem. Soc.* **2007**, *129*, 13277-13287.

(142) Saha, A.; Manna, S.; Nandi, A. K. *Langmuir* **2007**, *23*, 13126-13135.

(143) Ballabh, A.; Adalder, T. K.; Dastidar, P. *Cryst. Growth Des.* **2008**, *8*, 4144-4149.

(144) Adarsh, N. N.; Kumar, D. K.; Dastidar, P. *Tetrahedron* **2007**, *63*, 7386-7396.

(145) Sahoo, P.; Adarsh, N. N.; Chacko, G. E.; Raghavan, S. R.; Puranik, V. G.; Dastidar, P. *Langmuir* **2009**, *25*, 8742-8750.

(146) Džolić, Z.; Wolsperger, K.; Žinić, M. *New J. Chem.* **2006**, *30*, 1411-1419.

(147) Moffat, J. R.; Smith, D. K. *Chem. Commun.* **2009**, 316-318.

(148) Liang, G. L.; Xu, K. M.; Li, L. H.; Wang, L.; Kuang, Y.; Yang, Z. M.; Xu, B. *Chem. Commun.* **2007**, 4096-4098.

(149) Yang, Z. M.; Liang, G. L.; Ma, M. L.; Abbah, A. S.; Lu, W. W.; Xu, B. *Chem. Commun.* **2007**, 843-845.

(150) Jayawarna, V.; Ali, M.; Jowitt, T. A.; Miller, A. F.; Saiani, A.; Gough, J. E.; Ulijn, R. V. *Adv. Mater.* **2006**, *18*, 611-614.

(151) Mart, R. J.; Osborne, R. D.; Stevens, M. M.; Ulijn, R. V. *Soft Matter* **2006**, *2*, 822-835.

(152) Ulijn, R. V. *J. Mater. Chem.* **2006**, *16*, 2217-2225.

(153) Fiero, G. W. *J. Am. Pharm. Assoc.* **1940**, *29*, 502-5.

(154) Kishida, T.; Fujita, N.; Hirata, O.; Shinkai, S. *Org. Biomol. Chem.* **2006**, *4*, 1902-1909.

(155) Kishida, T.; Fujita, N.; Sada, K.; Shinkai, S. *Langmuir* **2005**, *21*, 9432-9439.

(156) Kishida, T.; Fujita, N.; Sada, K.; Shinkai, S. *J. Am. Chem. Soc.* **2005**, *127*, 7298-7299.

(157) Malik, S.; Kawano, S.; Fujita, N.; Shinkai, S. *Tetrahedron* **2007**, *63*, 7326-7333.

(158) Shirakawa, M.; Kawano, S.; Fujita, N.; Sada, K.; Shinkai, S. *J. Org. Chem.* **2003**, *68*, 5037-5044.

(159) Chen, J.; McNeil, A. J. *J. Am. Chem. Soc.* **2008**, *130*, 16496-16497.

(160) Liu, J.; He, P. L.; Yan, J. L.; Fang, X. H.; Peng, J. X.; Liu, K. Q.; Fang, Y. *Adv. Mater.* **2008**, *20*, 2508-2511.

(161) Liu, J.; Yan, J. L.; Yuan, X. W.; Liu, K. Q.; Peng, J. X.; Fang, Y. *J. Colloid Interface Sci.* **2008**, *318*, 397-404.

(162) Shirakawa, M.; Fujita, N.; Tani, T.; Kaneko, K.; Shinkai, S. *Chem. Commun.* **2005**, 4149-4151.

(163) Ziessel, R.; Pickaert, G.; Camerel, F.; Donnio, B.; Guillon, D.; Cesario, M.; Prangé, T. *J. Am. Chem. Soc* **2004**, *126*, 12403-12413.

(164) Camerel, F.; Ziessel, R.; Donnio, B.; Guillon, D. *New J. Chem.* **2006**, *30*, 135-139.

(165) Murata, K.; Aoki, M.; Nishi, T.; Ikeda, A.; Shinkai, S. *J. Chem. Soc., Chem. Commun.* **1991**, 1715-1718.

(166) Ghoussoub, A.; Lehn, J.-M. *Chem. Commun.* **2005**, 5763–5765.

(167) Miravet, J. F.; Escuder, B. *Chem. Commun.* **2005**, 5796-5798.

(168) Mieden-Gundert, G.; Klein, L.; Fischer, M.; Vögtle, F.; Heuzé, K.; Pozzo, J. L.; Vallier, M.; Fages, F. *Angew. Chem., Int. Ed.* **2001**, *40*, 3164-3166.

(169) D'Aléo, A.; Pozzo, J. L.; Fages, F.; Schmutz, M.; Mieden-Gundert, G.; Vögtle, F.; Caplar, V.; Žinić, M. *Chem. Commun.* **2004**, 190-191.

(170) Suzuki, M.; Nanbu, M.; Yumoto, M.; Shirai, H.; Hanabusa, K. *New J. Chem.* **2005**, *29*, 1439-1444.

(171) Suzuki, M.; Sato, T.; Shirai, H.; Hanabusa, K. *New J. Chem.* **2006**, *30*, 1184-1191.

(172) D'Aléo, A.; Pozzo, J. L.; Heuze, K.; Vögtle, F.; Fages, F. *Tetrahedron* **2007**, *63*, 7482-7488.

(173) Collier, J. H.; Hu, B. H.; Ruberti, J. W.; Zhang, J.; Shum, P.; Thompson, D. H.; Messersmith, P. B. *J. Am. Chem. Soc.* **2001**, *123*, 9463-9464.

(174) Diegelmann, S. R.; Gorham, J. M.; Tovar, J. D. *J. Am. Chem. Soc.* **2008**, *130*, 13840-13841.

(175) Ahmed, S. A.; Sallenave, X.; Fages, F.; Mieden-Gundert, G.; Müller, W. M.; Müller, U.; Vögtle, F.; Pozzo, J. L. *Langmuir* **2001**, *18*, 7096-7101.

(176) Page, M. G.; Warr, G. G. *Langmuir* **2009**, *25*, 8810-8816.

(177) Leong, W. L.; Batabyal, S. K.; Kasapis, S.; Vittal, J. J. *Chem. Eur. J.* **2008**, *14*, 8822-8829.

(178) Bardelang, D.; Camerel, F.; Hotze, A. C. G.; Kariuki, B.; Paik, B.; Schmutz, M.; Ziessel, R.; Hannon, M. J. *Chem. Eur. J.* **2007**, *13*, 9277-9285.

(179) Lenthall, J. T.; Steed, J. W. *Coord. Chem. Rev.* **2007**, *251*, 1747-1760.

(180) Steed, J. W. *Chem. Commun.* **2006**, 2637-2649.

(181) Steed, J. W.; Atwood, J. L. *Supramolecular Chemistry*; 2nd ed.; Wiley-Blackwell: Chichester, 2009.

(182) Sessler, J. L.; Gale, P. A.; Cho, W.-S. *Anion Receptor Chemistry*; Royal Society of Chemistry: Cambridge, 2006.

(183) Gale, P. A. *Coord. Chem. Rev.* **2006**, *250*, 2917 preface to the special issue and subsequent reviews.

(184) Yamanaka, M.; Nakamura, T.; Nakagawa, T.; Itagaki, H. *Tetrahedron Lett.* **2007**, *48*, 8990-8993.

(185) Hennrich, G.; Lynch, V. M.; Anslyn, E. V. *Chem.-Eur. J.* **2002**, *8*, 2274-2278.

(186) Wallace, K. J.; Belcher, W. J.; Turner, D. R.; Syed, K. F.; Steed, J. W. *J. Am. Chem. Soc.* **2003**, *125*, 9699-9715.

(187) Wang, C.; Zhang, D. Q.; Zhu, D. B. *Langmuir* **2007**, *23*, 1478-1482.

(188) Maeda, H.; Hasegawa, M.; Hashimoto, T.; Kakimoto, T.; Nishio, S.; Nakanishi, T. *J. Am. Chem. Soc.* **2006**, *128*, 10024-10025.

(189) Maeda, H.; Haketa, Y.; Nakanishi, T. *J. Am. Chem. Soc.* **2007**, *129*, 13661-13674.

(190) Stanley, C. E.; Clarke, N.; Anderson, K. M.; Lenthall, J. P.; Steed, J. W. *Chem. Commun.* **2006**, 3199-3201.

(191) Yang, H.; Yi, T.; Zhou, Z. G.; Zhou, Y. F.; Wu, J. C.; Xu, M.; Li, F. Y.; Huang, C. H. *Langmuir* **2007**, *23*, 8224-8230.

(192) van der Laan, S.; Feringa, B. L.; Kellogg, R. M.; van Esch, J. *Langmuir* **2001**, 7136-7140.

(193) Džolić, Z.; Cametti, M.; Cort, A. D.; Mandolini, L.; Žinić, M. *Chem. Commun.* **2007**, 3535-3537.

(194) Kim, T. H.; Choi, M. S.; Sohn, B. H.; Park, S. Y.; Lyoo, W. S.; Lee, T. S. *Chem. Commun.* **2008**, 2364-2366.

(195) Pinault, T.; Cannizzo, C.; Andrioletti, B.; Ducouret, G.; Lequeux, F.; Bouteiller, L. *Langmuir* **2009**, *25*, 8404-8407.

(196) Webb, J. E. A.; Crossley, M. J.; Turner, P.; Thordarson, P. *J. Am. Chem. Soc.* **2007**, *129*, 7155-7162.

(197) Zhang, J. Y.; Xu, X. L.; James, S. L. *Chem. Commun.* **2006**, 4218-4220.

(198) Becker, T.; Goh, C. Y.; Jones, F.; McIldowie, M. J.; Mocerino, M.; Ogden, M. I. *Chem. Commun.* **2008**, 3900 - 3902.

(199) Eds. Kanz, W. L. N., P.; Ninham, B. W. *Curr. Opin. Colloid Interface Sci.* **2004**, *9*, 1-197.

(200) Leontidis, E. *Curr. Opin. Colloid Interface Sci.* **2002**, *7*, 81-91.

(201) Cacace, M. G.; Landau, E. M.; Ramsden, J. J. *Q. Rev. Biophys.* **1997**, *30*, 241-278.

(202) Kim, H. J.; Lee, J. H.; Lee, M. *Angew. Chem., Int. Ed.* **2005**, *44*, 5810-5814.

(203) Kim, H. J.; Zin, W. C.; Lee, M. *J. Am. Chem. Soc.* **2004**, *126*, 7009-7014.

(204) Kim, H. J.; Jung, E. Y.; Jin, L. Y.; Lee, M. *Macromolecules* **2008**, *41*, 6066-6072.

(205) Beck, J. B.; Rowan, S. J. *J. Am. Chem. Soc.* **2003**, *125*, 13922-13923.

(206) Rowan, S. J.; Beck, J. B. In *Meeting on Self-Organising Polymers* Leeds, ENGLAND, 2004, p 43-53.

(207) Weng, W. G.; Beck, J. B.; Jamieson, A. M.; Rowan, S. J. *J. Am. Chem. Soc.* **2006**, *128*, 11663-11672.

(208) Weng, W. G.; Li, Z.; Jamieson, A. M.; Rowan, S. J. *Macromolecules* **2009**, *42*, 236-246.

(209) Zhao, Y. Q.; Beck, J. B.; Rowan, S. J.; Jamieson, A. M. *Macromolecules* **2004**, *37*, 3529-3531.

(210) Liu, Q. T.; Wang, Y. L.; Li, W.; Wu, L. X. *Langmuir* **2007**, *23*, 8217-8223.

(211) Shen, J. S.; Li, D. H.; Cai, Q. G.; Jiang, Y. B. *J. Mater. Chem.* **2009**, *19*, 6219-6224.

(212) Kishimura, A.; Yamashita, T.; Aida, T. *J. Am. Chem. Soc.* **2005**, *127*, 179-183.

(213) Henstock, H. *J. Am. Chem. Soc.* **1939**, *61*, 670–673.

(214) Abdallah, D. J.; Weiss, R. G. *Chem. Mater.* **2000**, *12*, 406-413.

(215) Trivedi, D. R.; Dastidar, P. *Chem. Mater.* **2006**, *18*, 1470-1478.

(216) Trivedi, D. R.; Dastidar, P. *Cryst. Growth Des.* **2006**, *6*, 2114-2121.

(217) Trivedi, D. R.; Ballabh, A.; Dastidar, P. *J. Mater. Chem.* **2005**, *15*, 2606-2614.

(218) Smith, P. J.; Reddington, M. V.; Wilcox, C. S. *Tetrahedron Lett.* **1992**, *33*, 6085-6088.

(219) Nishizawa, S.; Buhlmann, P.; Iwao, M.; Umezawa, Y. *Tetrahedron Lett.* **1995**, *36*, 6483-6486.

(220) Yamanaka, M.; Nakagawa, T.; Aoyama, R.; Nakamura, T. *Tetrahedron* **2008**, *64*, 11558–11567.

(221) van Esch, J.; Schoonbeek, F.; de Loos, M.; Kooijman, H.; Spek, A. L.; Kellogg, R. M.; Feringa, B. L. *Chem. Eur. J.* **1999**, *5*, 937-950.

(222) de Loos, M.; van Esch, J.; Kellogg, R. M.; Feringa, B. L. *Angew. Chem., Int. Ed.* **2001**, *40*, 613-616.

(223) van Esch, J.; DeFeyter, S.; Kellogg, R. M.; DeSchryver, F.; Feringa, B. L. *Chem. Eur. J.* **1997**, *3*, 1238-1243.

(224) Simic, V.; Bouteiller, L.; Jalabert, M. *J. Am. Chem. Soc.* **2003**, *125*, 13148-13154.

(225) Yabuuchi, K.; Marfo-Owusu, E.; Kato, T. *Org. Biomol. Chem.* **2003**, *1*, 3464-3469.

(226) George, M.; Tan, G.; John, V. T.; Weiss, R. G. *Chem. Eur. J.* **2005**, *11*, 3243-3254.

(227) Halcrow, M. A. *Dalton Trans.* **2009**, 2059-2073.

Chapter 2

Gelation and anion binding properties of a group of chiral bisurea compounds

2.1 Aims

The main aim of this research is to investigate low molecular weight gelators and their anion binding properties in order to produce anion tunable gels[1,2] for specific applications.[3] Chiral bisurea compounds were chosen because the anion binding capabilities of the urea group are well understood,[4,5] and the gel properties of compounds that contain urea groups have also been extensively studied.[6-10] Therefore it was easy to speculate that the two could be used together within the same system.[1,2,11] The choice of a resolved chiral end group comes through the reasoning that many gelators do contain chiral functionality and that chirality is a desirable property of self-assembled systems.[12-14] Moreover optically resolved systems frequently crystallise less readily than their racemic or achiral counterparts because of the restrictions placed on the possible space group symmetry by the asymmetric centre or moiety. The target compounds are to be tested for gelation ability and their gelation properties investigated. Addition of anions will be used as a means to test if the gelation ability of the compounds is affected by anion complexation. If the gelation properties are changed by the addition of anions the mechanism behind this change will be probed using such techniques as rheology and standard anion testing protocols like NMR spectroscopic titration. Finally two potential uses of LMWGs, crystal growth control[8,15] and controlled drug release,[16-27] will be tested with anion tuning playing an important role in the application of these properties.

2.2 Gelation study of 1-[(1*S*)-1-phenylethyl]-3-[2-({[(1*S*)-1-phenylethyl]carbamoyl} amino)ethyl] urea

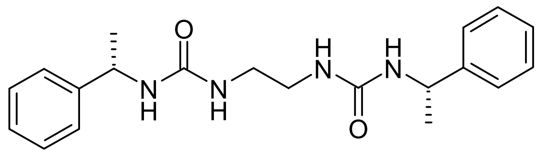

2.1a

1-[(1*S*)-1-Phenylethyl]-3-[2-({[(1*S*)-1-phenylethyl]carbamoyl}amino)ethyl]urea (**2.1a**) was readily synthesised by reaction of ethylene diamine with (*S*)-(-)-α-methylbenzyl isocyanate. The gelation ability of the compound was assessed by dissolving **2.1a** at 1% by weight in a variety of solvents, namely MeCN, $CHCl_3$, MeOH, EtOH, Toluene (Tol), EthylAcetate (EtOAc), $(CH_3)_2CO$, THF and solvent mixtures of H_2O or Tol (Table 2.1). The alcohols, DMSO and DMF dissolve **2.1a** very well and no gelation was observed. Compound **2.1a** did not dissolve in the non-polar solvents like hexane and toluene. Compound **2.1a** is only sparingly soluble in water and precipitates out of a hot solution. **2.1a** formed stable opaque gels in $CHCl_3$, EtOAc, $(CH_3)_2CO$, THF and MeCN.

In general sonication was found to significantly increase the rate of gelation and to improve the homogeneity of the organogels even though sonication was not necessary for gel formation.[28] The increase in homogeneity due to the sonication is due to the enhanced formation of nuclei and their dispersion throughout the solvent leading to the initial growth of more and finer fibres.[28] In the case of a brief sonication (less than a second) of **2.1a** at 0.3% by weight in MeCN a transparent gel results. Over time this clear gel (Figure 2.1a) becomes more opaque with the formation of thicker-fibred spherulitic networks of dendrimer appearance, Figure 2.1b.[29-32] This formation of the thicker-fibred spherulitic networks results in a stronger gel as indicated by the time dependence of the elastic shear modulus G' and the loss modulus G'' variables as measured by rheometry as shown in Figure 2.1. DMSO/H_2O, EtOH/H_2O, MeOH/H_2O and DMSO/Tol, MeCN/Tol, $CHCl_3$/Tol mixtures are also gelled by compound **2.1a** giving hydrogels (in the case of water based solvent mixtures)[33,34] and gels of nonpolar solvents. The gelling conditions for all solvents and solvent mixtures investigated are listed in Table 2.1. To form gels of hydrophobic solvents, such as Tol, where **2.1a** is not soluble, the gelator was dissolved in a minimum volume of DMSO (or a solvent that is miscible with the hydrophobic solvent and dissolves **2.1a**). This **2.1a** solution was added to a larger volume of the hydrophobic solvent resulting in a gel of **2.1a**. For example, gels, with Tol as the majority solvent, can be formed at a solvent ratio of 9.5:0.5 Tol to DMSO at 0.05% gelator by weight. These mixed solvent gels were thermally reversible.

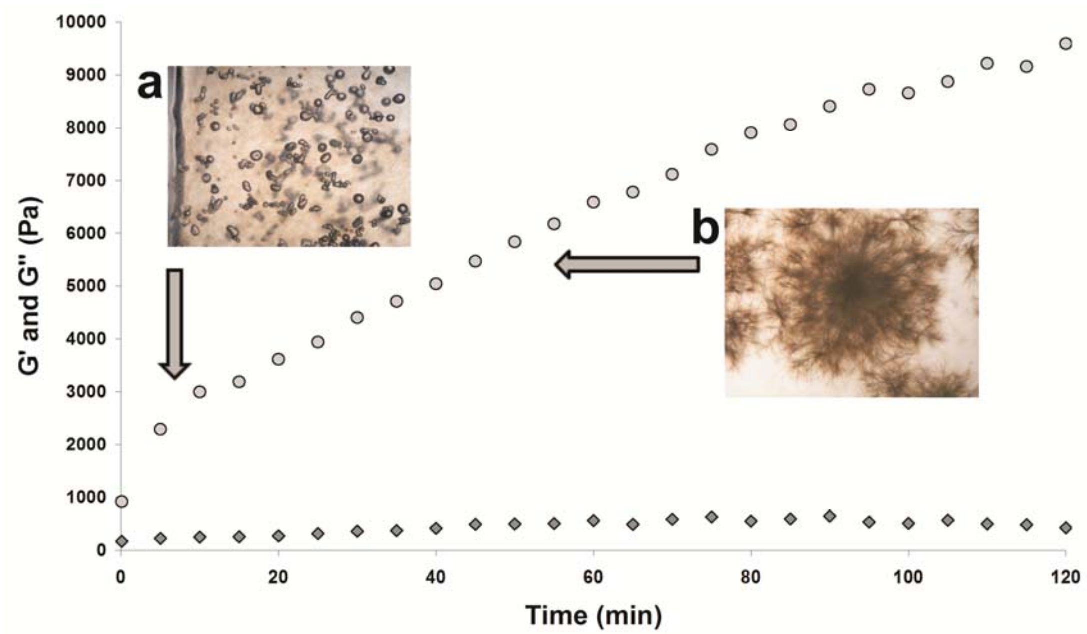

Figure 2.1. A time sweep of the rheological character of a gel of **2.1a** at 0.3% by weight in MeCN. It shows how even though a gel has formed instantaneously upon cooing the gel continues to 'mature'. The strengthening is highlighted by the increase in the *G′* value (Light grey filled ○) while the *G″* value (Grey filled ◇) stays relatively the same. **a)** Inset showing a micrograph image of air trapped in a clear gel as seen upon brief sonication of a gel solution. **b)** Inset shows the branching by growing fibres resulting spherulitic networks in a gel as it matures.

The gelation of **2.1a** at 1% in DMSO/ H_2O mixtures by the addition of water to a pre-dissolved DMSO solution is shown in Figure 2.2. These mixtures can be heated until compound **2.1a** dissolves and upon cooling the gels reform. In the case of the more aqueous samples, ratios 1:9; 2:8; 3:7, when water was added to the DMSO solution a mixture of gel material and precipitate was seen whereas when these same samples were heated and cooled a gel was formed (Figures 2.2 and 2.3). The 7:3 mixture shows the close relationship between gelation and crystallisation.[35] Adding water to the pre-dissolved **2.1a** in DMSO resulted in a gel, however, upon heating and cooling crystallisation occured (Figure 2.3).

Table 2.1. Gelation behaviour of compound **2.1a**.

Solvents	**Phase**[a]	**Appearance**	**CGC** (%)[b]
$CHCl_3$	G	Transparent to Opaque	0.02
MeCN	G	Opaque	0.05
THF	G	Opaque	0.05
Acetone	G	Opaque	0.05
Ethyl Acetate	G	Transparent to Opaque	0.03
Alcohols, DMSO, DMF	S	n/a	n/a
Tolune, Hexane, Cyclohexane	I	n/a	n/a
Water	P	n/a	n/a
DMSO:H_2O(c) / EtOH:H_2O(d) / MeOH:H_2O(e) /	G/C/S	Opaque	0.04
Tol:co-solvent(f)	G/S	Transparent to Opaque	0.06

[a] G = gel; I = Insoluble; S = Sol; P = Precipitate; C = Crystals [b] Gel formation is observed below this concentration however the gel does immobilise the entire solution of 1ml in a 1cm wide circular vessel [c] A ratio range of 7:3 to 1:9 results in gel formation (Figures 2 and 3) [d] A ratio range of 7:3 to 1:9 results in gel formation [e] A ratio range of 7:3 to 1:9 results in gel formation [f] **1** does not dissolve in toluene but dissolving it in a minimal amount of DMSO, MeCN or $CHCl_3$ and adding it to the toluene allows for gel formation.

Figure 2.2. DMSO:Water gels formed by the addition of water to a solution of **2.1a** in DMSO. From left to right the solvents are: pure water, ratios 1:9; 2:8; 3:7; 4:6; 5:5; 6:4; 7:3; 8:2; 9:1; pure DMSO. Note that the more aqueous samples, 1:9; 2:8; 3:7, are precipitated and/or form weak gels. Note the 8:2; 9:1 and pure DMSO samples are clear solutions.

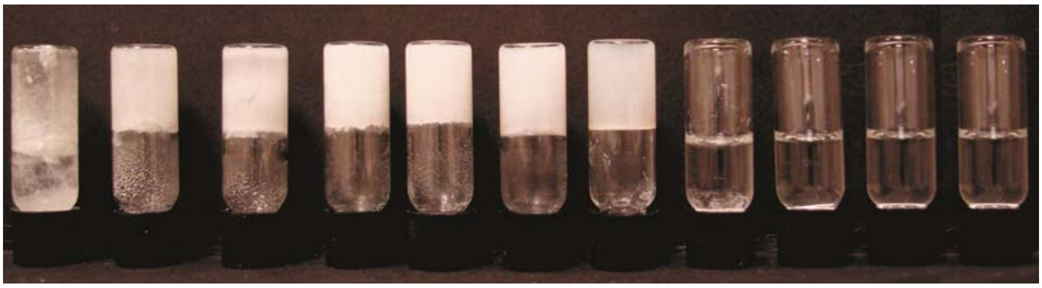

Figure 2.3. Image of the same samples as in Figure 2.2 but after heating to dissolution followed by cooling to room temperature. Homogenous gels were obtained for the more aqueous solutions. Only pure water and ratios 7:3; 8:2; 9:1 DMSO:H_2O and pure DMSO did not form gels. Compound **2.1a** is partially soluble in water but does not form a gel. Note that the vial containing the 7:3 solution contains small crystals which were used for the determination of the compound's crystal structure.

Given the ability of a concentrated solution of **2.1a** in DMSO to gel both water and non-polar solvents like Tol, we attempted to selectively gel one of these solvents from a mixture of the two in order to develop liquid-liquid separations applications.[36-40] A few drops of a concentrated solution of **2.1a** in DMSO were added to a mixture of water and Tol. The Tol is gelled upon addition of **2.1a**. If excess **2.1a** (above 2% by weight for the Tol gel) is added it begins to gel the water as well. Subsequent heating of this solution with water and the gelled Tol results in the toluene becoming a large mass of gel. This shows how **2.1a** can be used to separate a non-polar solvent from water. In addition the effect of small amounts of water on gel behaviour of organic solvent was investigated. In the case of MeCN and $CHCl_3$ the gels of these solvents were found to be stronger when the solvent was dried over molecular sieves to remove water compared to when the solvents were not dried over molecular sieves. This effect is more pronounced in the case of THF gels; addition of one or two drops of water results in the complete dissolution of the gels.

The behaviour of fibres of the gels when exposed to mechanical stress was investigated using rheology.[31,41-45] The gels were characterised by temperature sweep, stress sweep and frequency sweep rheometry. With a number of different samples varying in both concentration and solvent used, when a frequency sweep was performed with a small amplitude stress, the solid-like nature at 20 °C was reflected in the storage modulus, G', being typically an order of magnitude greater than the loss modulus, G'', thus demonstrating the elastic behaviour of the systems (Figure 2.4).[46] This viscoelastic behaviour is associated with classical gels, and therefore supports the notion that the cooling of these samples from a clear solution to a solid-like material results in a true gel state.

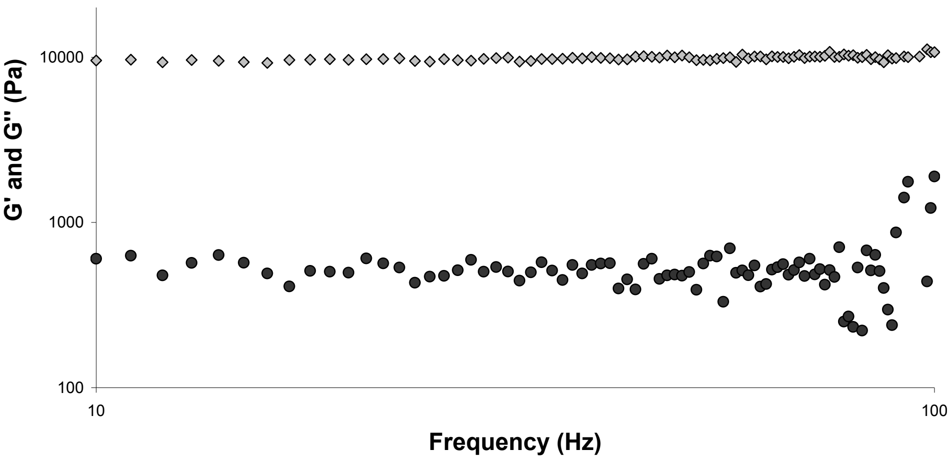

Figure 2.4. Rheology of **2.1a** showing a frequency sweep performed on a gel of **2.1a** at 0.3% by weight MeCN gel. Typically the consistency of the G' (Light grey filled ◇) and G'' (Dark grey filled ○) values over the frequency range indicates the solid-like nature of the gel material. The greater than a magnitude value of G' over the G'' value demonstrates the elastic behaviour of the gel. Both axis values are shown on a logarithmic (log) scale.

The non-linear rheological response was investigated using stress sweep experiments, during which an oscillatory torque was imposed with a fixed frequency (1 Hz) over a range of shear stress amplitudes. Example gels showed a typical instrument response with the small decrease in G' value, essentially constant, below the critical value of oscillatory torque, the "yield stress". At this "yield stress" point, where G' swaps from being greater in value than G'' to being lesser in value, the sample starts to flow providing the "yield strength/stress value" for the sample (Figure 2.5).[44,45]

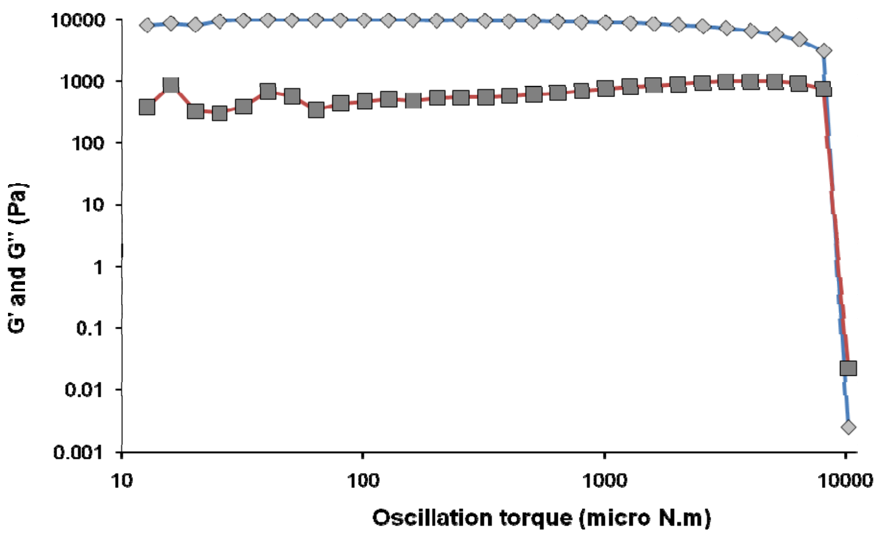

Figure 2.5. Rheology of **2.1a** showing a stress sweep, as a function of oscillation (osc.) torque, on a gel of **2.1a** at 0.3% by weight MeCN gel. The stress sweep shows the rigidity and strength of the gel which breaks at a relatively high shear strength. G' value (Light grey filled ◇) stays constant until the torque begins to become too strong and the struts start to break under the strain. Eventually G' for the samples drops to below the G'' value (Dark grey filled □) and the sample is said to be flowing, coloured guide lines show blue (G') passing red (G''). This transition point were the G'' value becomes greater the G' value gives the "yield stress". Both axis values are shown on a log scale.

The effect of the concentration on the gel strength was also investigated using rheology. Plotting G' against concentration of **2.1a** reveals concentration dependence similar to that seen often for the dependence of T_{gel} with concentration (Figure 2.6).[45] There have been theoretical models put forward for the mechanical properties of gels.[47]

Two examples that are pertinent to LMWGs are the colloidal gel description[48] and the cellular solid model.[41,49,50]

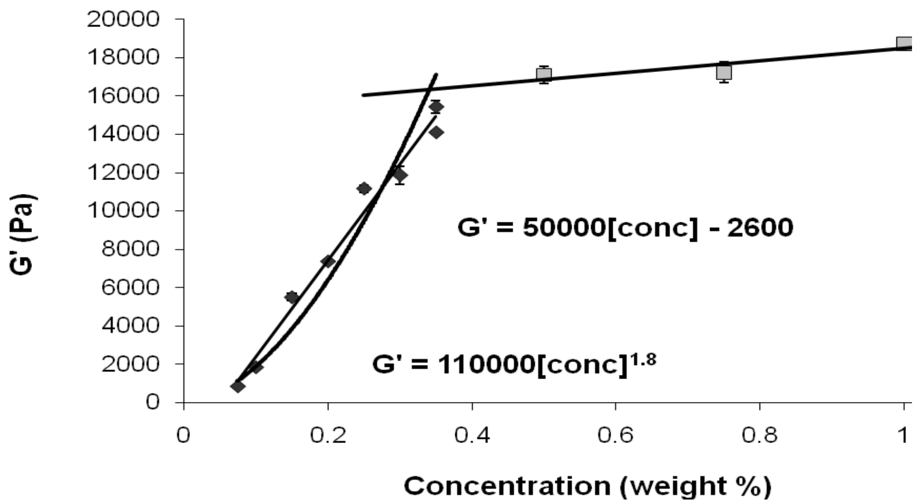

Figure 2.6. The G′ dependence on the concentration (indication of strength of gel) of compound **2.1a** in MeCN. The plateau point, at around 0.45 % by weight, is used as the cut off point for the determination of the $G' \propto$ [conc]^n relationship. Errors bars on all points represent standard deviation for ten determinations of G' values for a given sample. An example of the deviation in results for different samples at the same weight percent is represented by the two measurements on samples at 0.35% by weight. Lines are for a power law and a linear relation of best fits.

Attempting to fit either of the two models to the data shown in Figure 2.6 gives no obvious match. However, as can be seen clearly from the graph there is a saturation point (in terms of further strengthening) at approximately 0.45 % by weight. As neither model takes this into account, the use of data points below this weight percentage threshold should provide a set of data that can be modelled.[31,51] Doing this reveals a power law relationship fit between the strength of **2.1a** in MeCN and concentration of $G' \propto$ [conc]$^{1.8}$.This is in good agreement with the cellular solid model which is predicted to have a relationship of $G' \propto$ [conc]^n, where n can vary between 1 and 2.[50] A good fit for a linear relationship between G' and the concentration can also be found. Due to the inherently high errors involved in fitting data of this kind, no conclusive power law relationship can be made and therefore, a conclusive choice between the two models.

However, the cellular solid model parameters fit better than those for the colloidal gel description. The cellular solid model describes an open-cell cellular material which consists of load bearing struts interconnected via crosslinks or junction points which deform by bending. To further elucidate whether or not this model is correctly assigned to the gel structures formed by **2.1a**, imaging techniques were utilized to determine the gel morphology.

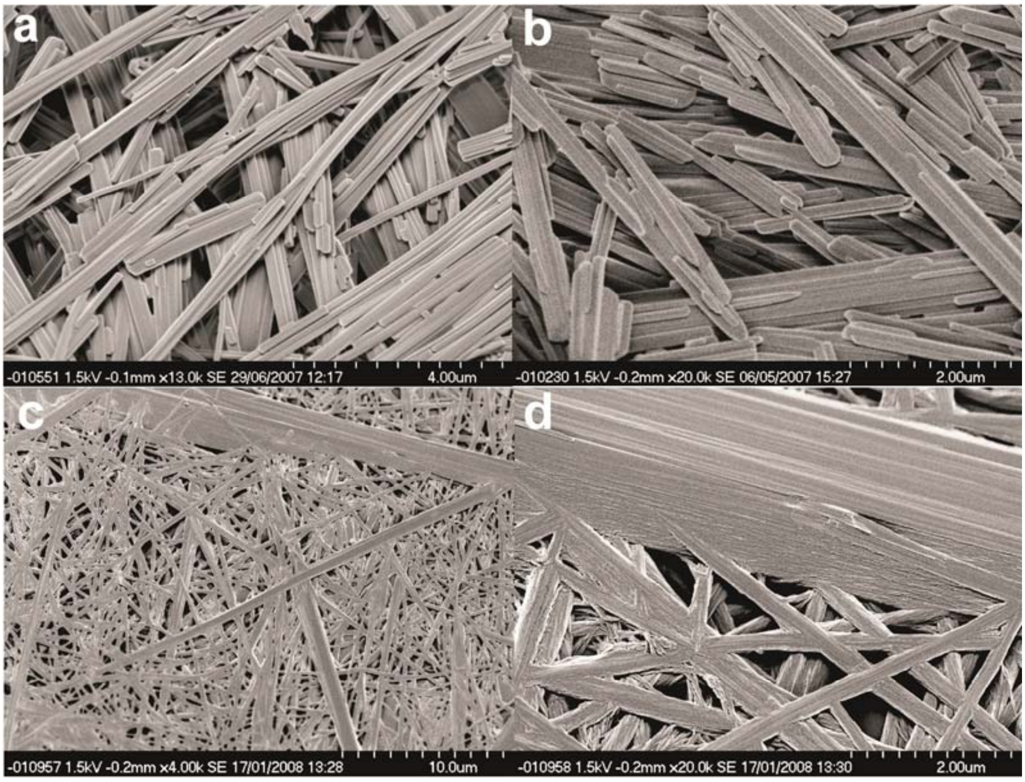

Figure 2.7. a) Crystalline material seen upon drying a gel sample of **2.1a** in MeCN using SEM. **b)** Crystalline material seen upon drying a gel sample of **2.1a** in $CHCl_3$ using SEM. **c)** SEM image of compound **2.1a** xerogel formed from a gel made in a DMSO:H_2O mixture at 6:4. This image is a better representation of the gel structure than images seen in parts a and b. Note how the gel fibres are rod-shaped and show no indication of the chirallity of the gelator. **d)** Higher resolution image of the fibre connections of the DMSO:H_2O gel. There are large fibres/crystals that are bound to the smaller gel fibres.

Gel morphologies were studied by scanning electron microscopy (SEM) imaging. Samples of **2.1a** were dried under vacuum and then coated with a thin layer of platinum metal. The rod-shaped morphologies seen in the SEM imaging of the gels are very different from the fibred network morphologies of the hydrogels (Figure 2.7). It is likely that the morphology difference is due to how the gels dry under dynamic vacuum. More specifically, the rod-shaped morphology is likely to be micro-crystalline material that does not truly represent the gel structure.

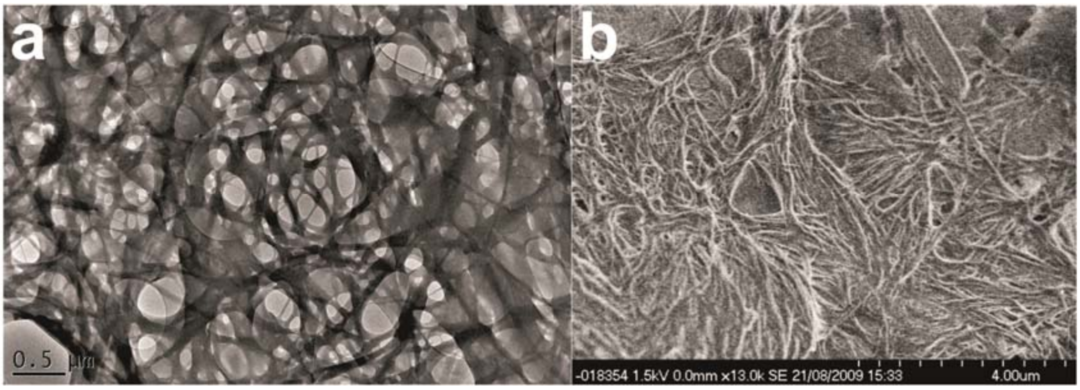

Figure 2.8. a) TEM image of compound **2.1a** gel formed in a $CHCl_3$ at 0.5% by weight. **b)** Cryo-SEM image of a $CHCl_3$ gel of **2.1a** showing the fibrous gelatinous morphology as seen in the TEM image, which is in strong contrast to the dried crystalline SEM samples of Figure 7a and 7b. To the top right of the image can be seen the edge of crystalline structure similar in morphology to the dried gel.

As this micro-crystalline material is not a true representation of the gel structure the $CHCl_3$ gels were also characterised using TEM imaging. The sample preparation for this imaging technique results in a fresh sample being exposed abruptly to high vacuum resulting in an altered drying process. The placement of thin layers of gel on the carbon mesh support and the imaging results revealed a more truly representative image of the gel. As shown in Figure 2.8a the TEM images show a much more fibrous morphology. We attempted to obtain an electron diffraction pattern from the larger fibres but failed due to the melting/break down of the fibres under the electron beam. The initial image under diffraction mode shows good diffraction that very quickly disappears. The morphology found using TEM was confirmed by running cryo-SEM (Figure 2.8b). With this technique the gels are frozen in liquid nitrogen and imaged as the frozen material. Initial imaging first showed no obvious gel features but by slowing heating the sample (under dynamic vacuum) the frozen solvent is slowly evaporated from the surface. This revealed a gel fibre network, confirming the gelatinous morphology seen in the TEM images. This technique of removing the solvent under high vacuum and low temperature results in less surface tension from evaporation, resulting in less disturbance of the gel morphologies.

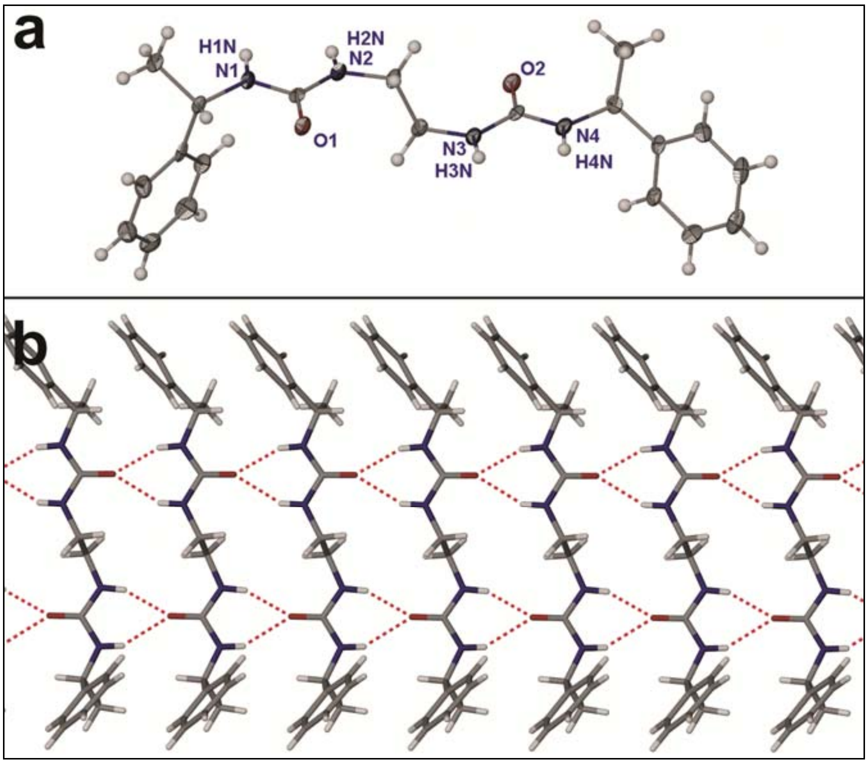

Figure 2.9. a) Ellipsoid plot of **2.1a**. Atoms shown as 50% ellipsoids with labels for atoms involved in the hydrogen bonding. **b)** Anti-parrallel urea-urea tapes formed within the structure of **2.1a**. Molecules shown in capped-stick representation. $R^1_2(6)$ hydrogen bonding shown by dashed red lines. Selected hydrogen bond distances: N1–H1N···O1 2.875(6) Å, N2–H2N···O1 2.956(6) Å, N3–H3N···O2 2.871(6) Å and N4–H4N···O2 2.939(6) Å.

Single crystals of **2.1a** were grown from 7:3 DMSO:water solution (Figure 2.3). The structure was determined using single crystal X-ray diffraction. The compound was found to crystallise in the chiral monoclinic space group $P2_1$, with the whole molecule as the asymmetric unit (ASU) (Figure 2.9a). The most obvious feature of the structure is the

$R_2^1(6)$ urea tape motif[9,52] formed by both urea substituents on each molecule (Figure 2.9b). The arrangement of the hydrogen bonding of the two urea tapes is in an anti-parallel chain. The antiparallel mode has been postulated in gels of a number of cyclic bis(ureas).[9] There is a gauche arrangement of the phenylethyl groups (Figure 2.9a). For this very short alkyl chain the two terminal C–N–C–C torsional angles are *ca.* 80^o rather than 180^o (of a perfect all-trans alkyl chain) resulting in a 'kink' in the chain. The crystal morphology is a long flat needle. This is similar to the fibre morphology seen in the gel state imaged by TEM and SEM. Face indexing the crystals showed that the growing face (i.e. the face that is growing fastest) is (010). The urea-tape packing direction is [010] and this matches the faster growing face of the crystal indicating that the urea–urea packing drives the faster growth of (010) face of the crystal. The flat longer face of the crystal is (100) and the thin face is the (001).

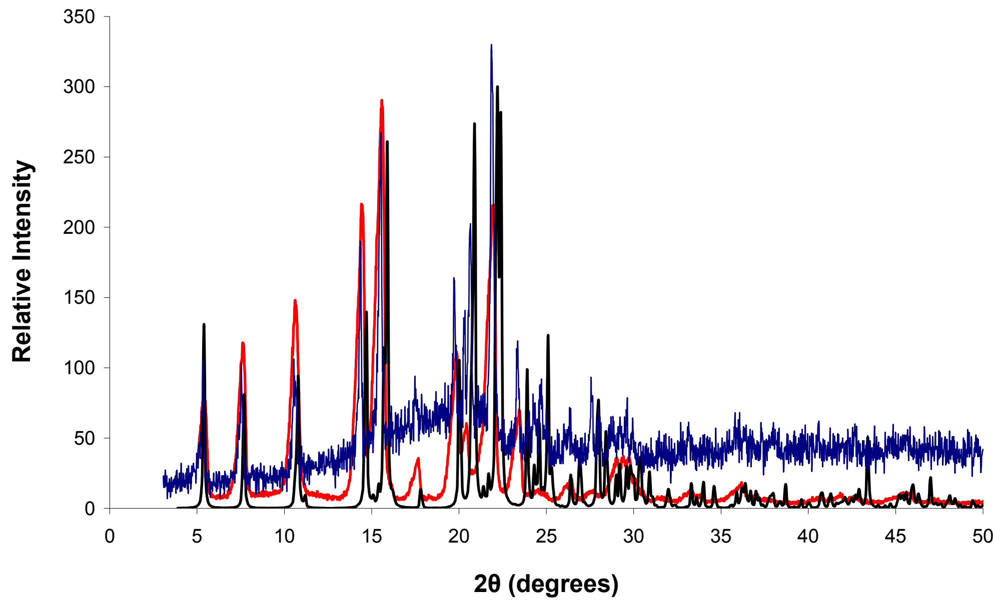

Figure 2.10. PXRD patterns of the xerogel of compound **2.1a** formed from the drying of the $CHCl_3$ gel (Blue line), drying of MeCN gel (Red line) and the simulated PXRD of the single crystal data of compound **2.1a** (Black line). The first three characteristic peaks match for all the samples. There is a systematic drift to lower 2θ values of the powder sample peaks compared to the simulated pattern due to the single crystal structure being obtained at 120K compared to the powder samples which were obtained are room temperature. Intensities have been normalised to the same scale.

The powder diffraction patterns of dried gel samples revealed that the dried crystalline material (as seen in the SEM images) has the same structure as the single crystal form (Figure 2.10). There is a variable amount of amorphous material within any particular sample (the base line of the gel sample pattern is elevated). From this crystallographic data, and taking the assumption that the structure of these fibrous crystals is the same of the fibres seen for the gel, we can take the density of the struts (ρ_s) joining junctions of a gel to be 1.262 g cm^{-3}. For a wide range of materials with a range of cellular concentrations, the formula $G' \approx 3E_s(c/\rho_s)^2/8$ holds true,[53] where E_s is the Young's modulus of the struts and c is the concentration of the compound making up those struts. The Young's modulus of the individual fibres determined using the data collected from the rheological study of the concentration of **2.1a** in MeCN can be calculated to be $E_s \sim 1.0$ GPa (+/- 0.1). This value is comparable to that calculated for other LMWGs and values associated with the macroscopic mechanical behaviour of semi-crystalline polymers.[11]

In tris(ureas), which mimic bis(ureas) in their crystal packing, the known gelator structure is anti-parallel,[54] whereas work on a tris(urea) analogue of **2.1a** (which is also a LMWG) resulted in a structure with a parallel arrangement being isolated in the presence of Cl^-.[11] The role of the anion may well be to switch the ureas from a gelling antiparallel arrangement to a crystalline colinear arrangement. If this postulated anion-induced rearrangement was the case then adding anions to gels based on **2.1a** should significantly reduce their gelling abilities according to the degree of interaction with the anion, resulting in tuneable rheology.[55] Addition of solid or dissolved excess amounts of tetrabutyl ammonnium (TBA^+) salts of varying anions to gels of **2.1a** were visually inspected to see if there had been any change. In the case of gels in MeCN, CH_3Cl, ethyl acetate, THF, acetone and Tol:MeCN the gel broke down to give a solution when at least one equivalent of F^-, Cl^-, Br^-, NO_3^- or $MeCO_2^-$ was added, either as a solid or solution. Weakly coordinating anions BF_4^- and PF_6^- had no effect indicating that the TBA^+ cation has no noticeable effect on the gel and acts as a spectator cation. Hydrogels are not affected by the addition of the anions, either in the form of TBA^+ salts or Na salts.

To test this theory of anion tuning we carried out stress sweep rheometry measurements and sol to gel temperature transition point (T_{sg}) determinations on **2.1a** in the presence of small amounts of a variety of simple anions as their TBA^+ salts, namely F^-, Cl^-, Br^-, NO_3^-, $MeCO_2^-$ and the non-coordinating BF_4^- as a control with MeCN as the solvent.

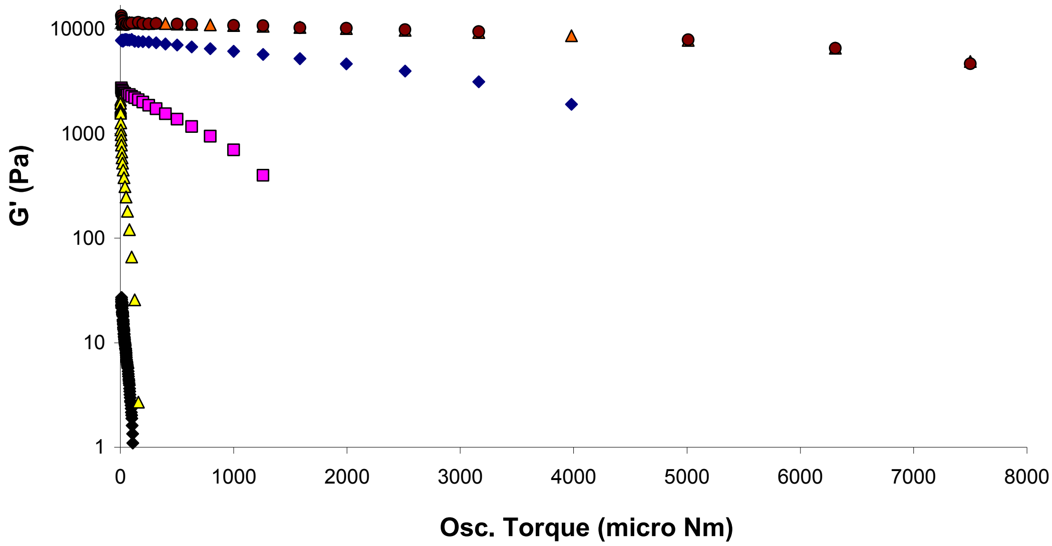

Figure 2.11. Influence of different anions (0.1 equivalents of anion added as their TBA^+ salts) on the storage modulus (G') at a frequency of 1 Hz and a temperature of 20 °C, as a function of osc. torque of the 0.3% by weight gel of compound **2.1a** in MeCN. The anions added were BF_4^- (Orange △); Br^- (Blue ◇); NO_3^- (Pink □); Cl^- (Yellow △) and $MeCO_2^-$ (Black ◇). The pure gel is represented as brown ○. F^- is not shown as it forms a liquid. G' and G'' axis values are shown on a log scale.

The addition of solids, or small volumes of dissolved anions, to preformed gels were found to give inconsistent rheological results as the breakdown of the gel was not homogenous. The most consistent results were found by predissolving both gelator and anion at a specific stoichiometry, and adding this hot solution to the rheometer. A homogenous gel would form over time. While BF_4^- had no effect on the observed storage and loss moduli (G' and G''), the other anions dramatically compromised the gel strength and greatly decreased the values of the moduli. Figure 2.11 shows that addition of small amounts of these anions (0.1 equivalents with respect to the gelator concentration) which results in the reduction in the storage modulus by up to two orders of magnitude depending on the identity of the anion, indeed addition of 0.1 equivalents of $MeCO_2^-$ and

F$^-$ totally disrupts gel formation. For a fixed concentration of gelator, such a decrease suggests a lower interconnectivity of the individual threads,[50] supporting our hypothesis that the anion disrupts the gelation process. In addition to the decrease in G', the anions cause a decrease in the "yield stress" of the gel and T_{sg},[45] also indicating a weakening of the gel (Figures 2.12 – 2.13). Increasing the amount of anion added results in the lowering of the G', G'' and T_{sg} values for the gel as revealed by temperature sweep rheometry (Figure 2.12). The sol to gel transition temperature can be defined by the when the G' and G'' values crossover, i.e. G' is smaller than G''. Hence for the samples shown in Figure 2.12, $T_{sg} = 58.5 \pm 1.5$ ^oC for when 0.1 equivalents of Cl$^-$ is added and $T_{sg} = 48.5 \pm 1.5$ ^oC for 0.2 equivalents added. The value of the osc. torque that results in a minimal, but measurable, value for G' also decreases as the anion concentration is increased (Figure 2.13), giving "yield stress" values of 794 micro Nm at 0.1 equivalents NO_3^- added to 158 micro Nm at 0.2 equivalents added to 79 micro Nm at 0.5 equivalents added. In addition to weakening the gels, time sweeps of gel formation reveal that the gel formation is slowed as generally the gels took longer to form if anions were added.

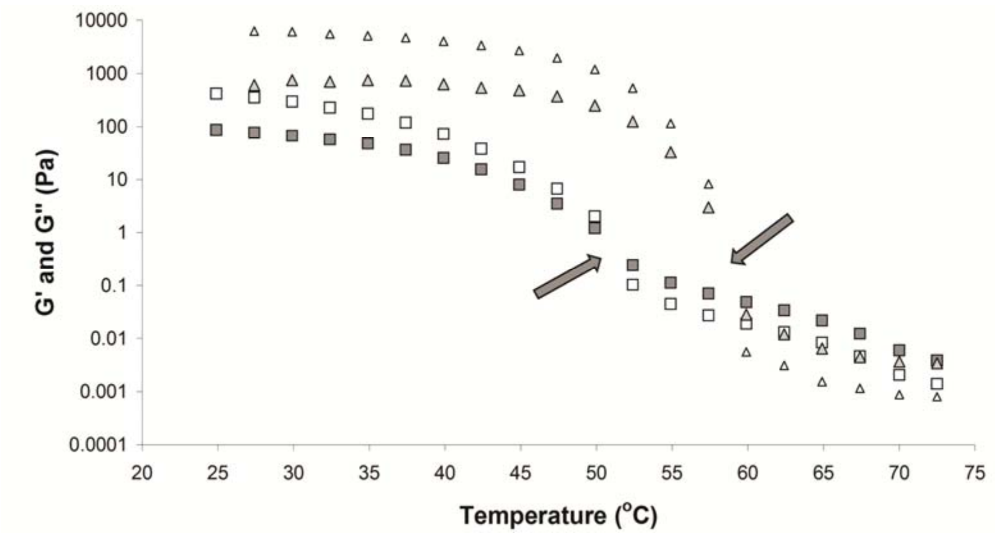

Figure 2.12. The effect of adding anion in form of TBA$^+$ Cl$^-$ on G', G'' and T_{sg} for a gel of **2.1a** at 0.3% by weight and in MeCN, as measured by varying the temperature from 70°C to 25°C. The △ symbols (G' open; G'' filled) represent 0.1 equivalents of anion added and the □ symbols (G' open; G'' filled) represent 0.2 equivalents added. Arrows indicate T_{sg} points. G' and G'' axis values are shown on a log scale.

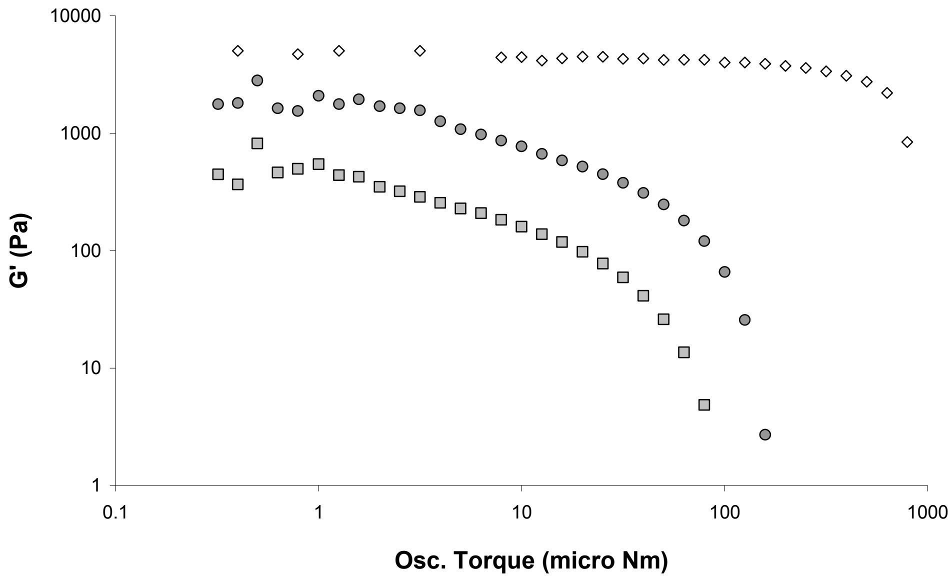

Figure 2.13. The effect of adding the anion TBA^+ NO_3^- on the storage moduli for a gel of **2.1a** at 0.3% by weight and in MeCN measured by varying the osc. torque from 10 micro N.m to 1000 micro N.m, at a fixed frequency of 1 Hz. The ◇ symbols represent 0.1 equivalents of anion added; the ○ symbols represent 0.2 equivalents added and the □ symbols represent 0.5 equivalents added. *G′* decreases as more anion is added to the gel. *G′* and *G″* axis are values shown in log scale.

As the gelator and anion are interacting in the solution state before the nucleation of the gel formation, anion binding by the gelators was probed using ^1H NMR spectroscopic titration techniques and the data were analysed using the program HypNMR[56,57] (Figure 2.14). By carrying out the titrations at 50 °C in MeCN, gelation was avoided, allowing the assessment of individual gelator-anion binding constants in the gel solvent. All titrations revealed the formation of 1:1 gelator-anion complexes. The host:guest stoichiometry was confirmed by Job plot analysis (Figures 2.15 – 2.16). Fluoride was not titrated as TBA^+ F^- occurs as a hydrate and water has a great effect on the self-association of **2.1a**. Addition of small amounts of TBA^+ F^- monohydrate breaks down the gel, but it is difficult to disentangle the effects of water and F^-. In addition to the 1:1 gelator-anion complex, the anion binding competes with the dimerisation of the molecule, an obvious precursor step to gel formation. $MeCO_2^-$ proved to be the strongest anion bound with a log β_{11} value of 4.24(1) in competition with dimerisation constant with a log β_{20} value of 3.96(1). Cl^- and NO_3^- are bound with log β_{11} values of 3.96(2) and 2.93(6), respectively, again in competition with the dimerisation process. For the BF_4^- and Br^- anions the binding was found to be too weak to determine binding strengths. The trend of the anion binding affinities in this pre-gel solution mirrors the inhibitory effect anions have on the gel formation, the gel rheology and the gel structure after forming. Thus $MeCO_2^-$, the strongest bound anion and the only one that competes effectively with solution dimerisation, has by far the most significant influence on G', G'', T_{sg} and "yield stress". This leads to the effect that the gel structure is completely broken and dissolution of **2.1a** occurs when as little as 0.05 equivalents of $MeCO_2^-$ are added to a gel. Similarly, chloride has a significantly greater effect than NO_3^- on the gel rheological properties. Therefore the order of anion binding in solution and the order of reduction in G', G'', T_{sg} and "yield stress" by addition of anions to the gels of **2.1a** are same and is $MeCO_2^- > Cl^- > NO_3^- > Br^- > BF_4^-$.

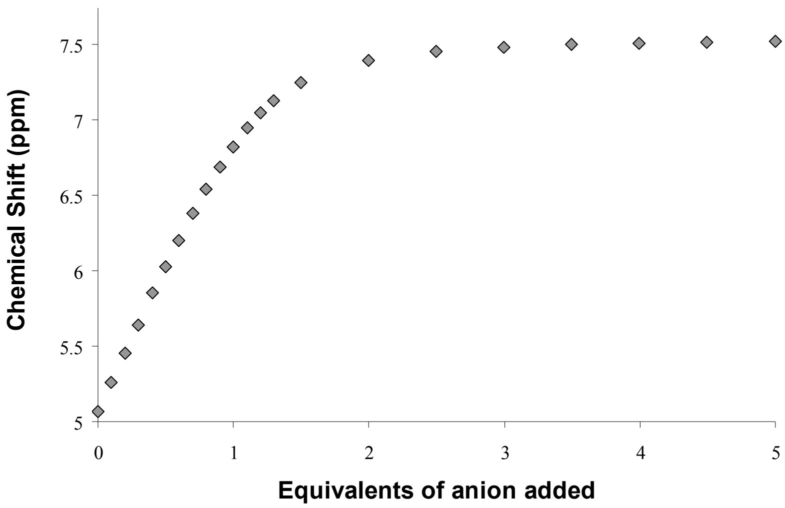

Figure 2.14. The change in chemical shift of one of the NH protons of compound **2.1a** during the titration of TBA^+ $MeCO_2^-$ done in MeCN at 50 °C from which the binding strengths of **2.1a** for the anion is determined.

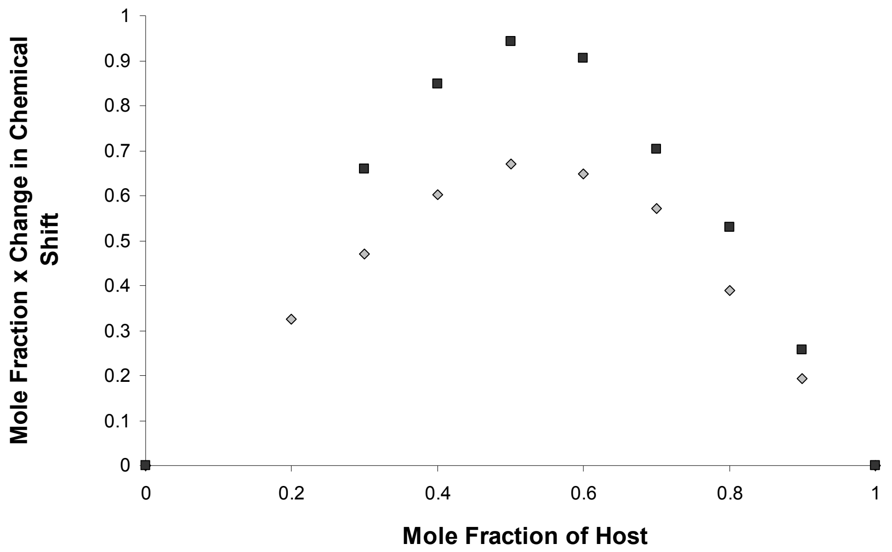

Figure 2.15. Figure showing the results of a Job Plot analysis for the binding of TBA^+ $MeCO_2^-$ by compound **2.1a** giving a 1:1 binding ratio (0.5 mole fraction of host). The two NMR signals, represented by the ◇ and □ symbols, are those assigned to the NH protons of the urea groups.

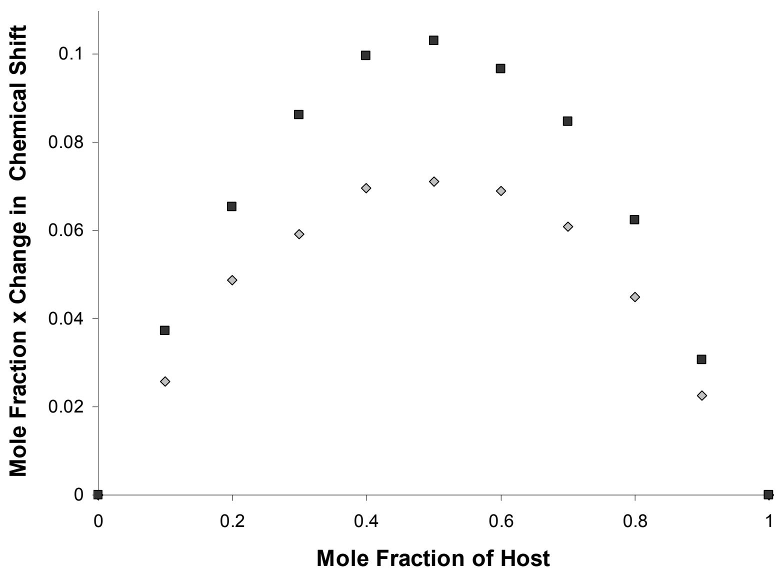

Figure 2.16. Figure showing the results of a Job Plot analysis for the binding of TBA^+ Cl^- by compound **2.1a** giving a 1:1 binding ratio (0.5 mole fraction of host). The two NMR signals, represented by the ◇ and □ symbols, are those assigned to the NH protons of the urea groups.

In summary compound **2.1a** gels a large variety of solvents. The fibre morphology is not always seen when imaged using SEM due to the crystallisation of gel upon drying, however, a fibrous gel structure is imaged using cryo-SEM and TEM. Rheological experiments identified the relationship between concentration and strength of the gels as $G' \propto [\text{conc}]^{1.8}$ which matches with the cellular solid model. The single crystal x-ray determination of the crystalline structure shows how the urea groups are hydrogen bonding together into anti-parallel tapes which provide the driving force for self-assembly into gel fibres. The gel self-association, and hence, rheology can be tuned by the introduction of sub-stoichiometric amounts of anions which compete with the self-association of the urea hydrogen bonding groups. The conjoined anions (with their TBA^+ counter ions) and molecules of **2.1a** are more soluble resulting in a shift of the equilibrium between the solid gel fibres and solution molecules from more solid to more solution. This shift in equilibrium results in weakening of the gels, and with the addition of the right quantity of anion, total dissolution of the gel results. Gel formation is also slowed by the addition of anions, as gel solutions containing anions were found to form more slowly in comparison to gels of equal strength or concentration of gelator. The degree to which anions inhibit gelation is to some extent correlated with the anion-gelator binding affinity when comparing the rheological tuning and the solution based determination of the binding between anions and **2.1a**.

2.3 Functional group orientation by variation in spacer group length between urea functionalities*

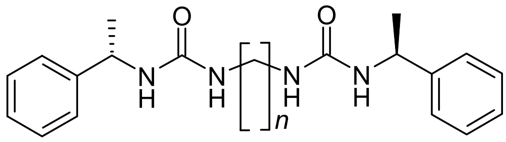

2.1a - g with *n* = 2 - 8

The seven compounds **2.1a** – **2.1g**, where the alkyl chain length (*n*) is varied from 2 – 8, respectively, are readily synthesised by reactions of the appropriate α,ω-diaminoalkane with (*S*)-(-)-α-methylbenzyl isocyanate.[55] The gelation ability of the compounds was assessed by dissolving the compounds at 1% by weight in a variety of solvents, namely MeCN, $CHCl_3$, MeOH, EtOH and solvent mixtures such as DMSO/H_2O and MeOH/H_2O (Table 2.2). The compounds **2.1e** (*n* = 6) and **2.1g** (*n* = 8) gelled $CHCl_3$ to form completely thermally reversible transparent gels at 1% weight and the compounds with **2.1a** (*n* = 2) and **2.1c** (*n* = 4) readily formed semi-transparent thermally reversible organogels in MeCN and $CHCl_3$ after slow cooling from the hot solutions. Gels for **2.1e** could also be obtained in MeCN, but were opaque, probably indicating larger (microscale) aggregates. For **2.1g** gels in MeCN could only be formed upon sonication of the compound in solution.[28] No gels were formed by the **2.1d** (*n* = 5) and **2.1f** (*n* = 7) compounds. The **2.1b** (*n* = 3) compound generally also did not form gels in any solvents, although in a few, poorly reproducible experiments, a weak gel or partial gel in $CHCl_3$ was observed. All compounds dissolved in MeOH, EtOH and DMSO and did not form gels in these solvents. Compounds with even numbered *n* were also found to gel mixtures of DMSO/H_2O and MeOH/H_2O. These gelation studies reveal that compounds with *n* = even formed gels and for *n* = odd did not (Figure 2.17).[58-63] In general sonication was found to significantly increase the rate of gelation and to improve the homogeneity of the organogels. The gel to sol transition temperatures, T_{gs}, of the even numbered compounds, as determined by the dropping ball method, decreased with an increase in oligomethylene linker length when measured at 1% by weight in $CHCl_3$.

* In collaboration with Dr. Marc-Oliver Piepenbrock. Dr. Piepenbrock performed synthesis, SEM studies and gelation studies of **2.1b – 2.1g**. All PXRD and single crystal diffraction studies performed by author.

Table 2.2. Gel formation for compounds **2.1a** – **2.1g**.

Compound	Solvents	Phase[a]
2.1a(b)	$CHCl_3$ / MeCN / DMSO:H_2O / EtOH:H_2O / MeOH:H_2O	G
2.1b	All solvents(c)	SP
2.1c	$CHCl_3$ / MeCN / DMSO:H_2O(d) MeOH:H_2O(e)	G G/C
2.1d	All solvents	SP
2.1e	$CHCl_3$ / MeCN / DMSO:H_2O(f) MeOH: H_2O(e)	G G/C
2.1f	All solvents	SP
2.1g	$CHCl_3$ / MeCN(g) / DMSO:H_2O(f) MeOH: H_2O(e)	G G/C

[a] G = gel; SP = Sol or Sol and Precipitate; C = Crystals [b] See Table 1.1 for more details [c] Occasionally forms gels in $CHCl_3$ [d] Range of 3:2 – 1:1 [e] gel + crystals mixed phases for all ratios [f] Range of 4:1 – 2:3 [g] Requires sonication for gelation to occur

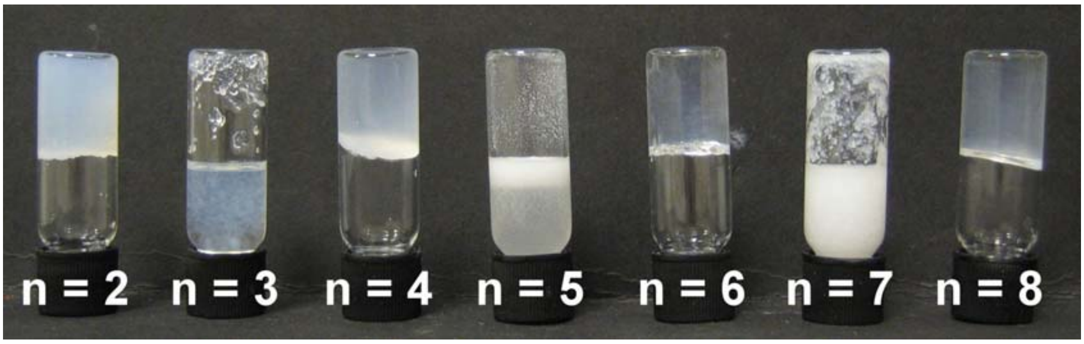

Figure 2.17. Alternation of gel (even *n*) and sol (odd *n*) formation in $CHCl_3$ by compounds **2.1a** – **2.1g**. All vials are at 1 % by weight in 2 ml of solvent.

For the even numbered spacers, the xerogels were imaged by SEM after drying under dynamic vacuum and coating with Pt, which revealed the characteristic threadlike morphology for gels from compounds **2.1c**, **2.1e** and **2.1g** (Figure 2.18). The morphology of the **2.1a** is discussed in the previous section but also shows similar threadlike morphology. The molecular chirality of the LWMG is manifested only in the gels of **2.1c** where a left-handed helical twist in the xerogel fibres is seen (Figure 2.18b).

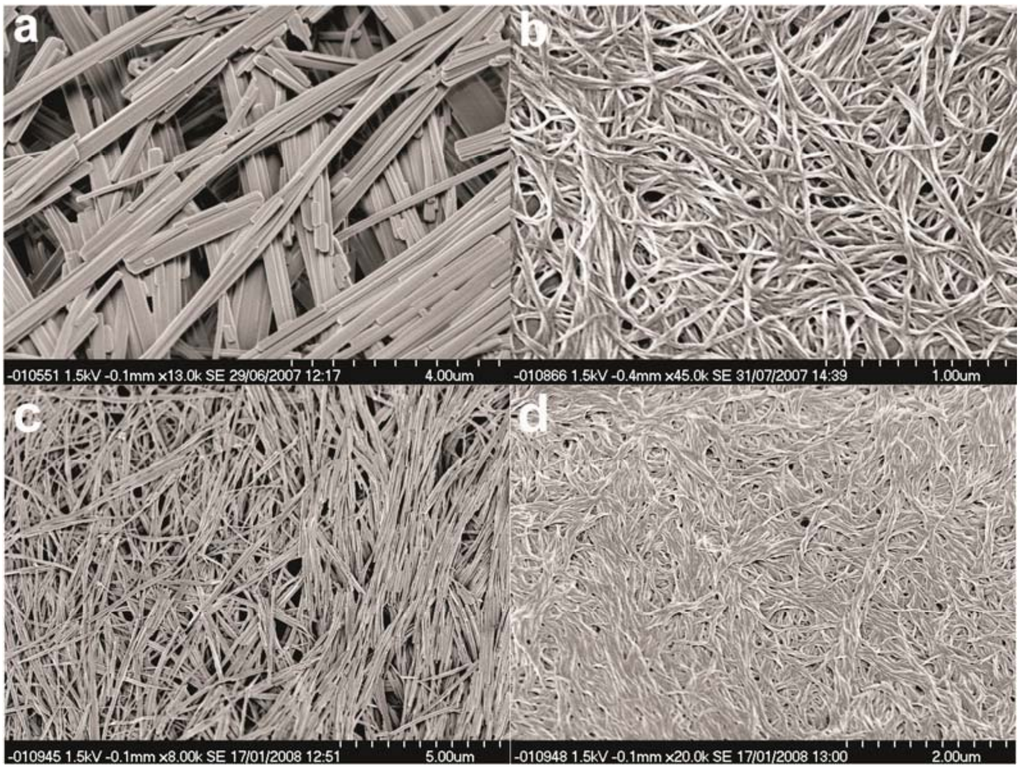

Figure 2.18. a) SEM image of the xerogel of **2.1a** gel from MeCN (solvent) showing the rod-shaped nature of the dried gel sample due to crystallisation. **b)** SEM image of the xerogel of **2.1c** gel from MeCN showing the thread-like nature of the gel fibres and the helical twist induced by the chiral gelator. **c)** SEM image of the xerogel of a MeCN gel of **2.1e** showing the brittle (more crystalline) fibrous nature of the gel fibres. **d)** SEM image of the xerogel of a MeCN gel of **2.1g**.

The n = 2, 4, 5 and 7 members of the series were characterised by single crystal X-ray crystallography. Crystals of the **2.1a** and **2.1c** compounds were obtained from aqueous DMSO, while the **2.1d** and **2.1f** samples were obtained from aqueous MeOH upon cooling of hot concnetrated solutions. In the cases of the **2.1a** and **2.1c**

(Figures 2.20) compounds PXRD measurements of xerogels showed that the single crystal structure was retained. The PXRD patterns of precipitates of **2.1e** show good crystallinity whereas the PXRD patterns of aerogels only shows marginal crystallinity. The PXRD patterns of precipitates and aerogels of **2.1g** show mostly amorphous character (Figures 2.20).

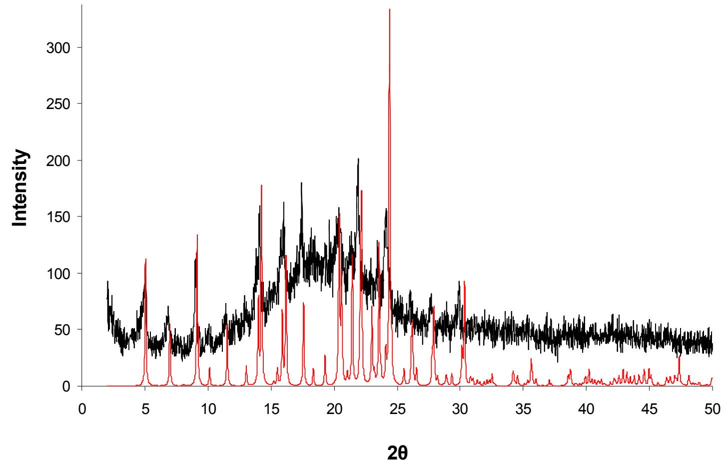

Figure 2.19. PXRD pattern of the xerogel of compound **2.1c** at room temperature formed from the drying of a $CHCl_3$ gel (Black line) and the simulated PXRD pattern from the single crystal determination (performed at 120 K) (Red line). Intensity of the simulated PXRD has been normalised to that of the xerogel.

In all cases the most obvious feature of the crystal packing is the $R_2^1(6)$ urea tape motif[5] formed by both urea substituents on each molecule (Figures 2.21 – 2.22). The structures of the **2.1c**, **2.1d** and **2.1f** materials display the expected all-trans conformations of the alkylenic chains and hence the two independent urea tapes are antiparallel for **2.1c**, whereas they are all co-aligned in the **2.1d** and **2.1f** case giving an overall polar as well as chiral structure, Figures 2.21 – 2.22. The orientation of the bulky phenylethyl groups is strongly correlated to the urea orientation because of the need to minimise steric bulk round the urea carbonyl group which acts as an acceptor for two NH donors.[64,65] This results in a gauche arrangement of the phenylethyl groups in the **2.1a** and **2.1c** cases and an anti arrangement for the **2.1d** and **2.1f** cases.

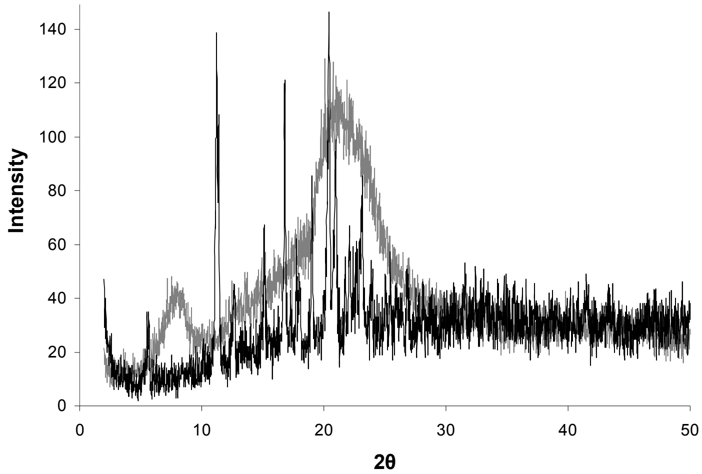

Figure 2.20. PXRD patterns at room temperature of a powder sample of the as synthesised **2.1e** from the precipitation/gel formation in the synthesis solvent $CHCl_3$ (Black line) and the xerogel of **2.1g** formed from the drying of the $CHCl_3$ gel (Grey line). Intensity of **2.1g** PXRD normalised to that of **2.1e**.

The expected packing for the *gauche* substituents should be more awkward compared to the anti substituents, however, there is little difference between these four compounds' densities. In the **2.1c** and **2.1f** cases a lower density is found (1.22 g cm^{-3}) compared to the **2.1c** and **2.1d** cases (1.26 g cm^{-3} and 1.25 g cm^{-3}, respectively). In the **2.1c**, case a less efficient packing mode is found as it crystallised in a space group with rotational rather than screw symmetry ($C2$ instead of $P2_1$).[66] The structure of the **2.1a** compound, which is also a good gelator, shows antiparallel chains for the urea tapes and a gauche arrangement of phenylethyl groups. For this very short chain, however, the two terminal C-N-C-C torsional angles are ca. 80^o rather than 180^o giving a 'kink' in the chain and allowing a higher density and more efficient packing than the **2.1c** case, in $P2_1$. Hence it is not poor crystallinity or bad packing that gives gelation but it is the antiparallel urea hydrogen bonded chains in bis(ureas) that resulted in gelation behaviour. A parallel, polar arrangement did not. The antiparallel mode has been postulated in gels of a number of cyclic bis(ureas).[9]

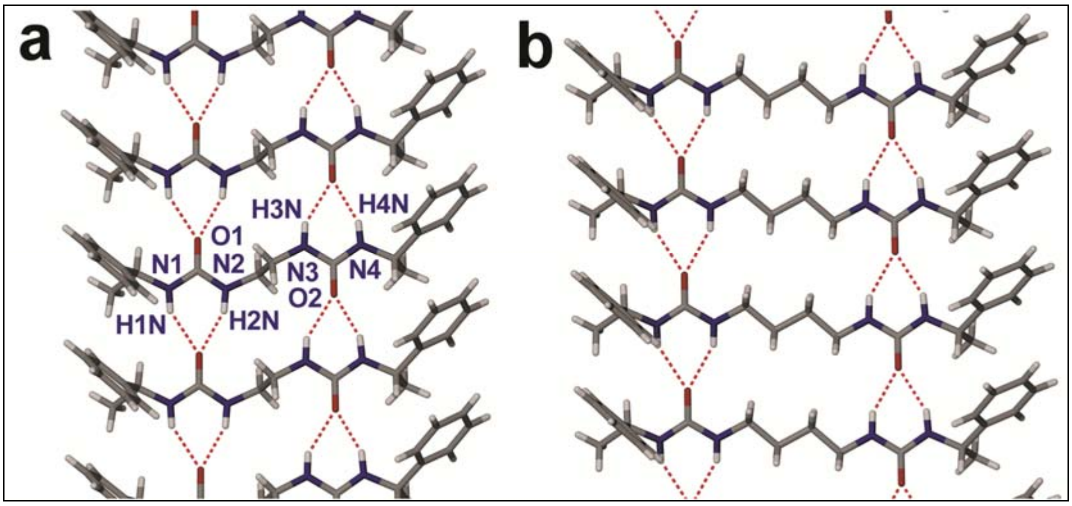

Figure 2.21. Crystal packing diagrams showing the urea tape motif of compounds **2.1a** (**a**), **2.1c** (**b**). Note how the urea tape motifs are anti-parallel and the phenylethyl groups are in a *gauche* arrangement. Selected hydrogen bond for **2.1c**: N1–H1N···O1 2.944(4) Å, N2–H2N···O1 2.923(4) Å, N3–H3N···O2 2.930(4) Å, N4–H4N···O2 2.905(4) Å.

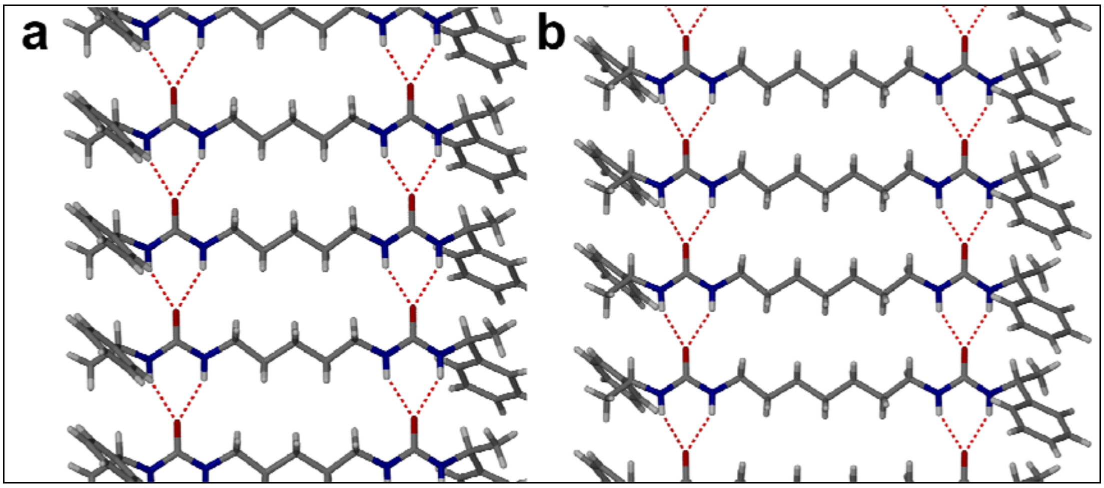

Figure 2.22. Crystal packing diagrams showing the urea tape motif of compounds **2.1d** (**a**), **2.1f** (**b**). Note how the urea tape motifs are parallel and the phenylethyl groups are in an *anti* arrangement. Selected hydrogen bonds: **2.1d** N1–H1N···O1 2.869(4) Å, N2–H2N···O1 2.939(4) Å, N3–H3N···O2 2.895(4) Å, N4–H4N···O2 2.866(4) Å and **2.1f** N1–H1N···O1 2.915(2) Å, N2–H2N···O1 2.881(2) Å, N3–H3N···O2 2.949(2) Å, N4–H4N···O2 2.886(2) Å.

When compound **2.1c** was crystallised from a MeOH:H_2O mixture a conformational polymorph was found (Figure 2.23).[67,68] Crystallisation of **2.1c** was performed by taking a room temperature concentrated solution of **2.1c** in MeOH and adding drops of water until crystallisation began. This polymorph (designated form II, with the C2 crystal form designated form I) crystallised in the space group $P2_1$. The density of form II was to be higher at 1.25 g cm^{-3} than that of form I. The $R^{1}_{2}(6)$ urea tape motif[5], formed by both urea substituents, are present once again. The two urea tapes are in an antiparrallel arrangment. The all-trans conformation of the alkylenic chain, as seen in form I, are also present in form II.

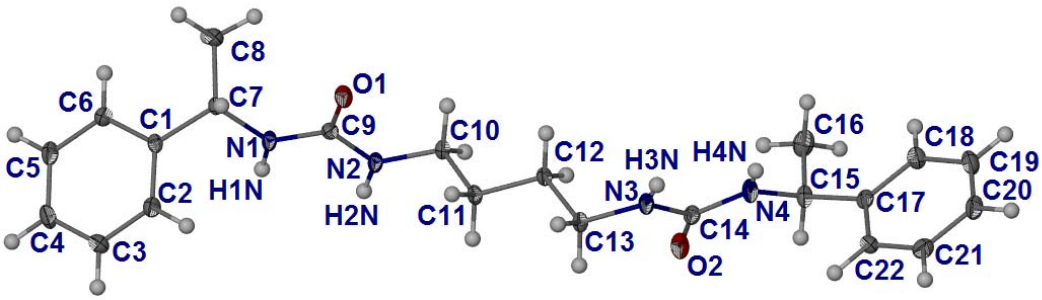

Figure 2.23. Molecular structure of **2.1c** in form II. Atoms are shown as ellipsoids at 50% probability. Selected hydrogen bonds: N1···O1^{i} = 2.8859(15) Å; ∠ N1–H1N···O1^{i} = 145.0°, N2···O1^{i} = 2.8565(15) Å; ∠ N2–H2N···O1^{i} = 143.8°, N3···O2^{ii} = 2.9111(15) Å; ∠ N3–H3N···O2^{ii} = 147.0°, N4···O2^{ii} = 2.8172(15) Å; ∠ N4–H4N···O2^{ii} = 154.8°, (*i* = 1+x, y, z and *ii* = x-1, y, z)

The significant change in the molecular structure of **2.1c** in form II compared with form I is the angle of the urea groups in relation to the all-trans alkyl chain. In form I, the C–N–C–C torsion angles are essentially linear at 171.6° and 177.2° (Figure 2.24a). In form II, the C–N–C–C torsion angles are 95.3° and -78.3° resulting in a 'kinked' molecule, similar to that seen in the structure of **2.1a** (Figure 2.24b). The phenylethyl groups are still in a *gauche* arrangement. The overall packing in form II is of a herringbone-like motif which is different to the interlocked motif of form I (Figure 2.24b).

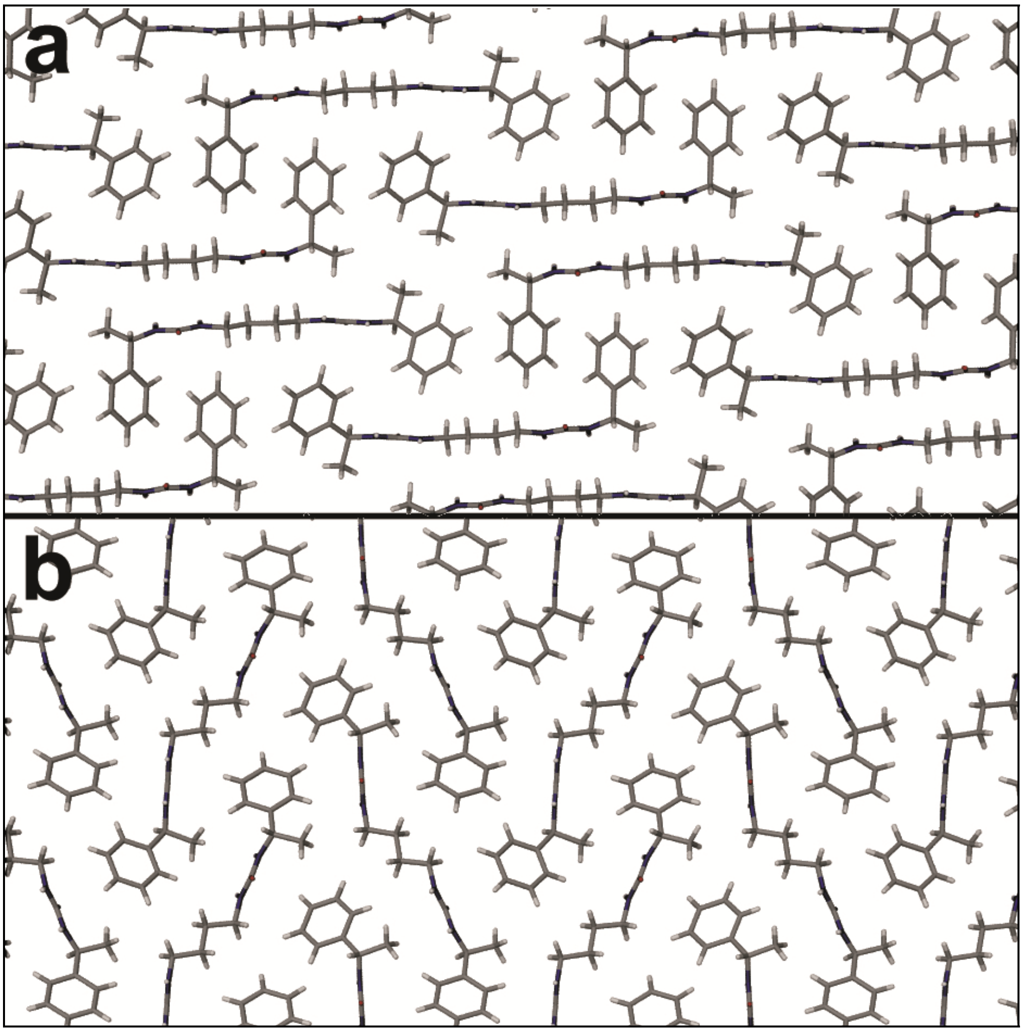

Figure 2.24. Packing arrangements of **2.1c** in **a)** form I and **b)** form II.

In summary we have shown that gelation in this series is a consequence of strong, anisotropic, multiple hydrogen bonding interactions coupled with packing difficulties perpendicular to the hydrogen bonded direction. There is a close relationship between molecular structure and hence hydrogen bonding group orientation and crystallisation or gelation tendency. Antiparallel arrangements of urea groups promote gelation while reducing crystallinity in some cases. While alternation effects are known in gels, the alternation between gelation and complete lack of gelator behaviour has not been observed previously.[58-63]

2.4 Gelation by 1-[(1*R*)-1-(1-naphthyl)ethyl]-3-[2-({[(1*R*)-1-(1-naphthyl)ethyl] carbamoyl}amino)ethyl]urea

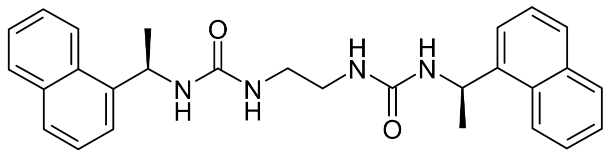

2.2

1-[(1*R*)-1-(1-Naphthyl)ethyl]-3-[2-({[(1*R*)-1-(1-naphthyl)ethyl]carbamoyl}amino) ethyl]urea, **2.2** (Scheme 2) was synthesised from the reaction of ethylene diamine with two equivalents of (*R*)-1-(1-naphthyl)ethyl isocyanate and was studied, as an analogue to compound **2.1a**, as a LMWG. Even though **2.2** has a lower solubility in most solvents, it formed gels readily in $CHCl_3$, MeCN, EtOAc and mixtures of DMSO/H_2O, MeOH/H_2O, EtOH/H_2O, Tol:MeCN (with a general weight percent range of 0.01% to 1.5% with a maximum limit due to poor solubility). Compound **2.2** showed identical gelation properties when it come to types and ratios of solvents as **2.1a** but have slightly lower CGCs. In contrast to **2.1a**, compound **2.2** showed no drying affects and the SEM images showed **2.2** to form fibrous strands (Figure 2.25). This difference could be seen by the naked eye as gels of **2.1a** are generally opaque with a fibrous crystalline nature under the microscope and gels of **2.2** were more transparent and were very gelatinous in nature. Compound **2.2** also showed helicity in the fibres which was not evident in gels of compound **2.1a** (Figure 2.26).

The behaviour of fibres of the gels formed by **2.2** when exposed to mechanical stress was investigated using rheology. The gels were characterised by time sweep (Figure 2.27), stress sweep and frequency sweep rheometry. With a number of different samples varying in both concentration and solvent used, when a frequency sweep was performed with a small amplitude stress, the solid-like nature at 20 °C was reflected in the G' being typically an order of magnitude greater than G'' thus demonstrating the elastic behaviour of the systems (Figure 2.28).[46] This viscoelastic behaviour is associated with classical gels, and therefore supports the notion that the cooling of these samples from a clear solution to a solid-like material resulted in a true gel state. In general, it was also found the gels of **2.2** were weaker than gels of **2.1a** when it came to the values of G' and "yield stress" (given that all things are equal such as weight % or concentration).

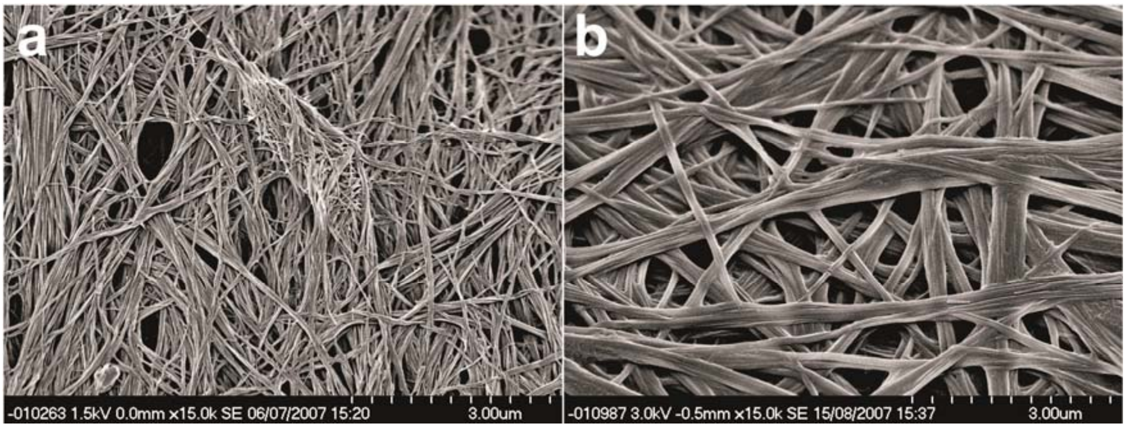

Figure 2.25. Fibrous strands of the gels formed by **2.2**. **a)** SEM image of a MeCN 0.06% by weight gel and **b)** is of a DMSO:H_2O 0.3% by weight gel. Note how the fibres are larger for the more concentrated gel (i.e. higher weight %) and how the fibres are joined together through both weaving and inter-growth of fibres.

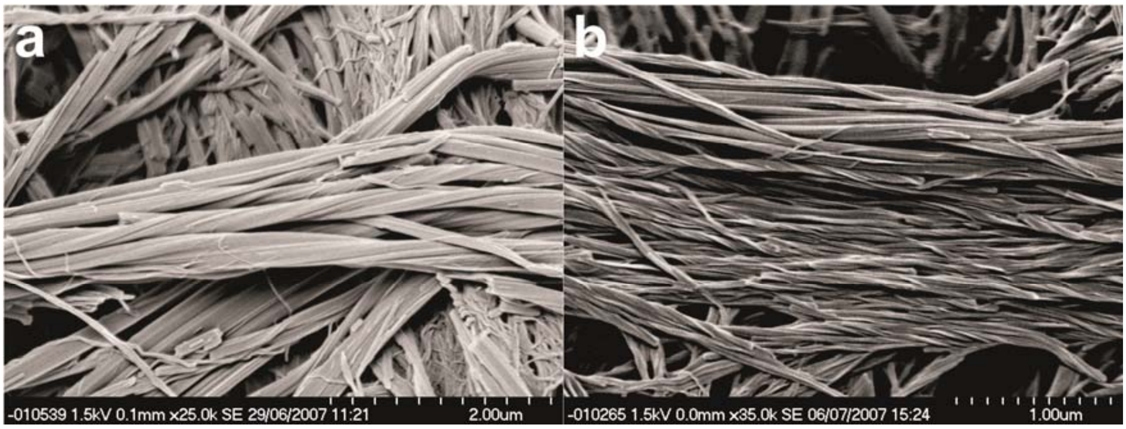

Figure 2.26. Helical fibres found within gels of compound **2.2**. **a)** is of a 0.1% by weight $CHCl_3$ gel and **b)** is of a 0.06% by weight MeCN gel. Note how the two images show two different sets of direction for the helical twist of the fibres. This indicates that the helicity direction is not determined by the chirality of compound **2.2**.

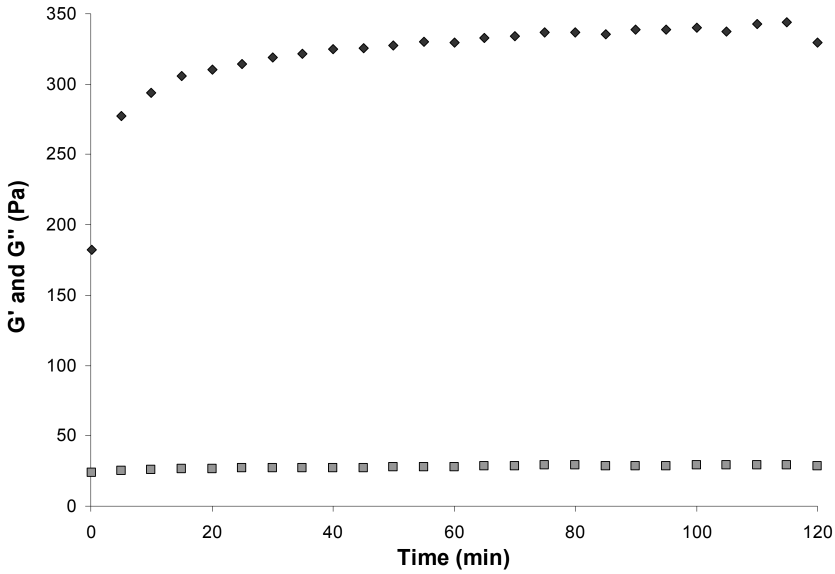

Figure 2.27. Rheology of **2.2** showing a time sweep performed on a gel of **2.2** at 0.1% by weight MeCN gel. Typically the gel's strength increases over time as shown by the increase in *G′* (Dark grey filled ◇) with time while *G″* (Light grey filled □) does not change.

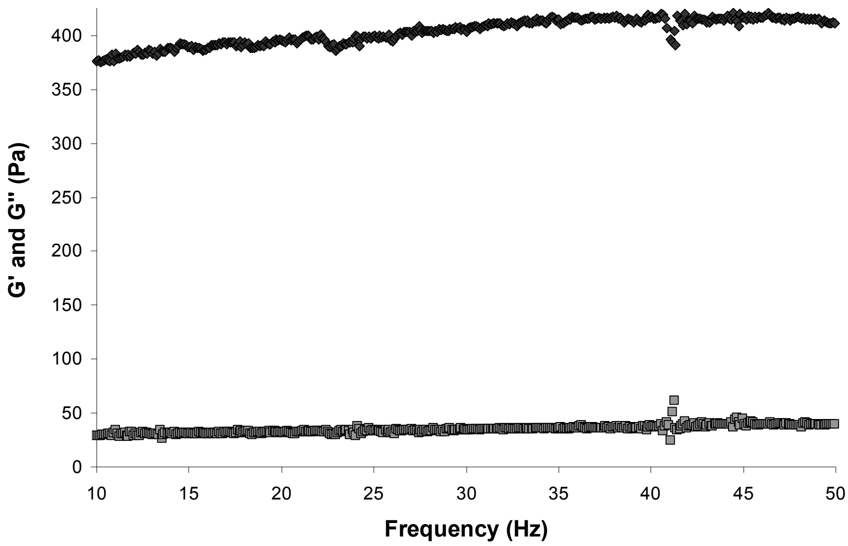

Figure 2.28. Rheology of **2.2** showing a frequency sweep performed on a gel of **2.2** at 0.1% by weight MeCN gel. Typically the consistency of the *G′* (Dark grey filled ◇) and *G″* (Light grey filled □) values over the frequency range indicates the solid-like nature of the gel material. The fact that the *G′* value is a magnitude of order larger than *G″* value, demonstrates the elastic behaviour of the gel.

The non-linear rheological response was investigated using stress sweep experiments, during which an oscillatory torque was imposed with a fixed frequency (1 Hz) over a range of shear stress amplitudes. Example gels showed a typical instrument response with the small decrease in *G′* value, essentially constant, below the critical value of shear stress, the "yield stress", until the sample started to flow providing the "yield strength/stress" value for the sample (Figure 2.29).

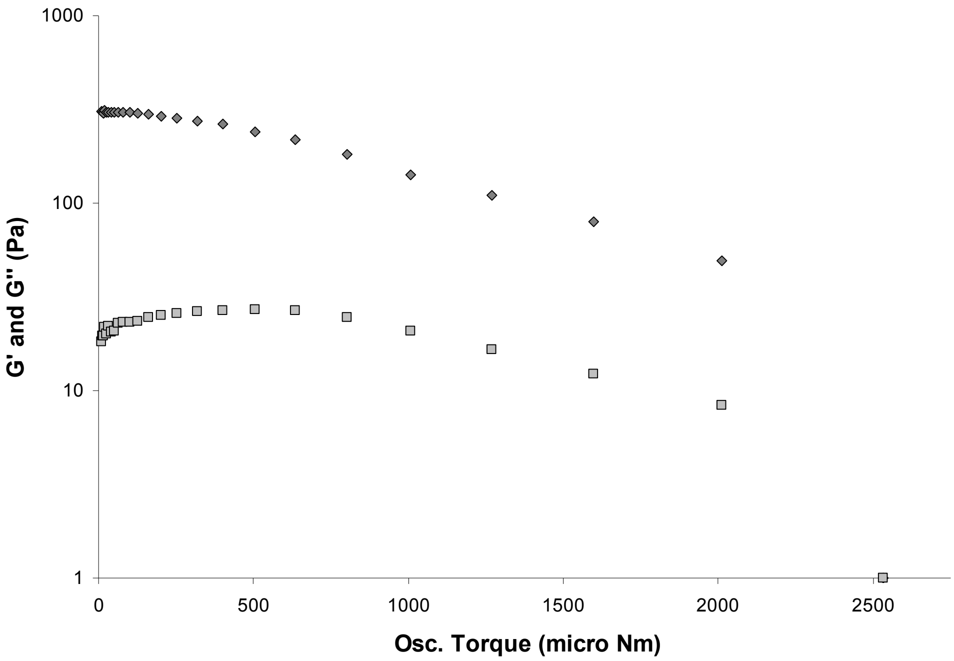

Figure 2.29. Rheology of **2.2** showing a stress sweep on a 0.1% by weight MeCN gel. The stress sweep shows the rigidity and strength of the gel, which breaks at a relatively high shear strength. *G′* value (Grey filled ◇) stayed relatively constant until the torque begins to become too strong and the struts start to break under the strain. Eventually *G′* for the samples dropped to below the *G″* value (Light grey filled □) and the sample are said to be flowing. *G′* and *G″* axis values shown on a log scale.

Unfortunately, no high quality single crystals of **2.2** could be obtained. Most often the crystallisation attempts from DMSO:H_2O and MeOH:H_2O mixtures resulted in very thin fibrous masses. As shown by the PXRD pattern of the as-synthesised compound (powder recovered from synthesis in $CHCl_3$) and the dried gels from $CHCl_3$ (xerogels) the two types of materials are crystalline and were found to contain the same peak positions and intensity ratios (Figure 2.30). The xerogels show considerable amorphous back ground scattering.

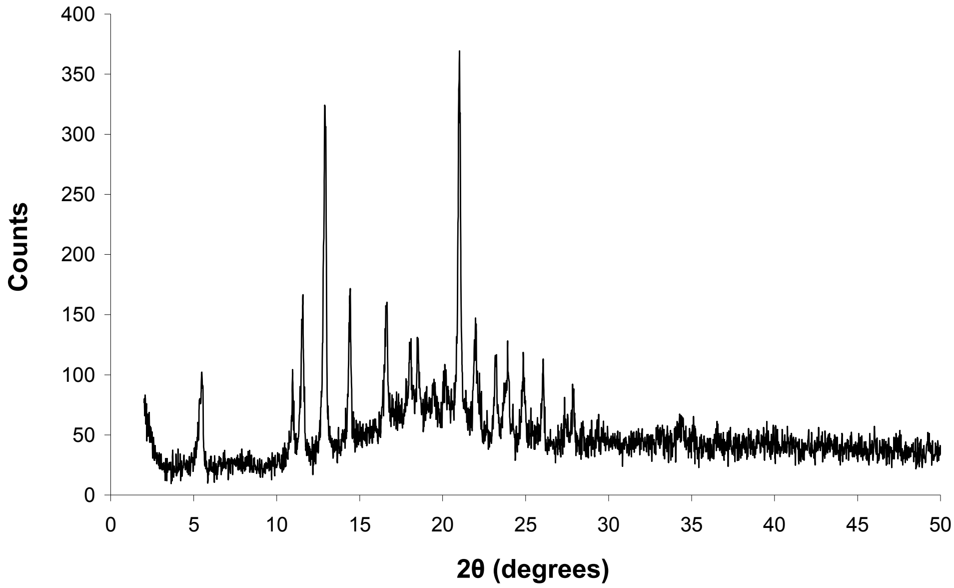

Figure 2.30. PXRD pattern of **2.2** from the as-synthesised materials.

Compound **2.2** readily formed gels in DMSO:H_2O mixtures. The gels showed thixotropic properties. Thixotropic gels are gels that lose their gel properties (i.e. begin to flow) by applying a shearing force to them, but upon removal of the shearing force the gel properties return (normally gels continue to flow once sheared). This "gel repair" property has been seen to occur in some gels but is still relatively uncommon phenomenon.[42,43,69-72] To investigate this process using rheometry a sample was allowed to gel. When the gel was found to be stable, a shear sweep was performed resulting in the breaking of the gel. The broken gel was then followed over time (Figure 2.31). The gel was shown to undergo shearing (time point 58 min, G' was measured at a lower value than G''). Upon removal of the shearing force the sample was seen to redevelop its gel characteristics with the gradual increase in G' with the G'' value staying practically the same eventually leading to a gel with a G' measurement of an approximate magnitude of order greater value than G'' but which was weaker (55% of the original G') than the originally set gel.

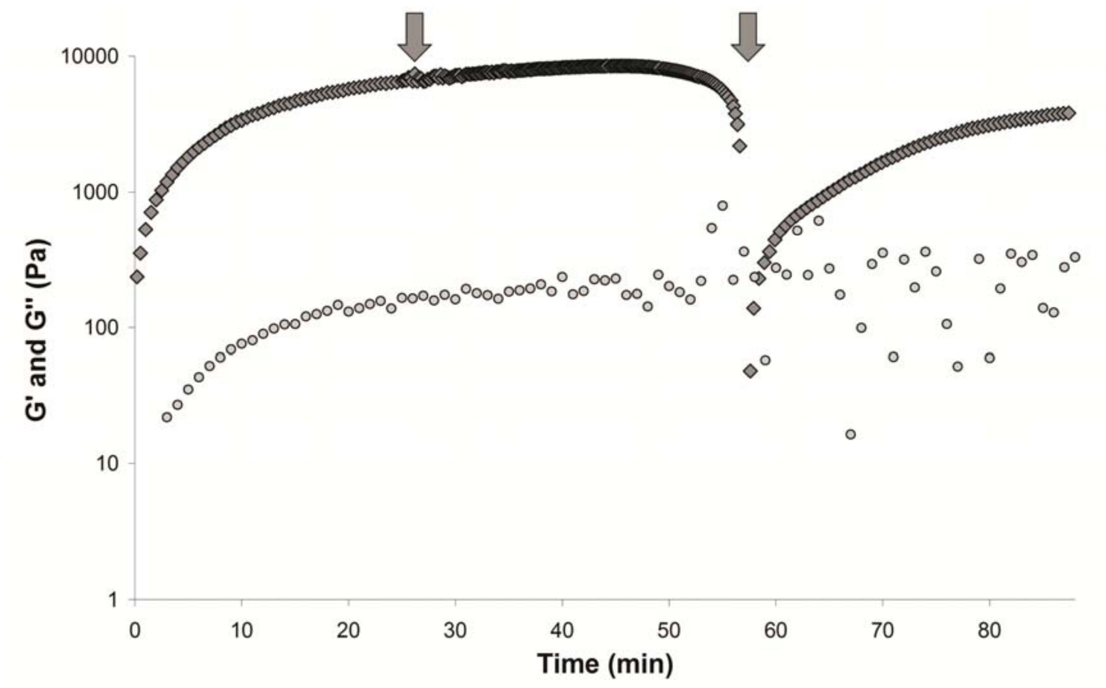

Figure 2.31. A gel of **2.2** at 0.6% by weight in a DMSO:H_2O 5:5 solvent mixture was shown to reform after being sheared to breaking point. The gel was allowed to set for 25mins upon which a stress sweep was performed from a range of 10 micro N.m to 15 000 micro N.m (Time 25.2 min to 57.4 min). The gel started to flow at around 10 000 micro N.m. Upon removal of this shear force the measurements were continued at a low frequency and stress value. As can be seen the gel reforms over time, the G' value reached ~ 55% of its original value. G' shown as grey filled ◇ and G'' as grey filled ○. G' and G'' axis values shown on a log scale.

A SEM study of the gel morphology gave good insight into how this particular gel system might be undergoing the shearing breakdown of the gel and “self-repair”. SEM imaging of a sample that has not been sheared revealed a well connected fibrous network (Figure 2.25b). Inspection of images of a sample that has been sheared and has “self-repaired”, Figure 2.32, revealed that the fibres have ends that were braided but still connect the fibres together into a network to bind the liquid in place. The liquid in this case, a DMSO:H_2O mixture, consisted of an excellent solvent for **2.2** in the form of DMSO, and H_2O, which is a poor solvent. This solvent mixture may allow for the growth and reconnection of the fibres, albeit at a small scale and formation of a weakened gel.

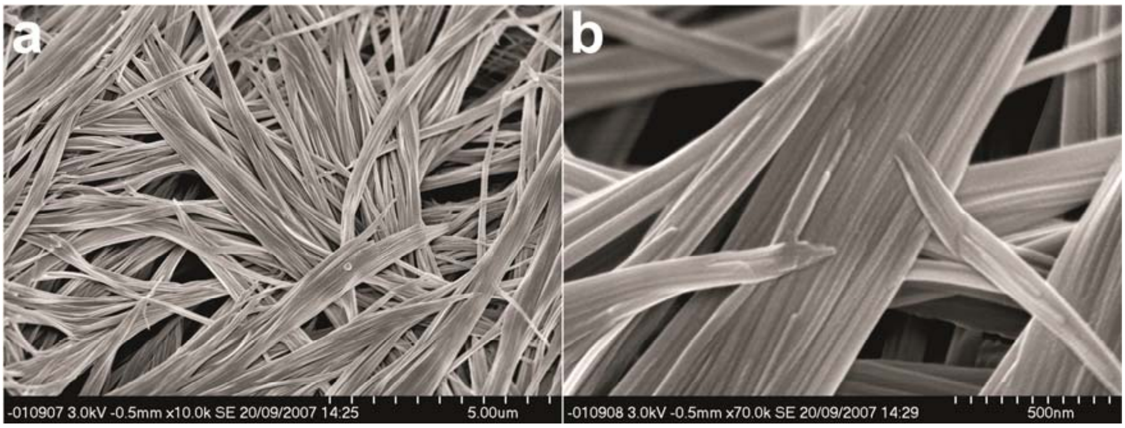

Figure 2.32. SEM images of the dried thixotopic gel formed by **2.2** in a DMSO:H_2O mixture after shearing and "self-repair". **a)** Note that the ends of fibres that join the fibres together are thinned. **b)** Close up SEM image of the areas that join the gel fibres of the thixotropic gel together. Note how the fibres join together and can be easily be broken and re-grown. The small fragile connections result in a weaker gel.

The naphthyl groups of **2.2** are a recognised fluorescent chromophore.[73] It was hoped that the gelation of **2.2** would result in a change in fluorescence of the naphthyl group allowing for determination of some of the structural details of the aggregation of **2.2**. Figure 2.33 shows the spectra found when a hot solution of **2.2** is cooled and gelation occurs. The split structural emission band (λ = 327, 335 and 353 nm) increases in intensity with a slight red shift (in the 335 nm peak) and loss of the fine structure. The aggregation of **2.2** within the gel fibres results in a restriction in the motion of the molecules and therefore reduces the non-radiative dynamic decay pathways of the naphthyl excited states resulting in the increase in the intensity (also known as the phenomenon of aggregation-induced enhanced emission (AIEE)).[74-83] The slight red shift can be attributed to the stacking of the naphthyl groups together, through π–π interactions, within the solid state of the gel (a hydrophobic environment).[84,85] This red shift in the band is characteristic of *J*-aggregation of the naphthyl groups.[74,76,86-88] In addition to this experiment, where a hot solution is cooled and gelation occurs fairly quickly, a second experiment was performed on a gel solution that was at the CGC level. Due to the gel not forming properly upon cooling the spectra do not change very much. But upon shaking the solution to initiate nucleation, and, therefore, gelation the spectra show gelation occurring with the red shift and intensity increase (Figure 2.34). This shows how important the nucleation event is for the growth of the gel fibres and the consequent gelation of the solution.

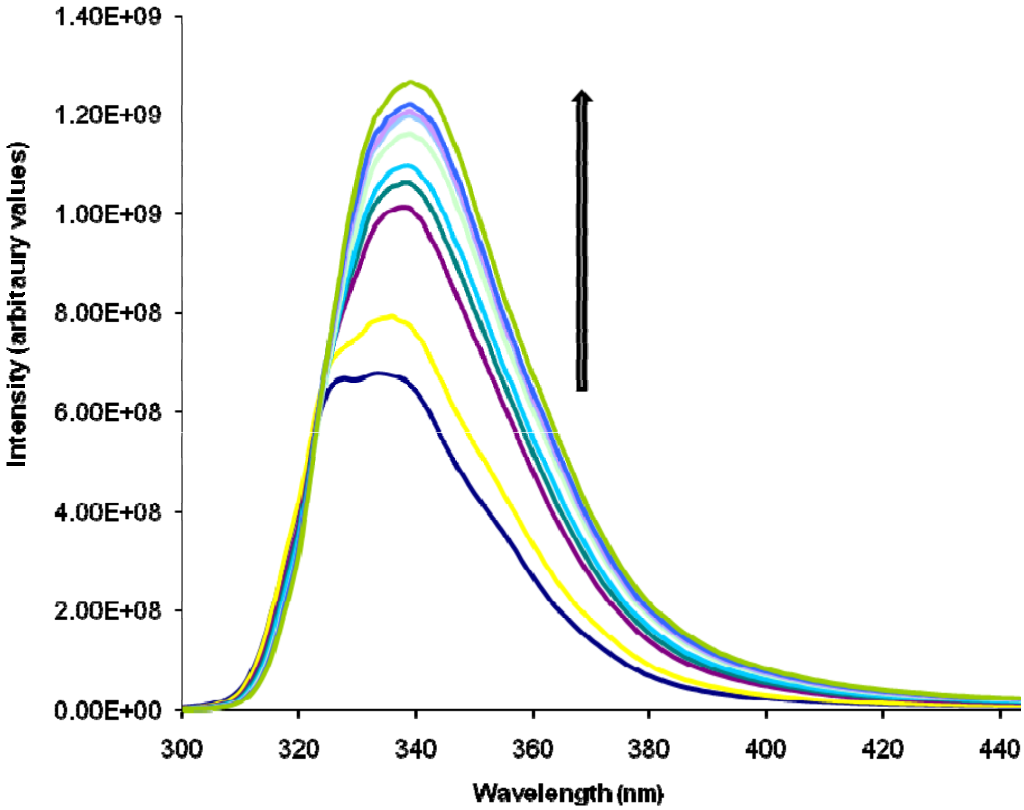

Figure 2.33. Fluorescence spectra of a gel of **2.2** at 0.06% by weight in DMSO:H_2O. The dark blue spectrum (lowest intensity spectrum) is of the hot solution. The general increase of the intensity, as indicated by the arrow, is seen as the temperature decreased. This decrease in temperature also resulted in gelation. There is also a small red shift in the band.

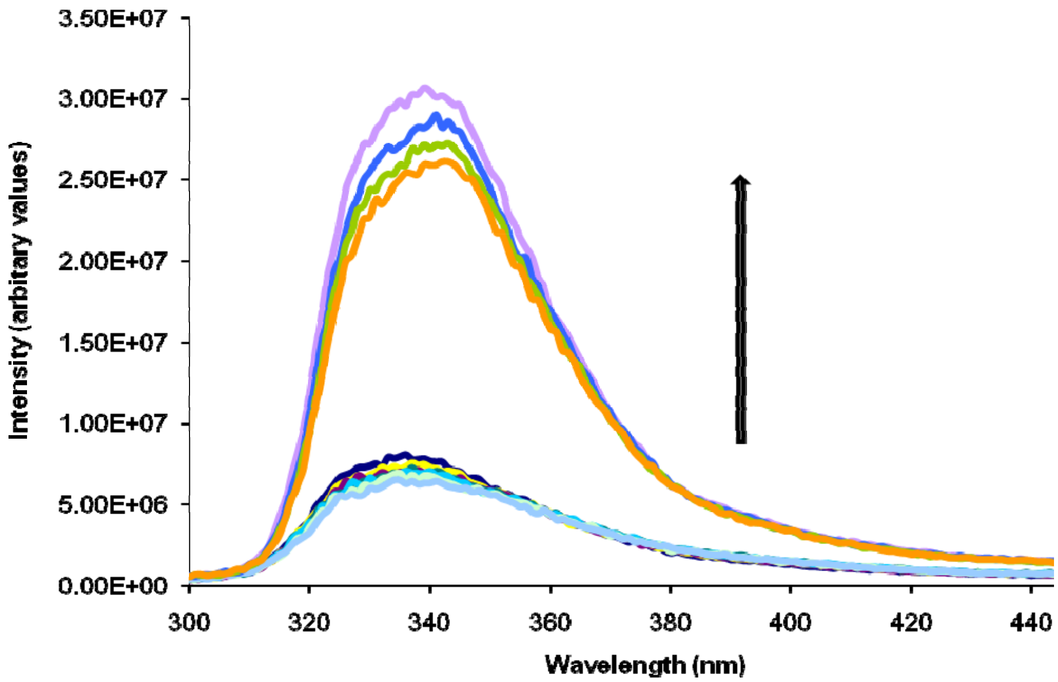

Figure 2.34. Fluorescence spectra of a gel of **2.2** at 0.003% by weight in DMSO:H_2O. The spectra do not change by much as the solution cooled. When the solution is given a shake, gel formation starts to occur and the band intensity increased (as shown by the arrow).

The anion tuning of the gels of **2.2** was also investigated. As with **2.1a** there gels show a gel to sol transformation upon addition of excess anion in the form of a TBA^+ salt, even though **2.2** is less soluble in most solvents when compared to **2.1a**. A determination of the binding of **2.2** to $MeCO_2^-$ at 50 °C in MeCN using NMR titration techniques gave binding data of β_{11} = 4.30(1); β_{20} = 2.92(10) and β_{21} = 7.63(3). The binding value for β_{11} is comparable to the β_{11} of **2.1a**. However, the dimerisation constant, β_{20}, is smaller. A two hosts to one guest complex is also evident in this experiment which contrasts with the behaviour of **2.1a**. This binding by $MeCO_2^-$ in comparison to **2.1a** should lead to comparable complex formation of **2.2** with $MeCO_2^-$ and therefore the breakdown of a gel of **2.2**. This is the case with **2.2** and is particularly evident when the tuning of gel strength is characterised using rheology (Figure 2.35). Compound **2.1a** forms gels in MeCN that can be easily "dissolved" with addition of 0.1 equivalents of TBA^+ $MeCO_2^-$. In comparison, **2.2** forms a gel in MeCN that requires a much larger concentration of anion to dissolve. One equivalent of TBA^+ $MeCO_2^-$ is required to fully dissolve the gel. This indicates that the binding strength between the host gel forming compound and the anion is not the only determining point in allowing the breakdown of these gels. The solubility of both the gel compound and the gel compound and anion complex, and the way in which the equilibrium between the solvated components and solid gel matrix is affected by these solubilities, plays a vital role in the anion tuning of these gels.

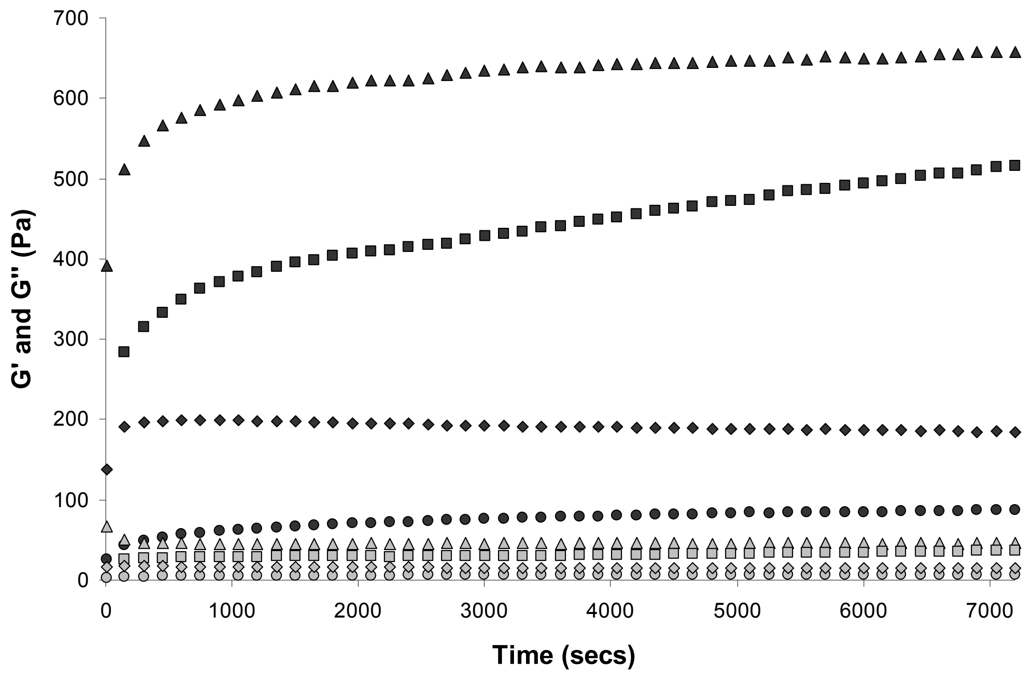

Figure 2.35. Rheological study of the tuning of gels of **2.2** using the addition of anion in the form of TBA^+ $MeCO_2^-$. Time sweep measurements were performed on gels of **2.2** at 0.1% by weight in MeCN with varied amounts of TBA^+ $MeCO_2^-$ added. *G′* represented as dark filled symbols and *G″* as light filled symbols. △ symbols are for the pure gel, □ symbols are for 0.05 equivalents of TBA^+ $MeCO_2^-$ added, ◇ symbols are for 0.2 equivalents of TBA^+ $MeCO_2^-$ added and ○ symbols are for 0. 5 equivalents of TBA^+ $MeCO_2^-$ added.

The rheological characterisation of the tuning of **2.2** by addition of TBA^+ $MeCO_2^-$ reveals how the strengths of the gels, as represented by *G′* values measured over the setting time of the gel, are decreased with increasing amounts of $TBA^+ MeCO_2^-$ added (Figure 2.35). The frequency sweep characterisations of the gels show how they are true gels. This is shown by the G' value being an order of magnitude larger than G'' and by the fact that over the frequency range measured the G' and G'' values are constant (Figure 2.36). The weakening of the gels by the addition of the $TBA^+ MeCO_2^-$ is also represented by the decrease in the "yield stress" of the gels as can be seen in Figure 2.37.

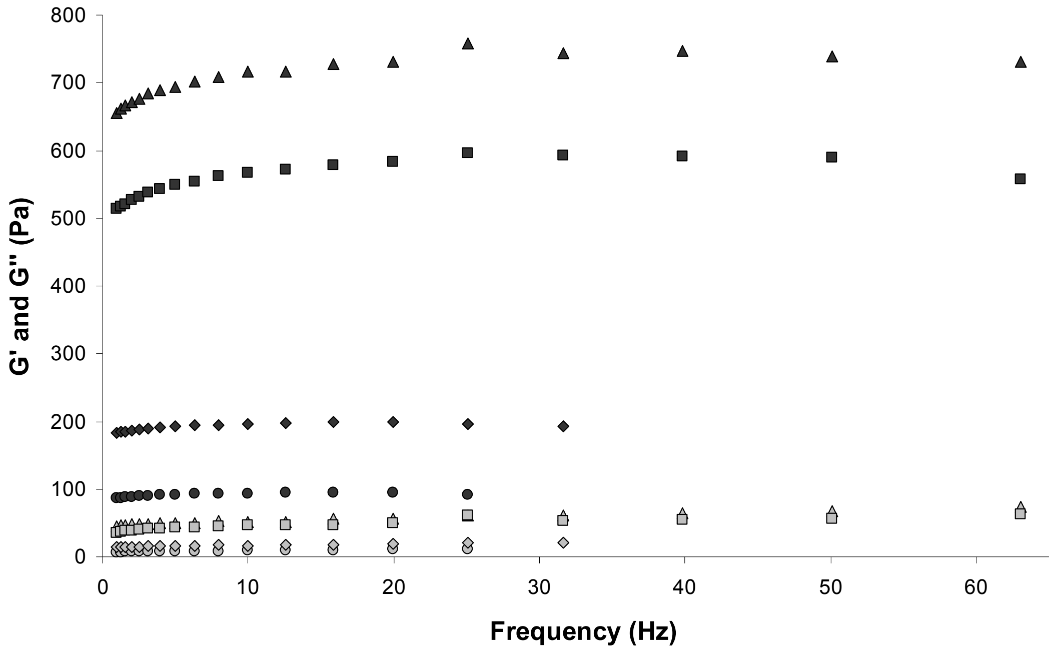

Figure 2.36. Rheological study of the tuning of gels of **2.2** using the addition of anion in the form of $TBA^+ MeCO_2^-$. Frequency sweep measurements were performed on gels of **2.2** at 0.1% by weight in MeCN with varied amounts of $TBA^+ MeCO_2^-$ added. G' represented as dark filled symbols and G'' as light filled symbols. △ symbols are for the pure gel, □ symbols are for 0.05 equivalents of $TBA^+ MeCO_2^-$ added, ◇ symbols are for 0.2 equivalents of $TBA^+ MeCO_2^-$ added and ○ symbols are for 0. 5 equivalents of $TBA^+ MeCO_2^-$ added.

In summary compound **2.2** gels a large variety of solvents and has low CGCs in most solvents (it can be characterised as a supergelator).[89] Although it forms weaker gels than compound **2.1a** (as shown by the rheology results) it shows similar gel qualities, one of them being the ability to have its rheological characteristics tuned using anion binding.

The fluorescence of the naphthyl group allows us to interpret structural details of the gel that cannot be seen using compound **2.1a**. The change in the fluorescence signal indicates that there is *J*-aggregation of the naphthyl groups within the gel fibres.

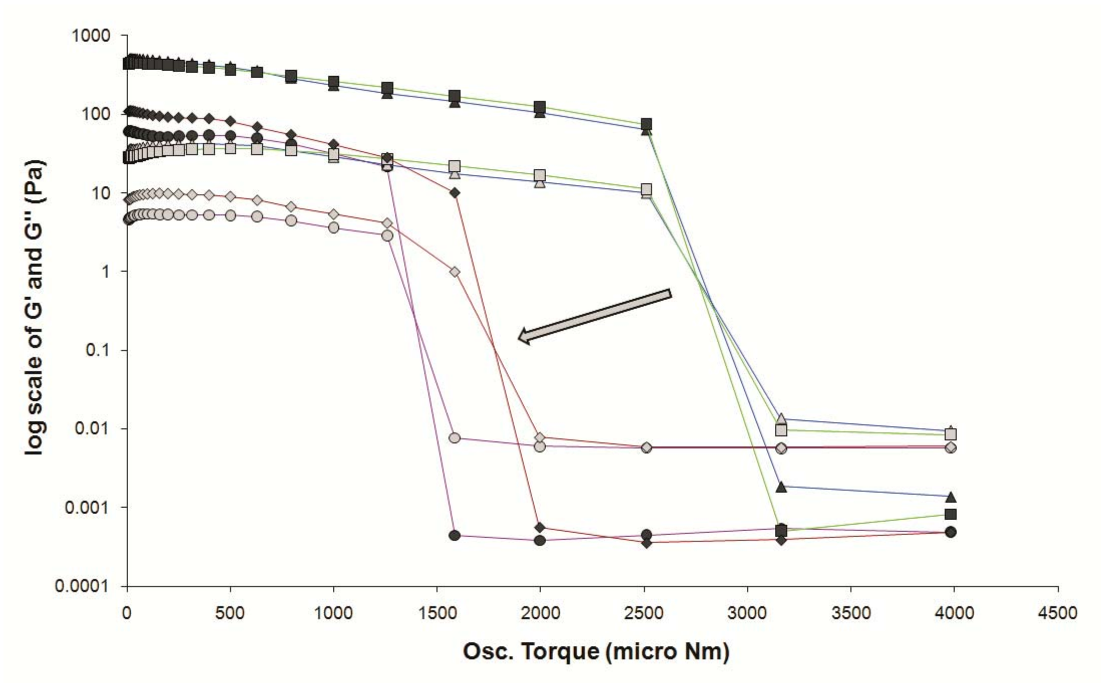

Figure 2.37. Rheological study of the tuning of gels of **2.2** using the addition of anion in the form of TBA^+ $MeCO_2^-$. Stress sweep measurements were performed on gels of **2.2** at 0.1% by weight in MeCN with varied amounts of TBA^+ $MeCO_2^-$ added. *G′* represented as dark filled symbols and *G″* as light filled symbols. △ symbols (blue guide line) are for the pure gel, □ symbols (green guide line) are for 0.05 equivalents of TBA^+ $MeCO_2^-$ added, ◇ (red guide line) symbols are for 0.2 equivalents of TBA^+ $MeCO_2^-$ added and ○ symbols (purple guide line) are for 0. 5 equivalents of TBA^+ $MeCO_2^-$ added. The "yield stress", as represented by the swapping of the *G′* being larger than *G″*, decreases with increasing equivalents of anion added (shown with an arrow). "Yield stress" values are estimated to be where the eye-guiding colour lines (linear plot between two points) intersect.

2.5 Anion Binding Study – 2-(3-{2-[3-((1*S*)-1-Methoxycarbonyl-2-methyl-propyl)-ureido]-ethyl}-ureido)-(1*S*)-3-methyl-butyric acid methyl ester

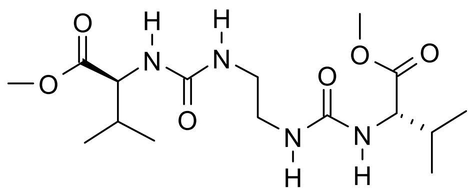

2.3

2-(3-{2-[3-((1*S*)-1-Methoxycarbonyl-2-methyl-propyl)-ureido]-ethyl}-ureido)-(1*S*)-3-methyl-butyric acid methyl ester, **2.3**, was synthesised from the reaction of methyl (*S*)-2-isocyanato-3-methylbutyrate with ethylene diamine. Compound **2.3** is soluble in most solvents and therefore did not form gels in any solvents tested. An anion binding study of compound **2.3** in $CHCl_3$ was performed to fully understand how the bisurea chiral compounds interact with different anions. Table 2.3 shows the resultant binding constants determined for compound **2.3** using the program HypNMR. $MeCO_2^-$ is bound most strongly by **2.3** with a much higher binding constant for the 1:1 (Host:Guest) complex compared to the other anions studied (the order is $MeCO_2^- > NO_3^- > Cl^- > Br^- > CF_3SO_3^-$).

Table 2.3. β values (Host:Guest) determined for the anion binding by **2.3** in $CHCl_3$.

Anion	log β_{11}	log β_{21}	log β_{12}
$CF_3SO_3^-$	0.84(3)	n/a	n/a
Br^-	1.52(4)	2.85(8)	2.63(4)
Cl^-	2.78(8)	5.42(10)	4.05(10)
NO_3^-	2.82(3)	4.70(13)	4.08(3)
$MeCO_2^-$	4.40(2)	6.75(5)	5.92(5)

This selectivity can be explained by the fact that urea groups are well-known to bind strongly to carboxylates through $R_2^2(8)$ hydrogen bonds and that the binding pocket shaped by the two urea groups of **2.3** probably matches the size of $MeCO_2^-$ well. Additionally, $MeCO_2^-$ is the most basic of the anions used. The relative size of the pocket, and therefore the presence of selectivity, is also shown by the slightly stronger binding of the NO_3^- compared to the Cl^-. The low binding constants for the 1:2 complexes indicates that both urea groups are possibly involved in the binding of the 1:1 complexes and that it is unfavourable to have an anion per urea group binding mode. The binding constants for the 2:1 complexes are interesting in that the Cl^- and Br^- complexes have comparably (to the related 1:1 complex value) higher binding constants than those of the other complexes. This pattern may be due to the size of the anions. The NO_3^- and $MeCO_2^-$ are likely to be too large and poorly shaped to receive the hydrogen bonds from two molecules of **2.3** whereas the Cl^- and Br^- are ideally shaped.[90]

The crystal structure of **2.3** was determined (Figure 2.38). Due to the steric bulkiness of the isopropyl and ester groups the urea tape motifs associated with the bisurea compounds studied so far in this report are slightly distorted (Figure 2.39). As the with the crystal structure of **2.1a**, the $R_2^1(6)$ urea tape motifs are present and are anti-parallel.[52] N4 forms an intra-molecularly hydrogen bond to O5 of the methylcarboxylate group (N4–H4N···O5 2.690(4) Å) showing how the orientation of the isopropyl groups and methylcarboxylate groups are very different on the two ends of **2.3**. This is partially the reason for the distorted urea hydrogen bonding. Similarly to compound **2.1a** the short chain results in a "kink" with the two terminal C–N–C–C torsional angles of ca. 80°. Unlike **2.1a**, the bisurea molecules are not hydrogen bonded together one on top of each other in a translation stacked one dimensional column. Each molecule of **2.3** hydrogen bonds to four different molecules via the donor and acceptor functionalities of the urea groups and the urea tapes are anti-parallel. This pattern results in a zigzag two-dimensional layer of molecules forming a two-dimensional hydrogen bonded sheet (Figure 2.40). Interdigitation of the two-dimensional layers and van der Waals interactions are the only interaction between the layers (Figure 2.41).

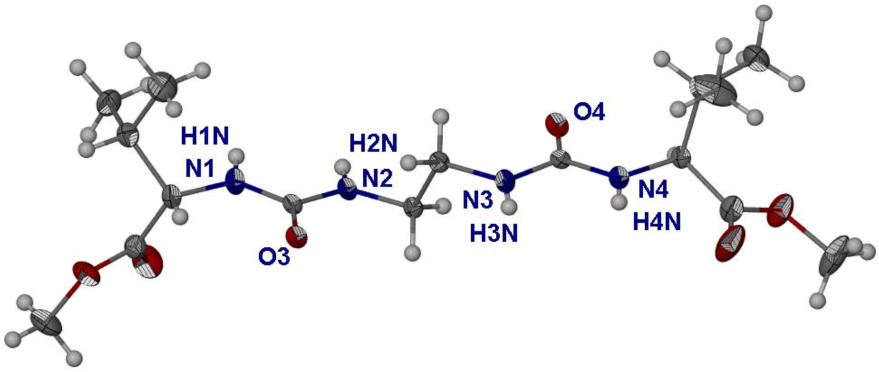

Figure 2.38. Molecular structure of **2.3**. Note how the urea groups are in an anti-parallel orientation. Atoms are shown at 50% probability ellipsoids.

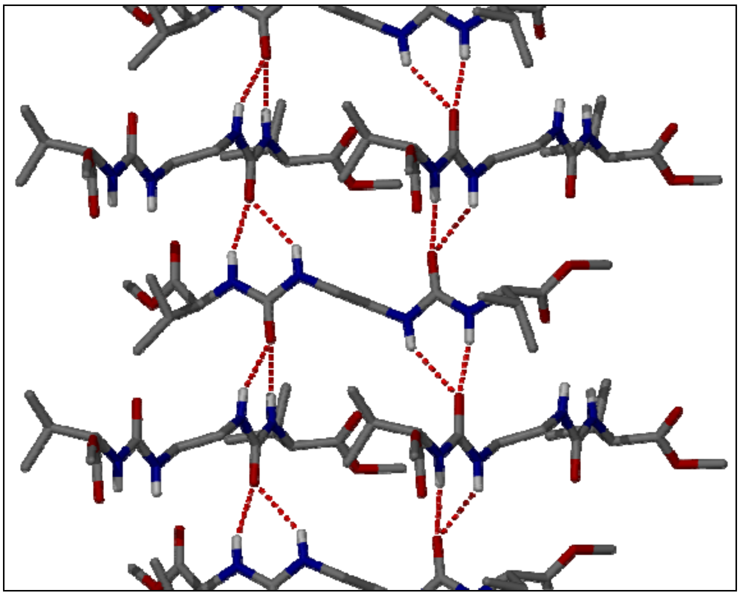

Figure 2.39. The urea tape motif of **2.3** in which each molecule is hydrogen bonded to four other molecules. C-H hydrogen atoms are omitted for clarity. Selected hydrogen bond distances: N1–H1N···O4 = 2.793(4) Å, N2–H2N···O4 = 3.056(4) Å, N3–H3N···O3 = 2.973(4) Å and N4–H4N···O3 2.933(3) Å

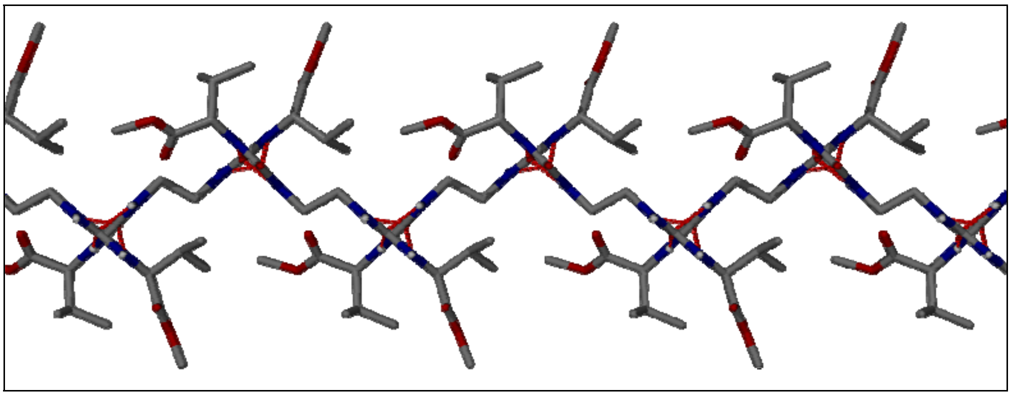

Figure 2.40. The two dimensional hydrogen bonded layer of the molecules of **2.3**. Structure viewed looking down [100]. C-H hydrogen atoms are omitted for clarity.

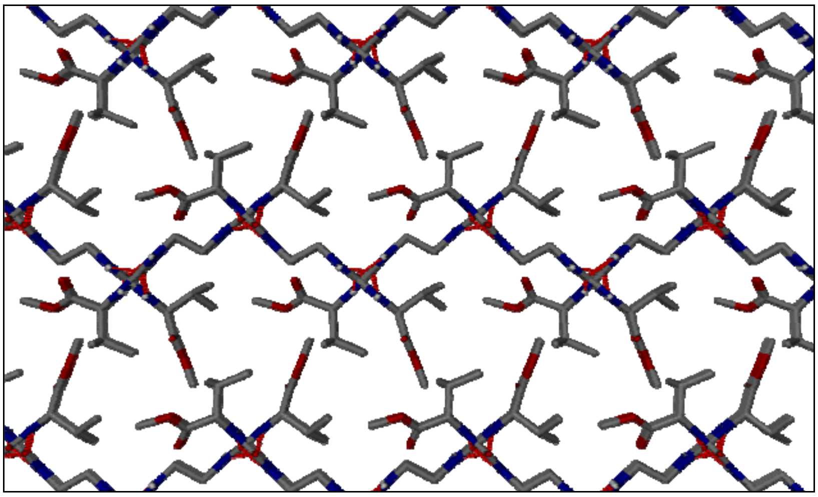

Figure 2.41. The overall packing of **2.3** as viewed looking down [100]. C-H hydrogen atoms are omitted for clarity.

In summary, compound **2.3** binds anions in a direct manner via the urea groups in a one host to one guest as well as a two guests to one host stoichiometry. There is indication that in the case of the spherical anions Cl^- and Br^- that there is enhanced binding of an anion by two hosts through a capsule-like assembly. The single crystal structure reveals that there is an anti-parallel arrangement for the urea tapes. However, the packing of the neighbouring molecules is not through translational stacking alone. Rather, rotational stacking is found which results in a two-dimensional hydrogen bonded sheet instead of a one-dimensional hydrogen bonded column. Combined with high solubility in most solvents and this alternating hydrogen bonding pattern, compound **2.3** does not form gels.

2.6 Crystal growth within LMWGs

Gel media have been utilised for over a century for controlling the growth of inorganic, organic and macromolecular crystals.[91-103] The improved physical characteristics (optical quality, improved size and fewer defects) and preferential crystallization of the more thermally stable polymorph of the gel-grown crystals over solution-grown crystals is usually ascribed to the suppression of convection currents, sedimentation and nucleation afforded by the viscous gel milieu.[94,95] It is generally accepted that the gel does not exert large mechanical forces on the growing crystal but there has been a recent increase in the understanding of the influence of chemical interactions between the gel and the molecules of the growing crystals.[96] Interestingly, LMWGs have not been reported as being used as the gel medium for crystal growth to date, despite the fact that Sangeetha and Maitra have stated in their 2005 review,[15] 'Supramolecular gels may be used as media for crystal growth'; Hamilton stated at the end of his paper of 2000 that 'we are currently investigating the use of these hydrogels to control the reactions and crystal growth within the matrix';[8] and Weiss has stated referring to LMWGs, 'They may allow novel morphs and specific sizes or shapes of crystals to be grown from the liquid component (i.e. crystal engineering)'.[104] In this section, crystal growth within gels of compounds **2.1a** and **2.2** is investigated with specific focus on the recovery of the grown crystals using the anion initiated degradation of the gel.

Three compounds were chosen for crystal growth within LMW gels. They were 1,3-bis(*m*-nitrophenyl)urea (NPU), carbamazepine (CBZ) and aspirin (ASP). All these compounds have been crystallised before and show polymorphism. 1,3-Bis(*m*-nitrophenyl)urea has similar functional groups to the two gelators **2.1a** and **2.2**.[105] Carbamazepine is a well studied drug compound that shows excellent crystallinity and polymorphism and with its hydrophobic and hydrophilic functional groups it also should interact well with the gelators.[106-111] Aspirin was also chosen as a drug compound which shows very little change in its structural crystallography in terms of polymorphism (there are two possible polymorphs) and habit growth.[112-116]

2.6.1 Aspirin

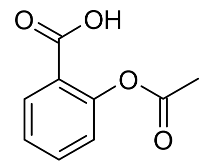

Asp

Aspirin (Asp) is a very well studied compound.[112-116] There are two known polymorphs. In the gel crystallisations, 2 ml gel with 100 mg of Asp at 0.3% by weight gelator in MeCN, crystallisation was found to have occurred after one week (Figure 3.42). Asp was found to crystallise in the most common form in all five experiments but of most interest is the manner of crystallisation. An equally concentrated solution of Asp in MeCN was found not to crystallise even when it is prepared at the same time and cooled at the same rate and subjected to sonication. This indicates that gel can be used to induce crystallisation by providing nuclei for crystal growth initiation.

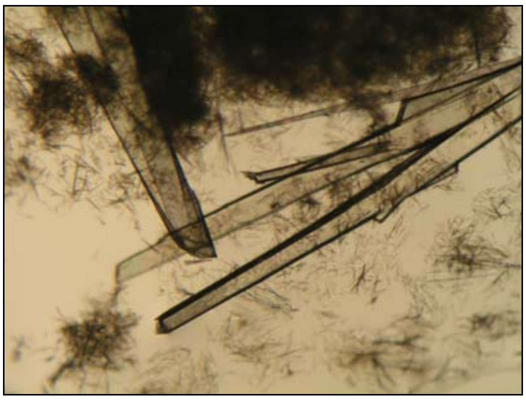

Figure 2.42. Photograph of the Asp crystals grown from a 0.3% by weight gel of **2.1a** in MeCN through a microscope at x40 magnification. Note the visible gel fibres that have been broken by smearing some of the gel that contains the crystals on a microscope.

2.6.2 1,3-Bis(*m*-nitrophenyl)urea

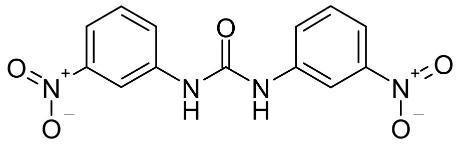

NPU

Three concomitant polymorphs of NPU were originally reported in 1899 and summarised by Groth a few years later.[105,117,118] More recently both Etter and Bernstein have studied this compound.[105,119,120] Bernstein in particularly showed that there are three polymorphs, designated as α, β and δ, and a hydrate which is more than likely the form designated as γ in the 1899 and Groth papers (Table 2.4).[105] Even though these studies have revealed a lot about the chemical crystallography of this compound it appears that there is no reliable means to obtain all of the pure states, i.e. control the crystallisation of a particular form. Slurry methods and fast cooling from a supersaturated acetic acid solution were found to be effective at producing pure β form but no other means were found to produce the other phases or the hydrate. For this reason this compound seemed well suited for testing crystallisation with LMWG based gel media.

Table 2.4 Crystal forms of NPU.

Form	Space Group	Habit Form	Stability	Pure Crystallisation Method
α	Monoclinic $P2_1/c$	Yellow Prisms	3	No means
β	Monoclinic *C2*	White Needle	1	Acetic acid slurry
δ	Monoclinic $P2_1/c$	White Needle	2	No means
γ (Hydrate)	Monoclinic *C2*	Yellow Plates	n/a	No means

Crystallisation from MeCN, EtOAc, $CHCl_3$ and MeOH:H_2O gels resulted in no control over crystal form. Often the yellow prism α form was found at the air/gel interface and the white needle β form within the gel matrix in $CHCl_3$, EtOAc and MeCN cases (characterisation of the form was done by determining the unit cells of several single crystals picked from the samples and visual characterisation by colour and morphology). Interestingly in the case of EtOAc the crystallisation from pure solvent in the absence of gel produced β form with plate morphology and from the gel a β needle morphology.[96,99,121] The hydrate form was mostly found in the case of the MeOH:H_2O gels but white needle, β form, crystals were also isolated. Testing the recovery of the crystals by adding anions to the gels resulted, unfortunately, in dissolution of not just the gel but also the crystals in the cases of gels in MeCN, EtOAc and $CHCl_3$. The gels and crystals of NPU in MeOH:H_2O were unaffected by the addition of anions. NPU interacts with anions, as highlighted by the $\beta_{11} = 3.67(10)$ for $MeCO_2^-$ in MeCN determined using the technique of NMR titration and the program HypNMR, [56,57] and the host:anion species was more soluble in the solvents used therefore leading to the rapid dissolution of any crystalline material.

2.6.3 Carbamazepine

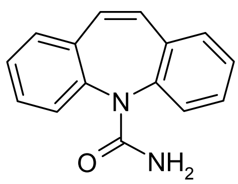

CBZ

Carbamazepine serves as a model compound for many groups engaged in the study of crystal polymorphism.[106,107,109-111,122] For this reason CBZ seemed ideal to test against crystallisation within our gels. CBZ, an anticonvulsant, crystallises in four known anhydrous, solventless forms (although the trigonal form could contain some solvent). Recently a fourth form was discovered that is grown by using polymer heteronuclei to induce the growth of this polymorph.[107,108] Table 2.5 below shows the relevant details of the different forms.

Table 2.5. CBZ polymorph characteristics

Form	Space Group	Habit Form	Stability	Crystallisation Method
I	Triclinic $P\bar{1}$	Needle	2	Melt
II	Trigonal $R\bar{3}$	Needle	4	Rapid cooling (5 ^{o}C) from EtOH
III	Monoclinic $P2_1/c$	Equant	1	Slow cooling (25 ^{o}C) from EtOH
IV	Monoclinic $C2c$	Prism	3	Polymer induced heteronucleation in MeOH

Crystallisations were attempted in $CHCl_3$, $MeOH:H_2O$, EtOAc, $(CH_3)_2CO$ and Tol:MeCN (9:1) gels. No gels of **2.1a** or **2.2** could be formed in $CHCl_3$ as CBZ retarded gel formation highlighting that there is interaction between the two compounds. The other solutions formed gels and crystallisation occurred (Table 2.6). The crystals were recovered, when crystallisation had occurred, by the addition of anions, namely adding at least five equivalents of TBA^+ $MeCO_2^-$ to dissolve the gel. This allows for the recovery of crystals without the use of mechanical separation, except in the case of the $MeOH:H_2O$ gels where addition of anions does not lead to break down of the gel, due to solvation of the anion. Acetone gels containing 50 mg of CBZ were found to contain crystals after a couple of weeks whereas parallel experiments in pure solvent did not. This is likely to be due to the large number of heteronuclei present within a gel sample compared to a solution based sample. Even though there are a large number of heteronuclei it is interesting to note that in most cases only a single large crystal was found to have grown within a gel sample. These large single crystals were found to be the acetone solvate form of CBZ. These crystals give a good example of the ease of recovery of the crystals by digestion of the gel using the addition of anions (Figure 3.43). The acetone crystallisation of CBZ in gels shows how the gel can induce crystallisation at lower concentrations than the level required for pure solvent crystallisation.

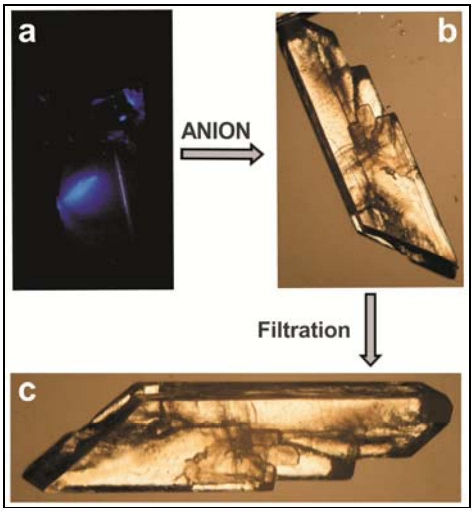

Figure 2.43. Pictures showing the result of crystallisation of CBZ from the gel state from acetone as a solvent resulting in a large single crystal of the acetone solvate of CBZ and its isolation from the gel by using the reversibility of the LMW gel. **a)** A photograph under UV irradiation of the vial containing the gel to highlight the crystal from the gel as the crystal was luminescent and the gel was not. **b)** The large single crystal forms within the gel which stays intact when anion in the form of TBA^{+} $MeCO_2^{-}$ was added to dissolve the gel to form a clear solution. **c)** The crystal was then easily separated for use.

Crystallisation of CBZ in MeOH:H_2O (8:2) gels of **2.1a** and **2.2** at 0.1% by weight containing 50mg of CBZ, and crystallisation from solvent without gel at the same concentration of CBZ, were found to give identical results. Crystals mechanically separated from the MeOH:H_2O gels were found to be the monohydrate form of CBZ and were similar in size and shape to those from the pure solvent crystallisation.[111,122] Crystallisation from EtOAc gels of **2.1a** and **2.2**, 0.1% by weight and 50 mg CBZ, resulted in the isolation of CBZ in form III. In the pure solvent crystallisations it was found that mixtures of block-shaped form III and needle-shaped form II formed when identical concentrations and cooling, compared to the gel crystallisations, were used. This is an example of how gel crystallisation can result in the more thermally stable polymorph being formed.[92,99] Although crystallisation from EtOAc often resulted in form III, if the cooling was rapid, form II was formed, as was often seen in these examples at the cooling rate and concentrations employed experimentally. Greater control of the habit and size of the crystals formed was found when utilising gels of a Tol and MeCN mixture. From a solvent crystallisation it was often found that the crystals were mostly of form III with occasional crystallisation of needles of form II. In the gel crystallisation, the more thermodynamically stable form III was found to crystallise in all cases. Some of the crystals showed different morphologies to the normal equant shape and were elongated block shaped.[96,99,121] It was found that these crystals were twinned explaining their different morphology.[123,124]

Table 2.6. Gel crystallisation results for CBZ in gels of compound **2.1a** and **2.2**.

Gel solvent[a]	Crystal forms in pure solvent[b]	Crystal forms from gel[b]	Habit from gel compared to solvent
$MeOH:H_2O$[c]	Dihydrate	Dihydrate	Identical
Ethyl Acetate	II leading to III over time	III	Same equant shape but larger in size
Acetone	No crystals[d]	Acetone solvate	n/a
$CHCl_3$	n/a	No gel formation	n/a
Tol:MeCN	III with some II	III (some crystals are twinned)	Same equant shape but larger in size[e]

[a] gels are at 0.1% by weight and 2 ml in volume. [b] Crystallisation was performed in a sealed 12 ml glass vial. Crystallisation performed at the same concentration, heating and cooling rates for samples of gel and pure solvent. Small variations were expected between the different solvents. [c] Crystals not retrieved by dissolving the gel with anions. [d] Crystallisation of the acetone solvate structure occured upon further super-saturation either by concentrating by evaporation or addition of more CBZ [e] Twinned crystal was different in habit, an elongated block shape.

In summary it was found that the crystallisation within gels formed from LMWGs could influence the crystallisation results of the three compounds studied. More importantly because of the ease with which LMWGs were be tuned, allowing for the recovery of the grown crystals by chemical decomposition of the gel fibres and without use of mechanical force (other than filtration), grown crystals were retrieved by simply dissolving the gels using the addition of anions. Of the three compounds tested using this crystallisation method, CBZ and Asp showed signs of enhanced crystallisation within the gel state. This is probably due to the high number of heteronuclei present within a LMW gel, which is not necessarily seen in the case of other forms of gels.[94,95] Interestingly, the opposite effect was also clear. In cases where prevention of convection currents and rapid nucleation by the formation of the gel were seen, fewer crystals grew in comparison to when a pure solvent mixture was used and found to be super-saturated upon which rapid crystallisations occurred.[94,95] Crystallisation from these LMWGs gels often led to the thermodynamically more stable polymorph being isolated from the gel state where commonly from pure solvents often both thermodynamic and kinetic forms are found.

2.7 Drug release from LMWGs

Gels are a well recognised means of controlling drug release.[125-131] LMWGs are now becoming an important medium for the release of drugs as they can represent a means of controlling the interaction of the drug with the gel and the controlled release of the drug, as most LMWGs can be tuned by external stimuli.[16-27] The fact that compound **2.1a** can form very stable hydrogels (albeit with a small amount of polar organic solvent present) and that the gels have been shown to be tuneable by the addition of anions, it was decided that this LMWG could act as media for controlled drug release.

Ibuprofen (IBU, as its sodium salt) was chosen as the model drug to be studied in the release studies from these gels. A gel of 1 ml in EtOH:H_2O, at a ratio of 3:7 at 0.3% by weight gelator and containing 10 mg of IBU was chosen as the ethanol represents a non-hazardous solvent (unlike DMSO and MeOH) and this gel is easily moved from the gel preparation vial into a cuvette for UV spectroscopic experiments. Once in the cuvette, a 3 ml layer of water was introduced into which the IBU could diffuse. Below in Figure 3.44 is shown a typical result in which the characteristic IBU UV spectra is seen increasing in intensity.

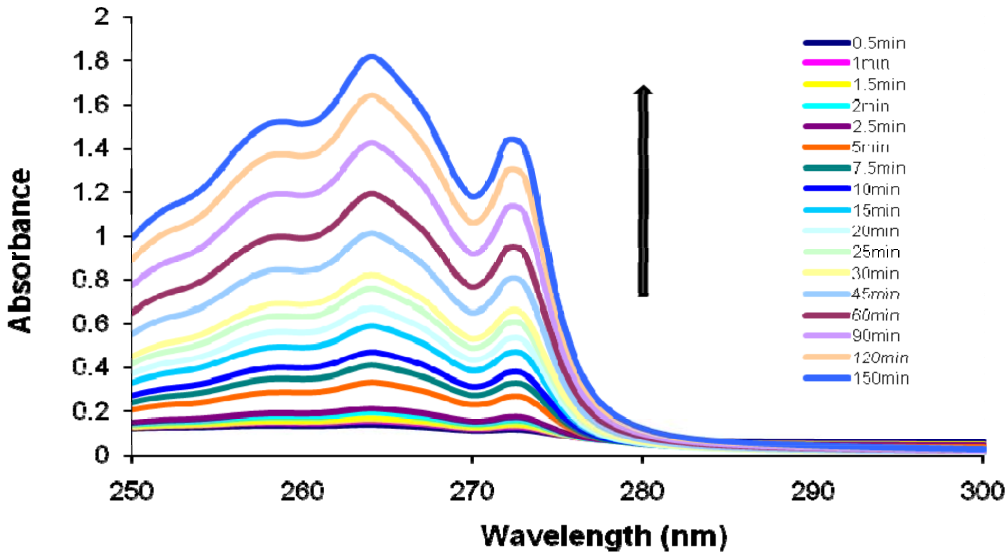

Figure 2.44. Release of ibuprofen (10 mg) from a gel of **2.1a** at 0.5% by weight 7:3 H_2O:EtOH into pure water over time.

According to the Beer Lambert Law (A = εcl) the concentration of a compound within a solution can be determined using its absorbance value and an extinction coefficient (ε) for the compound at a particular wavelength and path length. Using the literature value of 256.5 M^{-1} cm^{-1} at λ = 273 nm, for IBU, which was confirmed experimentally using the instrument utilised herein, the concentration increase from the release of IBU from the gel over time can be followed.[132] Simplifying the experiment by just following the absorbance at this specific wavelength over time gave results as shown in Figure 3.45, therefore allowing for the easy identification of the amount of drug released. From this data the concentration of the solution can be determined as 0.0113 M. This reveals that at equilibrium the concentration of the solution above the gel was less than that would be expected from the dilution of the 1 ml solution to 4 ml (it is approximately a third less, 0.0329 M) showing that there was a significant amount of drug compound retained within the gel.

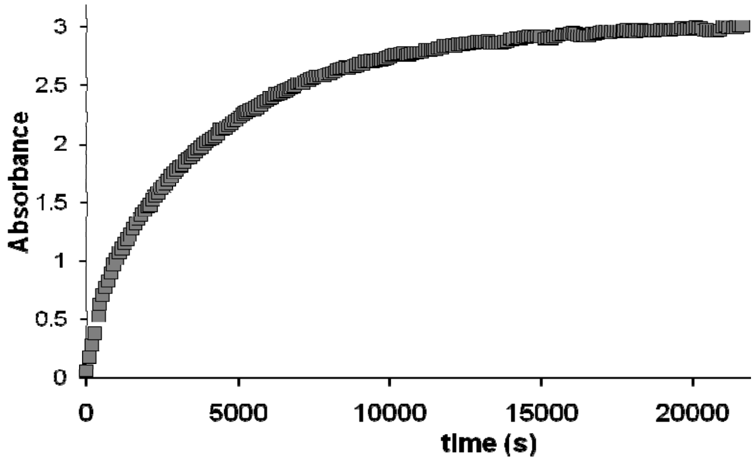

Figure 2.45. IBU release (30 mg in sample gel) over time from a 0.3% gel of **2.1a** in EtOH:H_2O 3:7 into pure water followed using UV spectroscopy.

By normalising the concentration level (α) to represent the amount released from the beginning of the experiment to the end point at equilibrium as 0 to 1, this allows the kinetics of the system to be probed. Doing this for the above data reveals that no known kinetic model for diffusion fits it. Within the literature[25,129,133] on drug release from gels (polymer, biological and LMWG) the release has been found to follow the one-dimensional law of $c \propto kt^{1/2}$. Using the initial 2 hours of data however produces a very good fit to this kinetic model (Figure 3.46).

A local Avrami plot is a means of determining whether or not more than one mechanism is involved in a process.[134] If one process is involved a consistent straight line is revealed. In the case of two or more processes a plot will tend to have a change in direction or curve. Plotting the above data showed a deviation in the slope indicating a two or more process for the release of IBU from these gels (Figure 3.47). The change in solvent mixture (water mixing with 3:7 EtOH:H_2O gel solvent) may account for the above results on the rate.

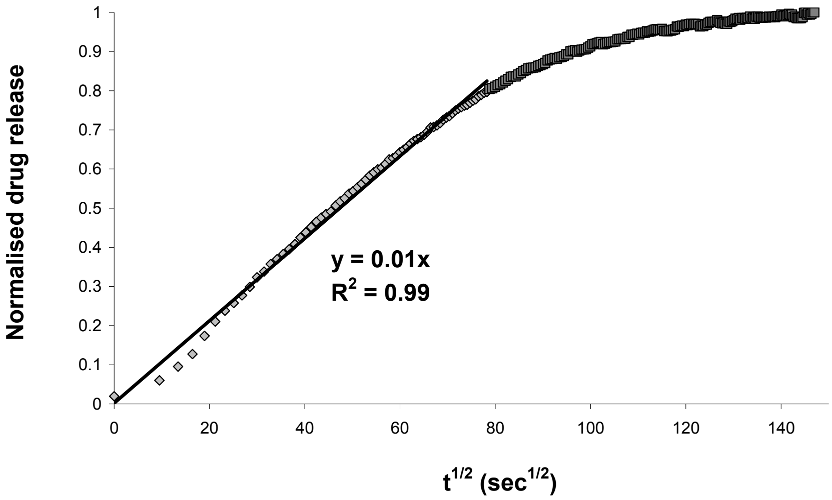

Figure 2.46. The initial release of IBU from the gel appears to follow the one-dimensional diffusion law $c \propto kt^{1/2}$ (Abscissa is $t^{1/2}$ and ordinate is the normalised concentration). However, after approximately two hours the rate has greatly slowed down and a second mechanism was evident.

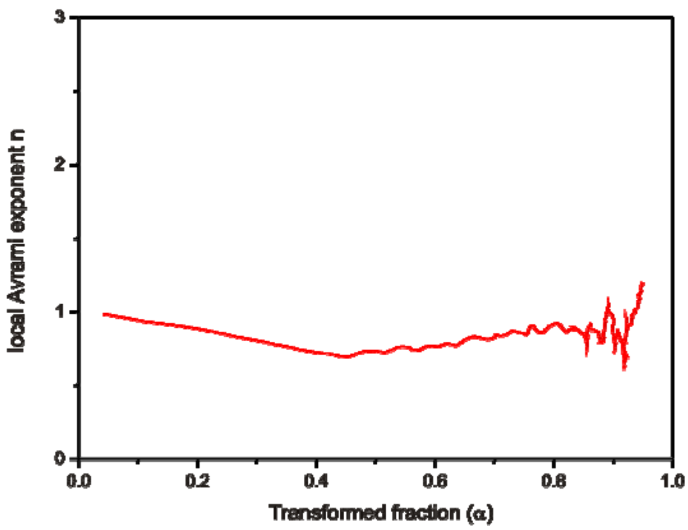

Figure 2.47. Local Avrami plot of the kinetics of drug release (IBU) from a gel of **2.1a** at 0.3% by weight of EtOH:H_2O 3:7 mixture into pure water. Note how the initial negative slope is linear but then deviates once approximately 0.45 α of the drug has been released compared to the equilibrium level of drug release. This shows a second mechanism of diffusion is occurring during the release of IBU from the gel.

The aim of this study was to investigate the effects of anions on the LMW gels. It has been shown that anions have no effects on hydrogels of **2.1a**. Nevertheless, the anions could have an effect on the interactions between the drug compounds and the gel matrix. The addition of anions in the form of TBA^+ $MeCO_2^-$ and NaCl was found to have no effect on the release of IBU. In additional to the anion study, the effect of pH of the solvents was investigated. As seen in Figure 3.48 the release of IBU from the gel was unaffected by a change to basic pH, however, the change to an acidic pH induced a reduction in the amount released. Although acidification does have an effect on the gel in that it slows the formation, it does not weaken the gel or affect it when viewed after it has formed by rheological studies. This means that the acidic conditions are affecting the way in which the IBU is interacting with the gel and/or released from the gel matrix. An obvious cause is the protonation of IBU from an anion to its neutral form. This neutral form will interact more strongly with the hydrophobic gel fibres in the water based media resulting in a drop in its release. Another cause is the solubility of the neutral form which is much reduced compared to the salt form of IBU (at high concentrations a change in pH results in precipitation of IBU from the solution).

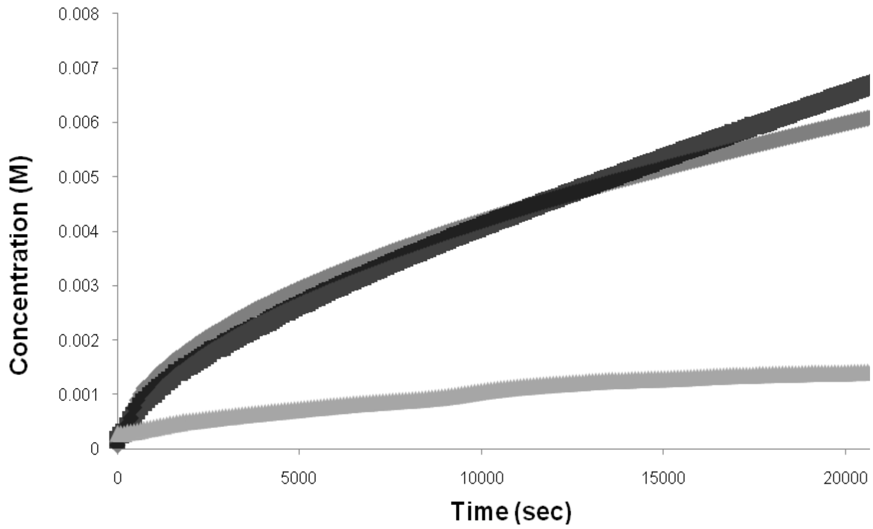

Figure 2.48. The effect to pH on the release of IBU (10 mg in sample of gel) from a 0.3% gel of **2.1a** in EtOH:H_2O 3:7 into water. The black points are the release into pure water, the dark grey points are the release into basic, pH 10, water and the light points are the release into acidic, pH 2, water.

In summary IBU release from hydrogels of **2.1a** is controlled, with the release of the drug taking several hours to diffuse out of the gel and to reach equilibrium. The equilibrium point indicates that a substantial amount of IBU is retained within the gel matrix indicating there is a strong interaction between the drug compound and the gel matrix. Kinetic studies of the drug release diffusion rates indicate that initial 2 hours does follow the one-dimensional diffusion law $c \propto kt^{1/2}$ as seen in other controlled drug release experiments.[25,129,133] However, there is evidence that there is a second mechanism involved that is more pronounced as the release approaches equilibrium as shown by inspecting the kinetics of the system by plotting a local Avrami graph. Unfortunately, the addition of anions in the form of NaCl or TBA^+ $MeCO_2^-$ did not affect the drug release. The change in pH revealed no change in the IBU release except when the pH was lowered. The change in solubility of IBU at low pH accounts for the change in release from the gel. The gel matrix may act as means to control the release of the drug as at low pH the solid IBU was retained within the gel solid where at neutral or higher pHs the drug was released in a controlled manner.

2.8 Conclusion

The chiral bisureas **2.1** and **2.2** show good gelation abilities and their gelation ability can be tuned using the addition of anions. Compound **2.1a** gels a wide variety of solvents forming organogels and mixtures of water forming hydrogels. The structural bonding through urea-urea tapes, as revealed by the crystallographic determination of the single crystal form, represents the unidirectional driving force for the growth of the fibrous structures that constitute the gel. As revealed by the electron microscopy studies of the gel the drying of samples can lead to crystallisation in some cases with a fibrous microstructure of a gel shown when crystallisation has not occurred. This microstructural determination of the gel was confirmed by the rheological study in which the cellular solid model matches with the experimental results therefore connecting theory and experimental results. The anion tuning shows how other than just fully breaking down a gel to a solution, anions can be used to tune the rheological characteristics of the gel. The rheological characteristics that are tuned by the addition of anions, which show a decrease in their value with increasing amounts of anion added, include the T_{gel}, shear value and G' parameters.

The alternation of the urea tapes from antiparallel to parallel upon changing the alkyl chain length within the heart of the compounds **2.1a-g** caused an alternation in the gelation ability. Single crystal x-ray determination of the structures of some of these compounds (**2.1a**,**c**,**d** and **f**) reveals the antiparallel and parallel relationship with the length of the alkyl chain. An even numbered chain length, which gave the antiparallel urea tapes, results in gelation and an odd numbered chain length, which gave the parallel urea tapes, results in no gelation character. While alternation effects are known in gels, the alternation between gelation and complete lack of gelator behaviour has not been observed previously.[58-63]

Compound **2** showed very similar gelation abilities to compound **2.1a**. Compound **2.2** forms weaker gels (as shown by the rheological measurements) than **2.1a**, however it did gel at lower CGC in all the solvents investigated allowing for its classification as a super gelator.[89] The fibrous structure shown by scanning electron spectroscopy demonstrates helical twisting, although the chirality of the compound is not evidenced in these helical twists. The fluorescence of the naphthyl group shows that stacking of the compounds within the gel follows a *J*-aggregation mode. Similarly to **2.1a**, compound **2.2** can have its rheological characteristics tuned by the addition of anions.

Compound **2.3** did not gel due to high solubility and different packing within the solid state. Compound **2.3** forms the antiparallel urea tape motif, as seen in compounds **2.1** when the spacer is even, but did not form it through translation stacking as revealed by single crystal x-ray diffraction. Rather it formed through rotational stacking resulting in a two-dimensional hydrogen bonded sheet instead of a one-dimensional hydrogen bonded column. Anion binding by this compound showed how the anions interact with the urea groups with the more basic anions being bound more strongly. There was also evidence of a capsule-like binding assembly with two hosts to one anion formed with the stronger binding in this mode seen for the spherical anions.

Gels formed from LMWGs were found to influence the crystallisation results of the three compounds studied. More importantly because of the ease with which LMWGs can be tuned, allowing for the recovery of the grown crystals without use of mechanical force, grown crystals were retrieved by simply dissolving the gels using the addition of anions. The three compounds tested with this crystallisation method all showed signs of enhanced crystallisation within the gel state. This is probably due to the high number of heteronuclei present within a LMW gel which is not necessarily seen in the case of other forms of gels.[94,95] Interestingly the opposite effect was also clear, due to the prevention of convection currents and rapid nucleation by the formation of the gel, resulting in the growth of fewer crystals within a gel sample compared to when a pure solvent mixture was found to be super-saturated and rapid crystallisation occurred.[94,95] Polymorphic crystallisation from these LMWG gels often led to the thermodynamically more stable polymorph being isolated from the gel state where commonly from pure solvents often both thermodynamic and kinetic forms are found.

Ibuprofen release from hydrogels of **2.1a** is controlled with the release of the drug taking several hours to diffuse out of the gel to reach equilibrium. The equilibrium point indicates that a substantial amount of IBU is retained within the gel matrix indicating there is a strong interaction between the drug compound and the gel matrix. Kinetic studies of the drug release indicate that initial drug release does follow the one-dimensional diffusion law $c \propto kt^{1/2}$ as seen in other controlled drug release experiments.[25,129,133] However, there is evidence that there is a second mechanism involved that is more pronounced as the release approaches equilibrium as shown by inspecting the kinetics of the system by plotting an local Avrami graph. Unfortunately, the addition of anions in the form of NaCl or TBA^+ $MeCO_2^-$ did not affect the drug release. The change in pH revealed no change in the IBU release except when the pH was lowered. The change in solubility of IBU at low pH accounts for the change in release from the gel.

In general it was found that chiral bisureas could gel a large variety of solvents and within most of these solvents, anion tuning of the rheological characteristics of the gels could be obtained. This may lead to application of these gels and this property as shown by the use of the LMW gels a growth medium for crystallisation and the ease of recovery for the grown crystals by the anion induced reversibility of gel formation.

2.9 References

(1) Lloyd, G. O.; Steed, J. W. *Nat. Chem.* **2009**, *1*, 437-442.
(2) Maeda, H. *Chem. Eur. J.* **2008**, *14*, 11274-11282.
(3) Hirst, A. R.; Escuder, B.; Miravet, J. F.; Smith, D. K. *Angew. Chem., Int. Ed.* **2008**, *47*, 8002-8018.
(4) Smith, P. J.; Reddington, M. V.; Wilcox, C. S. *Tetrahedron Lett.* **1992**, *33*, 6085-6088.
(5) Nishizawa, S.; Buhlmann, P.; Iwao, M.; Umezawa, Y. *Tetrahedron Lett.* **1995**, *36*, 6483-6486.
(6) Fages, F.; Vögtle, F.; Žinić, M. *Top. Curr. Chem.* **2005**, *256*, 77-131.
(7) Yamanaka, M.; Nakagawa, T.; Aoyama, R.; Nakamura, T. *Tetrahedron* **2008**, *64*, 11558–11567.
(8) Estroff, L. A.; Hamilton, A. D. *Angew. Chem., Int. Ed.* **2000**, *39*, 3447-3450.
(9) van Esch, J.; Schoonbeek, F.; de Loos, M.; Kooijman, H.; Spek, A. L.; Kellogg, R. M.; Feringa, B. L. *Chem. Eur. J.* **1999**, *5*, 937-950.
(10) de Loos, M.; van Esch, J.; Kellogg, R. M.; Feringa, B. L. *Angew. Chem., Int. Ed.* **2001**, *40*, 613-616.
(11) Stanley, C. E.; Clarke, N.; Anderson, K. M.; Lenthall, J. P.; Steed, J. W. *Chem. Commun.* **2006**, 3199-3201.
(12) Smith, D. K. *Chem. Soc. Rev.* **2009**, *38*, 684-694.
(13) Brizard, A.; Oda, R.; Huc, I. In *Low Molecular Mass Gelators: Design, Self-Assembly, Function*; Springer-Verlag Berlin: Berlin, 2005; Vol. 256, p 167-218.
(14) Palmans, A. R. A.; Meijer, E. W. *Angew. Chem., Int. Ed.* **2007**, *46*, 8948-8968.
(15) Sangeetha, N. M.; Maitra, U. *Chem. Soc. Rev.* **2005**, *34*, 821-836.
(16) Matsumoto, S.; Yamaguchi, S.; Ueno, S.; Komatsu, H.; Ikeda, M.; Ishizuka, K.; Iko, Y.; Tabata, K. V.; Aoki, H.; Ito, S.; Noji, H.; Hamachi, I. *Chem. Eur. J.* **2008**, *14*, 3977-3986.
(17) Liang, G. L.; Yang, Z. M.; Zhang, R. J.; Li, L. H.; Fan, Y. J.; Kuang, Y.; Gao, Y.; Wang, T.; Lu, W. W.; Xu, B. *Langmuir* **2009**, *25*, 8419-8422.
(18) Adhikari, B.; Palui, G.; Banerjee, A. *Soft Matter* **2009**, *5*, 3452-3460.
(19) van Bommel, K. J. C.; Stuart, M. C. A.; Feringa, B. L.; van Esch, J. *Org. Biomol. Chem.* **2005**, *3*, 2917-2920.
(20) Karinaga, R.; Jeong, Y.; Shinkai, S.; Kaneko, K.; Sakurai, K. *Langmuir* **2005**, *21*, 9398-9401.
(21) Vemula, P. K.; Li, J.; John, G. *J. Am. Chem. Soc.* **2006**, *128*, 8932-8938.
(22) Shome, A.; Debnath, S.; Das, P. K. *Langmuir* **2008**, *24*, 4280-4288.
(23) Panda, J. J.; Mishra, A.; Basu, A.; Chauhan, V. S. *Biomacromolecules* **2008**, *9*, 2244-2250.
(24) Feng, G. L.; Xiong, Y.; Wang, H.; Yang, Y. J. *Eur. J. Pharm. Biopharm.* **2009**, *71*, 297-302.
(25) Friggeri, A.; Feringa, B. L.; van Esch, J. *J. Control. Release* **2004**, *97*, 241-248.
(26) Komatsu, H.; Matsumoto, S.; Tamaru, S.; Kaneko, K.; Ikeda, M.; Hamachi, I. *J. Am. Chem. Soc.* **2009**, *131*, 5580-5585.
(27) Yang, Z. M.; Gu, H. W.; Zhang, Y.; Wang, L.; Xu, B. *Chem. Commun.* **2004**, 208-209.
(28) Cravotto, G.; Cintas, P. *Chem. Soc. Rev.* **2009**, *38*, 2684-2697.
(29) Liu, X. Y. In *Low Molecular Mass Gelators: Design, Self-Assembly, Function*; Springer-Verlag Berlin: Berlin, 2005; Vol. 256, p 1-37.
(30) Wang, R. Y.; Liu, X. Y.; Xiong, J. Y.; Li, J. L. *J. Phys. Chem. B* **2006**, *110*, 7275-7280.
(31) Li, J. L.; Liu, X. Y.; Wang, R. Y.; Xiong, J. Y. *J. Phys. Chem. B* **2005**, *109*, 24231-24235.
(32) Lescanne, M.; Colin, A.; Mondain-Monval, O.; Fages, F.; Pozzo, J. L. *Langmuir* **2003**, *19*, 2013-2020.
(33) Estroff, L. A.; Hamilton, A. D. *Chem. Rev.* **2004**, *104*, 1201-1217.
(34) de Loos, M.; Feringa, B. L.; van Esch, J. H. *Eur. J. Org. Chem.* **2005**, 3615-3631.
(35) Terech, P.; Weiss, R. G. *Chem. Rev.* **1997**, *97*, 3133-3159.
(36) Bhattacharya, S.; Krishnan-Ghosh, Y. *Chem. Commun.* **2001**, 185-186.
(37) Suzuki, M.; Sato, T.; Shirai, H.; Hanabusa, K. *New J. Chem.* **2006**, *30*, 1184-1191.
(38) Peng, J. X.; Liu, K. Q.; Liu, X. F.; Xia, H. Y.; Liu, J.; Fang, Y. *New J. Chem.* **2008**, *32*, 2218-2224.
(39) Debnath, S.; Shome, A.; Dutta, S.; Das, P. K. *Chem. Eur. J.* **2008**, *14*, 6870-6881.
(40) Bardelang, D.; Camerel, F.; Margeson, J. C.; Leek, D. M.; Schmutz, M.; Zaman, M. B.; Yu, K.;

Soldatov, D. V.; Ziessel, R.; Ratcliffe, C. I.; Ripmeester, J. A. *J. Am. Chem. Soc.* **2008**, *130*, 3313-3315.
(41) Terech, P.; Pasquier, D.; Bordas, V.; Rossat, C. *Langmuir* **2000**, *16*, 4485-4494.
(42) Brinksma, J.; Feringa, B. L.; Kellogg, R. M.; Vreeker, R.; van Esch, J. *Langmuir* **2000**, *16*, 9249-9255.
(43) Terech, P.; Friol, S. *Tetrahedron* **2007**, *63*, 7366-7374.
(44) Menger, F. M.; Caran, K. L. *J. Am. Chem. Soc.* **2000**, *122*, 11679-11691.
(45) Terech, P.; Rossat, C.; Volino, F. *Journal of Colloid and Interface Science* **2000**, *227*, 363-370.
(46) Larson, R. G. *The Structure and Rheology of Complex Fluids*; Oxford University Press: Oxford, 1999.
(47) Sangeetha, N. M.; Bhat, S.; Choudhury, A. R.; Maitra, U.; Terech, P. *J. Phys. Chem. B* **2004**, *108*, 16056-16063.
(48) Shih, W. H.; Shih, W. Y.; Kim, S. I.; Liu, J.; Aksay, I. A. *Phys. Rev. A* **1990**, *42*, 4772-4779.
(49) Gibson, L. J.; Ashby, M. F. *Proc. Royal Soc. London Ser. A* **1982**, *382*, 43-59.
(50) Buxton, G. A.; Clarke, N. *Phys. Rev. Lett.* **2007**, *98*.
(51) Hirst, A. R.; Coates, I. A.; Boucheteau, T. R.; Miravet, J. F.; Escuder, B.; Castelletto, V.; Hamley, I. W.; Smith, D. K. *J. Am. Chem. Soc.* **2008**, *130*, 9113-9121.
(52) Byrne, P.; Turner, D. R.; Lloyd, G. O.; Clarke, N.; Steed, J. W. *Cryst. Growth Des.* **2008**, *8*, 3335-3344.
(53) Gibson, L. J.; Ashby, M. F. *Cellular Solids: Structures and Properties*; 2nd ed.; Cambridge University Press: Cambridge, 1997.
(54) de Loos, M.; Ligtenbarg, A. G. J.; van Esch, J.; Kooijman, H.; Spek, A. L.; Hage, R.; Kellogg, R. M.; Feringa, B. L. *Eur. J. Org. Chem.* **2000**, 3675-3678.
(55) Piepenbrock, M. O. M.; Lloyd, G. O.; Clarke, N.; Steed, J. W. *Chem. Commun.* **2008**, 2644-2646.
(56) Frassineti, C.; Ghelli, S.; Gans, P.; Sabatini, A.; Moruzzi, M. S.; Vacca, A. *Anal. Biochem.* **1995**, *231*, 374-382.
(57) Gans, P.; University of Leeds: Leeds, 2006.
(58) Fujita, N.; Sakamoto, Y.; Shirakawa, M.; Ojima, M.; Fujii, A.; Ozaki, M.; Shinkai, S. *J. Am. Chem. Soc.* **2007**, *129*, 4134-4135.
(59) Suzuki, M.; Nanbu, M.; Yumoto, M.; Shirai, H.; Hanabusa, K. *New J. Chem.* **2005**, *29*, 1439-1444.
(60) Aoki, K.; Kudo, M.; Tamaoki, N. *Org. Lett.* **2004**, *6*, 4009-4012.
(61) Ishi-i, T.; Iguchi, R.; Snip, E.; Ikeda, M.; Shinkai, S. *Langmuir* **2001**, *17*, 5825-5833.
(62) Sumiyoshi, T.; Nishimura, K.; Nakano, M.; Handa, T.; Miwa, Y.; Tomioka, K. *J. Am. Chem. Soc.* **2003**, *125*, 12137-12142.
(63) Jung, J. H.; Shinkai, S. *J. Chem. Soc., Perkin Trans 2* **2000**, 2393-2398.
(64) Reddy, L. S.; Basavoju, S.; Vangala, V. R.; Nangia, A. *Cryst. Growth Des.* **2006**, *6*, 161-173.
(65) Hoffmann, R. W. *Chem. Rev.* **1989**, *89*, 1841-1860.
(66) Brock, C. P.; Dunitz, J. D. *Chem. Mater.* **1994**, *6*, 1118 - 1127.
(67) Nangia, A. *Acc. Chem. Res.* **2008**, *41*, 595-604.
(68) Bernstein, J. *Chem. Commun.* **2005**, 5007-5012.
(69) Percec, V.; Peterca, M.; Yurchenko, M. E.; Rudick, J. G.; Heiney, P. A. *Chem. Eur. J.* **2008**, *14*, 909-918.
(70) Weng, W. G.; Jamieson, A. M.; Rowan, S. J. *Tetrahedron* **2007**, *63*, 7419-7431.
(71) Shirakawa, M.; Fujita, N.; Shinkai, S. *J. Am. Chem. Soc.* **2005**, *127*, 4164-4165.
(72) Lescanne, M.; Grondin, P.; d'Aleo, A.; Fages, F.; Pozzo, J. L.; Monval, O. M.; Reinheimer, P.; Colin, A. *Langmuir* **2004**, *20*, 3032-3041.
(73) Yang, Z. M.; Liang, G. L.; Xu, B. *Chem. Commun.* **2006**, 738-740.
(74) Seo, J.; Chung, J. W.; Jo, E. H.; Park, S. Y. *Chem. Commun.* **2008**, 2794-2796.
(75) Chen, J. W.; Law, C. C. W.; Lam, J. W. Y.; Dong, Y. P.; Lo, S. M. F.; Williams, I. D.; Zhu, D. B.; Tang, B. Z. *Chem. Mat.* **2003**, *15*, 1535-1546.
(76) Chung, J. W.; An, B. K.; Park, S. Y. *Chem. Mat.* **2008**, *20*, 6750-6755.
(77) Desvergne, J. P.; Olive, A. G. L.; Sangeetha, N. M.; Reichwagen, J.; Hopf, H.; Del Guerzo, A. *Pure Appl. Chem.* **2006**, *78*, 2333-2339.
(78) Zhu, L. L.; Ma, X.; Ji, F. Y.; Wang, Q. C.; Tian, H. *Chem. Eur. J.* **2007**, *13*, 9216-9222.
(79) An, B. K.; Kwon, S. K.; Jung, S. D.; Park, S. Y. *J. Am. Chem. Soc.* **2002**, *124*, 14410-14415.
(80) Tam, A. Y. Y.; Wong, K. M. C.; Yam, V. W. W. *J. Am. Chem. Soc.* **2009**, *131*, 6253-6260.

(81) Saha, A.; Manna, S.; Nandi, A. K. *Langmuir* **2007**, *23*, 13126-13135.
(82) Leong, W. L.; Batabyal, S. K.; Kasapis, S.; Vittal, J. J. *Chem. Eur. J.* **2008**, *14*, 8822-8829.
(83) An, B. K.; Lee, D. S.; Lee, J. S.; Park, Y. S.; Song, H. S.; Park, S. Y. *J. Am. Chem. Soc.* **2004**, *126*, 10232-10233.
(84) Asai, M.; Sugiyasu, K.; Fujita, N.; Shinkai, S. *Chem. Lett.* **2004**, *33*, 120-121.
(85) Kim, T. H.; Seo, J.; Lee, S. J.; Lee, S. S.; Kim, J.; Jung, J. H. *Chem. Mat.* **2007**, *19*, 5815-5817.
(86) Saha, A.; Manna, S.; Nandi, A. K. *Chem. Commun.* **2008**, 3732-3734.
(87) Pham, Q. N.; Brosse, N.; Frochot, C.; Dumas, D.; Hocquet, A.; Jamart-Gregoire, B. *New J. Chem.* **2008**, *32*, 1131-1139.
(88) Wurthner, F.; Bauer, C.; Stepanenko, V.; Yagai, S. *Adv. Mater.* **2008**, *20*, 1695-+.
(89) Žinić, M.; Vögtle, F.; Fages, F. In *Low Molecular Mass Gelators: Design, Self-Assembly, Function*; Springer-Verlag Berlin: Berlin, 2005; Vol. 256, p 39-76.
(90) Bowman-James, K. *Acc. Chem. Res.* **2005**, *38*, 671-678.
(91) Henisch, H. K. *Crystal Growth in Gels*; The Pennsylvania State University Press: University Park, PA, 1976.
(92) Henisch, H. K. *Crystals in Gels and Liesegang rings*; Cambridge University Press: New York, 1988.
(93) Henisch, H. K.; Garcia-Ruiz, J. M. *J. Cryst. Growth* **1986**, *75*, 195-202.
(94) Henisch, H. K.; Garcia-Ruiz, J. M. *J. Cryst. Growth* **1986**, *75*, 203-211.
(95) Petrova, R. I.; Swift, J. A. *J. Am. Chem. Soc.* **2004**, *126*, 1168-1173.
(96) Petrova, R. I.; Patel, R.; Swift, J. A. *Cryst. Growth Des.* **2006**, *6*, 2709-2715.
(97) Daiguebonne, C.; Deluzet, A.; Camara, M.; Boubekeur, K.; Audebrand, N.; Gerault, Y.; Baux, C.; Guillou, O. *Cryst. Growth Des.* **2003**, *3*, 1015-1020.
(98) Desiraju, G. R.; Curtin, D. Y.; Paul, I. C. *J. Am. Chem. Soc.* **1977**, *99*, 6148-6148.
(99) Pauchet, M.; Morelli, T.; Coste, S.; Malandain, J. J.; Coquerel, G. *Cryst. Growth Des.* **2006**, *6*, 1881-1889.
(100) Yaghi, O. M.; Li, G. M.; Li, H. L. *Chem. Mat.* **1997**, *9*, 1074-1076.
(101) Li, H. Y.; Estroff, L. A. *CrystEngComm* **2007**, *9*, 1153-1155.
(102) Oaki, Y.; Imai, H. *J. Am. Chem. Soc.* **2004**, *126*, 9271-9275.
(103) Imai, H.; Oaki, Y. *Angew. Chem., Int. Ed.* **2004**, *43*, 1363-1368.
(104) Abdallah, D. J.; Weiss, R. G. *Adv. Mater.* **2000**, *12*, 1237-1247.
(105) Rafilovich, M.; Bernstein, J.; Harris, R. K.; Apperley, D. C.; Karamertzanis, P. G.; Price, S. L. *Cryst. Growth Des.* **2005**, *5*, 2197-2209.
(106) Grzesiak, A. L.; Lang, M. D.; Kim, K.; Matzger, A. J. *J. Pharm. Sci.* **2003**, *92*, 2260-2271.
(107) Lang, M. D.; Grzesiak, A. L.; Matzger, A. J. *J. Am. Chem. Soc.* **2002**, *124*, 14834-14835.
(108) Lang, M. D.; Kampf, J. W.; Matzger, A. J. *J. Pharm. Sci.* **2002**, *91*, 1186-1190.
(109) Dabros, M.; Thalladi, V. R. *Chem. Commun.* **2007**, 2476-2478.
(110) Johnston, A.; Johnston, B. F.; Kennedy, A. R.; Florence, A. J. *CrystEngComm* **2008**, *10*, 23-25.
(111) Gelbrich, T.; Hursthouse, M. B. *CrystEngComm* **2006**, *8*, 448-460.
(112) Vishweshwar, P.; McMahon, J. A.; Oliveira, M.; Peterson, M. L.; Zaworotko, M. J. *J. Am. Chem. Soc.* **2005**, *127*, 16802-16803.
(113) Bond, A. D.; Boese, R.; Desiraju, G. R. *Angew. Chem., Int. Ed.* **2007**, *46*, 615-617.
(114) Bond, A. D.; Boese, R.; Desiraju, G. R. *Angew. Chem., Int. Ed.* **2007**, *46*, 618-622.
(115) Heng, J. Y. Y.; Bismarck, A.; Lee, A. F.; Wilson, K.; Williams, D. R. *J. Pharm. Sci.* **2007**, *96*, 2134-2144.
(116) Aubrey-Medendorp, C.; Parkin, S.; Li, T. L. *J. Pharm. Sci.* **2008**, *97*, 1361-1367.
(117) Offret, A.; Vittenet, H. *Bull. Soc. Chim. Fr.* **1899**, 788-797.
(118) Groth, P. H. *An Introduction to Chemical Crystallography (trans. H. Marshall)*; Gurnery & Jackson: London, 1906.
(119) Etter, M. C.; Urbanczyklipkowska, Z.; Ziaebrahimi, M.; Panunto, T. W. *J. Am. Chem. Soc.* **1990**, *112*, 8415-8426.
(120) Etter, M. C. *Acc. Chem. Res.* **1990**, *23*, 120-126.
(121) Oaki, Y.; Imai, H. *Cryst. Growth Des.* **2003**, *3*, 711-716.
(122) Harris, R. K.; Ghi, P. Y.; Puschmann, H.; Apperley, D. C.; Griesser, U. J.; Hammond, R. B.; Ma, C. Y.; Roberts, K. J.; Pearce, G. J.; Yates, J. R.; Pickard, C. J. *Org. Process Res. Dev.* **2005**, *9*, 902-910.
(123) Davey, R. J.; Williams-Seton, L.; Lieberman, H. F.; Blagden, N. *Nature* **1999**, *402*, 797-799.

(124) Williams-Seton, L.; Davey, R. J.; Lieberman, H. F. *J. Am. Chem. Soc.* **1999**, *121*, 4563-4567.
(125) Kabanov, A. V.; Vinogradov, S. V. *Angew. Chem., Int. Ed.* **2009**, *48*, 5418-5429.
(126) Soussan, E.; Cassel, S.; Blanzat, M.; Rico-Lattes, I. *Angew. Chem., Int. Ed.* **2009**, *48*, 274-288.
(127) Ehrbar, M.; Schoenmakers, R.; Christen, E. H.; Fussenegger, M.; Weber, W. *Nat. Mater.* **2008**, *7*, 800-804.
(128) Gao, P.; Nixon, P. R.; Skoug, J. W. *Pharm. Res.* **1995**, *12*, 965-971.
(129) Peschka, R.; Dennehy, C.; Szoka, F. C. *J. Control. Release* **1998**, *56*, 41-51.
(130) Ammar, H. O.; Ghorab, M.; El-Nahhas, S. A.; Kamel, R. *Int. J. Pharm.* **2006**, *327*, 81-88.
(131) Godeau, G.; Bernard, J.; Staedel, C.; Barthelemy, P. *Chem. Commun.* **2009**, 5127-5129.
(132) Stephenson, B. C.; Rangel-Yagui, C. O.; Pessoa, A.; Tavares, L. C.; Beers, K.; Blankschtein, D. *Langmuir* **2006**, *22*, 1514-1525.
(133) Higuchi, T. *J. Pharm. Sci.* **1963**, *52*, 1145-1149.
(134) Wang, J.; Kou, H. C.; Gu, X. F.; Li, J. S.; Xing, L. Q.; Hu, R.; Zhou, L. *Mater. Lett.* **2009**, *63*, 1153-1155.

Chapter 3

Gelation and coordination chemistry of Pyrazole derived compounds

3.1 Aims

The main aims for this research were to investigate the coordination chemistry of metals and anions of a set of pyrazole derived compounds in order to characterise the ligands' metal and anion coordination modes, and hence design new pyrazole-based LWMGs. Additional studies on pyrazolate coordination chemistry were undertaken in collaboration with Prof. Peter Junk at Monash University, Australia. The pyrazole group, a five membered heteroaromatic ring with two adjacent nitrogen atoms, has been studied extensively, particularly in metal coordination chemistry.[1-7] The derivatisation of the pyrazole group has led to many important ligand classes, particularly the "scorpionate" ligands.[2-6,8-13] Simple pyrazoles have the ability to coordinate to metals through the Lewis basic pyrazolyl N-donor group and coordinate via hydrogen bonds to anions through the Lewis acidic pyrrolic N–H group. This has led to studies in the co-coordination of cations and anions by pyrazole ligands. Anion binding by these kinds of coordination complexes includes work particularly by Halcrow and Pérez.[12-19] The use of pyrazoles within LMWGs has been limited, with the work of Aida, with a trinuclear Au(I) pyrazolate complex, being one of the more recognisable examples.[20] Far greater use has been made of pyridyl moieties as an N-donor group in metal and anion tunable LMWGs.[21-37] The work presented here complements these pyridyl examples with the use of the pyrazole group and is aimed at producing LWMGs that can be tuned using anions. The addition of urea functionality to the pyrazole will aid the search for a LWMG that can be tuned using anions as the anion binding capabilities of the urea group are well understood,[38,39] and the gel properties of compounds that contain urea groups have also been extensively studied.[40-44] Initial studies on simple urea derivatised pyrazole compounds were performed to understand the coordination chemistry of these compounds with both anions and metals in the hope of producing a LMWG. The LWMGs that formed were tested for their anion tunability.[45,46]

3.2 Synthesis of Pyrazole Ureas

The following results describe the synthesis of the target urea and thiourea pyrazole derivatives. All the compounds synthesised were tested for gelation ability in the solvents H_2O, $CHCl_3$, Acetone, MeCN, MeOH, EtOH, Hexane, Toluene and DMSO. The synthesis of urea-functionalised pyrazole derivatives was first attempted by reacting 3-amino-5-methylpyrazole with isocyanates and isothiocyanates. There are three possible reaction products for the addition of an isocyanate to 3-amino-5-methylpyrazole. These products involve either reaction at the primary amino group to form a urea, or the reaction on either of the ring nitrogen positions to give a carboxamide (or carboxylic acid amide) (Scheme 3.1).[7,47,48] The large majority of the literature on this type of reaction between an amino-pyrazole and an isocyanate suggests that the carboxamide derivatives are the most common products.[7,47,49] However, as shown by Graubaum and others, temperature plays an important role in determining which of the three possible products is obtained.[47,50] Indeed even heating the products can lead to the conversion from one isomer to another, with the urea often being the most stable product.[47,50]

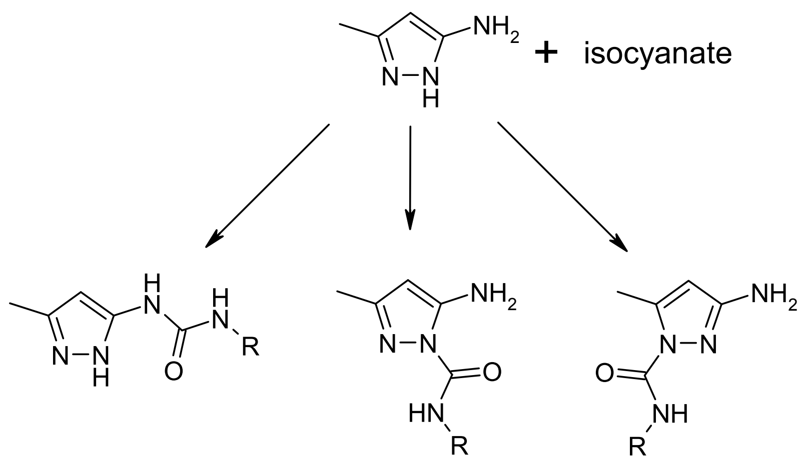

Scheme 3.1 Possible products from the reaction of 3-amino-5-methylpyrazole with an isocyanate to give, from left to right, desired urea, 2-carboxamide, 1-carboxamide.

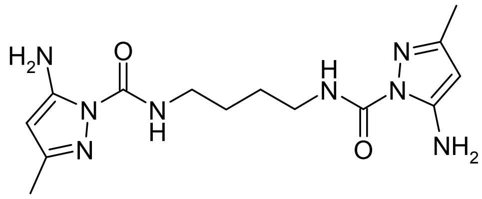

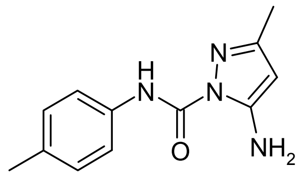

3.1 **3.2**

Reaction of 3-amino-5-methylpyrazole with 1,4-diisocyanatobutane and *p*-tolyl isocyanate in refluxing $CHCl_3$ resulted in the two carboxamide products **3.1** and **3.2**, in agreement with previous work on related compounds.[47-49] The X-ray crystal structures of **3.1** (both in pure form and as a chloroform solvate) and **3.2** confirm the carboxamide has indeed been formed and that the addition of the isocyanate to form the carboxamide has occurred on the nitrogen atom next to the primary amine group (Figure 3.1). Attempting to convert the carboxamides to ureas using the protocol described by Graubaum, where heating of the carboxamide under an inert atmosphere resulted in the isolation of the urea form,[47] only resulted in mixtures of products. These mixtures of products could not be satisfactorily separated to give the urea in high yield and purity. Neither compound **3.1** nor **3.2** were found to form gels. Crystalline materials were produced from solution. The determination of the crystal structures of **3.1** as the pure compound and as a $CHCl_3$ solvate, as well as the structure of **3.2** revealed that intra-molecular hydrogen bonding plays a role in the behaviour of these compounds (Figure 3.1). Formation of 1D hydrogen bond chains by amide and urea groups has been recognised as a structural directing motif in LMWGs.[40,51,52] The presence of the carboxamide group within compounds **3.1** and **3.2** did not lead to 1D chains of hydrogen bonds. The intra-molecular hydrogen bonding between N–H of the amide group and the Lewis basic pyrazolyl N-donor group of the pyrazole moiety, and the amine group and the carbonyl group of the amide group within the three structures determined for **3.1** and **3.2** prevents the formation of the amide hydrogen bond chains. The conjugation between the amide group and the pyrazole aids planarisation of the pyrazole and amide groups orientating the hydrogen bonding groups in such a way to allow the formation of the intra-molecular hydrogen bonds.

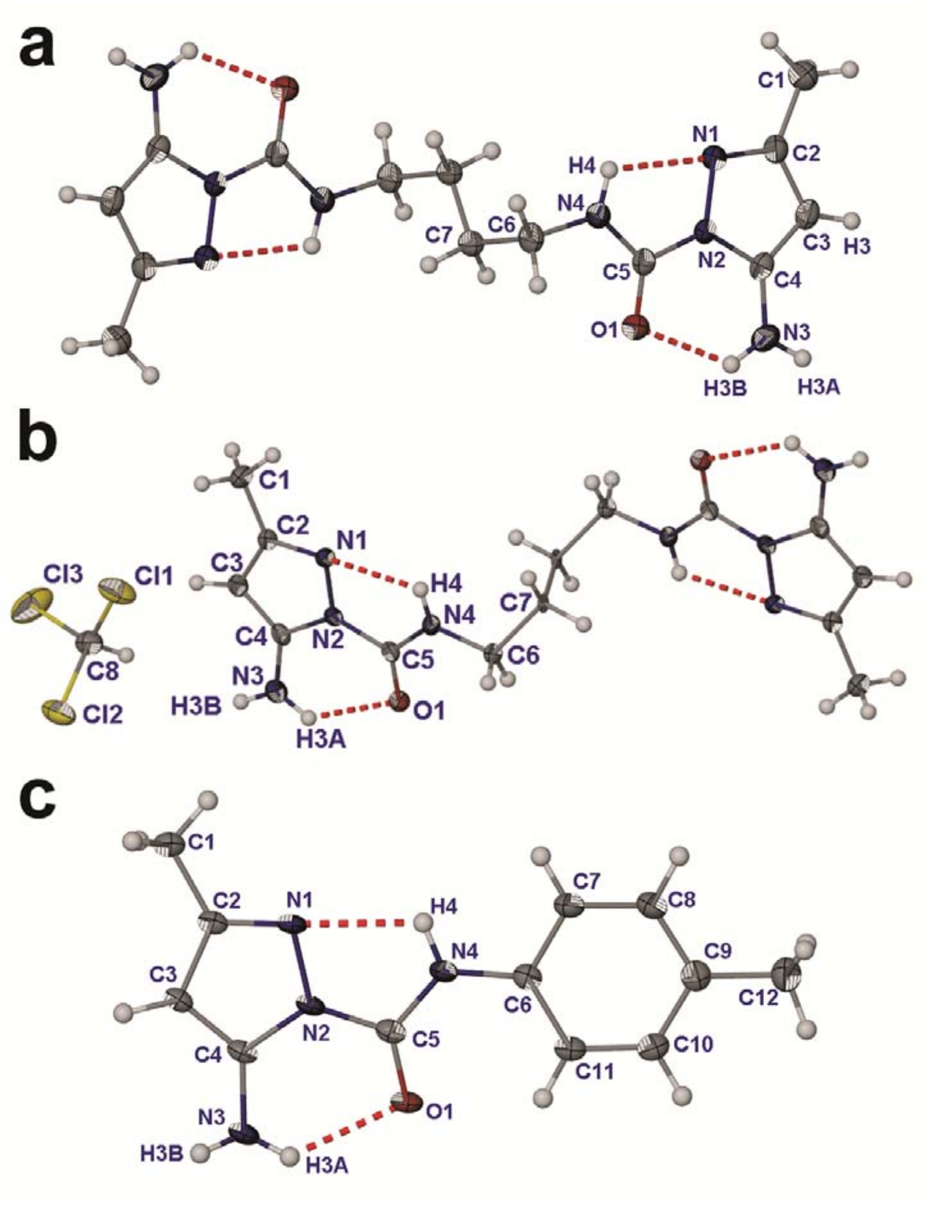

Figure 3.1. Molecular structures of **3.1** and **3.2**. **a)** Compound **3.2**. **b)** Compound **3.2** chloroform solvate. **c)** Compound **3.1**. Atoms are shown as ellipsoids at 50% probability. Selected hydrogen bonds: **3.2** N3···O1 = 2.736(2) Å; ∠ N3–H3B···O1 = 126.4°, N4···N1 = 2.681(2) Å; ∠ N4–H4···N1 = 107.5°, **3.2**·2$CHCl_3$ N3···O1 = 2.743(3) Å; ∠ N3–H3A···O1 = 126.0°, N4···N1 = 2.667(3) Å; ∠ N4–H4···N1 = 108.3°, **3.1** N3···O1 = 2.768(2) Å; ∠ N3–H3A···O1 = 126.1° and N4···N1 = 2.627(2) Å; ∠ N4–H4···N1 = 111.7°.

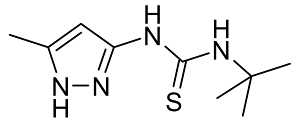

3.3

Reaction of *t*-butyl isothiocyanate with 3-amino-5-methylpyrazole in refluxing $CHCl_3$ gave compound **3.3** in good yield. All analytical data, including the single crystal x-ray structure determinations, indicate that the isothiocyanate reacted at the 3-amino position giving a thiourea as desired. Reactions between aminopyrazoles and isothiocyanates reported in the literature all appear to produce a thiourea except in one case.[7,48,53-55] In this one case, where carbothioamides were produced, the reactions were performed at room temperature in acetone whereas in the other examples the reactions were performed in a refluxing solvent.[54] This result shows that the temperature and solvent of the reaction play important roles in determining the product of the reaction between a thioisocyanate and an aminopyrazole. [47]

Compound **3.3** was not found to form gels. The crystal structures of **3.3** are of interest when it comes to the interpretation of the anion and metal coordination properties of the urea pyrazole compounds and their potential for gel formation. Compound **3.3** was crystallised from MeCN (Figure 3.2). The structure shows how there is an intra-molecular hydrogen bond between the NH group next to the *t*-butyl group and the Lewis basic pyrazolyl N-donor group. This results in the thiourea group being in an *anti* conformation (Figure 3.2a). The rest of the thiourea group, not involved in the intra-molecular hydrogen bond, hydrogen bonds in a $R_2^2(8)$ motif resulting in a dimer of **3.3** (Figure 3.2b). These dimers pack in a herringbone-like motif (Figure 3.2c) with the Lewis acidic pyrrolic N–H group interacting with the neighbouring dimers through a hydrogen bond to the sulfur resulting in a 3D hydrogen bonded lattice. The conformation of **3.3** with the intra-molecular hydrogen bond and dimer formation is the same as that seen for a wide variety of 2-pyridylthiourea compounds.[56-67] The second crystallographically determined structure of **3.3** is of a $CHCl_3$ clathrate from the crystallisation of **3.3** in $CHCl_3$. The molecular structures of the two **3.3** molecules of the ASU (Figure 3.3a) of this structure are identical to that of the previous structure, with the intra-molecular hydrogen bond and the *anti* conformation of the thiourea both being present.

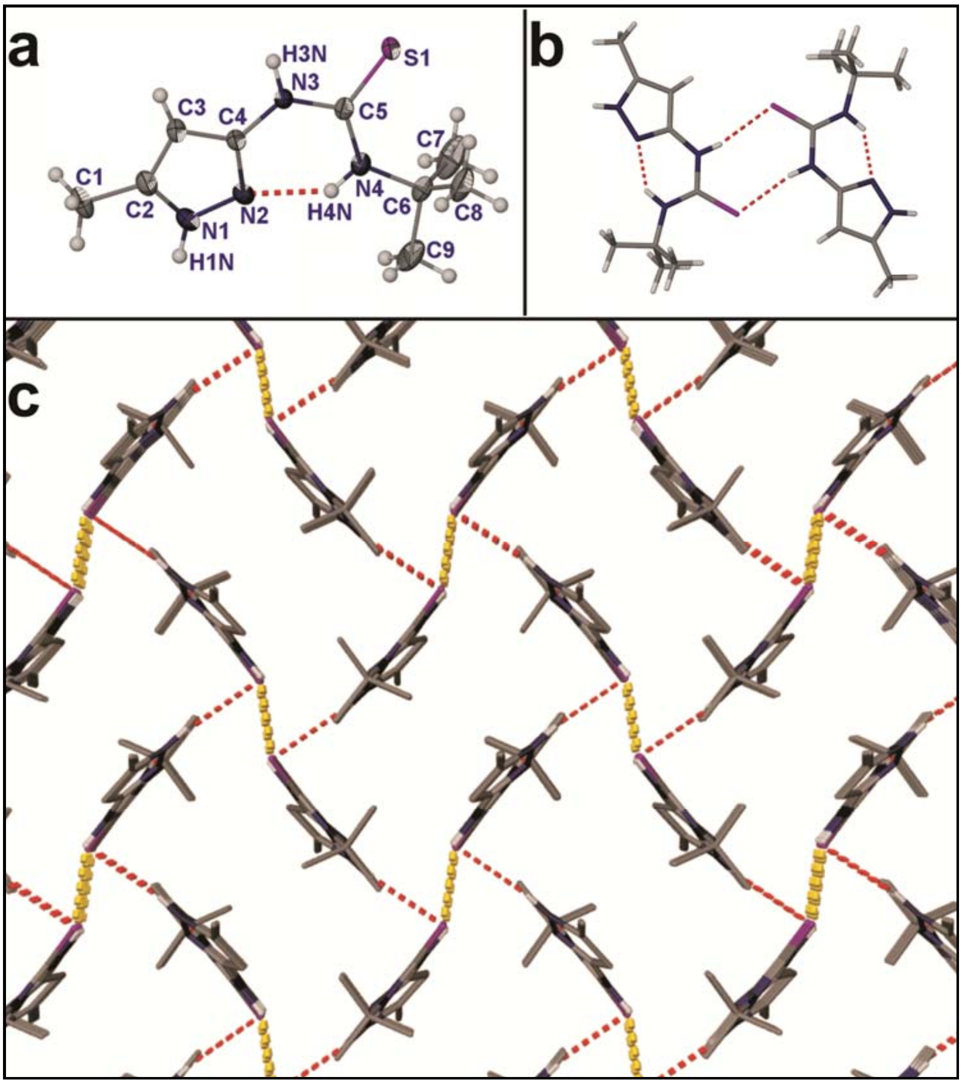

Figure 3.2. The crystal structure of **3.3**. **a)** Molecular structure of **3.3**. Atoms are shown as ellipsoids at 50% probability. **b)** Dimer formation through the hydrogen bonding of the thiourea groups. **c)** Herringbone-like packing of the dimers. Hydrogen bonds from the N–H of the pyrazole to the S1 are shown as dashed red lines. Hydrogen bonds between dimers shown as dashed yellow lines. Selected hydrogen bonds: N4⋯N2 = 2.687(2) Å; ∠ N4–H4N⋯N2 = 140.6°, N3⋯S1^{i} = 3.345(1) Å; ∠ N3–H3N⋯S1^{i} = 148.3° and N1⋯S1^{ii} = 3.285(2) Å; ∠ N1–H1N⋯S1^{ii} = 152.4° (*i* = 2-x, 1-y, -z and *ii* = x-½, ½-y, z-½).

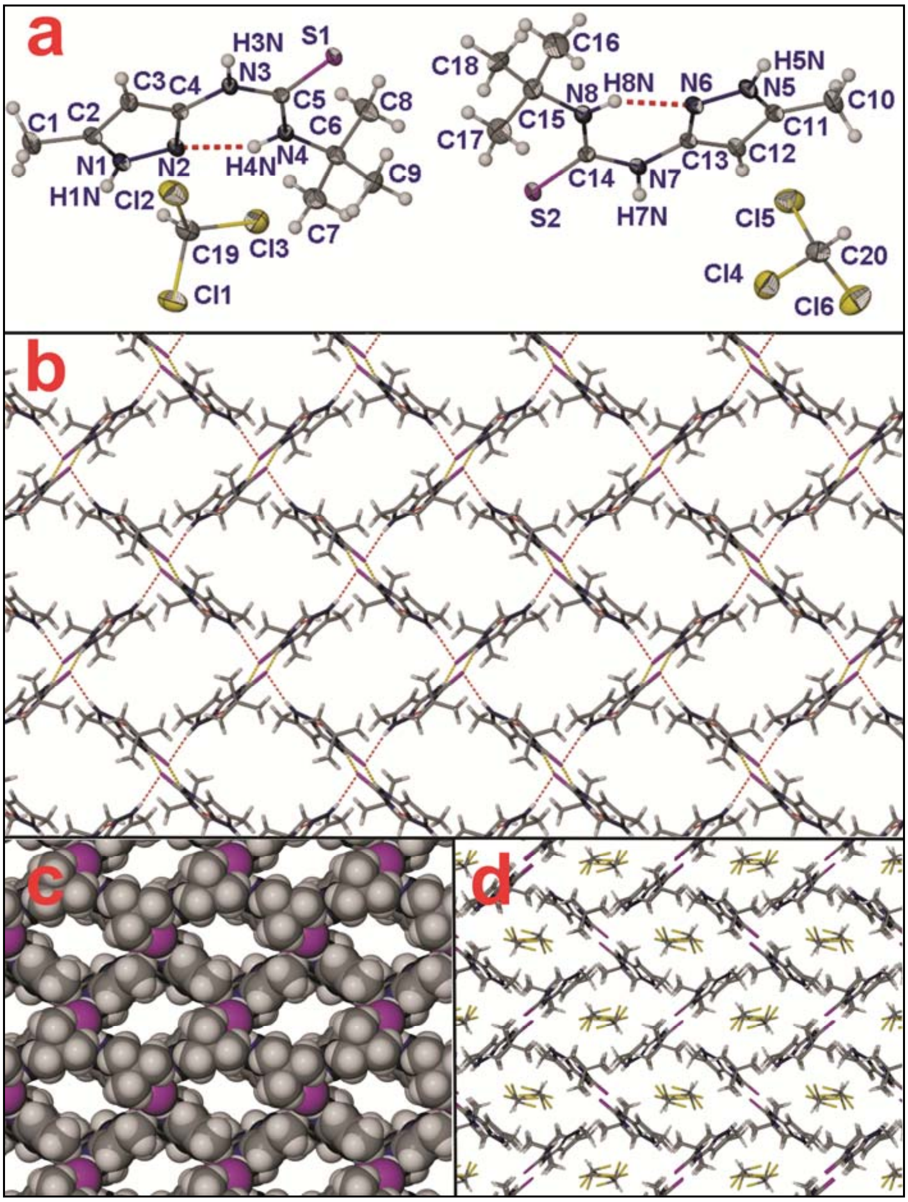

Figure 3.3. a) ASU of **3.3**.$CHCl_3$. Atoms are shown as ellipsoids at 50% probability. **b)** Packing of the dimers of **3.3** to form a 2D hydrogen bonded sheet. Hydrogen bonds between dimers are shown as yellow dashed lines. Hydrogen bonds involving the pyrazole N–H group are shown as red dashed lines. **c)** Packing of these sheets one on top of each other results in channels. **d)** These channels are occupied by the $CHCl_3$. Selected hydrogen bonds: N4···N2 = 2.684(3) Å; ∠ N4–H4N···N2 = 141.1°, N8···N6 = 2.703(3) Å; ∠ N8–H8N···N6 = 140.7°, N3···S1^{i} = 3.367(2) Å; ∠ N3–H3N···S1^{i} = 162.0°, N7···S2^{ii} = 3.328(2) Å; ∠ N7–H7N···S2^{ii} = 162.1°, N1···S1^{ii} = 3.296(2) Å; ∠ N1–H1N···S1^{ii} = 169.5° and N5···S2^{ii} = 3.346(2) Å; ∠ N5–H5N···S2^{ii} = 166.3° (*i* = -x, 1-y, 1-z, *ii* = 1-x, 1-y, 1-z).

The dimer formation, through the $R_2^2(8)$ hydrogen bond motif interaction between the urea functionalities, is also present in the **3.3**·$CHCl_3$ structure. Once again these dimers interact through the Lewis acidic pyrrolic N–H group. Unlike the previous structure where this hydrogen bonding led to a 3D packing arrangement of edge-to-face dimer packing the solvate structure has 2D hydrogen bonded sheets with the same edge-to-face packing of dimers (Figure 3.3b). These sheets pack one on top of each other forming tubular channels that contain the chloroform guests (Figure 3.3c–d).

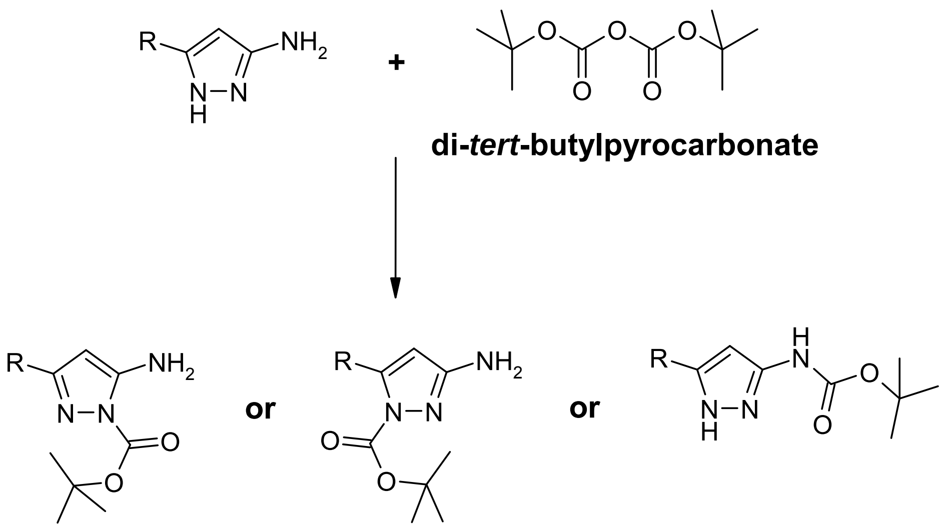

Scheme 3.2 Possible reaction products from the reaction of 3-amino-5-methylpyrazole with di-*tert*-butylpyrocarbonate, the BOC-protection reaction.

As a result of the reaction between 3-amino-5-methylpyrazole and isocyanates leading to carboxamide compounds **3.1** and **3.2**, an alternative method was used to obtain the desired pyrazole ureas. *tert*-Butyloxycarbonyl (BOC) protection is a very well known method in chemical synthesis and protection of the pyrazole group has indeed been used to synthesis pyrazole amides and ureas of 3-amino-5-methylpyrazole and other aminopyrazoles.[68-75] The reaction of one equivalent of di-*tert*-butylpyrocarbonate with one equivalent of 3-amino-5-R–pyrazole (where R = H, methyl or phenyl) in $CHCl_3$ at room temperature gave compounds **3.4**, **3.5** and **3.6** in yields of 69%, 96% and 96%, respectively (Scheme 3.2 and Figure 3.4).

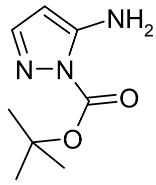

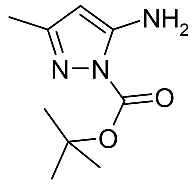

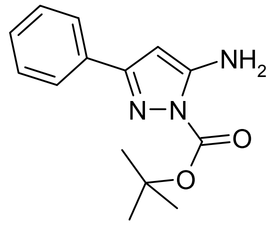

3.4 **3.5** **3.6**

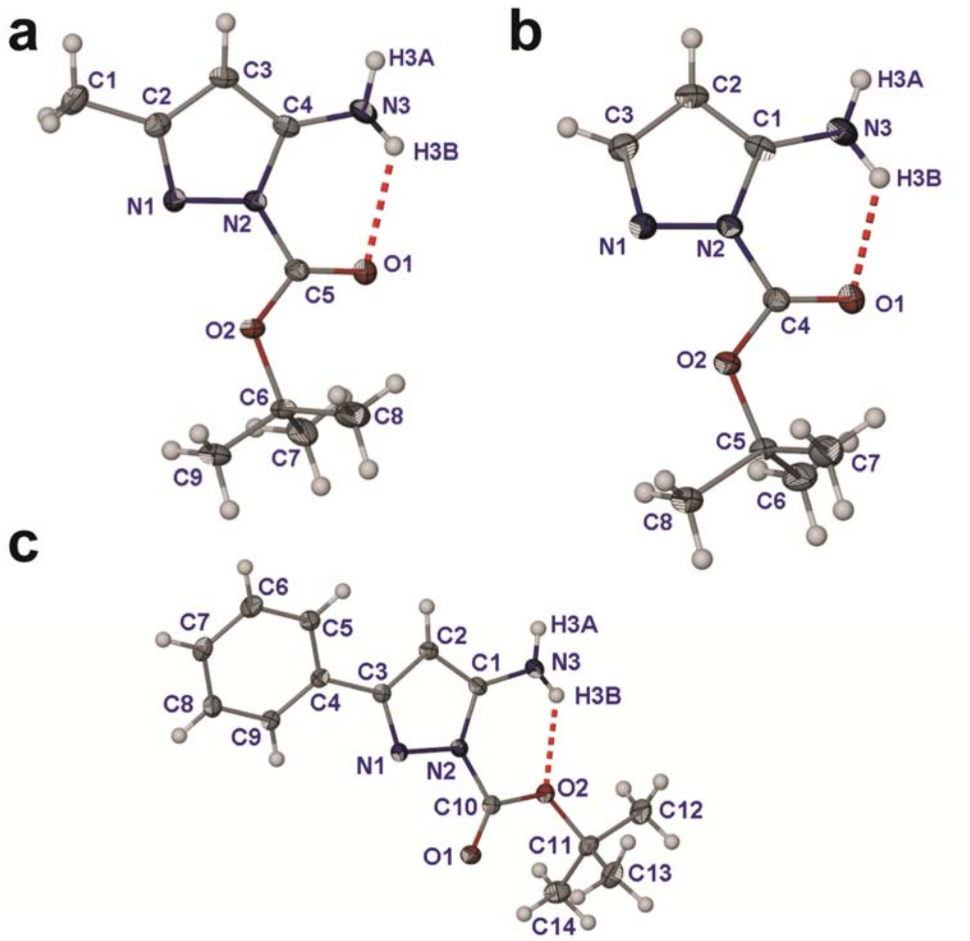

Figure 3.4. Molecular structures of **3.4**, **3.5** and **3.6**. **a)** BOC protected 3-amino-5-methylpyrazole, **3.5**. **b)** BOC protected 3-aminopyrazole, **3.4**. **c)** BOC protected 3-amino-5-phenylpyrazole, **3.6**. Selected hydrogen bonds: **3.5** N3···O1 = 2.7812(16) Å; ∠ N3–H3N···O1 = 119.8°, **3.4** N3···O1 = 2.735(2) Å; ∠ N3–H3N···O1 = 128.1° and **3.6** N3···O2 = 2.6918(11) Å; ∠ N3–H3N···O2 = 121.6°. Atoms are shown as ellipsoids at 50% probability.

The analytical and spectroscopic data, along with the crystallographically determined molecular structures (Figure 3.4), showed that "protection" of the nitrogen position next to the amine had occurred. These results agree with the reported literature results for similar reactions.[70,75] There is an intra-molecular hydrogen bond between the amine group and the BOC group within each of the structures of **3.4**, **3.5** and **3.6**. The hydrogen bond is to the carbonyl group of the BOC group in the structures of **3.4** and **3.5** and to the ether oxygen of the BOC group in the structure of **3.6**. This BOC protection of the Lewis acidic pyrrolic N–H group leaves the amino group available for further derivatisation.

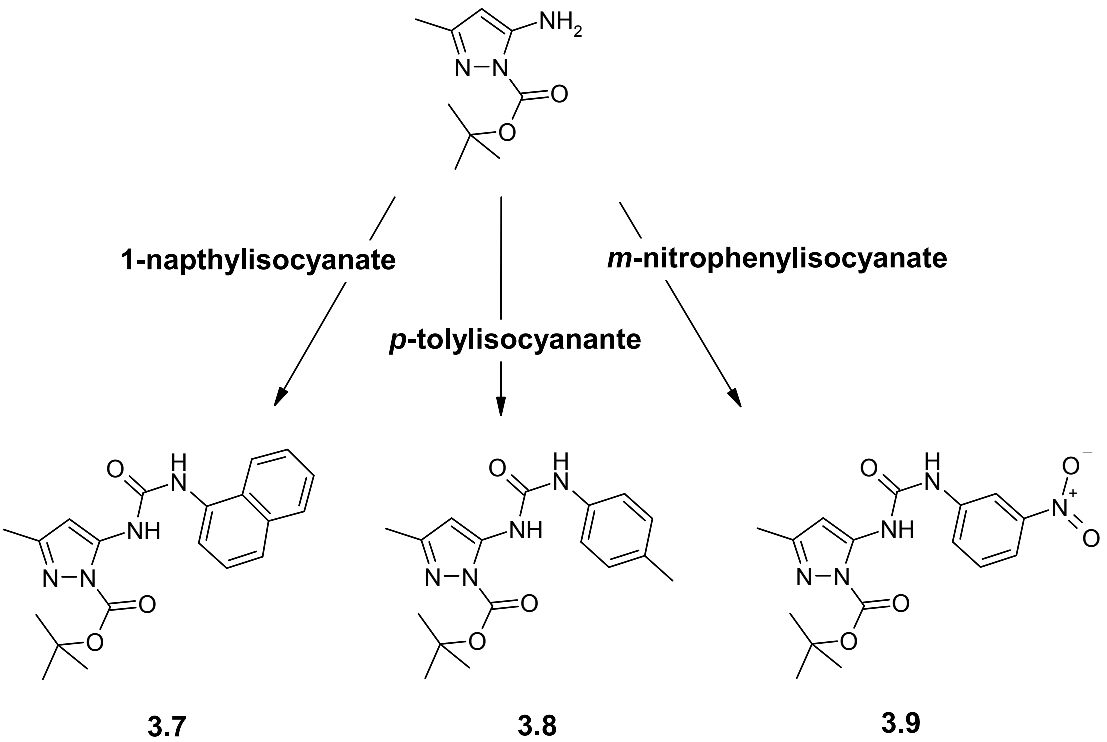

Scheme 3.3 Reaction products, **3.7**, **3.8** and **3.9**, of the pyrazole urea synthesis by reacting **3.5** with three different isocyanates.

Derivatisation of the free amine group of **3.5** by reaction with the isocyanates 1-napthylisocyanate, *p*-tolylisocyanate, *m*-nitrophenylisocyanate in refluxing $CHCl_3$ gave the BOC-protected urea derivatised pyrazoles **3.7**, **3.8** and **3.9**, respectively, in relatively high yields (Scheme 3.3). Compounds **3.7**, **3.8** and **3.9** did not form gels. The crystal structure determined for **3.8** shows how the BOC-protecting group has remained on the same position on the pyrazole and the amine has been derivatised to a urea (Figure 3.5). This Z′ = 2 structure (two of the same molecules in the ASU)[76] shows how **3.8** has intra-molecular hydrogen bonds between the urea NH next to the pyrazole to the carbonyl of the BOC moiety (similar to what is seen in compound **3.5**) and the other NH of the urea group hydrogen bonds the Lewis basic pyrazolyl N-donor group of neighbouring molecules. This hydrogen bonding results in helical columns (Figure 3.6).

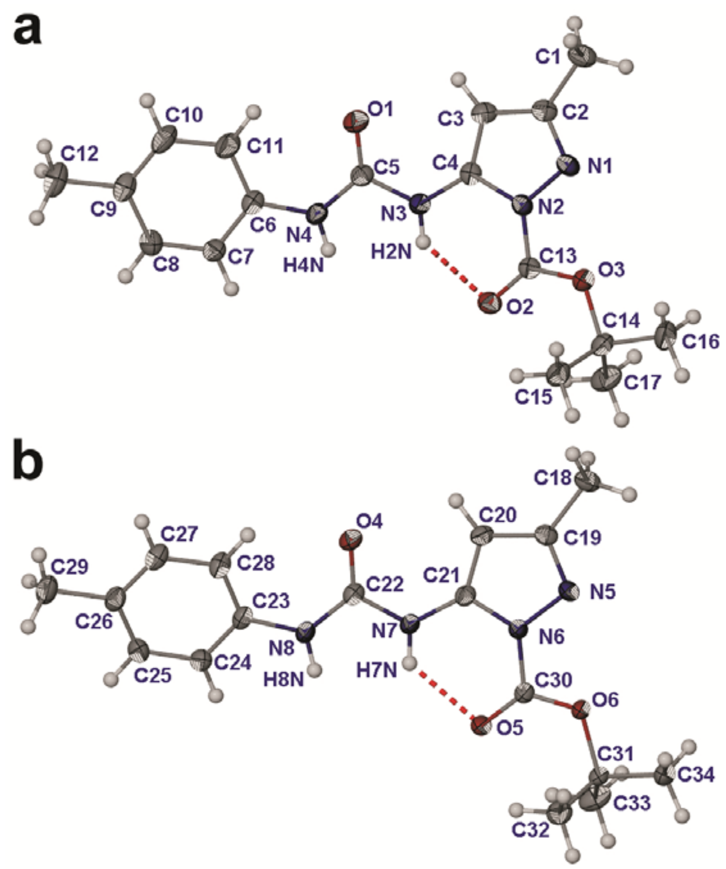

Figure 3.5. The two molecular structures of the two molecules of the ASU of the crystal structure of **3.8.** Atoms are shown as ellipsoids at 50% probability. Selected hydrogen bonds: N3···O2 = 2.7338(18) Å; ∠ N3–H3N···O2 = 120.5° and N7···O5 = 2.7049(17) Å; ∠ N7–H7N···O5 = 125.9°.

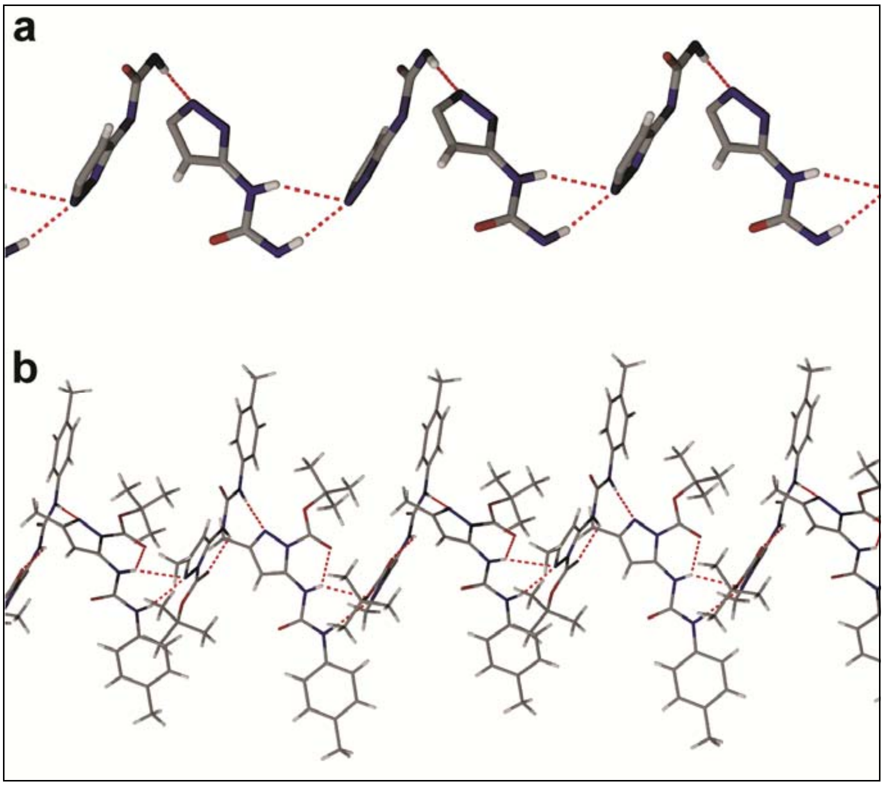

Figure 3.6. a) Simplified diagram showing the donor and acceptor groups. b) Helix formed by **3.8**. Selected hydrogen bonds: N4···N5 = 3.0243(19) Å; ∠ N4–H4N···N2 = 173.0° and N8···N1^{i} = 2.9437(19) Å; ∠ N8–H8N···N1^{i} = 150.1° (*i* = -x, y, -z).

BOC deprotection of **3.9** by refluxing in acetic acid overnight yielded compound **3.10**. The crystal structure of compound **3.10** was determined (Scheme 3.4 and Figure 3.7). The structure exhibits an intra-molecular hydrogen bond between N4 and N2 within the ASU of **3.10** which results in an *anti* conformation for the urea group. This is similar to the conformation found for the structures of thiourea-containing compound **3.3**. A few 2-pyridylureas and 2-pyrrolyleurea derivatives show similar behaviour, namely forming an intra-molecular hydrogen bond and causing the urea to be in an *anti* conformation.[77-80] The rest of the urea group that is not involved in the intra-molecular hydrogen bond forms a dimer with the neighbouring molecule via a $R_2^2(8)$ hydrogen bond motif, similar to the structures of **3.3** and related compounds.[56-67,77-80] These dimers form a 1D hydrogen bonded chain with N1–H1···O3 hydrogen bond between the pyrazole and nitro groups (Figure 3.8). These flat chains stack one on top of each other resulting in 2D stacks (stack distance 3.3 Å). These stacks run perpendicular to each other (Figure 3.9). This stacking is possible due to the flatness of **3.10**, RMS value of 0.0694 Å.[81]

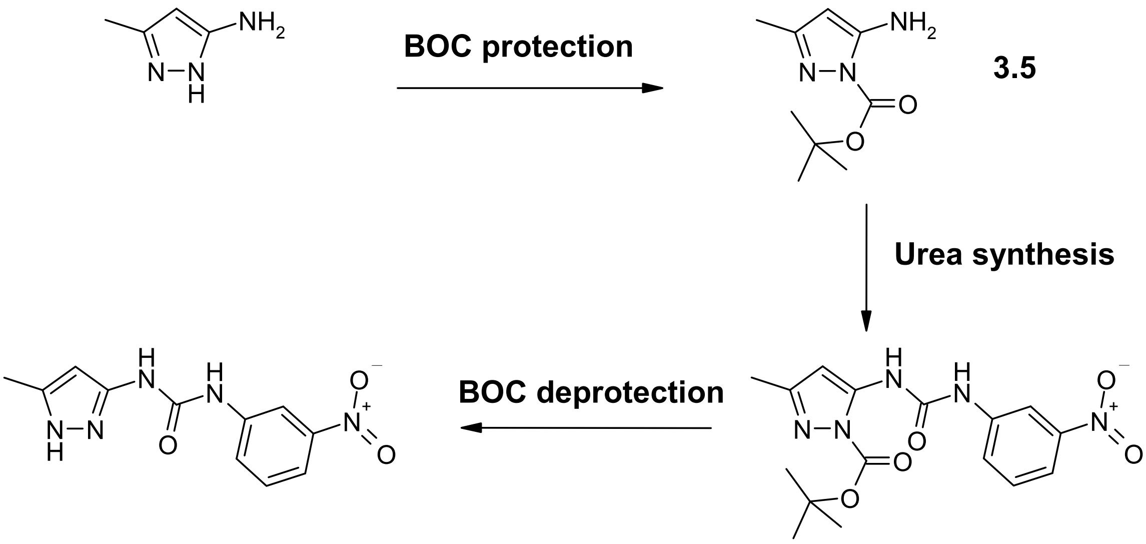

Scheme 3.4 The synthetic route to the synthesis of **3.10** from 3-amino-5-methylpyrazole via a BOC-protection of the pyrazole ring.

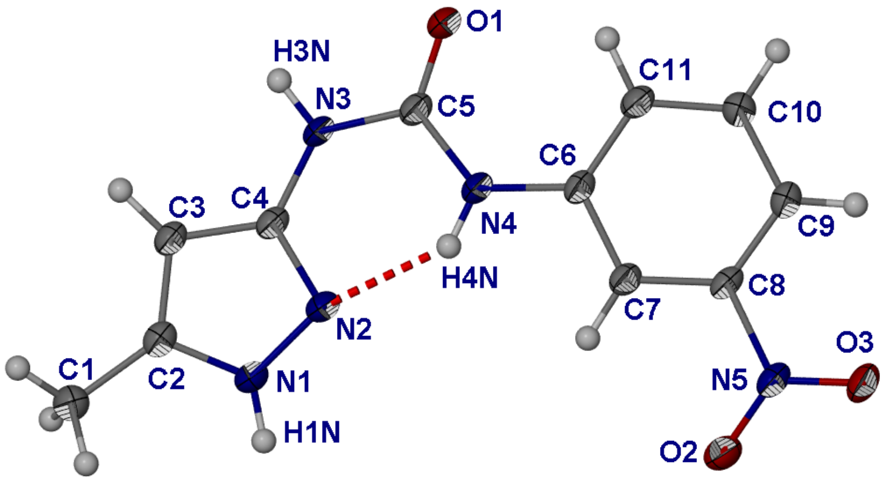

Figure 3.7. Molecular structure of **3.10**. Atoms are shown as ellipsoids at 50% probability. Selected hydrogen bond: N4···N2 = 2.6651(17) Å; ∠ N4–H4N···N2 = 139.4°.

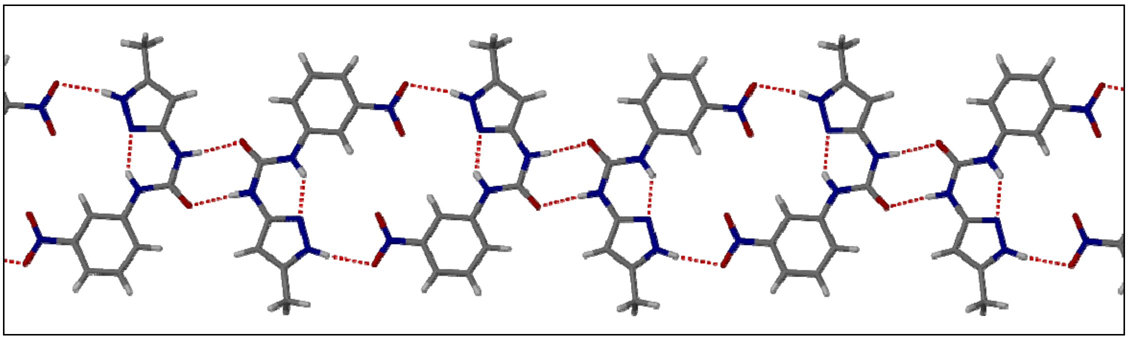

Figure 3.8. Hydrogen bonding of the dimers of **3.10** to form a hydrogen bond chain. Selected hydrogen bonds: N3···O1^{i} = 2.8153(15) Å; ∠ N3–H3N···O1^{i} = 166.3° and N1···O3^{ii} = 2.9703(16) Å; ∠ N1–H1N···O3^{ii} = 171.1° (*i* = -x, 1-y, -z and *ii* = 1-x, -y-1, -z)

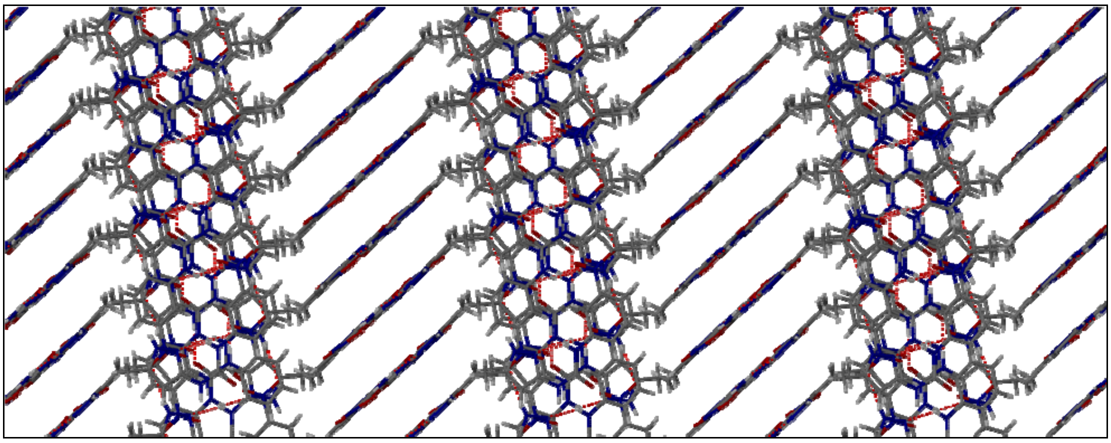

Figure 3.9. Perpendicular inter-chain packing of **3.10**.

As the synthesis of the carboxamides from reaction of the aminopyrazole with an isocyanate results in an unreacted primary amine group, we attempted to react 3-amino-5-methylpyrazole with two equivalents of *p*-tolyl isocyanate in refluxing $CHCl_3$ in order to derivatise both primary and ring nitrogen atoms. This would give a compound with both amide and urea groups. There are two possible isomers that can be produced in this reaction (Scheme 3.5). The reaction was performed overnight in refluxing $CHCl_3$. The ^{1}H NMR spectrum of the crude product showed that both isomers, **3.11a** and **3.11b**, are produced as there are two resonances for every proton type. The existence of the two isomers was confirmed by the observation of two spots by thin layer chromatography

(TLC) with ethyl acetate as the solvent.

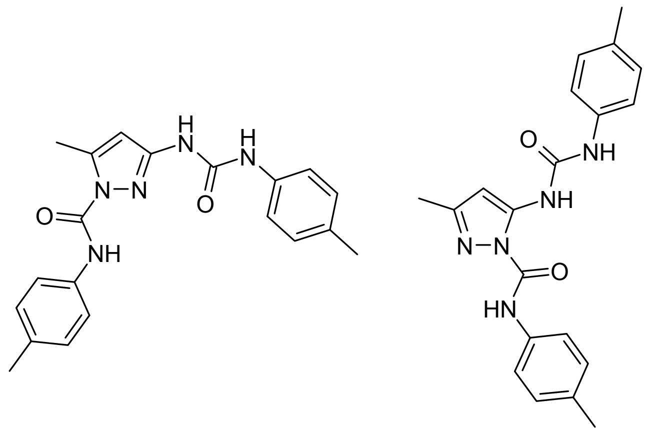

3.11a **3.11b**

Scheme 3.5 The two possible isomers from the reaction of two equivalents of *p*-tolylisocyanate with 3-amino-5-methylpyrazole. **3.11a** 1-carboxamide-3-urea isomer and **3.11b** 2-carboxamide-3-urea isomer.

Recrystallisation of the mixtures of products from hot $CHCl_3$ resulted in the isolation of compound **3.11a**, and therefore separation of the isomers. Compound **3.11a** was found not to form gels. The structure of this crystalline material from $CHCl_3$, **3.11a** polymorph I, was determined (Figure 3.10). In this structure the urea is in an anti conformation resulting from a hydrogen bond to the Lewis basic pyrazolyl N-donor group of the pyrazole from the N4–H4N.[77-80] The carboxamide N5–H5N group also forms intra-molecular hydrogen bonds to the same Lewis basic pyrazolyl N-donor group. The rest of the urea group forms a dimer motif through a $R_2^2(8)$ hydrogen bond motif (Figure 3.11).[56-67,77-80] There are only weak C–H···O interactions with the carbonyl of the carboxamide group leading to a 1D chain of these V-shaped molecules. Subsequent packing by van der Waals space filling completes the structural description. This structure shows how even though there is already a hydrogen bond to the Lewis basic pyrazolyl N-donor group that the urea has a propensity to go into an *anti* conformation and hydrogen bond to the N-donor group of the pyrazole.

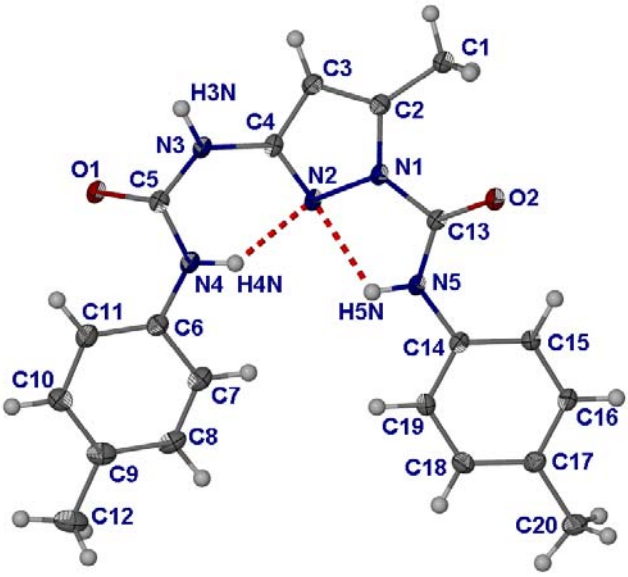

Figure 3.10. Molecular structure of **3.11a** in form I. Atoms are shown as ellipsoids at 50% probability. Selected hydrogen bonds: N4···N2 = 2.7328(18) Å; ∠ N4–H4N···N2 = 139.0^{o} and N5···N2 = 2.6153(17) Å; ∠ N5–H5N···N2 = 112.7^{o}.

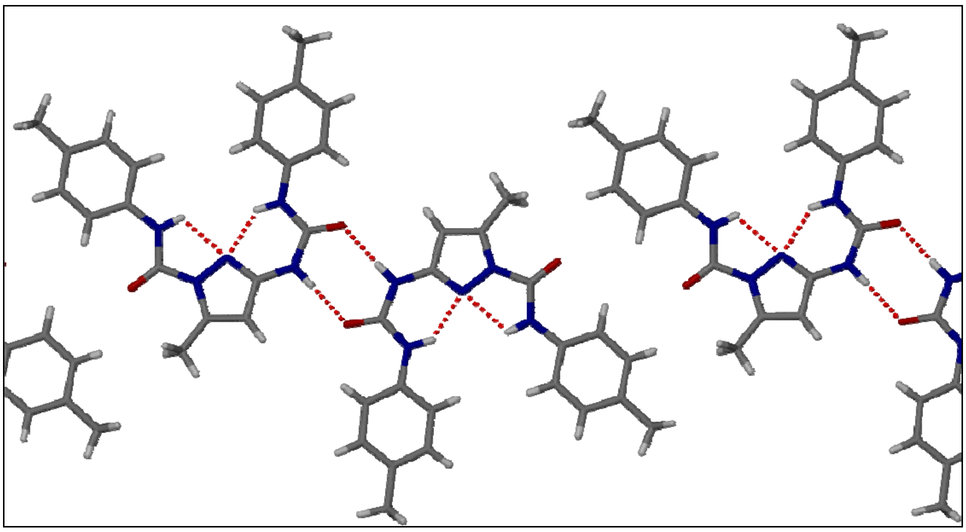

Figure 3.11. Dimer formation by **3.11a** in form I. Selected hydrogen bonds: N3···O1^{i} = 2.7859(16) Å; ∠ N3–H3N···O1^{i} = 166.0^{o} (i = -x, y, -z).

Interestingly, when **3.11a** was crystallised from the more polar solvent MeOH a conformational polymorph,[82] form II, was found (Figure 3.12). Polymorphism is an important phenomenon, especially in pharmaceutical compounds.[83-85] The conformational differences of compound **3.11a** in these two forms involves the *syn* and *anti* isomers of the urea group. In the structure of form II the urea group is in a *syn* conformation (Figure 3.12) and as a result only the N–H group of the carboxamide group hydrogen bonds to the Lewis basic pyrazolyl N-donor group of the pyrazole which has similar bond lengths and angles to that in form I. This leaves the urea group to form a urea tape motif with a hydrogen bond of $R_2^1(6)$ (Figure 3.13).[86] The resultant V-shaped columns interact weakly through C–H···O hydrogen bonding of the carbonyl group of the carboxamide moiety to give 2D layers that stack next to each other through filling of space in an anti-parallel fashion. This conformation change due to recrystallisation from a more polar solvent demonstrates how even though the urea or thiourea group on these urea and thiourea functionalised pyrazoles has a strong propensity to form an *anti* conformation and an intra-molecular hydrogen bond, it can be induced to form a *syn* conformation.[77,80]

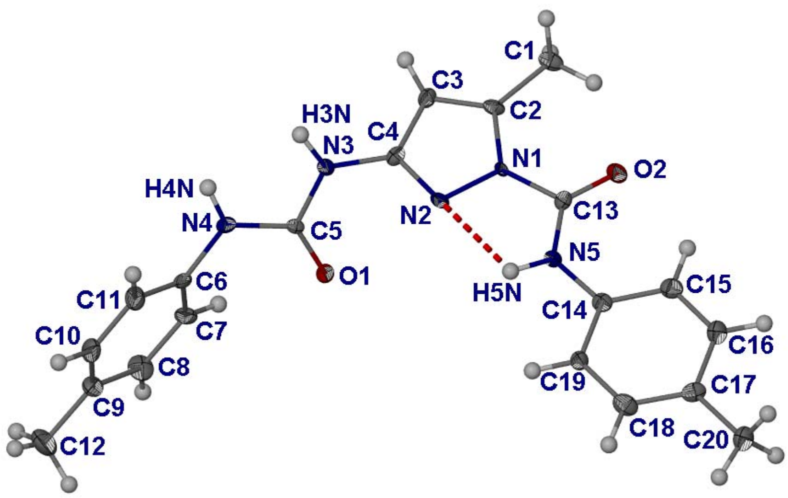

Figure 3.12. Molecular structure of **3.11a** in form II. Atoms are shown as ellipsoids at 50% probability. Selected hydrogen bond: N5···N2 = 2.660(12) Å; ∠ N4–H4N···N2 = 112.0°.

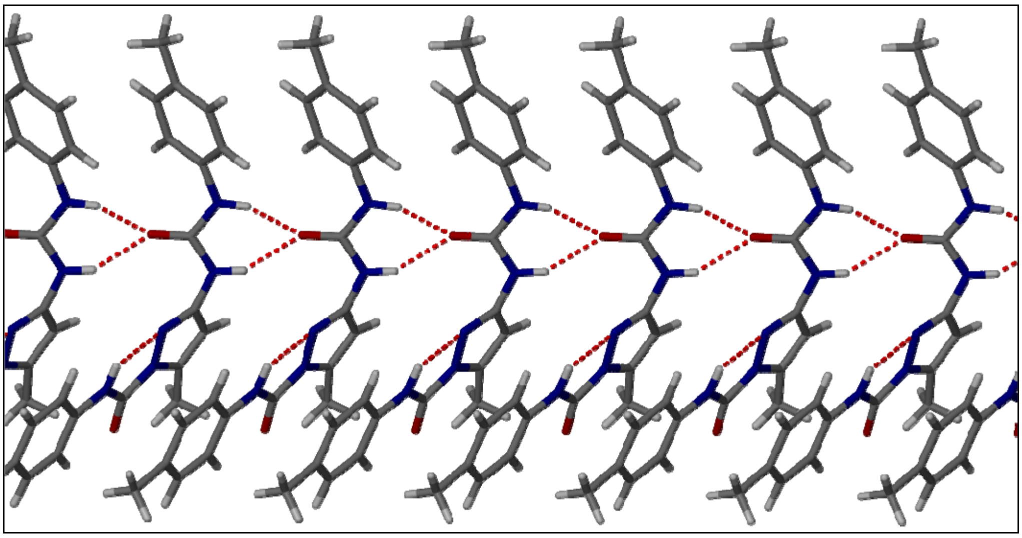

Figure 3.13. Formation of a urea tape by **3.11a**, form II. Selected hydrogen bonds: N3···O1^i = 2.902(11) Å; ∠ N3–H3N···O1^i = 151.3° and N4···O1^i = 2.822(11) Å; ∠ N4–H4N···O1^i = 156.5° (*i* = x-1, y, z).

In summary, it was found that synthesis of urea and thiourea derivatised pyrazoles was not as straightforward as it at first appeared, i.e. reacting the isocyanate or isothiocyanate with the aminopyrazole did not always lead to a urea or thiourea. The reaction of *t*-butyl isothiocyanate with 3-amino-5-methylpyrazole in refluxing $CHCl_3$ was performed, and in agreement with literature results, the derived thiourea compound **3.3** was isolated.[7,48,53-55] The reaction of isocyanates with 3-amino-5-methylpyrazole results in the formation of carboxamides, compounds **3.1** and **3.2** being two examples.[7,47,48] This problem was circumvented by BOC-protection of the pyrazole ring allowing for the urea functionalisation of the amine group to yield the desired urea functionalised pyrazole compounds. The reaction of two equivalents of *p*-tolyl isocyanate with 3-amino-5-methylpyrazole yielded a mixture of isomeric products. Compound **3.11a**, isolated by crystallisation from hot $CHCl_3$, showed conformational polymorphism due to the transition from *anti* to *syn* conformations of the urea group. The propensity of the thiourea and urea groups of compounds **3.3** and **3.10**, respectively, to form an intra-molecular hydrogen bond and therefore be in an *anti* conformation will be an obstacle that needs to be circumvented to allow for the urea and thiourea groups to interact with themselves and/or anions in the study of any gel formation and subsequent anion tuning of any gels. The following sections that follow are, therefore, studies to determine ways of breaking the inter-molecular hydrogen bond, to allow for anion interaction and gel formation.

3.3 Metal coordination chemistry of urea functionalised ligands

Urea-derivatised pyrazoles have not been studied as ligands for transition metals,[48] although Kraatz has studied the coordination chemistry of related amide-derivatised pyrazoles.[68,72] We have undertaken the reaction of urea pyrazole ligands **3.10** and **3.11** with a range of transition metal salts in order to obtain insight into possible assembly and anion interaction modes that may be found within gels. While a number of single crystals were obtained that give interesting structural details, no gels were formed and no pure compounds were isolated in large quantities, and hence, no claim is made that the structures presented herein are representative of the bulk material. However, the structural results do represent useful information into the coordination modes of the urea-derivatised pyrazoles.

The first row transition metals, Ag(I) and Cd(II) were used in the coordination experiments because of their softness. On this basis we expected them to coordinate to the pyrazole ligand, as seen in the studies of Halcrow and Kraatz.[14-17,48,68,72,87] There is an increasing interest in coordination metal-tuned LMWGs, especially those formed by the first row transition metals because of the interesting properties shown by these metals, such as their redox chemistry, spectroscopic properties, catalytic properties and magnetism, to name but a few.[22] The studies of the transition metal complexes presented here, were driven by the need to better understand the coordination chemistry of the ligands. With this information in hand we hoped to be able to further tune the properties of LMW gels formed by utilising urea-derivatised pyrazoles. The reactions between ligand **3.10** and the first row transition metals often led to mixtures of precipitates, from which it was difficult to isolate pure compounds. In the case of Ag(I) salts with **3.10**, sticky precipitates that resembled gels were formed but these were not crystalline nor gelatinous. In a few cases, with Zn(II), Cu(II) and Cd(II) salts, crystalline materials were isolated, and these are described in the following section.

As a direct comparison with the anion-binding systems reported by Halcrow and co-workers,[14-17,48,87] compound **3.10** was mixed in a MeOH solution with $ZnCl_2$ in a 3:1 ratio. The reaction yielded single crystals of formula [$Zn_2Cl_2(\mu\text{-}Cl)_2(\kappa\text{-}N,O\text{-}\mathbf{3.10})_2$] which were characterised by single crystal x-ray diffraction (Figure 3.14). The dimetallic complex is made up of two ligands of **3.10** each coordinated to a different zinc(II) centres. Each zinc(II) ion also binds to one terminal and two bridging chloride ligands to give a chloride-bridged dimer involving five coordinate zinc centres in a distorted trigonal bipyramidal geometry. The ASU consists of half of the complex. Ligand **3.10** acts a bidentate chelate forming a six-membered ring in which the Lewis basic pyrazolyl N-donor group, N2, in this case the nitrogen nearest the urea group of the pyrazole ring and the oxygen of the carbonyl group of the urea group, O1, coordinate to the zinc. The ligand is planar, rms deviation for all non–hydrogen atoms is 0.04 Å. The bidentate character precludes any chances of **3.10** forming a tripodal complex like that seen with the anion-binding systems of Halcrow and coworkers.[14-17,48,87] The bidentate coordination of **3.10** is similar to the amide pyrazole complexes reported by Kraatz and to complexes of triazole amides.[68,72,88,89] The bidentate coordination is also similar to that of the coordination complexes of 2-pyridylureas.[78,90,91]

The observed hydrogen bonding motifs are essential to the understanding of this ligand, its coordination complexes and the gelation possibilities of both. The Lewis acidic pyrrolic N1–H1 group intra-molecularly hydrogen bonds to the bridging chloride Cl2. The CH group C7–H7 also forms intra-molecular hydrogen bonds with the coordinated O1 and O2 of the nitro group helping to constrain ligand **3.10** into a planar conformation. The urea NH donor groups are free to hydrogen bond to the coordinated chlorides resulting in 1D stacks of [$Zn_2Cl_2(\mu\text{-}Cl)_2(\kappa\text{-}N,O\text{-}\mathbf{3.10})_2$] (Figure 3.15a). The NH group (N4-H4) nearest the nitrophenyl group hydrogen bonds to the equatorial (non-bridging) chloride. The NH group (N3-H3) next to the pyrazole group hydrogen bonds to the bridging chloride. The Lewis acidic pyrrolic N1–H1 group interacts with neighbouring stacks by hydrogen bonding to the equatorial chloride $Cl1^{ii}$ (Figure 3.15b).

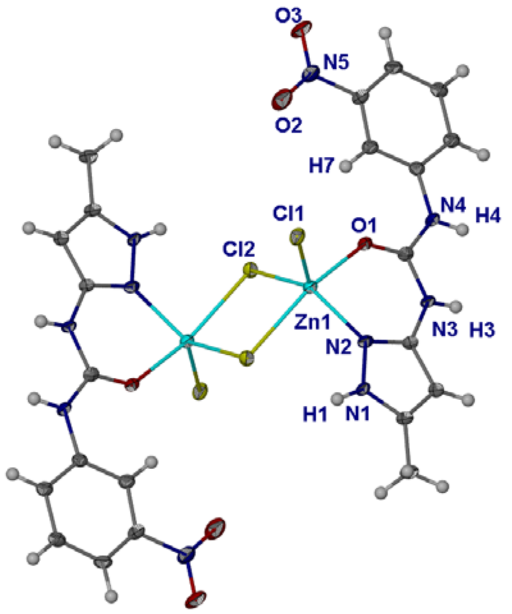

Figure 3.14. X-ray molecular structure of [$Zn_2Cl_2(\mu\text{-}Cl)_2(\kappa\text{-}N,O\text{-}\mathbf{3.10})_2$] (50 % ellipsoids). Selected bond distances: Zn1···N2 = 2.013(5) Å, Zn1···O1 = 2.093(4) Å, Zn1···Cl2 = 2.5845(17) Å, Zn1···Cl1 = 2.2492(17) Å and Zn1···Cl2^{i} = 2.3289(18) Å (*i* = -x, 2-y, -z).

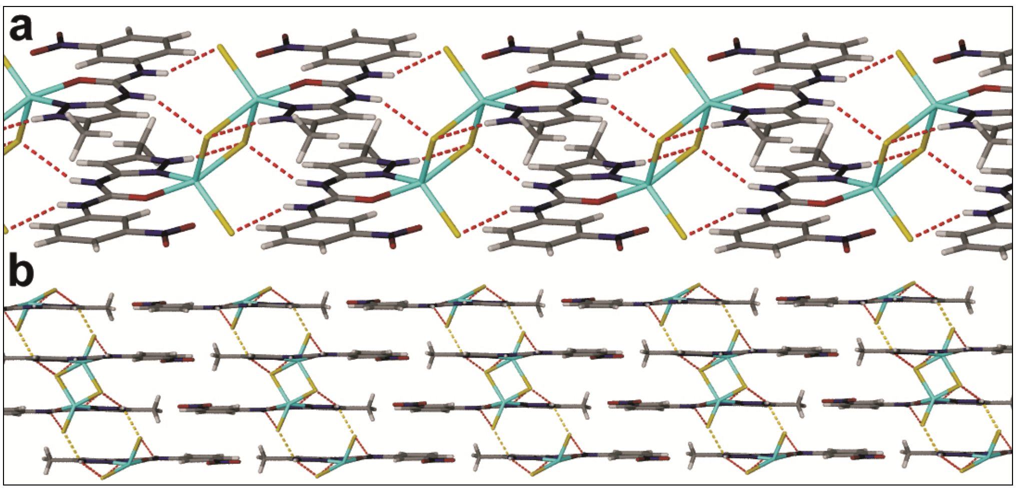

Figure 3.15. Hydrogen bonding of complexes [$Zn_2Cl_2(\mu\text{-}Cl)_2(\kappa\text{-}N,O\text{-}\mathbf{3.10})_2$] into columns **(a)** which are stacked next to each other **(b)**. Selected hydrogen bonds: N1···Cl2 = 3.126(4) Å; ∠ N1–H1···Cl2 = 120.7°, N1···Cl1^{ii} = 3.314(4) Å; ∠ N1–H1···Cl1^{ii} = 128.3°, C7···O1 = 2.813(4) Å; ∠ C7–H7···O1 = 120.9°, C7···O2 = 2.705(4) Å; ∠ C7–H7···O2 = 97.6°, N4···Cl1^{iii} = 3.257(4) Å; ∠ N4–H4···Cl1^{iii} = 152.3° and N3···Cl1^{iii} = 3.292(4) Å; ∠ N3–H3···Cl1^{iii} = 146.1° (*ii* = -x, y, ½ - z and *iii* = x, y-1, z).

Copper coordination compounds with pyridyl ureas have become an interesting class of LMWGs.[21-37] The coordination chemistry of **3.10** with several copper salts was, therefore, investigated to elucidate the coordination chemistry of this metal to the urea-derivatised pyrazole ligand. Reaction of **3.10** with copper (II) bromide in a 2:1 ratio in MeOH gave [CuBr(*κ*-*N*,*O*-**3.10**)$_2$]Br·2H_2O (Figure 3.16).

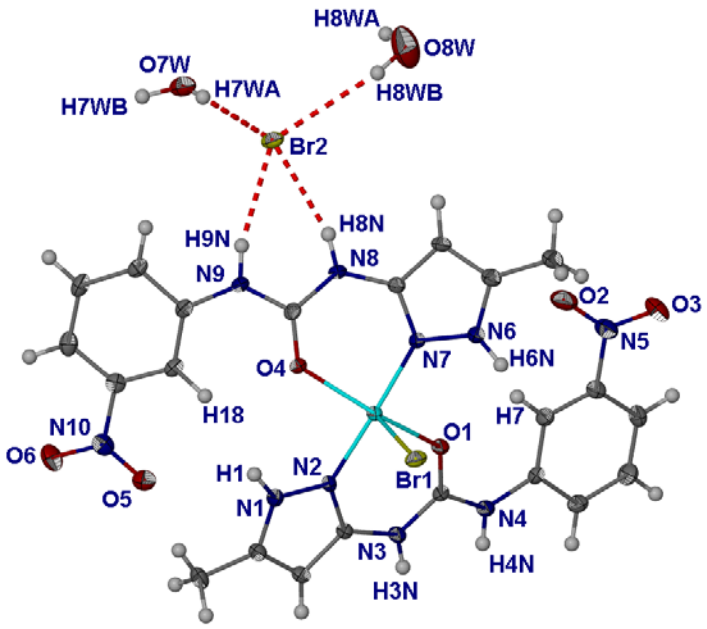

Figure 3.16. The ASU of [CuBr(*κ*-*N,O*-**3.10**)$_2$]Br.2H_2O showing the chelating coordination of compound **3.10** to copper and the hydrogen bonding to the anion by the urea group of **3.10**. Atoms shown as ellipsoids at 50 % probability. Selected coordination bonds: Cu1···O1 = 2.034(2) Å; Cu1···O4 = 2.025(2) Å; Cu1···N2 = 1.923(2) Å; Cu1···N2 = 1.923(2) Å; Cu–Br 2.693(1) Å with angles of ∠ N2–Cu1–N7 = 176.7(1)^o and ∠ O1–Cu1–O4 = 144.5(1)^o. Selected hydrogen bonds: N8···Br2 = 3.370(2) Å; ∠ N8–H8N···Br2 = 149.6^o, N9···Br2 = 3.370(2) Å; ∠ N9–H9N···Br2 = 149.6^o, O7W···Br2 = 3.481(2) Å; ∠ O7W –H7W···Br2 = 165.6^o, O8W···Br2 = 3.706(2) Å; ∠ O8W –H8W ···Br2 = 154.7^o, C7···O1 = 2.854(3) Å; ∠ C7–H7···O1 = 119.8^o, C7···O2 = 2.711(4) Å; ∠ C7–H7···O2 = 96.5^o, C18···O4 = 2.984(3) Å; ∠ C18–H18···O4 = 116.2^o and C18···O5 = 2.721(3) Å; ∠ C18–H18···O5 = 96.6^o.

The two **3.10** ligands once again bind as bidentate chelates *via* the N and O atoms. The coordination sphere is completed by a bromide ligand to give a five coordinate copper centre with a distorted trigonal bipyramidal geometry. The distortion from square pyramidal geometry is due to the steric bulkiness of the nitrophenyl groups and the hydrogen bonding of the Lewis acidic pyrrolic N–H groups not being intra-molecular. The distorted trigonal bipyramidal geometry of this complex is different to the reported copper complexes of the amide pyrazole, triazole amides and 2-pyridylureas, where either an octahedral or square pyramidal geometry has been seen.[68,72,78,88-91] The two ligands adopt a mutually *trans* orientation with the oxygen and nitrogen coordinated opposite each other with the oxygen coordinated in the equatorial plane of the copper centre and the nitrogens in the axial positions. The *trans* coordination is similar to that seen with the complexes formed by amide pyrazole, triazole amides and 2-pyridylureas ligands.[68,72,78,88-91] The **3.10** molecules within this complex are slightly less planar, with the RMS deviation from planarity being 0.141 Å and 0.120 Å.

Once again the hydrogen bonding is of interest in this structure, to give information on how the complexes interact with anions. The availability of six NH hydrogen bond donors within this complex results in an extensive hydrogen bonding network. The Lewis acidic pyrrolic N1–H1 group hydrogen bonds to the interstitial (secondary coordination sphere) bromide. The Lewis acidic pyrrolic group, N6–H6N, hydrogen bonds to one of the interstitial waters. Both urea groups hydrogen bond to bromides through $R_2^1(6)$ hydrogen bonding motifs (Figure 3.16), one to the coordinated bromide and the other to the interstitial bromide. The interstitial bromide receives one hydrogen bond each from the two interstitial waters meaning it receives a total of five hydrogen bonds. The hydrogen bonding of the urea groups and the Lewis acidic pyrrolic N1–H1 group to the bromides leads to a ribbon of [CuBr(*κ*-*N,O*-**3.10**)$_2$]Br with the planarity of **3.10** aiding the assembly (Figure 3.17). The interstitial waters hydrogen bond to each other and the coordinated bromide connecting the ribbons of [CuBr(*κ*-*N,O*-**3.10**)$_2$]Br together to complete the packing.

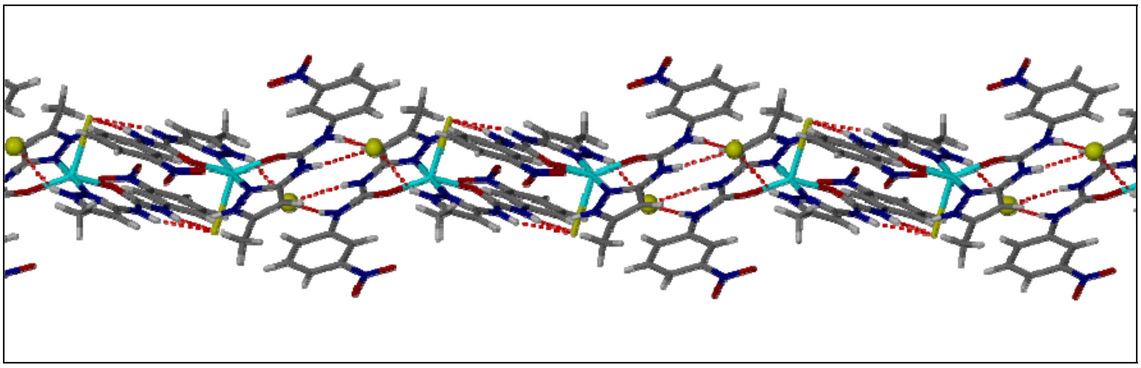

Figure 3.17. Extensive hydrogen bonding of [CuBr(κ-*N,O*-**3.10**)$_2$]Br.2H$_2$O. Selected hydrogen bonds: N1⋯Br2^{i} = 3.370(2) Å; ∠ N1–H1⋯Br2^{i} = 149.6°, N6⋯O7W^{ii} = 2.806(3) Å; ∠ N6–H6N⋯ O7W^{ii} = 152.2°, N3⋯Br1^{iii} = 3.304(2) Å; ∠ N3–H3N⋯Br1^{iii} = 158.7°; N4⋯Br1^{iii} = 3.371(2) Å; ∠ N4–H4N⋯Br1^{iii} = 157.2°, O7W⋯O8W^{iv} = 2.885(4) Å; ∠ O7W –H7W⋯O8W^{iv} = 164.9° and O8W⋯Br1^{v} = 3.293(2) Å; ∠ O8W –H8W⋯Br1^{v} = 162.9° (*i* = 1-x, 1-y , -z; *ii* = 1-x, ½+y , ½-z; *iii* = -x, 1-y , -z; *iv* = x, ½-y, z-½ and *v* = 1-x, y-½, ½-z).

The reaction of two equivalents of **3.10** with Cu(BF$_4$)$_2$ in MeOH results in the complex [Cu(κ-*N,O*-**3.10**)$_2$(MeOH)$_2$] 2BF$_4$ being isolated as blue plate crystals (Figure 3.18). Once again the ligand **3.10** is coordinated to the transition metal in a bidentate manner. The two ligands are coordinated *trans* to each other with the O and N opposite each other as seen in the structure of [CuBr(κ-*N,O*-**3.10**)$_2$]Br·2H$_2$O and the complexes formed by amide pyrazole, triazole amides and 2-pyridylureas ligands.[68,72,78,88-91] The MeOH is coordinated in the axial positions of a Jahn-Teller distorted octahedral copper centre. Unlike the two previous complexes in which ligand **3.10** is planar, the ligand **3.10** within this structure is not planar. This is due to the two ligands coordinating to the metal in an ideal square planar manner resulting in steric hindrance between the nitrophenyl groups causing the non-planar character of the ligand. The Lewis acidic pyrrolic N1–H1 group is hydrogen bonded to the coordinated oxygen of the carbonyl group of the urea functionality aiding the planarity of the coordination.

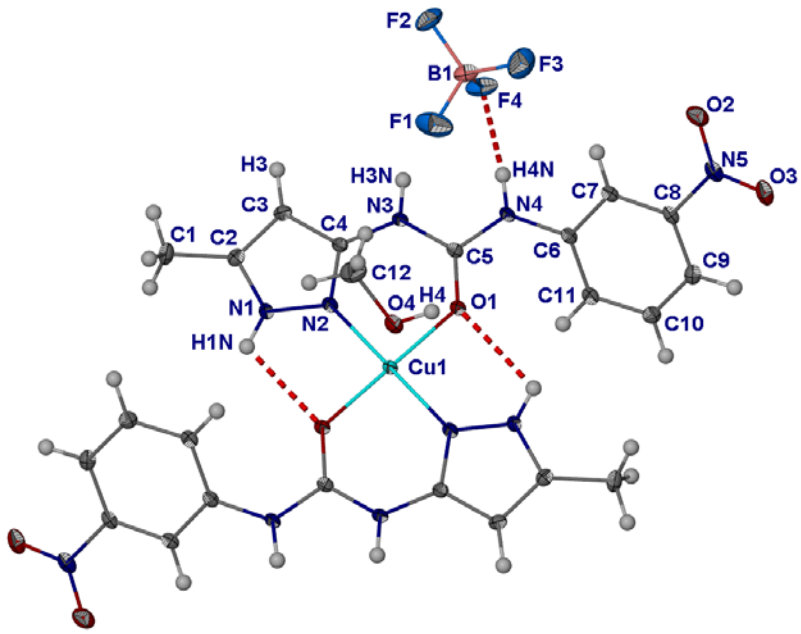

Figure 3.18. The complex of [Cu(*κ-N,O*-**3.10**)$_2$(MeOH)$_2$](BF$_4$)$_2$ showing the chelating coordination of compound **3.10** to copper and the hydrogen bonding to the anion by the urea group of **3.10**. Atoms shown as ellipsoids at 50 % probability and labelled atoms represent the asymmetric unit. Selected bond distances: Cu1···N2 = 1.9209(15) and Cu1···O1 = 1.9706(11) Cu1···O4 = 2.5243(13). Selected hydrogen bonds: N1···O1^i = 2.898(2); ∠ N1-H1N···O1^i = 111.4° (i = -x, -y, -z).

The N3–H3N group of the urea functionality hydrogen bonds to the MeOH while the other NH group of the urea, N4–H4N, hydrogen bonds to the BF_4. The MeOH hydrogen bonds to the nitro group of a neighbouring complex. The nitrophenyl groups that twist out from the coordination centres are able to stack together indicative of π-π stacking, as shown in Figure 3.19.

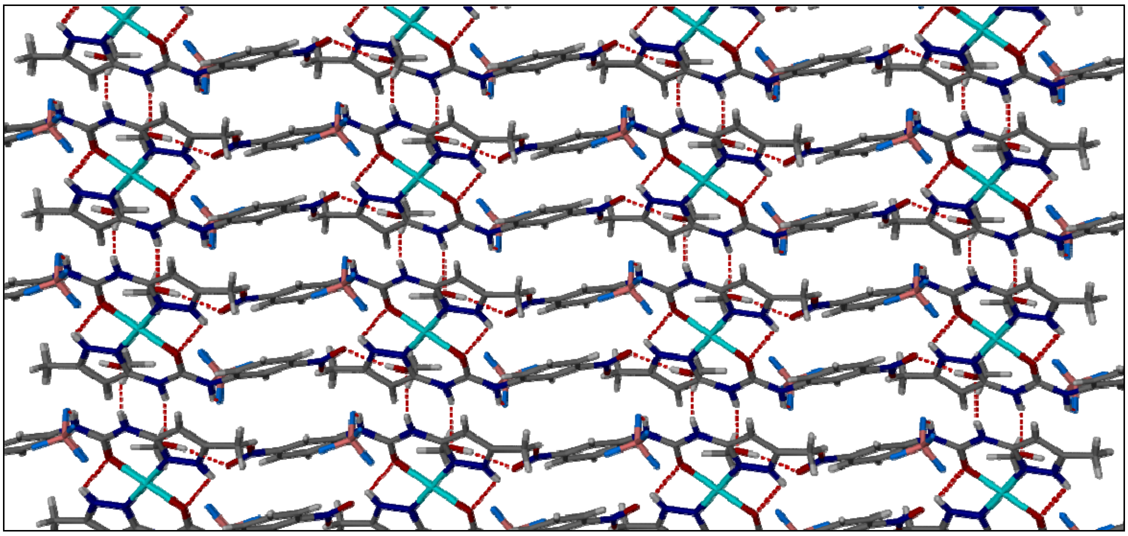

Figure 3.19. Packing of [Cu(κ-*N,O*-**3.10**)$_2$(MeOH)$_2$](BF$_4$)$_2$. Selected hydrogen bonds: N3···O4^{ii} = 2.968(2); ∠ N3-H3N···O4^{ii} = 155.5°, N3···F4 = 2.802(2); ∠ N3-H3N···F4 = 139.5° and O4···O3^{iii} = 2.868(2); ∠ O4-H4···O3^{iii} = 162.8° (*ii* = 1+x, y, z and *iii* = -x, -y, 1-z).

The coordination chemistry of compound **3.11a** was also investigated. Crystallisation of Cu(MeCO$_2^-$)$_2$ and **3.11a** in MeOH resulted in the isolation of crystals in which **3.11a** has been deprotonated to give the compound [{Cu(μ-κ-*O,O,N,N*-**3.11a**)(MeOH)}$_6$](MeCO$_2$)$_6$·6MeOH (Figure 3.20). The deprotonation occurred on the carboxamide nitrogen. This creates a cleft in which the copper is chelated by the tridentate **3.11a** through bonds to the deprotonated N5, pyrazole Lewis basic pyrazolyl N-donor group N2 and the oxygen of the carbonyl group of the urea moiety O1. There are, therefore, two chelate rings present from the coordination of the deprotonated **3.11a**. They are a five-membered ring involving the deprotonated carboxamide and pyrazole (-Cu1-N5-C13-N1-N2-) and a six-membered ring involving the carbonyl of the urea group and the same pyrazole (-Cu1-O1-C5-N3-C4-N2-). The tridentate coordination by the deprotonated **3.11a** is similar to some Schiff base ligands and similar ligands used in the supramolecular assembly of multi-metal centred grids.[92-108] The coordination geometry of the copper is that of a distorted trigonal bipyramidal. The fifth coordination is to the carbonyl oxygen (O2) of the carboxamide group of a neighbouring **3.11a**. The urea NH groups hydrogen bond to the MeCO$_2^-$ through an $R_2^2(8)$ hydrogen bond motif. Both of the symmetry-independent methanol molecules are hydrogen bonding to the $MeCO_2^-$ (one to each of the $MeCO_2^-$ oxygen atoms) and in addition, one of the $MeCO_2^-$ is coordinated to the copper(II) centre.

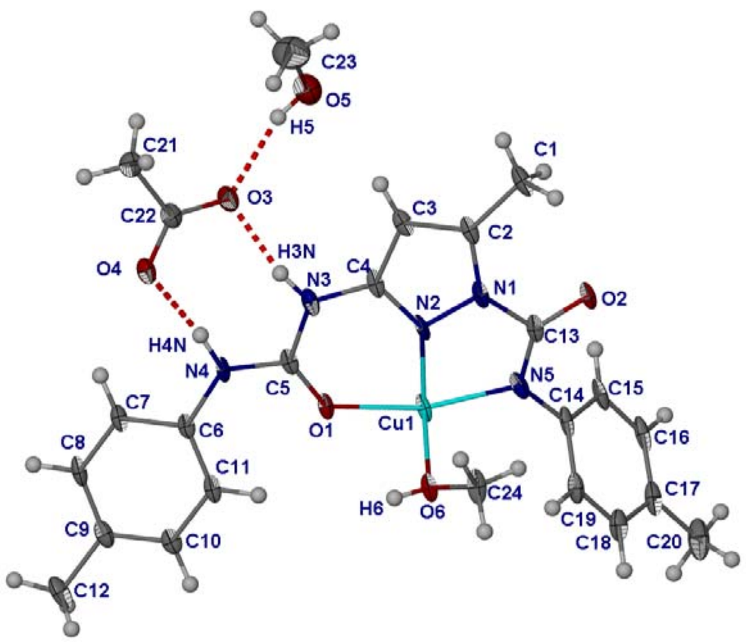

Figure 3.20. ASU of [{Cu(μ-κ-*O,O,N,N*-**3.11a**)(MeOH)}$_6$]$(MeCO_2)_6$·6MeOH. Atoms are shown as ellipsoids at 30% probability. Selected bond lengths: N5···Cu1 = 2.001(4) Å, N2···Cu1 = 1.882(5) Å, O1···Cu1 = 2.004(3) Å, O6···Cu1 = 2.216(4) Å and O2^i···Cu1 = 1.939(3) Å. Selected hydrogen bonds: N3···O3 = 2.730(6); ∠ N3-H3N···O3 = 165.3° and N4···O4 = 2.765(6); ∠ N4-H4N···O4 = 169.9°, O5···O3 = 2.824(6); ∠ O5-H5···O3 = 164.9° and O6···O4^{ii} = 2.679(5); ∠ O6-H6···O4^{ii} = 173.4° (*i* = 1+y, 1-x+y, -z and *ii* = $^5/_3$-x, ⅓-y, ⅓-z).

The space group for this crystal structure is $R\overline{3}$. The coordination of the neighbouring (Cu(μ-κ-*O,O,N,N*-**3.11a**) through the carboxamide group continues in a $\overline{3}$ symmetry pattern resulting in hexamer of formula [{Cu(μ-κ-*O,O,N,N*-**3.11a**)(MeOH)}$_6$]$^{6+}$ (Figure 3.21).[101] These hexamers have an acetate anion hydrogen bonded to each of the urea groups with the tolyl group alternating up and down on the outer rim of the hexamer. The tolyl group bound to the carboxamide group can be seen alternating up and down within the centre of the hexamer. The hexamers stack one on top of each other resulting in columns that are packed into the hexagonal lattice, with the hydrogen bond between the coordinated MeOH and the $MeCO_2^-$ aiding the stacking assembly (Figure 3.22). When the crystals were dissolved in MeOH the mass spectra data indicated that the hexamer was not fully broken down as indicated by the 1574 *m/z* signal which had a half *m/z* pattern which corresponds to $[\{Cu(\mu\text{-}\kappa\text{-}O,O,N,N\text{-}\mathbf{3.11a})(MeOH)\}_6]^{6+}$ plus $6MeCO_2^-$ and $2Na^+$. There were other peaks observed which are indicative of fragments of the $[\{Cu(\mu\text{-}\kappa\text{-}O,O,N,N\text{-}\mathbf{3.11a})(MeOH)\}_6]^{6+}$ assembly.

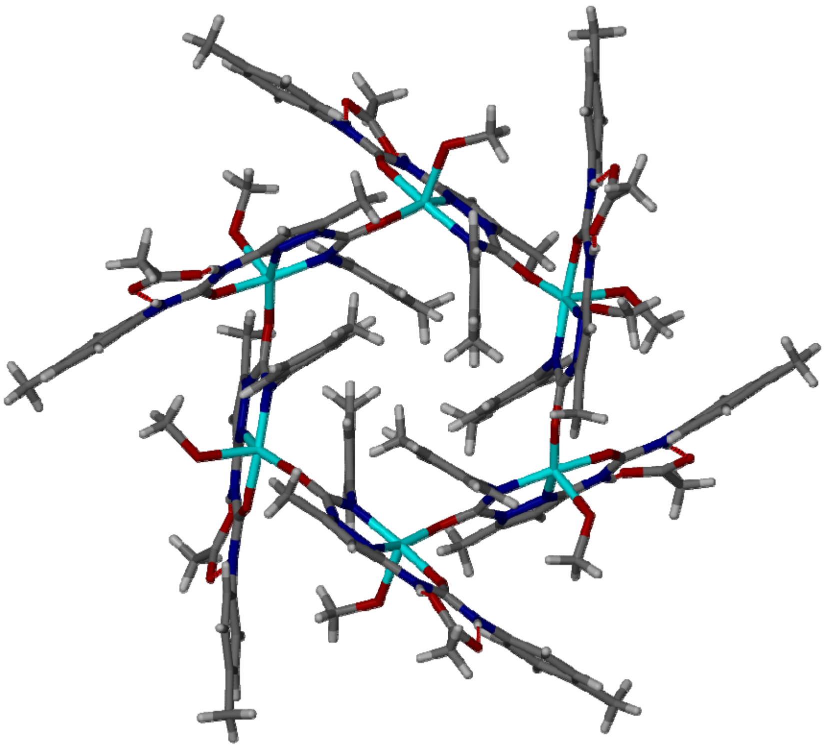

Figure 3.21. Hexamer ring of $[\{Cu(\mu\text{-}\kappa\text{-}O,O,N,N\text{-}\mathbf{3.11a})(MeOH)\}_6](MeCO_2)_6\cdot 6MeOH$. Non-coordinated MeOH has been removed for clarity.

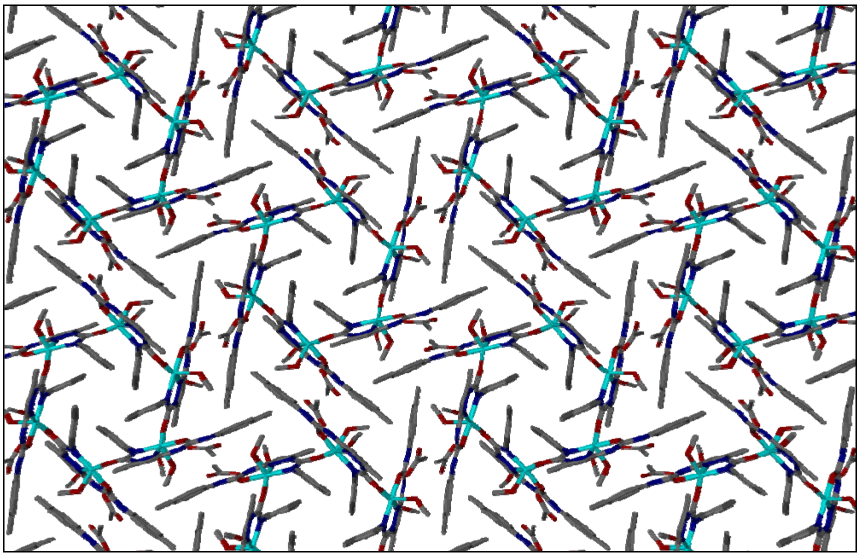

Figure 3.22. Overall packing of stacks of [{Cu(μ-κ-*O,O,N,N*-**3.11a**)(MeOH)}$_6$]$^{6+}$. Hydrogens and hydrogen bonds are not shown for clarity.

A second coordination complex of compound **3.11a** was obtained from crystallisation of **3.11a** with $Cd(MeCO_2)_2{\cdot}6H_2O$ from MeOH. Cadmium was chosen because it is slightly larger than copper, and, thus, its use should test the robustness of the hexamer unit to variations in metal ion size. Once again deprotonation of **3.11a** occurred at the carboxamide group but with two of the ligands bound to the metal. The resultant complex *mer*-[Cd(κ-*O,N,N*-**3.11a**)$_2$] was isolated in the crystalline form *mer*-[Cd(κ-*O,N,N*-**3.11a**)$_2$]·2MeOH·H_2O with the crystal structure having the space group $P2_1$ (Figure 3.23). The two deprotonated **3.11a** ligands chelate to the cadmium through the same mode as seen in the copper structure forming the five-membered and six-membered rings. As the tridentate chelating deprotonated **3.11a** is rigid and planar the coordination of two ligands around a metal centre results in the *mer* isomer, which has been isolated in this crystallisation.[109,110] As *mer*-[Cd(κ-*O,N,N*-**3.11a**)$_2$] is neutral the urea groups are free to hydrogen bond to the included solvent. The hydrogen bonding is in a cyclic motif, $R_2^3(8)$, to neighbouring complexes, with the methanol molecules and NH groups closest to the pyrazole substituent interacting with the carbonyl group of the deprotonated **3.11a** and the other NH groups hydrogen bonding to the methanol. These interactions result in a hydrogen bonded 2D layer of complexes (Figure 3.24). The disordered water molecule resides within the interstitial space created between the mismatching of 2D layers.

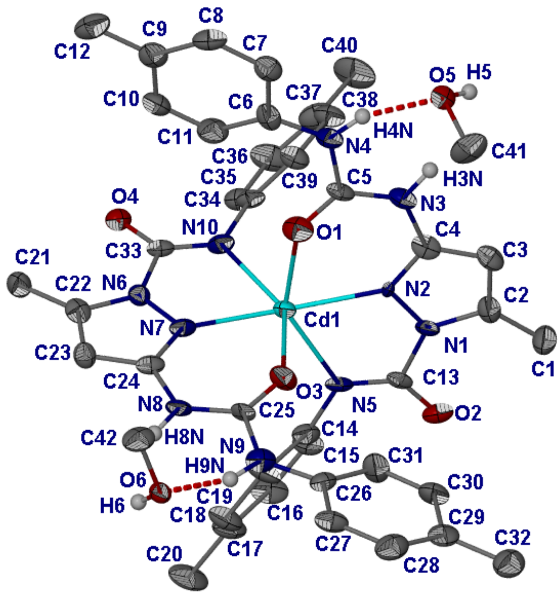

Figure 3.23. Molecular structures of [*mer*-Cd(κ-*O,N,N*-**3.11a**)$_2$]. Water and hydrogen atoms bound to carbon atoms are not shown for clarity. Atoms are shown as ellipsoids at 50% probability. Selected bond distances: Cd2···O1 = 2.393(9), Cd2···N2 = 2.234(7), Cd2···N5 = 2.304(8); Cd2···O3 = 2.398(9), Cd2···N7 2.251(9) and Cd2···N10 = 2.312(8)

In summary, the coordination chemistry of the soft transition first row metals, silver and cadmium with ligands **3.10** and **3.11a** were investigated to see whether metal ion coordination could induce gel formation. No gels were formed, but some crystalline complexes with zinc, copper and cadmium were isolated and investigated. The complexes of **3.10** show how the urea-derivatised pyrazole acts as a bidentate ligand with copper and zinc, coordinating through the carbonyl group of the urea (a hard donor) and the nitrogen in the 2 position on the pyrazole (a soft donor). The bidentate coordination is similar to that found for amide-derivatised pyrazole.[68,72] The coordination to the metal ion results in the urea group going from the *anti* conformation seen in the crystal structure of **3.10** (section 3.2) to a *syn* conformation. The *syn* conformation suggests that the urea is free from intra-molecular hydrogen bonding and is able to interact with anions and solvent. This, however, does not lead to gel formation as hoped, probably because of the coordination of the metal ion to the carbonyl group, preventing formation of the urea tape motif. Deprotonation of **3.11a** and its coordination to copper and cadmium results in a chiral *mer* complex of cadmium (that exists as a spontaneous conglomerate) and a hexameric copper assembly. The larger cadmium cation allows for the coordination of two deprotonated **3.11a** ligands around a distorted octahedral metal centre, whereas with the smaller copper cation, a distorted trigonal bipyramidal coordination arose and a cationic hexameric assemble was formed.

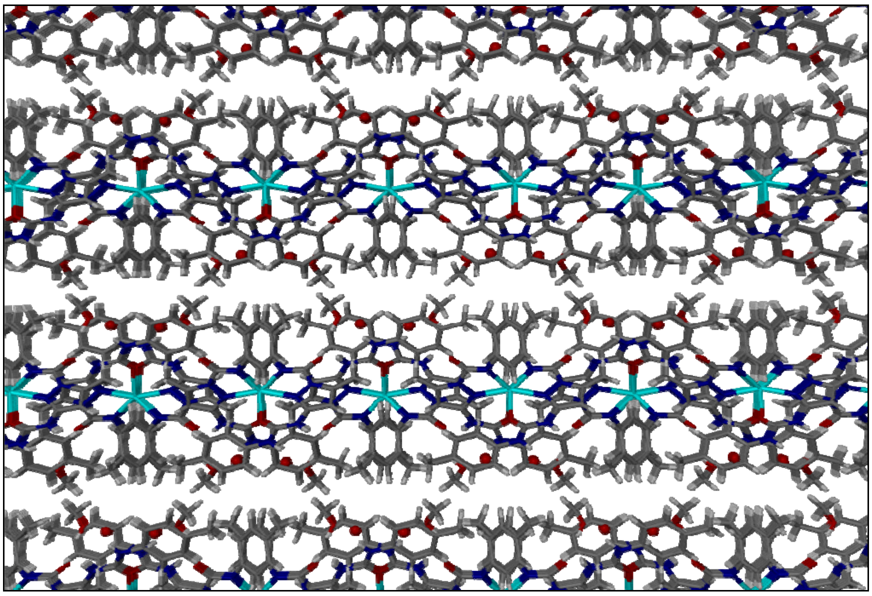

Figure 3.24. Packing of *mer*-[Cd(*κ-O,N,N*-**3.11a**)$_2$] through hydrogen bonds between the urea groups and included methanol resulting in interstitial spaces filled by disordered water, N4···O5 = 2.892(13); ∠ N4-H4N···O5 = 157.4°, N3···O2^{i} = 2.850(10); ∠ N3-H3N···O5^{i} = 152.4°, O5···O2^{i} = 2.721(11); ∠ O5-H5···O2^{i} = 150.2°, N9···O6 = 2.729(14); ∠ N9-H9N···O6 = 159.9°, N8···O4^{ii} = 2.821(10); ∠ N8-H8N···O4^{ii} = 150.5° and O6···O4^{ii} = 2.729(11); ∠ O6-H6···O4^{ii} = 169.6° (*i* = -x, ½-y, 1-z and *ii* = -x, y-½, 2-z).

3.4 Redox Transmetallation/Ligand Exchange reactions*

The coordination chemistry of pyrazolate anions and pyrazole has become a

* Work performed by the author in the group of Prof. Peter Junk, Monash University, Melbourne, Australia

mainstay of inorganic chemistry.[1-5,8,18,111-118] Prior to 1997, the coordination modes established for pyrazolate by crystallographic means consisted of just the simple μ-η^1:η^1, η^1 and η^2 modes.[1,119] However, post-1997 the increase in the possible modes of coordination increased substantially to over twenty, resulting in such extreme cases as μ-η^1:η^2:η^1 (to K^+) and η^5 (to Ru^{2+}).[1,119-122] The synthesis of homoleptic pyrazolate complexes of both d-block, f-block and main group metals has also been achieved.[119,123,124] In all these cases, there is significant competition between the formation of the homoleptic complex and complexes with coordinated solvent. 3,5-Di-*t*-butylpyrazole (TBPH) is an archetypal ligand when it comes to the coordination chemistry of the pyrazolates.[112,124,125] Due to its simplicity in structure and its lack of steric bulk it forms many types of complex with all known metal types.[119,123,124] The homoleptic [Al(TBP)$_3$] has been synthesised (Compound **3.12**, a hexane solvate trigonal crystal structure was determined) using a metathesis method.[119] In this study, we further investigate the prospective coordination chemistry of aluminium with this ligand and investigate the use of the redox transmetallation/ligand exchange reaction [126,127] as a means to produce novel aluminium complexes.[128,129]

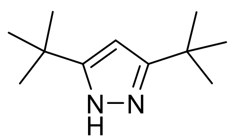

TBPH

$$6\text{TBPH} + 2\text{Al(s)} + 3\text{Hg}(\text{C}_6\text{H}_5)_2 \xrightarrow[\text{Hg}]{\text{Solvent}} 2\text{Al(TBP)}_3 + 6\text{C}_6\text{F}_5\text{H} + \text{Hg}$$

Scheme 3.6. Redox transmetallation ligand exchange reaction between Aluminium metal and 3,5-*t*-butylpyrazole (TBPH) and dipentaflourophenylmercury.

Carrying out the redox transmetallation/ligand exchange reaction shown in Scheme 3.6 using THF as the solvent resulted in a complex of formula [Al(TBP)$_3$THF]·THF (**3.13**). The best yields of *ca.* 60% were achieved when the aluminium metal was cut into strips as small as possible. Elemental mercury was used as an activator and the reaction was performed in a sonic bath for between 48 and 72 hours. Crystals were formed over time after filtration and reducing the volume of the solution. Single crystal X-ray diffraction confirmed the formulation (Figure 3.25). Compound **3.13** exhibits η^2 coordination of the TBP ligand in the same way as in **3.12**. However, the η^1 THF coordination distorts the metal environment resulting in one of the three TBP ligands becoming η^1, N1···Al1 1.8770(18). Even though the other two TBP ligands are still η^2 they are distorted with asymmetric Al–N binding; bond lengths N3···Al1 1.8542(19)Å; N4···Al1 2.3894(19)Å; N5···Al1 1.8794(18)Å and N6···Al 2.0304(18)Å. Additionally the pyrazolate ring is distorted away from planarity with the coordination plane of the aluminium centre; interplanar angles between the plane of TBP and N1-N2-Al1 6.07(17)^o; N3-N4-Al1 17.06(14)^o; N4-N5-Al1 25.49(14)^o; calculated using MPLA function in SHELXL.[81,130] The complex formed a solvate with THF.

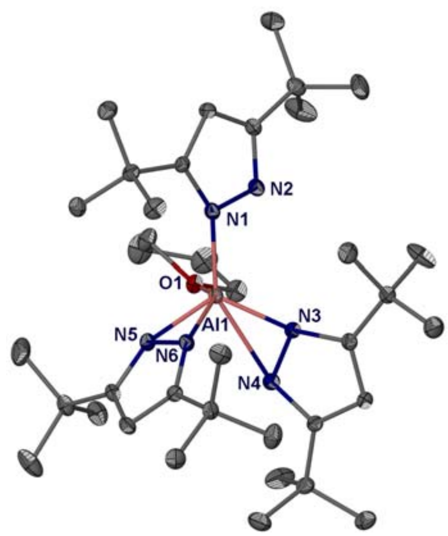

Figure 3.25. Ellipsoid plot of compound **3.13** showing the η^2 and η^1 coordination by TBP and THF to the aluminium centre. Hydrogen atoms and the interstitial THF have been removed for clarity. Ellipsoids are shown at 50% probability.

In the trigonal crystal form found for the homoleptic compound, recrystallised from hexane, the complex has approximate D_{3h} symmetry. The original metathesis was carried out in THF as well, but we now believe reduction of the solution to dryness under vacuum removed the THF from **3.13** to produce the homoleptic compound, which was recrystallised from hexane to give the reported trigonal structure. This is evidenced in the mass spectrum of a sample of **3.13** as no signal is seen for **3.13**, but **3.12** is detected. The redox transmetallation/ligand exchange reaction, therefore, effectively works as a means to synthesise the desired products of ligated aluminium.

The solvent THF plays an important role in the formation of the above complex in terms of the formation of **3.13** and **3.12**. We attempted to study the effect a change of solvent would have on the reaction product in terms of the coordination of solvent and rate of reaction. We chose to use 1,2-dimethylether (DME) in the hope that the bidentate coordinating ability of the solvent would reveal if it is possible for the aluminium coordination sphere to accommodate three pyrazolate ligands and two coordinated solvent oxygen atoms. The product isolated from the first crystallisation of this reaction has the formula $[Al_2(TBP)_3(PFP)_2(MG)]\cdot DME$ (**3.14**) (Figure 3.26).

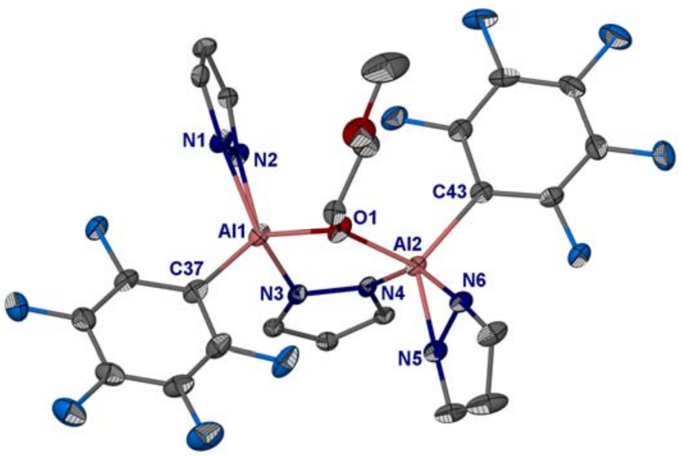

Figure 3.26. Ellipsoid plot of compound **3.14** showing the ligation of aluminium by PFB, TBP and a methoxyglycol anion in a bimetallic complex. Hydrogen atoms and the interstitial DME have been removed for clarity. *t*-butyl groups on the TBP ligands have been removed for clarity and the disordered groups as well. Ellipsoids are shown at 30% probability.

The complex is dinuclear and contains three different ligands; the desired pyrazolate anion, the precursor pentafluorophenyl ligand (PFP) and a methoxyglycol anion (MG) arising from the cleavage of DME. One of the three pyrazolate ligands and a methoxyglycol ligand bridge the two metal centres. The bridging pyrazolate ligand, μ-η^1:η^1 binds to the two metals with bond lengths of Al1···N3 1.954(3)Å and Al2···N4 1.949(3)Å and a torsion angle of ∠ Al1·N3·N4·Al2 34.3(3)°. The five membered ring involving the bridged TBP and MG ligands -Al1-N3-N4-Al2-O1- is not a common motif (only three rings involving -Al-N-N-Al-O- were found in the CSD[131] and all have pyrazolate ligands)[132-134] and is not planar (RMS deviation from plane = 0.136 Å).[130] The η^2 pyrazolate ligands have bond lengths of Al1···N1 1.974(3)Å; Al1···N2 1.870(3)Å and Al2···N5 1.858(3)Å; Al2···N6 2.054(3)Å. These two ligands are coplanar with the Al/N coordination plane (interplanar angles of N1-N2-Al1 2.67(15)° and N5-N6-Al2 3.37(9)° The methoxyglycol is the product of the cleavage of the solvent DME and is relatively unusual, although well precedented.[135-141] The bonds between the aluminium and the PFP ligands are Al1···C37 2.008(4)Å and Al2···C43 2.007(4)Å. This matches well with the average distance Al···C 1.997(52)Å for PFP to Al in the crystal structures observed and reported in the CSD.[131] The serendipitous formation of compound **3.14** provides evidence that the redox transmetallation/ligand exchange reaction does indeed go through a metal PFP complex intermediate and not a mercurial TBP complex. Compound **3.14** represents a small percentage of the reaction products (*ca.* 23%). As well as **3.14**, unreacted TBP (*ca.* 40%) and the homoleptic compound [Al(TBP)$_3$] (**3.12**, *ca.* 37%) were found.

The second product, from the second crystallisation, obtained in the DME reaction is the homoleptic complex [Al(TBP)$_3$] (**3.12**) which does not contain metal-bound DME solvent. The formulation of the complex suggests that it may not be possible to cleave more than one Al–N bond (as in **3.13**), even in the presence of a bidentate hard donor such as DME. The crystal structure reported previously of **3.12** is a hexane clathrate (or solvate, the solvent is present in channels and is incommensurate and therefore is not modelled in the reported structure) with a *Z*' value of 1 (Figure 3.27a).[76,142-145] However, in the new structure of **3.12** there is no solvent present, and the packing is compact (Figure 3.27b). The four crystallographically independent molecules found within this structure all show a similar approximate D_{3h} symmetry to the hexane structure of **3.12** (almost C_3 symmetry due to the twisting of the planes of the pyrazolate ligands, this twisting is opposite on neighbouring columns (related by $P\bar{1}$ symmetry) in both structures of **3.12**). One of the most noticeable differences between the two structures of **3.12** is the orientation of the two t-butyl groups on TBP in relation to each other. In the hexane structure of **3.12** the orientation is staggered, with a torsion angle of ca. 32.5^{o}. In the new high Z' structure this is not always the case, of the twelve examples, two are eclipsed (torsion angles of *ca.* 1.2^{o} and *ca.* 5.6^{o}). The other ten staggered groups have torsion angles ranging from *ca.* 25^{o} to *ca.* 52^{o}. As recently described by Anderson *et al.*,[142] the occurrence of high Z' crystalline structures of a compound in its pure state can be related to its ability to form host:guest complexes. The structures of **3.12** are a good example of a high Z' organometallic complex that forms a low Z' clathrate structure.

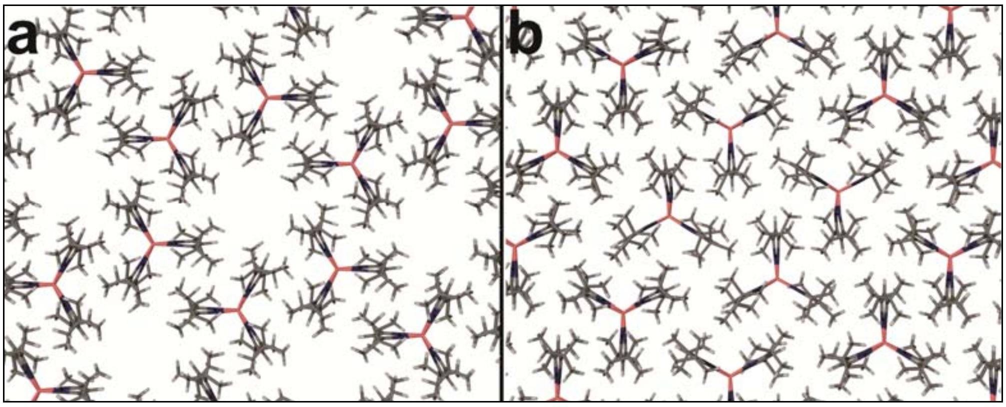

Figure 3.27. a) Crystal packing in the homoleptic compound Al(TBP)$_3$ channel structure of the hexane solvate of **3.12**. **b)** High Z' structure (Z' = 4) of the homoleptic compound Al(TBP)$_3$, **3.12**.

In summary it has been shown that the redox transmetallation/ligand exchange reaction can be used to prepare Al complexes starting with simple “off the supermarket shelf” aluminium foil in reasonable yield. The ease of isolation of the pure product due to the production of volatile pentafluorobenzene and amalgamated Hg (with the excess metal reactant) is also advantageous. The complexes reported herein reveal the solvent ligand binding ability of the [Al(TBP)$_3$] complex. THF can coordinate, but more sterically demanding solvents such as DME do not appear to be able to, even though they are potential chelators. The cleavage of DME by this reaction is also interesting and provides us with evidence of the $Al(PFP)_n$ intermediate. The crystallisation of the homoleptic $[Al(TBP)_3]$ complex from DME reveals its interesting clathrate chemistry especially relating to its high Z' characteristics. Further experiments are underway to investigate the possibilities of using the redox transmetallation/ligand exchange reaction with other metals and other ligands with aluminium.

3.5 Anion coordination chemistry of urea functionalised pyrazole ligands

The ability of the NH group of the pyrazole functionality to bind to anions is a well recognised phenomenon that has been utilised by the groups of Halcrow and Pérez amongst others.[12-19] However, in these cases, the pyrazole group has been pre-organised for anion binding by the coordination to a metal. In this study, titrations were performed to look at the anion binding properties of the pure urea functionalised pyrazoles to see whether the urea group can be induced to change from an *anti* conformation to a *syn* conformation through the binding of an anion.

As can been seen from the structures of **3.3** the thiourea group forms an intra-molecular hydrogen bond and may not be available for hydrogen bonding to an anion. ^{1}H-NMR spectroscopic titrations were performed on **3.3** in $CHCl_3$ with the anions Cl^-, Br^-, NO_3^- and $MeCO_2^-$, and the results were interpreted using the HYPNMR program.[146,147] The resulting anion binding constants are presented in Table 3.1.

Table 3.1. Binding constants for compound **3.3** with various anions in $CDCl_3$

Anion	log β_{20}[a]	log β_{11}	log β_{21}
Cl^-	1.11	2.07(3)	3.74(6)
Br^-	1.11	1.73(1)	2.53(1)
NO_3^-	1.11	1.93(5)	3.34(12)
$MeCO_2^-$	1.11(1)	2.03(5)	3.68(7)

[a] Constant determined from $MeCO_2^-$ data and kept constant for the other anions (Other anion studies were found to give similar values).

From the raw data it is immediately clear that one of the NH groups' resonances shifts upfield a small amount ($\Delta\delta$ = 0.3 ppm for $MeCO_2^-$), one NH resonance shifts downfield a small amount after initially moving upfield ($\Delta\delta$ = 0.25 ppm for $MeCO_2^-$) and the last NH proton resonance shifts significantly upfield ($\Delta\delta$ = 4.5 ppm for $MeCO_2^-$) for all the anions studied. The resonance that shifts downfield is assigned to the pyrazole NH proton. The NH resonance that shifts upfield a little is the thiourea NH involved in the intra-molecular hydrogen bond as seen in the crystal structures, leaving the resonance that shifts the most as the other NH group of the thiourea. Interestingly, the data indicate that **3.3** forms a dimer, with β_{20} = 1.11(1). The ES^- mass spectrometry results corroborate the dimer formation with the dimer minus a proton and the dimer plus a Cl^- seen. The dimer formation through the $R_2^2(8)$ hydrogen bond motif of the thiourea groups as seen in the two crystal structures of **3.3** also corroborates the dimer formation in solution. A concentration study to confirm this constant is not possible in $CHCl_3$ due to the poor solubility of **3.3**. The intra-molecular hydrogen bond, seen in the two crystal structures of **3.3**, appears to be still present in the titration experiments as there was little shift in the NH proton resonance peaks for two of the three NH proton resonance peaks. It is of interest to see that the order of strength of binding for the anions with the 1:1 complex is $Cl^- > MeCO_2^- > NO_3^- > Br^-$. $MeCO_2^-$ normally binds much more strongly to urea/thiourea groups due to the formation of an $R_2^2(8)$ hydrogen bond, but with this compound, Cl^- and $MeCO_2^-$ bind comparably. This can be explained by the formation of the intra-molecular bond which prevents the formation of the $R_2^2(8)$ hydrogen bond motif. The 1:1 anion binding order is also observed in the β_{21} values for a two hosts to one guest binding ratio in which the Cl^- binds better than $MeCO_2^-$. The Job plot for $MeCO_2^-$ confirms the two hosts to one guest binding ratio (Figure 3.28). The structural determination of (**3.3**)(TBA^+)($MeCO_2^-$)·H_2O crystals grown from the evaporation of the $CHCl_3$ solutions of **3.3** and TBA^+ $MeCO_2^-$ shows a host:guest ratio of 1:1 and a binding mode that supports the mode of binding of the anion by **3.3** described above (Figure 3.29).

The ASU of the anion host crystal consists of **3.3**, TBA^+, $MeCO_2^-$ and H_2O. The intra-molecular hydrogen bond between the NH of the thiourea and the Lewis basic pyrazolyl N-donor group is present as seen in the two other crystal structures of **3.3**. The thiourea group has not gone from the *anti* conformation to the *syn* conformation by binding of the acetate anion. The free NH group of thiourea group is hydrogen bonded to the $MeCO_2^-$. The water is then hydrogen bonded to the $MeCO_2^-$ and the sulfur of the thiourea resulting in a $R_3^3(10)$ hydrogen bond motif. The pyrazole NH also binds to the $MeCO_2^-$ resulting in 1D chains of alternating left then right complexes of (**3.3** $MeCO_2^-$ $H_2O)_n$ (Figure 3.30a),. These chains stack next to each other forming an anionic layer (Figure 3.30a). These layers alternate with cationic layers of TBA^+ (Figure 3.30b).

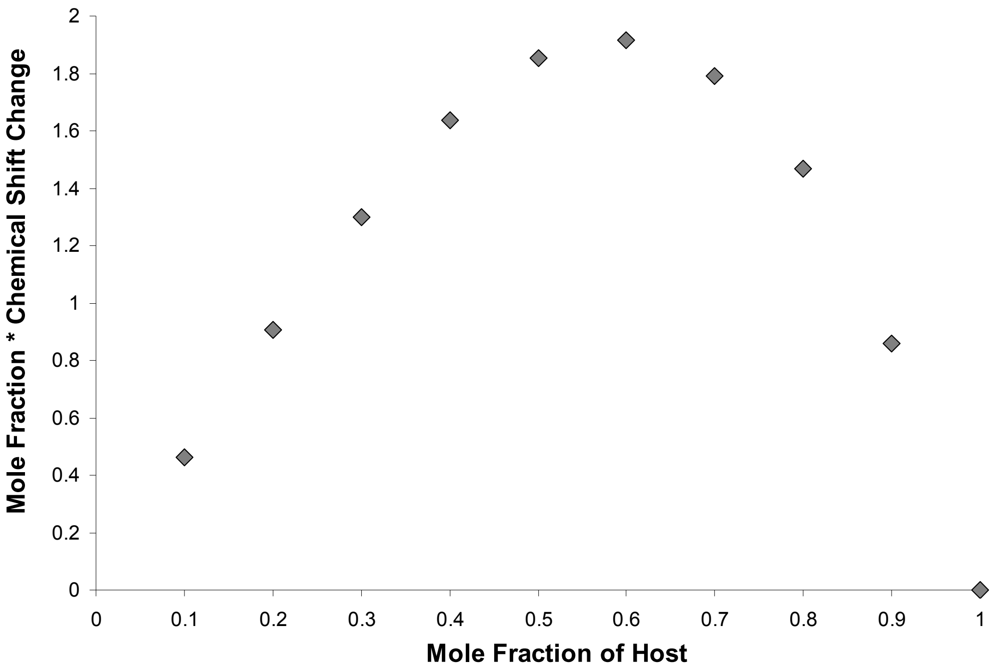

Figure 3.28. Job plot of binding by **3.3** with $MeCO_2^-$ showing the 2:1 host to guest ratio. Only the N3–H3N resonance which shows the maximum amount of shift during the titration is plotted for clarity.

In summary, anion binding by **3.3** does not appear to cause the breaking of the intra-molecular hydrogen bond between the thiourea group and the Lewis basic pyrazolyl N-donor group.[148] The anion binding strengths are in the order Cl^- > $MeCO_2^-$ > NO_3^- > Br^-. This indicates that the $R_2^2(8)$ binding of $MeCO_2^-$ by ureas and thioureas which results in stronger binding of $MeCO_2^-$ over Cl^- is not present as Cl^- is bound more strongly than $MeCO_2^-$. This is confirmed by the elucidation of the structure of the host:guest complex between **3.3** and $MeCO_2^-$ in the crystal of (**3.3**)(TBA^+)($MeCO_2^-$)·H_2O. The structure shows the intra-molecular hydrogen bond still present. As anion addition did not result in the formation of gel, protonation was studied as a means to induce gel formation by compound **3.10**.

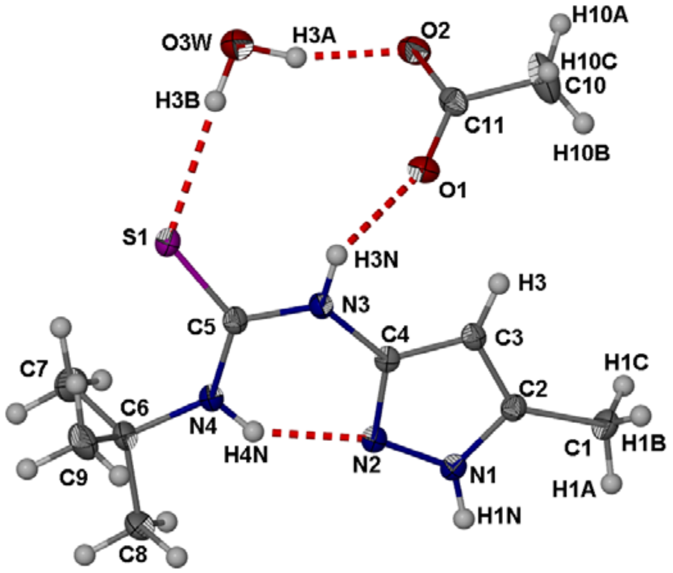

Figure 3.29. Molecular structure of (**3.3**)(TBA^+)($MeCO_2^-$)·H_2O with the TBA^+ removed for clarity. Atoms are shown as ellipsoids at 50% probability. Selected hydrogen bonds: N4···N2 = 2.660(3) Å; ∠ N4–H4N···N2 = 143.3°, N3···O1 = 2.856(3) Å; ∠ N3–H3N···O1 = 143.3°, O3W···O2 = 2.777(3) Å; ∠ O3W–H3A···O2 = 163.5° and O3W···S1 = 3.315(3) Å; ∠ N3–H3N···O1 = 175.1°.

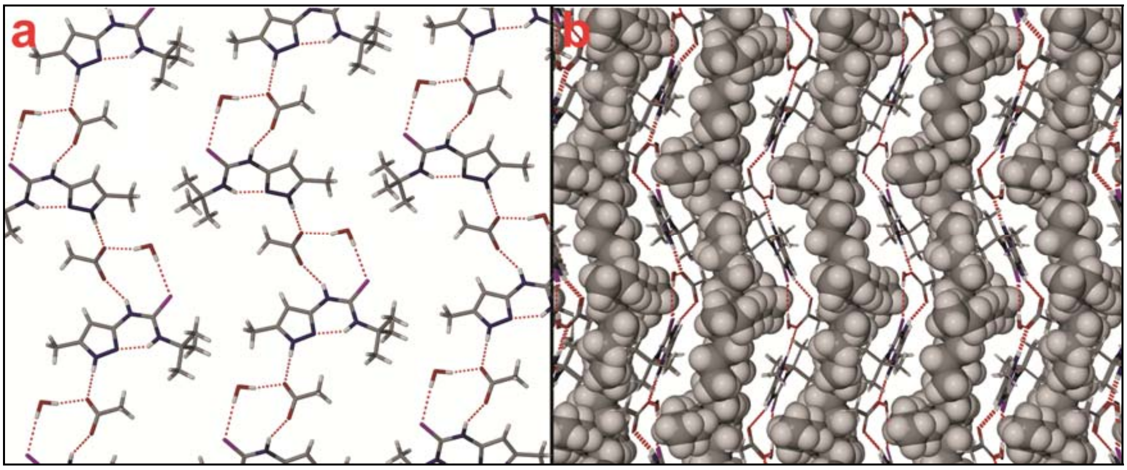

Figure 3.30. Packing of (**3.3**)(TBA^+)($MeCO_2^-$)·H_2O. **a)** 1D hydrogen bonded stacking of **3.3** hydrogen bonded to $MeCO_2^-$ and the H_2O as viewed down [001]. **b)** Layer pattern of the packing with negatively charged layers of **3.3** $MeCO_2^-$ H_2O (shown in capped stick representation) alternating with positively charged TBA^+ layers (shown in space-filled representation). Selected hydrogen bond: N1···O2^i = 2.687(3) Å; ∠ N1–H1N···O2^i = 175.1^o (i = -x, y-½, ½-z).

3.6 Gelation by urea functionalised pyrazole ligands and their anion tuning

3.6.1 Gel formation by compound 1-(3-methyl-1*H*-pyrazol-5-yl)-3-(3-nitrophenyl)urea

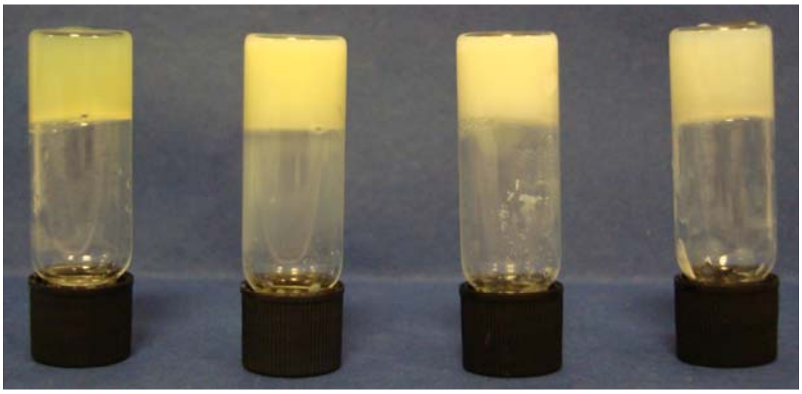

Figure 3.31. Photograph of the gels of compound **3.10** at 1% by weight in water acidified with, from left to right, H_3PO_4; H_2SO_4; HPF_6 and HBF_4.

The urea-functionalised pyrazole compounds were investigated to find examples of LMWGs as simple organic compounds, metal complexes and/or salts. The investigations into metal complexes and pure compounds resulted in isolation of crystalline materials as shown in sections 3.1 to 3.5. Serendipitously, salt formation proved to be the means to produce LMWGs. More specifically, compound **3.10** was found to gel water in acidic conditions indicating that the protonated form, as part of a salt, can form hydrogels (Figure 3.31). The importance of pH and therefore the formation of a salt (acidity required to protonate the pyrazole group giving **3.10H**$^+$) is highlighted by the fact that **3.10** precipitates/crystallises out of neutral water (and all organic solvents tested) in the crystalline form described in section 3.2. In basic conditions, pH > 10, **3.10** stays in solution presumably as a deprotonated **3.10** pyrazolate sodium salt. At very low pH, below 1, **3.10** was also found to not gel and instead stays in solution. It was found that **3.10** forms hydrogels in the narrow pH range of 1 to 2. This makes compound **3.10** a hydrogel with pH tunable gelation ability.[25,42,149-168] As well as being a pH tunable LMWG the ability of **3.10** to gelate water in this pH range allows for the study of the influence of the anion species on gelation ability of this compound in water. Table 3.2 shows the results of the systematic study of the gelation ability of **3.10** in acidified water using different inorganic acids to provide the anion variation. The pH of the solution was varied as well for each of the acids to find the optimum pH at which gels formed for the different anions. Gels were consistently formed when HBF_4, HPF_6, H_2SO_4 and H_3PO_4 were used as acids (CGC for each of these acids and pH ranges resulting in gelation are shown in Table 3.2).

Table 3.2. Conditions for gel formation for compound **3.10**.

Acid	HBF_4	HPF_6	HCl	HNO_3	H_3PO_4	H_2SO_4
pH range	1 – 2.0	1 – 1.7	n/a	1 – 2.5	1 – 2.1	1 – 2.0
CGC (Weight %)[a]	0.30	0.20	n/a	n/a	0.11	0.12
Appearance	Opaque Cream Gel	Opaque Cream Gel	Light Cream Precipitate	Unstable Opaque Cream-Yellow Gel	Clear to Opaque Yellow Gel	Clear to Opaque Yellow Gel

[a] Weight percent in 1 ml of solvent that will hold a gel up upon upturning a vial of diameter of 1 cm.

Water acidified with HCl containing **3.10** never gave a gel at any pH and concentration of **3.10**. A light cream coloured precipitate always formed under acidic conditions. Water acidified with HNO_3 could be gelled by **3.10**, however, these gels were unstable. When **3.10** was dissolved in a small volume of conc. HNO_3 (0.05 ml) and diluted by the addition of water (0.95 ml) a gel formed. However, this gel was unstable and formed a precipitate upon standing for a few minutes.[169,170] The gel could be reformed by heating the sample until the precipitate dissolved followed by slow cooling on a bench (sonication resulted in the precipitate). However, within a few minutes the gel broke down again to a precipitate. Due to the precipitation of a solution of **3.10** in water acidified with HCl the addition of chloride salt to gels of the other acids was investigated as a means to tune the gel with anions. Addition of NaCl as solid to gels of **3.10** in water acidified with H_2SO_4 or H_3PO_4 resulted in the gradual disintegration of the gel to a precipitate. The precipitation caused by the addition of Cl^- provides the ability tune a gel of **3.10** (a salting out effect).[152,162,168,171]

3.6.2 Gel formation with H_2SO_4

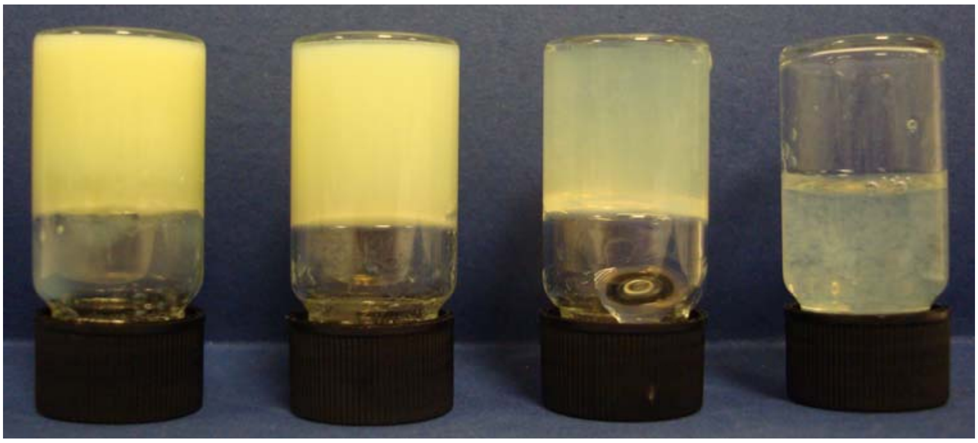

Figure 3.32. Gels formed by compound **3.10** in water at pH 1.0 acidified with H_2SO_4. From left to right the concentrations are 1.3%, 0.6%, 0.15% and 0.1% by weight in 5 ml of solution. The 0.1% by weight solution only partially gels and therefore does not survive the inversion test.

Hydrogels formed by compound **3.10** in water acidified with H_2SO_4 were found to be the most stable over time (Figure 3.32). Gel formation occured in the pH range of 1 – 2 and the CGC for **3.10** with this acid was 0.12% by weight. Sonication of samples resulted in more uniform gels.[172] The behaviour of the gels when exposed to mechanical stress was investigated using rheology to understand the gels and their characteristics.[173-178] The gels were characterised by stress sweep and frequency sweep rheometry. When a frequency sweep was performed with a small amplitude stress, with a number of different samples varying in concentration, the solid-like nature at 20 °C was reflected in the storage modulus, G', being, typically, five times greater than the loss modulus, G'', thus demonstrating the elastic behaviour of the systems (Figure 3.33).[179] This viscoelastic behaviour is associated with classical gels, and therefore supports the notion that the cooling of these samples from a solution to a solid-like material resulted in a true gel state.

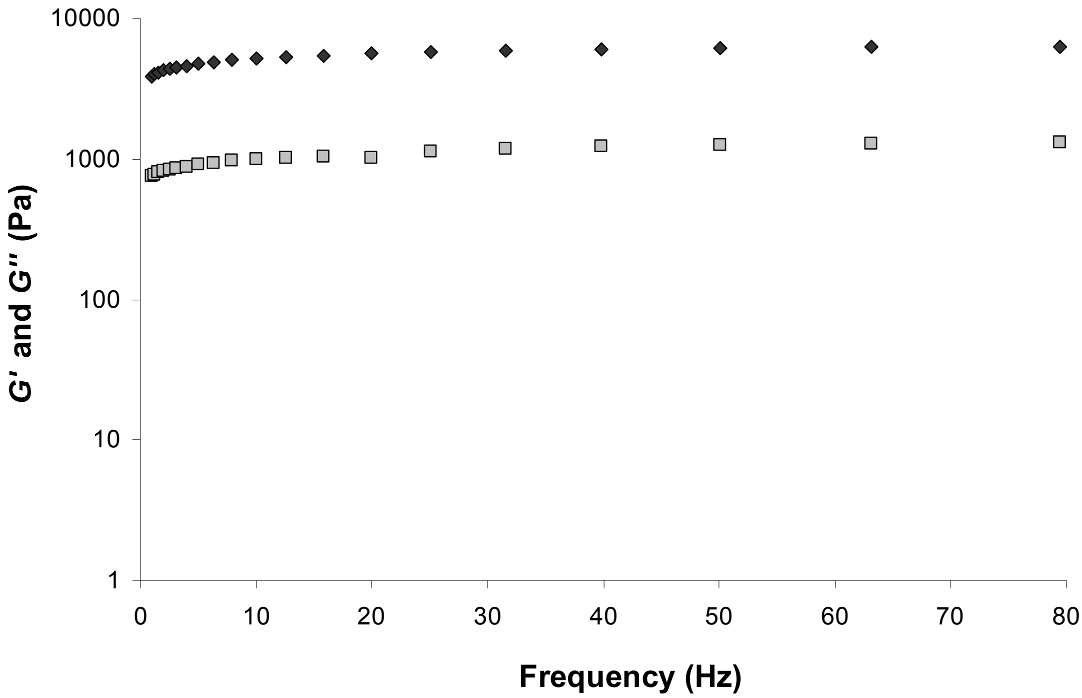

Figure 3.33. Rheology of gelation by **3.10** showing a frequency sweep performed on a gel of **3.10** at 0.1% by weight in water acidified with H_2SO_4 to a pH of 1.0. Typically the consistency of the *G*′ (Dark grey filled ◇) and *G*″ (Light grey filled ○) values over the frequency range indicates the solid-like nature of the gel material. The value of *G*′ was typically five times greater than the *G*″ value and constant with respect to the frequency demonstrating the elastic behaviour of the gel. The *G*′ and *G*″ axis is shown on a log scale.

The non-linear rheological response was investigated using stress sweep experiments, during which an oscillatory stress was imposed with a fixed frequency (1 Hz) over a range of shear stress amplitudes. Example gels showed a typical response with the small decrease in *G*′ value, essentially constant, below the critical value of shear stress, the "yield stress", whereupon the sample started to flow (Figure 3.34).

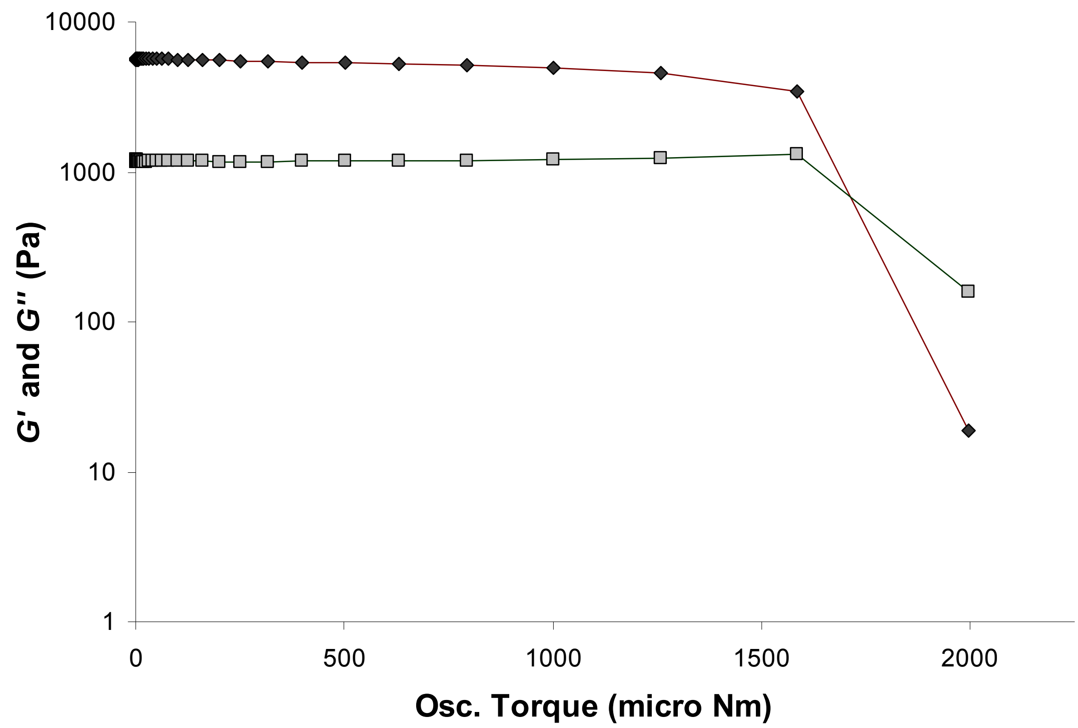

Figure 3.34. Rheology of the gelation by **3.10** showing a stress sweep on a gel of **3.10** at 0.1% by weight in water acidified with H_2SO_4 to a pH of 1.0. The stress sweep shows the rigidity and strength of the gel which breaks at a relatively high shear strength. *G′* value (Dark grey filled ◇ with brown line) stays constant until the torque begins to become too strong and the struts start to break under the strain where upon *G′* becomes less than *G″* (Light grey filled □ with green line). Lines are there to aid the eye. The *G′* and *G″* axis is shown on a log scale.

The effect of the concentration on the gel strength, in the form of *G′* and "yield stress" values was also investigated using rheology. The two theoretical models put forward for the mechanical properties of gels[180] that are pertinent to LMWGs are the colloidal gel description[180,181] and the cellular solid model.[173,180,182,183] A power law relationships between the strength of the gel of **3.10,** in water acidified to pH 1 with H_2SO_4, and the concentration of **3.10** of $G' \propto [\text{conc}]^{2.2}$ (Figure 3.35) and "yield stress" $\propto [\text{conc}]^{1.5}$ (Figure 3.36) was found. This is in good agreement with the cellular solid model which is predicted to have a relationship of $G' \propto [\text{conc}]^n$ and "yield stress" $\propto [\text{conc}]^n$, where n can vary between 1 and 2.[183] The cellular solid model describes an open-cell cellular material which consists of load bearing struts interconnected via crosslinks or junction points which deform by bending. To confirm this model for the gel structure formed by **3.10** imaging techniques were utilized to try to determine the gel morphology.

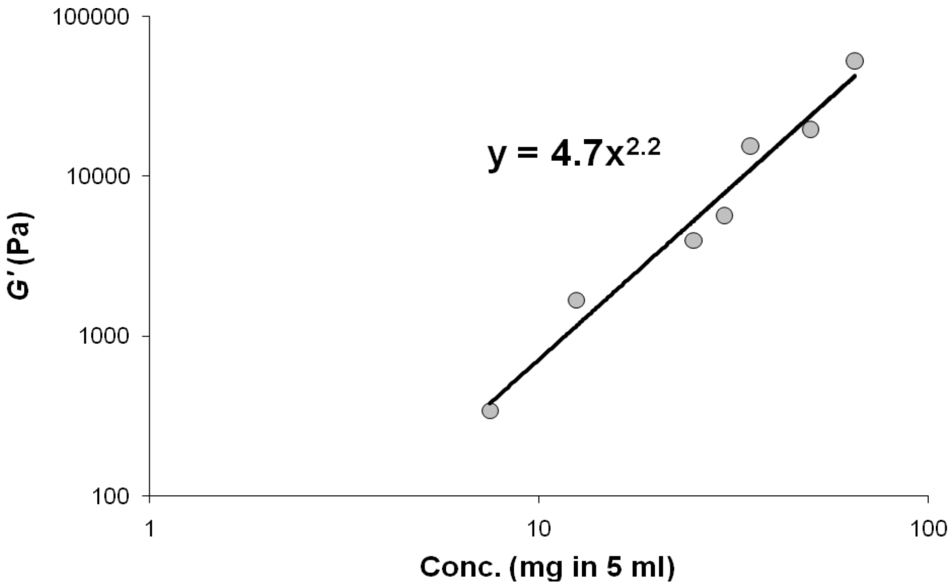

Figure 3.35. Study in the variation in *G′* with change in concentration for gels of **3.10** in acidified water at pH 1.0 using H_2SO_4 (y = *G′* (Pa) and x = concentration in mg in 5 ml). $G' \propto [\text{conc}]^n$ relationship is confirmed with *n* = 2.2. Errors on data points, determined as standard deviations of ten measurements on a sample, are smaller than symbol size used. Both the *G′* axis and concentration axis are shown on a log scale.

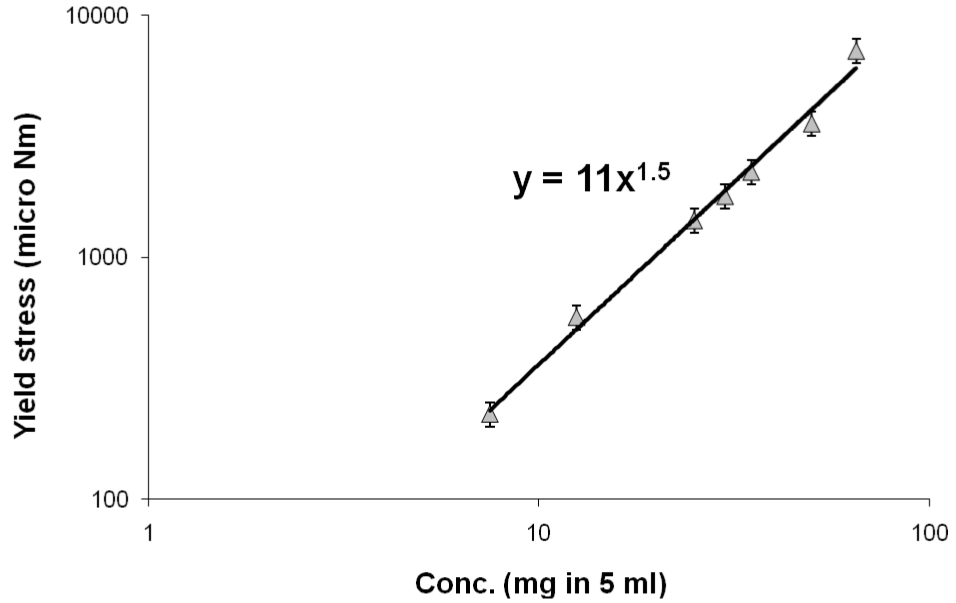

Figure 3.36. Study in the variation in "yield stress" with change in concentration for gels of **3.10** in acidified water at pH 1.0 using H_2SO_4 (y = "Yield Stress" (micro Nm) and x = concentration in mg in 5ml). "Yield stress" $\propto$ [conc]^n relationship is confirmed with n = 1.5. Errors on plotted points are determined as the standard deviation for the point determined by taking the average of the measured points either side of the "yield stress" (see Figure3.34 for example). Both the "yield stress" axis and concentration axis are shown on a log scale.

The gel morphology was studied by SEM and TEM imaging (Figure 3.37). Samples of gels of **3.10** acidified with H_2SO_4 to a pH of 1.0 for SEM imaging were dried under vacuum and then coated with a thin layer of platinum metal. As can be seen from Figure 3.37a the imaging reveals a porous sponge-like morphology. The Pt coating has created a smooth surface on the gel struts with the pores of the gels appearing darker. The gel morphology from the TEM images, as shown in Figure 3.37b, appears, essentially, to be the same as that seen in the SEM images. The gel material broke down under the electron beam, but the porous sponge-like morphology of the gel structure remained visible. The visible edge of a large circular pore, which the gel transverses, is the edge of the carbon mesh grid used to hold the gel sample.

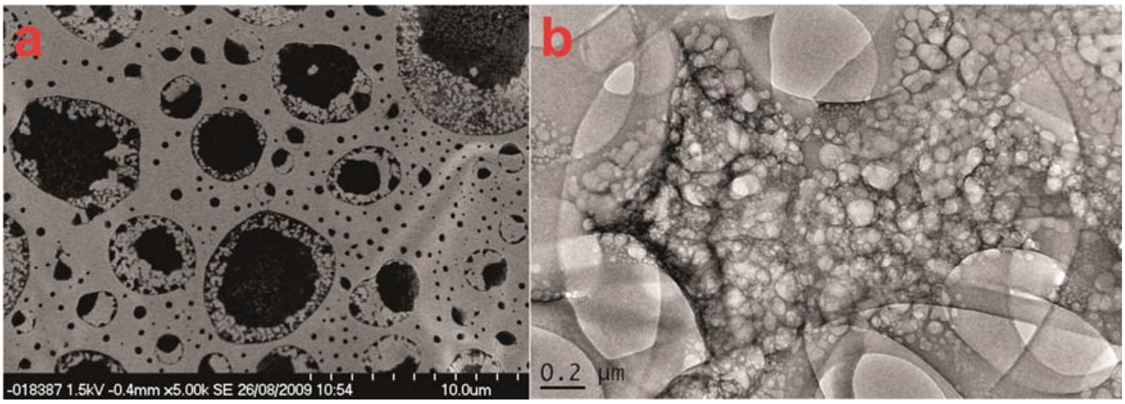

Figure 3.37. a) SEM image of dried gels of **3.10** in water acidified with H_2SO_4 to a pH of 1.0 that has been covered with a thin layer of Pt. b) TEM image of a gel of **3.10** in water acidified with H_2SO_4 to a pH of 1.0.

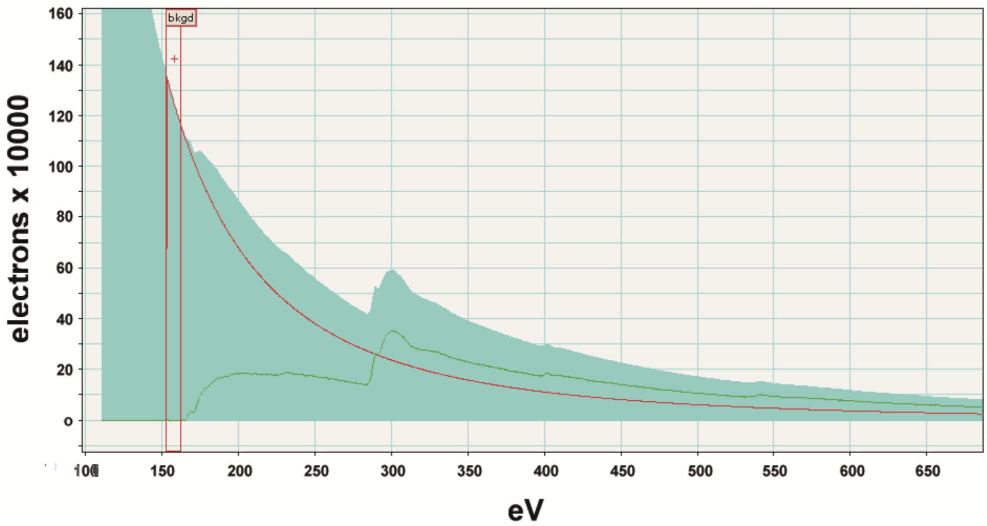

Figure 3.38. EELS data from the gel sample of **3.10** in water acidified to pH 1.0 with H_2SO_4. The collected spectra (Filled blue area) is baseline corrected (Red line) to give the EELS data (Green line). This reveals peaks at 164 eV (S), 284 eV (C), 401 eV (N) and 532 eV (O).

Electron energy-loss spectroscopy (EELS) was run on the TEM samples to confirm that SO_4^{2-} or HSO_4^{-} were incorporated into the gel and that the gel was a salt (Figure 3.38). As the samples were under high vacuum there was no liquid present so any sulfur found to be present was due to that in the gel struts as counter ion to the protonated

3.10, although it could have been deposited from the evaporation of the solvent but the amount would be small and the signal weak. The EELS clearly shows a peak at 164 eV which can be assigned to the 2p shell electron peak of sulfur confirming the presence of sulphur and therefore SO_4^{2-} or HSO_4^{-}.[184] The other elements that were expected to be present in this gel, carbon, nitrogen and oxygen can also be identified at 284 eV, 401 eV and 532 eV, respectively.[184]

The gels of **3.10** formed in water acidified at pH 1.0 with H_2SO_4 were induced to crystallise by addition of salt in the form of Na_2SO_4 or by mechanical stress. Stirring with a spatula, which creates nuclei for crystallisation to occur, resulted in crystallisation after a few weeks with the gel slowly converting to crystal form.[170] The crystals were dissolved by heating the solution, and upon cooling, the gel reformed. The structure of these crystals, $(\mathbf{3.10H^+})_2(SO_4^{2-})\cdot 7H_2O$ provides a "snap shot" into the structural characteristics of the gel.[25] The ASU consists of two **3.10H**$^+$, a SO_4^{2-} anion and seven water molecules (Figure 3.39).

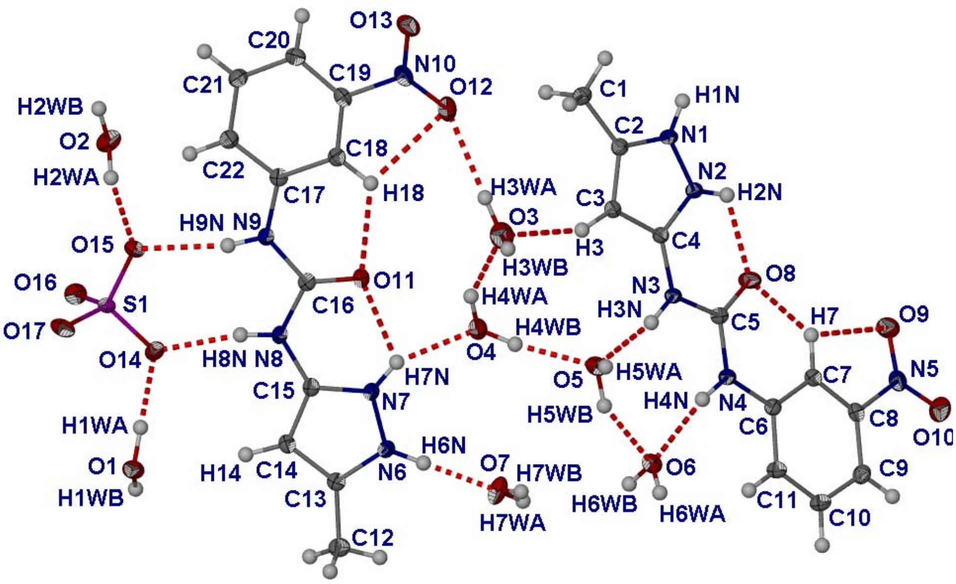

Figure 3.39. ASU of $(\mathbf{3.10H^+})_2(SO_4^{2-})\cdot 7H_2O$. Atoms are shown as ellipsoids at 50% probability. Selected hydrogen bonds: N2···O8 = 2.575(2) Å; ∠ N2–H2N···O8 = 118.4°, C7···O8 = 2.750(2) Å; ∠ C7–H7···O8 = 121.5°, N7···O11 = 2.663(2) Å; ∠ N7–H7N···O11 = 118.3° and C18···O11 = 2.836(2) Å; ∠ C18–H18···O11 = 121.1°, N8···O14 = 2.8184(19) Å; ∠ N8–H8N···O14 = 169.4°, N9···O15 = 2.9459(18) Å; ∠ N9–H9N···O15 = 168.2° and N1···O17^i = 2.7439(18) Å; ∠ N1–H1N···O17^i = 171.9° (*i* = x, y-1, z).

Table 3.3. Hydrogen bond parameter details for hydrogen bonds involving the water molecules within the structure of ($\mathbf{3.10H^{+}}$)$_2$(SO_4^{2-})$\cdot$7H_2O.

Water Donor or Acceptor[a]	Hydrogen bond Atoms[b]	Donor – Acceptor Distance (Å)	Hydrogen bond Angle (Degrees)
Acceptor	N7–H7N···O4	2.742(2)	145.9
Acceptor	N6–H6N···O7	2.6405(19)	175.6
Donor	O2–H2WA···O15	2.8887(19)	167.3
Donor	O1–H1WA···O14	2.6901(19)	160.5
Donor	O4–H4WA···O3	2.877(2)	150.3
Donor	O5–H5WB···O6	2.7185(18)	153.1
Donor	O4–H4WB···O5	2.828(2)	167.0
Acceptor	N4–H4N···O6	2.9226(18)	170.2
Acceptor	N3–H3N···O5	2.8797(18)	165.6
Donor	O3–H3WA···O12	3.069(2)	168.2
Acceptor	N2–H2N...O1^{i}	2.7514(19)	152.9
Donor	O1–H1WB...O4^{ii}	2.931(2)	170.1
Donor	O2–H2WB...O17^{iii}	2.8721(19)	174.3
Donor	O3–H3WB...O14^{iv}	3.134(2)	145.2
Donor	O5–H5WA...O15^{iv}	2.9319(19)	172.7
Donor	O6–H6WA...O16^{v}	2.8173(18)	170.3
Donor	O7–H7WB...O2^{v}	2.674(2)	165.4
Donor	O6–H6WB...O16^{vi}	2.7833(19)	177.1
Donor	O7–H7WA...O16^{vi}	2.8333(19)	168.2

[a] Denotes if the water molecule is a donor or acceptor of an hydrogen bond. [b] *ii* = 1-x, ½+y, ½-z; *iii* = -x, 3-y, 1-z; *iv* = -x, y-½, ½-z; *v* = x, ⁵/₂–y, z-½; *vi* = 1-x, y-½, ½-z.

The pyrazole group is protonated resulting in the breaking of the intra-molecular hydrogen bond seen in crystal structure of **3.10**. The **3.10H⁺** molecules are flat (RMS deviation of 0.102 Å and 0.08 Å for the molecules with atoms C1 and C12, respectively) with intra-molecular hydrogen bonds between the carbonyl group of the urea and the pyrazole NH nearest the urea group, and the carbonyl group of the urea and the CH on the nitrophenyl group. As there are a large number of water molecules in this structure there is extensive hydrogen bonding. All hydrogen bonds involving water, both as an acceptor and as a donor, are listed in Table 3.3. Hydrogen bonds involving just atoms within the ASU are shown in Figure 3.39. There are just three hydrogen bonds that do not involve water molecules and these involve the hydrogen bonding of the urea group (N8 and N9) to the SO_4^{2-} anion in a $R_2^2(8)$ motif and the pyrazole (N1) to the SO_4^{2-} anion through a linear hydrogen bond. The overall packing of the molecules of **3.10H⁺** one on top of each other in a π stacking motif (the distance between the molecules varies from 3.33 Å to 3.49 Å) results in columns that contain the SO_4^{2-} and water molecules surrounded by four stacks of **3.10H⁺** (Figure 3.40). This packing is similar to that seen by Dastidar, Das and coworkers in a bispyridyl urea hydrogelator with ethylene glycol and water "snap shot" single crystal structure.[25] 1D growth of gel fibres due to 1D supramolecular bonds is considered an important consideration in designing LMWGs.[51] Keeping this in mind, the needle-shaped crystals were face indexed to determine what the driving force is for the "quicker" growth of the face that determines the needle morphology. This quicker growing face was determined to be (100). The packing of the **3.10H⁺** molecules within the structure one on top of each other through π stacking is in the [100] direction, in correlation to the (100) quicker growing face. This shows that the π stacking, the hydrophobic supramolecular driving force that is important in aqueous conditions, of the planarised **3.10H⁺** drives 1D growth and may do so as well in the gel formation. No PXRD pattern of the H_2SO_4 gel samples could be obtained.

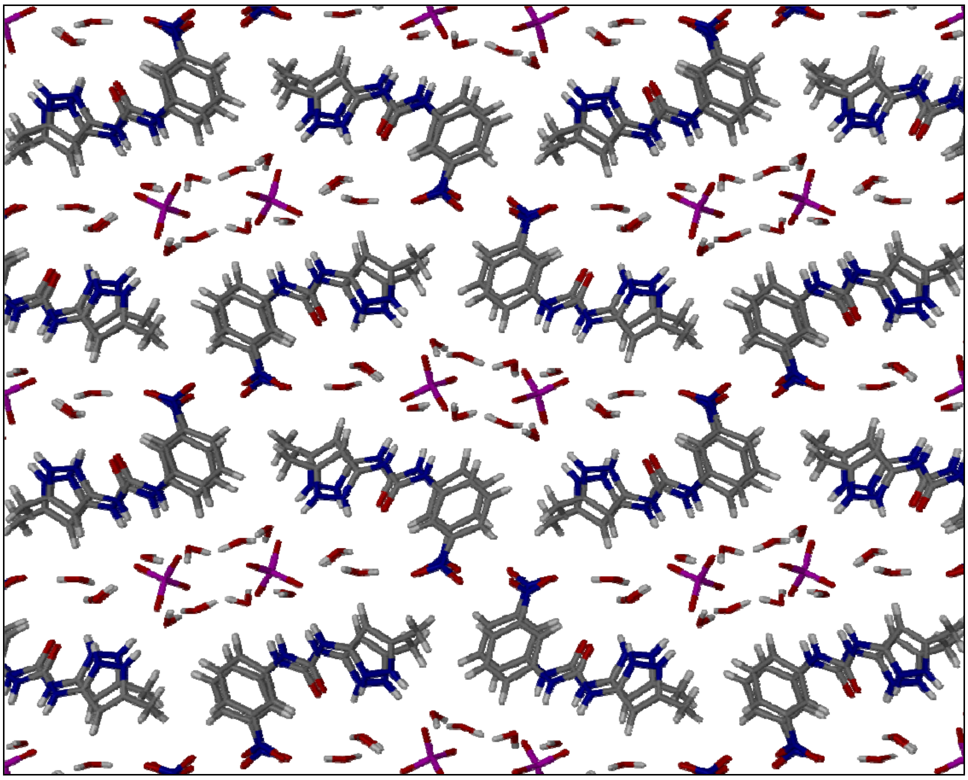

Figure 3.40. Packing diagram of ($\mathbf{3.10H^+}$)$_2$(SO_4^{2-})·$7H_2O$ showing the stacking of $\mathbf{3.10H^+}$ one on top of each other resulting in a column in which the SO_4^{2-} and water are located. Packing viewed down [100].

3.6.3 Gel formation with HBF_4 and HPF_4

Solutions of **3.10** in water that have been acidified to a general pH range of 1 to 2 with HBF_4 or HPF_6 also formed gels (see Table 3.2 for details). When hot solutions were allowed to cool to room temperature irregular gel formation was seen, however, more regular gels were obtained by sonication of the solution until gel formation was complete.[172] The gels were, in appearance, different to gels of **3.10** with H_2SO_4 (and the metastable nitrate gel) in that they were more opaque and were pale cream in colour instead of the more yellow colour of the other gels (Figure 3.31). The rheological characterization by stress sweep and frequency sweep reveals that the HBF_4 and HPF_6 acidified gels were true gels with G' values being 2 to 4 times greater than the G'' values, and there values were essentially constant over a range of frequencies or stress levels

(Figure 3.41).[179] The HBF_4 and HPF_6 acidified gels were found to be weaker than those of H_2SO_4.

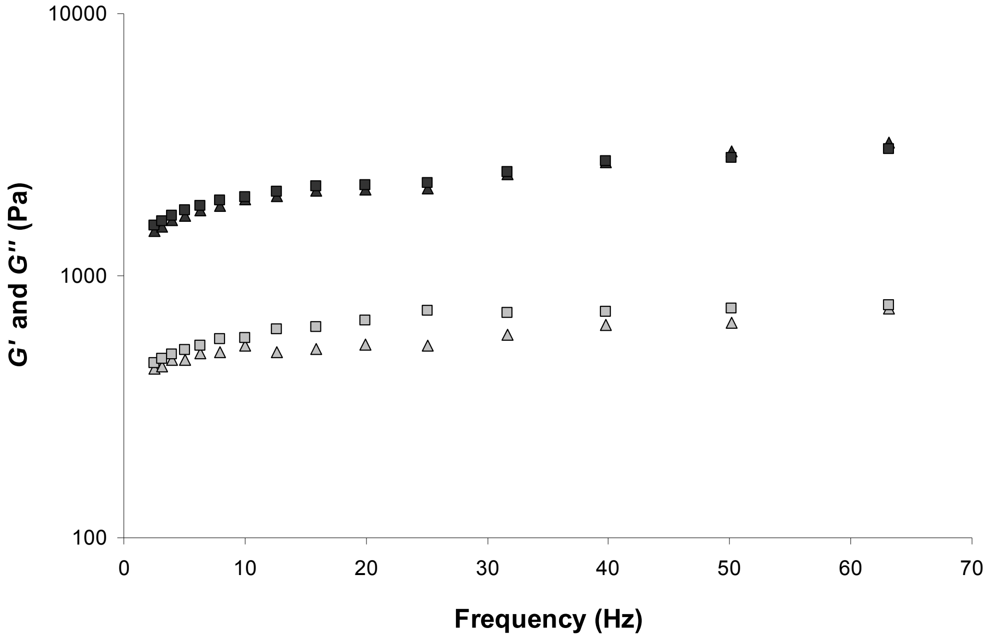

Figure 3.41. Rheology by frequency sweep of the HBF_4 (△) and HPF_6 (□) acidified gels.

TEM imaging of the HBF_4 and HPF_6 acidified gels reveals that the microstructure was different to that of the H_2SO_4 acidified gels (Figure 3.42). Both gels showed a particle-based gel structure.[185-187] The images of the HBF_4 acidified gels showed a porous structure with struts consisting of small particles ranging in size from 10 to 50 nm with the gel spanning the pores of the carbon mesh holding the samples. The images of the HPF_6 gels showed a similar gel structure with struts consisting of nano-sized particles. The particles of the HBF_4 and HPF_6 acidified gels were crystalline in nature as shown by their ability to diffract the electron beam in diffraction mode on the TEM instrument (Figure 3.43). SEM images of gel samples acidified with HBF_4 and HPF_6 that had been dried under high vacuum and covered in a thin layer of Pt showed that the HBF_4 acidified gels form crystalline flakes upon drying (Figure 3.44a). The SEM images of the HPF_6 acidified gels showed porous structures which are similar to those seen for the H_2SO_4 acidified gels (Figure 3.44b).

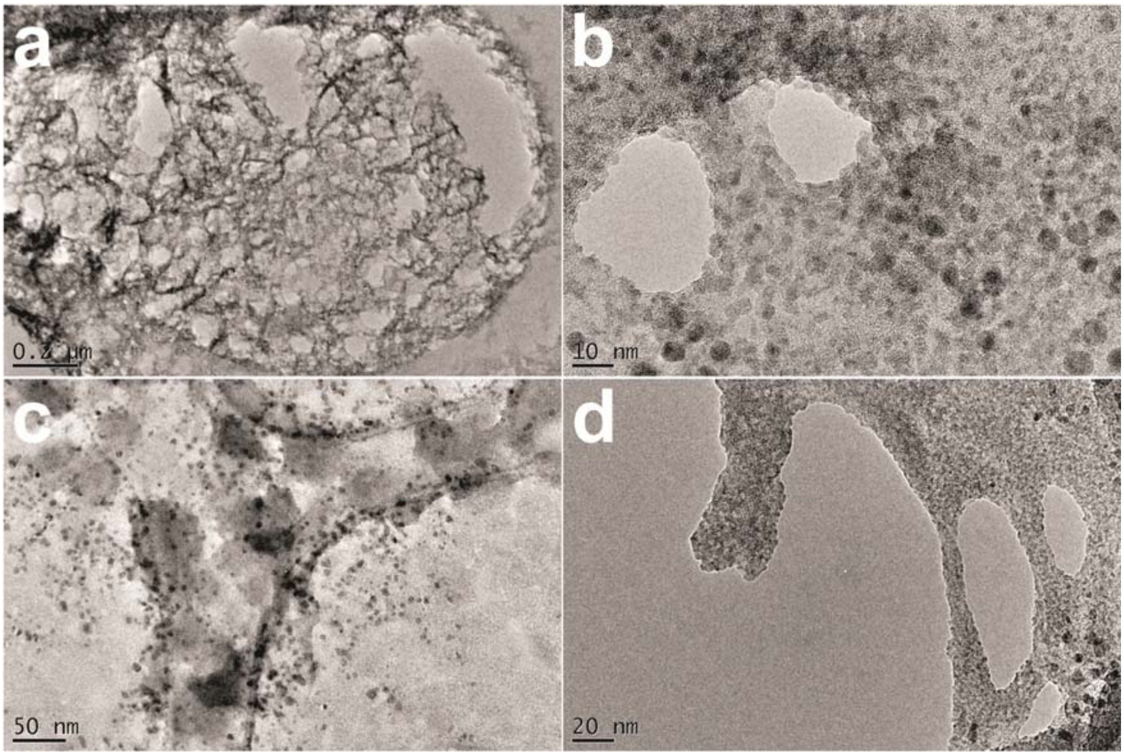

Figure 3.42. TEM images of gels of **3.10** acidified with **a,b)** HBF_4, **c,d)** HPF_6.

Single crystal structure determinations of the structure of the acidified water gels with HBF_4 or HPF_6 were attempted by inducing salt formation by adding salts such as NaCl and Na_2HPO_4 to the gels and by growing single crystals from MeOH solutions of **3.10** acidified with the acids. No single crystals were obtained with HPF_6 but the HBF_4 sample yielded block-shaped crystals of formula (**3.10H$^+$)**(BF_4^-)·H_2O from a MeOH solution acidified with HBF_4 that was allowed to evaporate for one week (Figure 3.45). A **3.10H$^+$** cation was found in this structure. The nitrophenyl group is twisted away from the plane set by the pyrazole and urea groups, the torsion angle ∠ C5–N4–C6–C7 = –30.1^o (in other structures of **3.10** the angle is less than 12^o and as little as 1^o in structure of (**3.10H$^+$**)$_2$(SO_4^{2-})·7H_2O). The RMS deviation from planarity of 0.3081 Å for the **3.10H$^+$** molecule within the (**3.10H$^+$)**(BF_4^-)·H_2O structure also highlights this twisting. The twisted conformation of the **3.10** molecule also disrupts the intra-molecular hydrogen bonds involving the carbonyl group of the urea, in particularly the hydrogen bond with the nitrophenyl group, in comparison to the structure of **3.10** and the structure of (**3.10H**$^+$)$_2$(SO_4^{2-})·$7H_2O$), N2···O1 = 2.626(2) Å; ∠ N2–H2N···O1 = 119.0°, C7···O1 = 2.905(18) Å; ∠ C7–H7···O1 = 111.5° and the H···O distance is longer at 2.42 Å (compared to the 2.24 Å and 2.12 Å of the SO_4^{2-} structure). The $R_2^2(8)$ hydrogen bonding to the BF_4^- through the urea group is shifted resulting in a weaker interaction for the N3–H3N···F3 bond compared to the N4–H4N···F1 and results in the hydrogen bond N3–H3N···F1 leading to an asymmetric hydrogen bonding pattern (Figure 3.45).

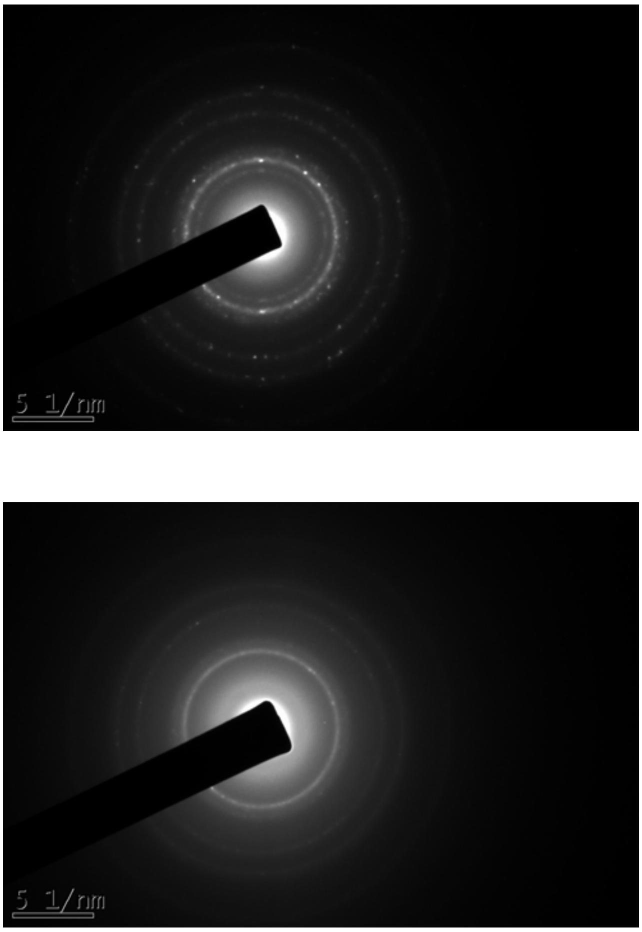

Figure 3.43. Electron diffraction images of gels of **3.10** acidified with HBF_4 (top) and HPF_6 (bottom). Top diffraction *d*–spacing for the HBF_4 acidified gels are 2.46 Å; 2.11 Å; 1.86 Å; 1.55 Å; 1.32 Å and 1.12 Å. Bottom diffraction *d*–spacing for the HPF_6 acidified gels are 2.07 Å; 1.81 Å; 1.31 Å and 1.10 Å.

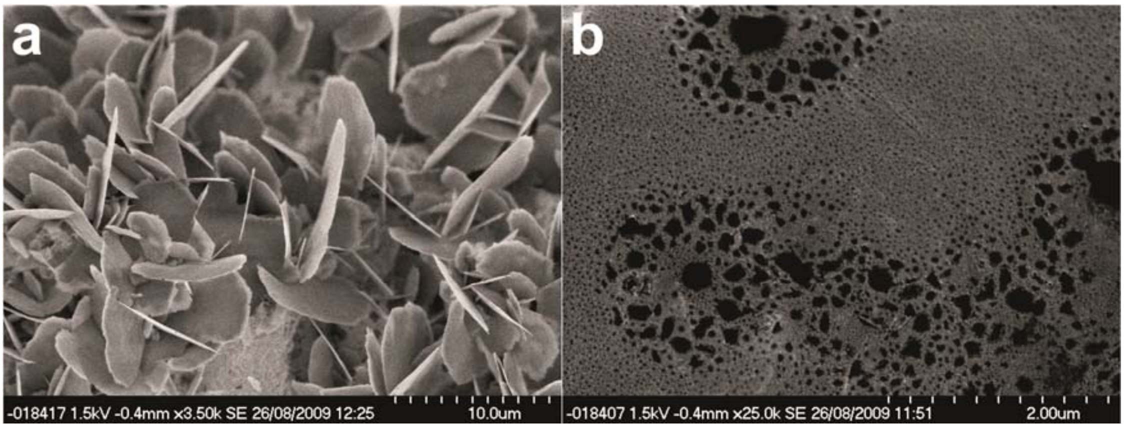

Figure 3.44. SEM images of dried gels of **3.10** acidified with **a)** HBF_4 and **b)** HPF_6..

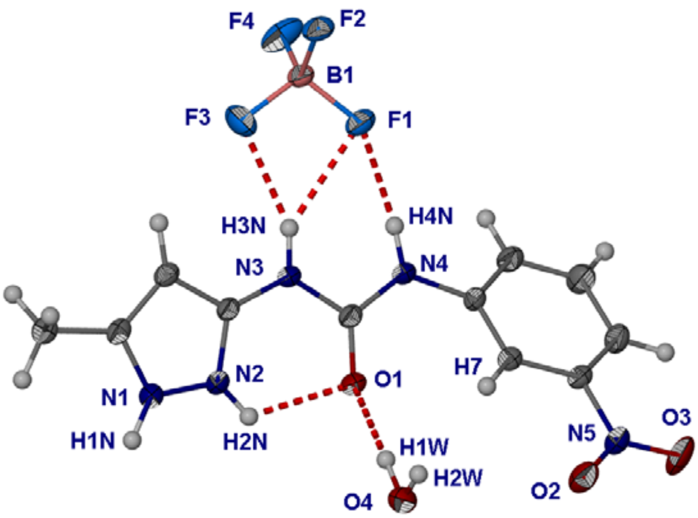

Figure 3.45. Molecular structure of (**3.10H$^+$**)(BF_4^-)·H_2O. Atoms are shown as ellipsoids at 50% probability. Selected hydrogen bonds: BF_4^- are N3···F3 = 2.965(2) Å; ∠ N3–H3N··· F3 = 148.4^o, N3···F1 = 3.069(2) Å; ∠ N3–H3N··· F1 = 145.9^o, N4···F1 = 2.9275(19) Å; ∠ N4–H4N··· F1 = 149.4^o, O4···O1 = 2.814(2) Å; ∠ O4–H4W··· O1 = 177.3^o, N1···O4^i = 2.653(2) Å; ∠ N1–H1N··· O4^i = 170.5^o, O4···F3^{ii} = 2.981(2) Å; ∠ O4–H4W··· F3^{ii} = 149.4^o and N2···F2^{iii} = 2.7539(19) Å; ∠ N2–H2N··· F2^{iii} = 140.9^o (*i* = -x, 1-y, 1-z and *ii* = x, y-1, z and *iii* = x-1, y-1, z).

There is one water molecule that hydrogen bonds to both the **3.10H$^+$** (as both a donor and an acceptor) and the BF_4^- anion. The intra-molecularly hydrogen bonded N2–H2N also hydrogen bonds to the BF_4^-. Due to the twisting of the nitrophenyl group in

3.10H$^+$ the **3.10H**$^+$ cations do not quite pack one on top of each other as seen in the other structures containing **3.10H**$^+$ (Figure 3.46a). The π-π stacking of the nitrophenyl groups can be viewed when the entire structure is packed out and viewed down (010) (the *c* axis length of 7.7509(4) Å being double the π stacking distance) (Figure 3.46b).

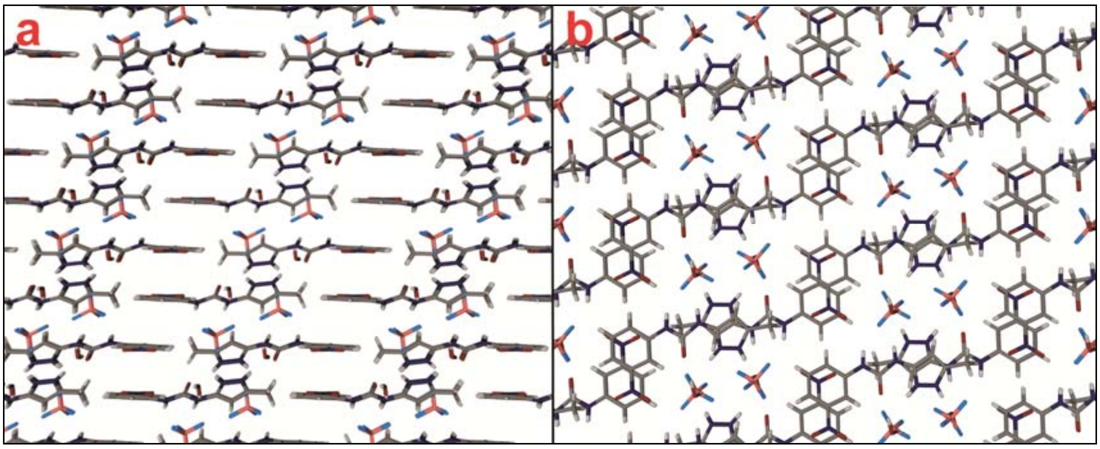

Figure 3.46. a) Structure of **3.10H**$^+$ BF_4^- H_2O as viewed down (100). **b)** Structure of **3.10H**$^+$ BF_4^- H_2O as viewed down (010). Hydrogen bonds not shown for clarity.

Crystals of formula (**3.10H**$^+$)(BF_4^-)·**3.10,** obtained by adding Na_2HPO_4 (50 mg to a 3 ml 0.2% by weight gel) to a gel in water acidified with HBF_4, were found to be a cocrystal[188-192] consisting of both protonated and unprotonated **3.10** (Figure 3.47). The acidic proton is disordered equally between N2 and N7 of neighbouring molecules of **3.10** with the hydrogen bonding between the two compounds changing with the position of the proton. The two molecules of **3.10** are still planar but the nitrophenyl groups are twisted slightly due to steric hindrance arising from the interactions between the pyrazole groups, RMS deviations of 0.1190 Å (**3.10** molecular with C1 atom) and 0.2161 Å (C12 compound). Indeed, the nitrophenyl group of the second molecule (based on C12 to O6) has a "transoid" orientation in relation to the pyrazole group orientation rather than the "cisoid" orientation seen in all the other structures of **3.10**. When the proton is on N2, in addition to it hydrogen bonding to N7, the pyrazole group forms a $R_1^2(8)$ hydrogen bond with the carbonyl of the neutral **3.10** helping to open up the urea group from the intra-molecular hydrogen bond of crystal structure of pure **3.10**. When the proton is on N7 the hydrogen bonding is slightly different. The hydrogen bonding to the now acceptor N1 means that there is an intra-molecular hydrogen bond to the urea carbonyl group as seen in the other structures. The intra-molecular hydrogen bonds from the nitrophenyl moiety are slightly different due to the already mentioned twisting of the nitrophenyl group to a different orientation. With the first **3.10** compound (labelled C1 to O3) the previously noted intra-molecular hydrogen bonding, C7–H7···O1, was found. However, the second **3.10** molecule (labelled C12 to O6) has a hydrogen bond from C22, C22–H22···O4, instead of C18.

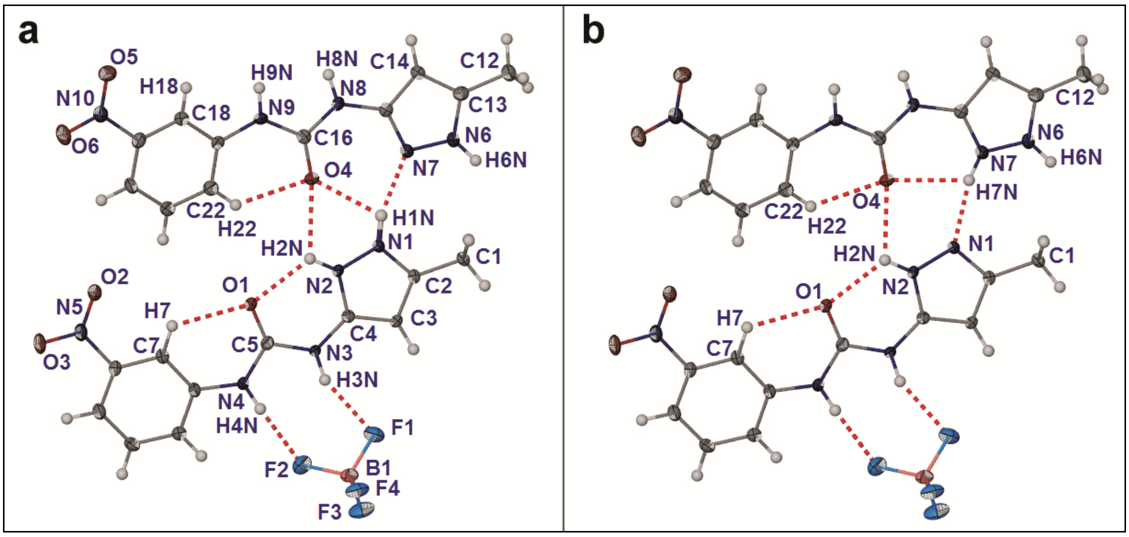

Figure 3.47. Molecular structure of (**3.10H**$^+$)(BF_4^-)·**3.10**. Atoms are shown as ellipsoids at 50% probability. **a)** Disordered proton on N1. Selected hydrogen bonds: N1···O4 = 2.722(3) Å; ∠ N1–H1N··· O4 = 113.2°, N2··· O4 = 2.743(3) Å; ∠ N2–H2N··· O4 = 111.7°, N2···O1 = 2.685(3) Å; ∠ N2–H2N··· O1 = 119.3°, C7···O1 = 2.930(3) Å; ∠ C7–H7··· O1 = 118.9° N1···N7 = 2.843(3) Å; ∠ N1–H1N···N7 = 162.5° or N7···N1 = 2.843(3) Å; ∠ N7–H7N···N1 = 167.6° N7···O4 = 2.838(3) Å; ∠ N7–H7N··· O4 = 114.7° C22···O4 = 2.905(3) Å; ∠ C22–H22··· O4 = 118.3°. **b)** Disordered proton on N7. Selected hydrogen bonds: N3···F1 = 2.935(3) Å; ∠ N3–H3N···F1 = 155.6° and N4···F2 = 2.897(3) Å; ∠ N4–H4N···F2 = 160.9° N8···F4^{i} = 2.908 (3) Å; ∠ N8–H8N···F4^{i} = 145.9°, N9···F4^{ii} = 2.958(3) Å; ∠ N9–H9N···F4^{ii} = 157.4° and N6···O3^{iii} = 3.192(3) Å; ∠ N6–H6N··· O3^{iii} = 164.8° (*i* = 1-x, 1-y, 2-z; *ii* = 1+x, 1+y, z and *iii* = 1+x, y, 1+z).

This hydrogen bonding between a neutral **3.10** species and a protonated species via their carbonyl and pyrazole groups results in the NH groups of the urea moieties and one NH group of the pyrazole group, N6–H6N, being available as hydrogen bond donors. The urea groups hydrogen bond to the BF_4^- with the N3–H3N and N4–H4N groups forming a $R_2^2(8)$ hydrogen bond pattern. The other urea group (N8 and N9) hydrogen bonds to F4 on two symmetry independent BF_4^- ions. The free NH group of the pyrazole group hydrogen bonds to O3 of neighbouring nitro groups which results in a hydrogen bonded thread of **3.10H$^+$·3.10**. These threads are stacked one on top of each other (the stacking distance being a quarter of the a–c unit cell diagonal distance) giving a 2D dimensional layer that alternates with layers of the BF_4^- ions (Figure 3.48).

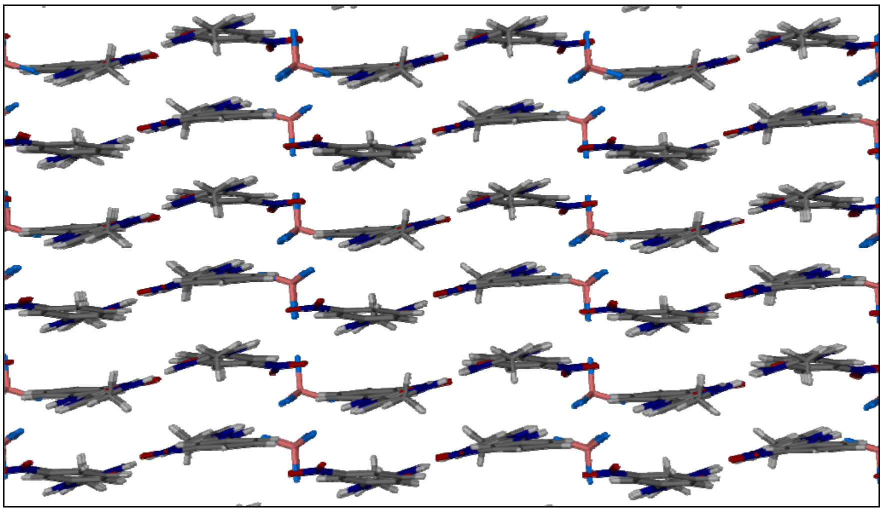

Figure 3.48. Packing diagram of (**3.10H$^+$**)(BF_4^-)·**3.10** showing the stacking of 1D hydrogen bonded **3.10H$^+$ 3.10** threads alternating with the layers of BF_4^-. Hydrogen bonds are not shown for clarity.

The formation of this cocrystal may be due to the change in pH induced by the addition of the Na_2HPO_4. Simulation of the PXRD patterns of either of these BF_4^- **3.10H$^+$** single crystal structures resulted in no confirmed match with the *d*-spacings found from either the electron diffraction of the particles of the TEM gel samples (Figure 3.43) or the PXRD patterns measured of dried gel samples (Figures 3.49 and 3.50). The dried gel PXRD patterns of the HBF_4 and HPF_6 acidified gels show some similarities, but are not perfectly matched.

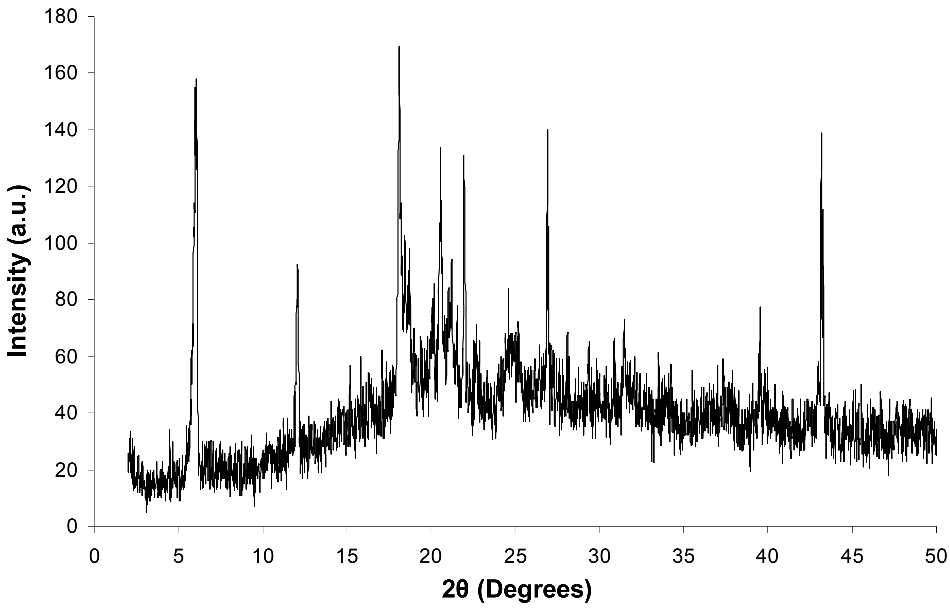

Figure 3.49. PXRD pattern for dried **3.10** gel acidified with HPF_6. Selected *d*-spacings: 2.08 Å; 1.85 Å; 1.70 Å; 1.21 Å and 1.13 Å.

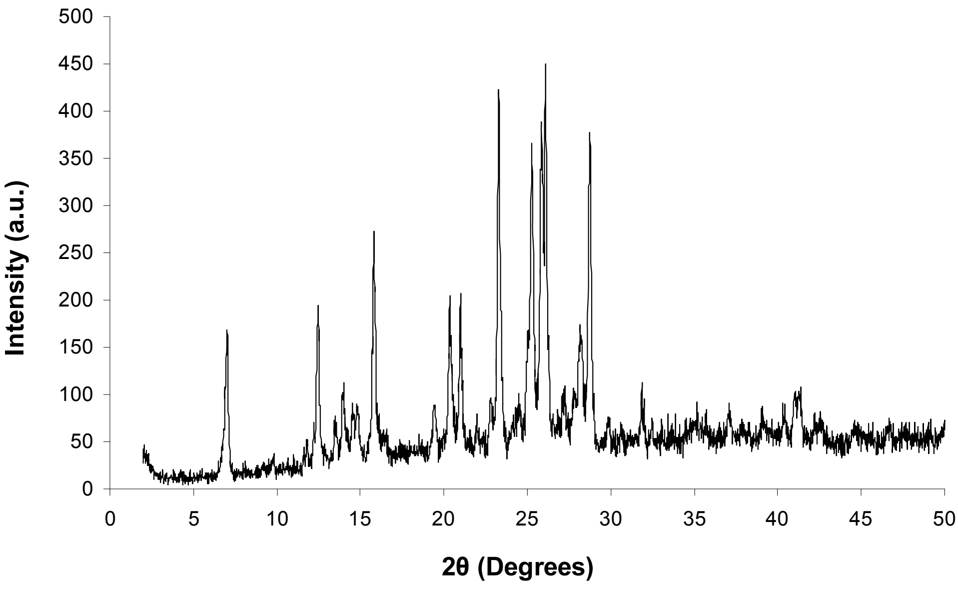

Figure 3.50. PXRD pattern for dried **3.10** gels acidified with HBF_4. Selected *d*-spacings: 2.15 Å; 1.95 Å; 1.81 Å; 1.77 Å; 1.75 Å; 1.60 Å and 1.46 Å.

3.6.4 Gel formation with H_3PO_4 and organic acids

The use of inorganic acids to protonate **3.10** to give gels in acidified water showed the trend that the multiple oxygen-containing anions formed much more stable and reproducible gels. The acids used were H_2SO_4 and H_3PO_4. As both of these acids give multiply charged conjugate anions that can be derivatised with organic groups a study of simple organic sulfonic and phosphonic acids as well as carboxylic acids was performed and the results were compared with the H_3PO_4 acidified gels. The following organic acids were tested with compound **3.10** for gelation in water by dissolving the acid in water to give an acidic solution: acetic acid, trifluoroacetic acid, methanesulfonic acid, trifluoromethanesulfonic acid, *p*-toluene sulfonic acid, methylphosphonic acid ($MePO_3H_2$) and ethylphosphonic acid ($EtPO_3H_2$). The use of $MePO_3H_2$ and $EtPO_3H_2$ resulted in gels, whereas the other acids only gave precipitates. In a similar way to the inorganic acids, gels were formed with $MePO_3H_2$ and $EtPO_3H_2$ at a pH between 1 and 2. The CGC for the $MePO_3H_2$ gels was 0.13 % by weight, 0.18 % by weight for $EtPO_3H_2$ and 0.11 % by weight for H_3PO_4. The visual appearance of these two phosphonate gels was similar to the H_3PO_4 and H_2SO_4 gels. The $MePO_3H_2$ based gels were found to be stable for months, whereas the $EtPO_3H_2$-based gels broke down to a precipitate within 30 min.[170]

Rheological characterisation of gels acidified with H_3PO_4, $MePO_3H_2$ or $EtPO_3H_2$ by both stress sweep and frequency sweep rheometry confirmed that these solid-like materials were true gels with their G' values being five times greater than their G'' values. These values were essentially constant over a range of frequencies or stresses (Figure 3.51).[179] The $MePO_3H_2$ acidified gels were found to be stronger (larger G' and "yield stress" values) than the H_3PO_4 acidified gels, but weaker than the H_2SO_4 acidified gels with the H_3PO_4 acidified gels being comparable to the HBF_4 and HPF_6 acidified gels in strength. The $EtPO_3H_2$ acidified gels were found to be very weak, often forming precipitates when transferred to the rheometer for measurement, therefore, resulting in poor measurement data. The TEM imaging of the H_3PO_4, $MePO_3H_2$ and $EtPO_3H_2$ acidified gels revealed a porous sponge-like structure similar to that seen for the H_2SO_4

acidified gels (Figure 3.52). PXRD patterns of the of dried $MePO_3H_2$ and $EtPO_3H_2$ acidified gels show how the gel materials transform to crystalline materials (Figures 3.53 and 3.54) No PXRD patterns could be obtained for the H_3PO_4 gel samples as samples formed sticky amorphous materials.

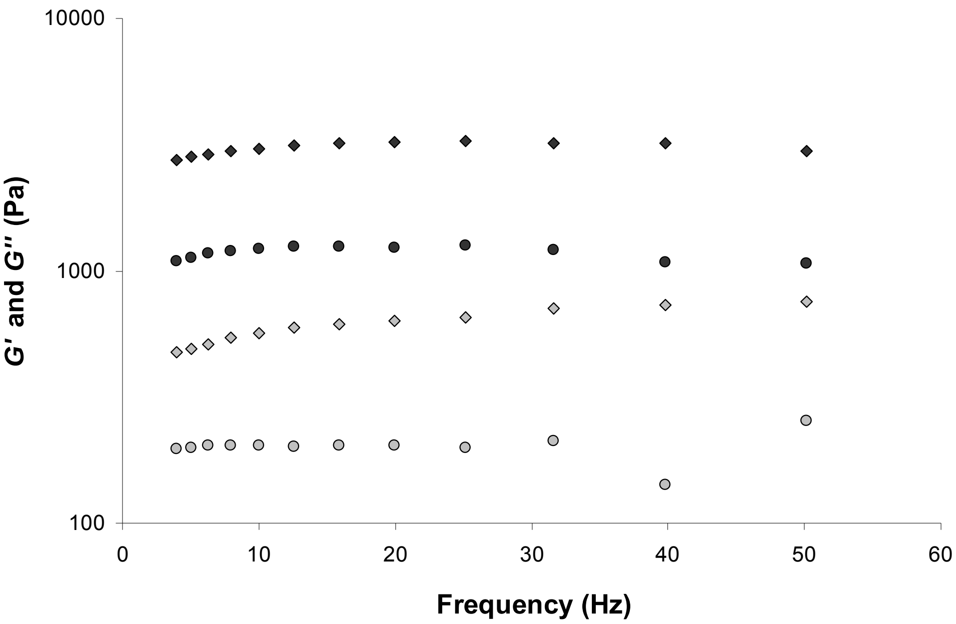

Figure 3.51. Frequency sweep rheometry of **3.10** gels acidified with H_3PO_4 (○) and $MePO_3H_2$ (◇). Dark grey filled symbols are of *G′* and light grey filled symbols are of *G′′*.

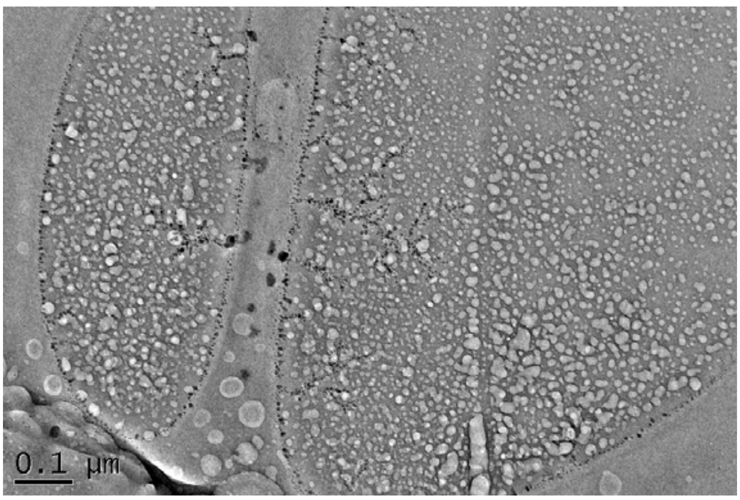

Figure 3.52. TEM image of **3.10** gel acidified with H_3PO_4 at room temperature.

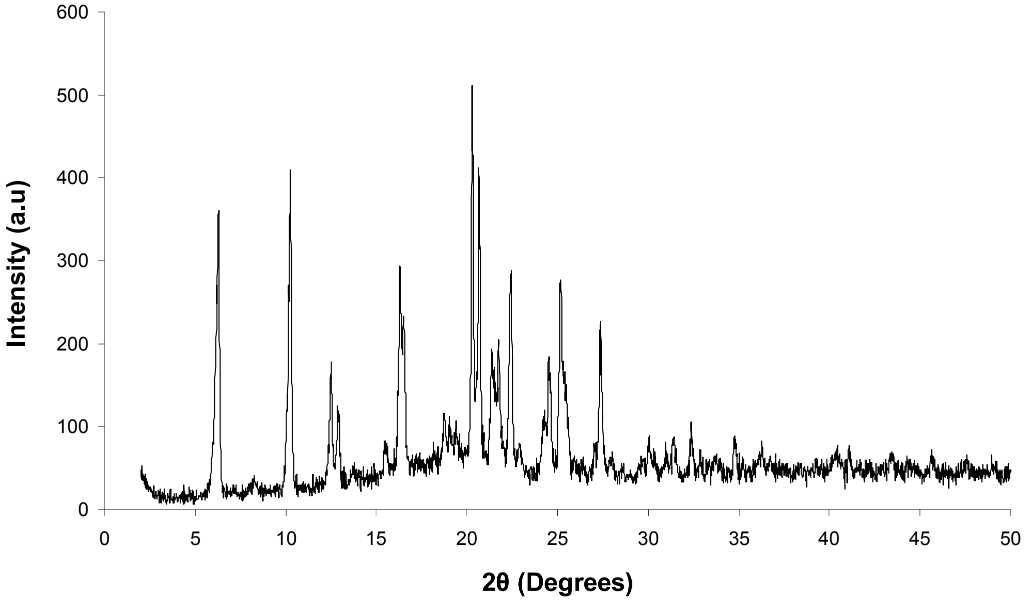

Figure 3.53. PXRD pattern for dried **3.10** gel acidified with $MePO_3H_2$.

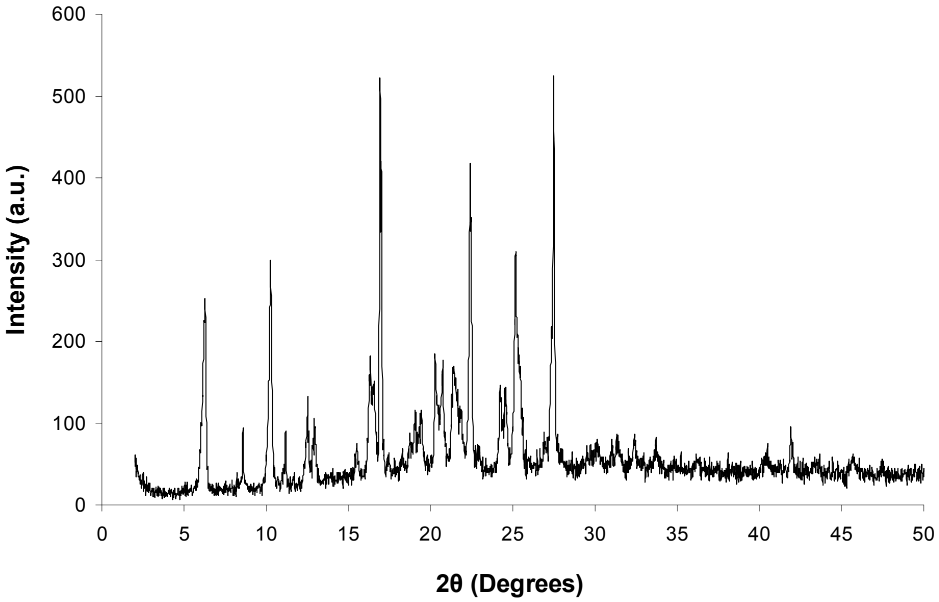

Figure 3.54. PXRD pattern for dried **3.10** gels acidified with $EtPO_3H_2$.

3.6.5 Precipitation of 3.10 by NO_3^- and Cl^-

As already noted, the nitrate- and chloride-based solutions of **3.10** resulted in precipitates instead of gels. A study of the crystalline materials of **3.10** with these two anions was undertaken to ascertain why these anions result in precipitates and not stable gels. The transient nature of the nitrate-acidified gel, that turns into a precipitate, meant that it was studied using the technique of rheology. However, it could have been investigated using TEM imaging (Figure 3.55).[170] Taking images of a gel that had just formed allowed for some characterisation of the gel. Interestingly, the transformation from gel to crystal could be observed directly, as clusters of nanocrystals grew on what appeared to be the gel fibres. The Cl^- and NO_3^- gel tests and the transformation of the nitrate, sulphate and ethylphosphate **3.10** gels to crystals revealed a close relationship between gel formation and crystal formation.[51,193,194]

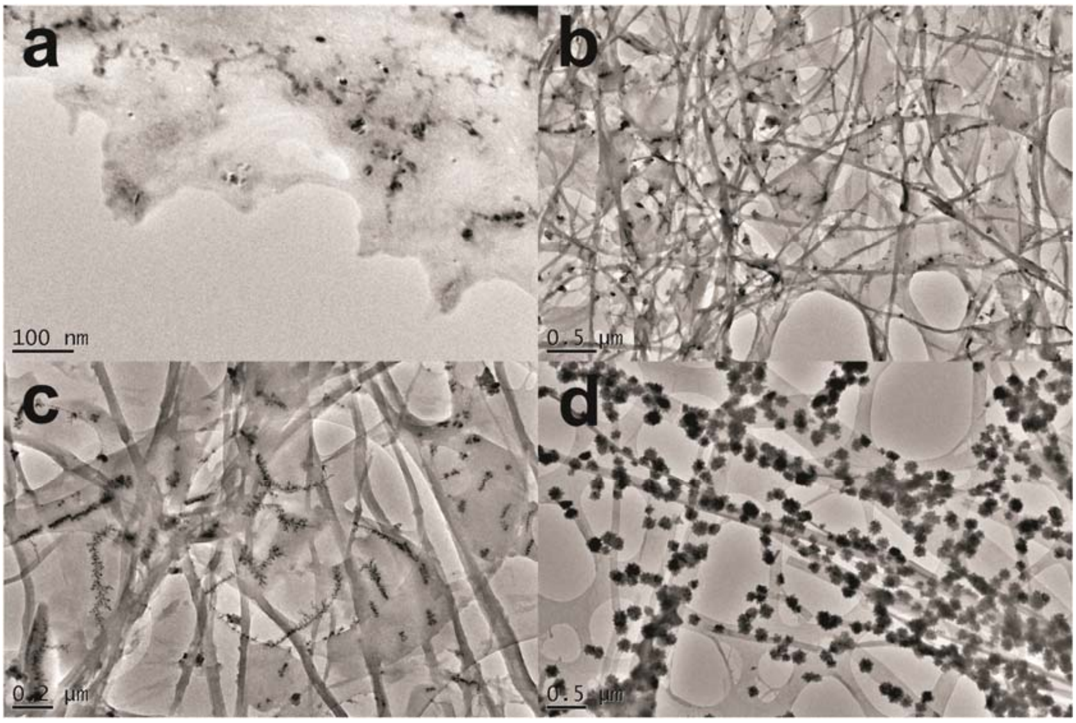

Figure 3.55. TEM images of the gels from acidification of a water solution of **3.10** with HNO_3. **a)** and **b)** are from a **3.10** with HNO_3 gel sample. **c)** and **d)** are from a **3.10** with HNO_3 gel that has started to break down to a precipitate.

As no single crystals of these crystalline materials could be obtained from acidified water, an organic polar solvent was added to slow down crystal formation. This resulted in the formation and characterisation of a methanol solvate of **3.10H**$^+$ Cl^- and a methanol and water solvate of **3.10H**$^+$ NO_3^- when **3.10** was crystallised from a MeOH solution acidified with an equal volume of concentrated acid. The (**3.10H**$^+$)(NO_3^-)·MeOH structure has an ASU consisting of two each of **3.10H**$^+$, NO_3^- and MeOH, i.e. $Z' = 2$ (Figure 3.56). Once again, the **3.10H**$^+$ cations are planar with the pyrazole being protonated, RMS deviations of 0.105 Å (C1 containing molecule) and 0.0396 Å (C12 containing molecule). The intra-molecular hydrogen bonds between the pyrazole and the carbonyl of the urea and the carbonyl group of the urea and the CH on the nitrophenyl group aids with the formation of the planar **3.10**$^+$ cation. One of the nitrate anions is asymmetrically chelated between two urea groups with hydrogen bonds that are in an asymmetric $R_2^2(8)$ motif.[195] The hydrogen bond details for the $R_2^2(8)$ motif of the urea group containing N3 and N4 show that the hydrogen bond pattern is symmetrical. The urea containing N8 and N9 is not symmetric, with particularly the N8–H8N hydrogen bond being weaker in strength than the N9–H9N hydrogen bond. The N8 part of the urea group can ,therefore, be considered to be forming a $R_2^1(6)$ motif and the N9 forming a linear hydrogen bond.[196] The pyrazole group containing N1 and N2, hydrogen bonds to the second nitrate anion, but due to the divergent character of the pyrazole NH groups only the N–H···O11 hydrogen bond is strong. The MeOH molecules hydrogen bond (as donors) to this nitrate and are hydrogen bonded (as acceptors) to the other pyrazole group. The planar **3.10H**$^+$ molecules, once again, pack one on top of each other, but this time in an alternating pattern (Figure 3.57). There are four stacks of **3.10H**$^+$ that surround a column of the MeOH and NO_3^-.

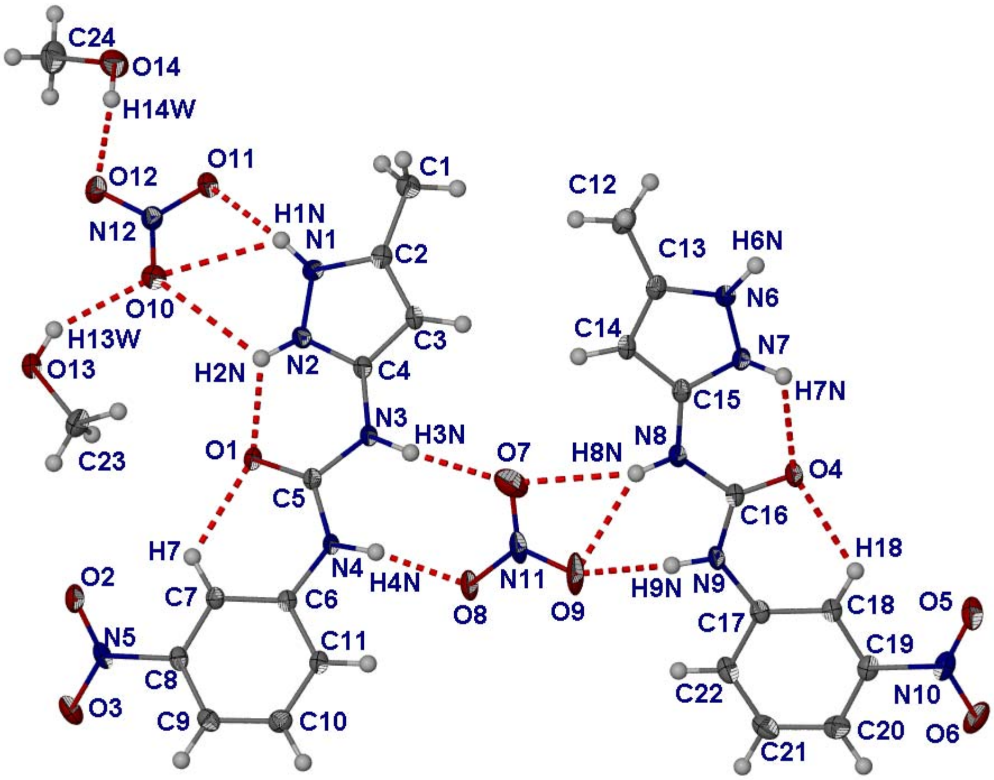

Figure 3.56. Molecular structure of (**3.10H$^+$**)(NO_3^-)·MeOH. Atoms are shown as ellipsoids at 50% probability. Selected hydrogen bonds for intra-molecular bonds: N2⋯O1 = 2.598(2) Å; ∠ N2–H2N⋯O1 = 120.3°, C7⋯O1 = 2.855(3) Å; ∠ C7–H7⋯O1 = 120.4°, N7⋯O4 = 2.667(2) Å; ∠ N7–H7N⋯O4 = 118.3° and C18⋯O4 = 2.884(3) Å; ∠ C18–H18⋯O4 = 120.2°. Selected hydrogen bonds for chelated nitrate: N3⋯O7 = 2.982(3) Å; ∠ N3–H3N⋯O7 = 170.7°, N4⋯O8 = 2.785(2) Å; ∠ N4–H4N⋯O8 = 165.9°, N8⋯O7 = 3.318(3) Å; ∠ N8–H8N⋯O7 = 161.8°, N8⋯O9 = 3.040(3) Å; ∠ N8–H8N⋯O9 = 144.4° and N9⋯O9 = 2.778(3) Å; ∠ N9–H9N⋯O9 = 157.5°. Selected hydrogen bonds for methanol and methanol hydrogen bonded nitrate: N1⋯O11 = 2.687(3) Å; ∠ N1–H1N⋯O11 = 172.9°, N1⋯O10 = 3.080(3) Å; ∠ N1–H1N⋯O10 = 117.2° and N2⋯O10 = 3.097(3) Å; ∠ N2–H2N⋯O10 = 115.3°, O14⋯O12 = 2.835(3) Å; ∠ O14–H14W⋯O12 = 171.5°, O13⋯O10 = 2.969(2) Å; ∠ O13–H13W⋯O10 = 150.1°, N6⋯O14 = 2.645(3) Å; ∠ N6–H6N⋯O14 = 169.6° and N7⋯O13 = 2.803(2) Å; ∠ N7–H7N⋯O13 = 146.5° (*i* = 1-x, 1-y, 1-z and *ii* = 1+x, y, 1+z).

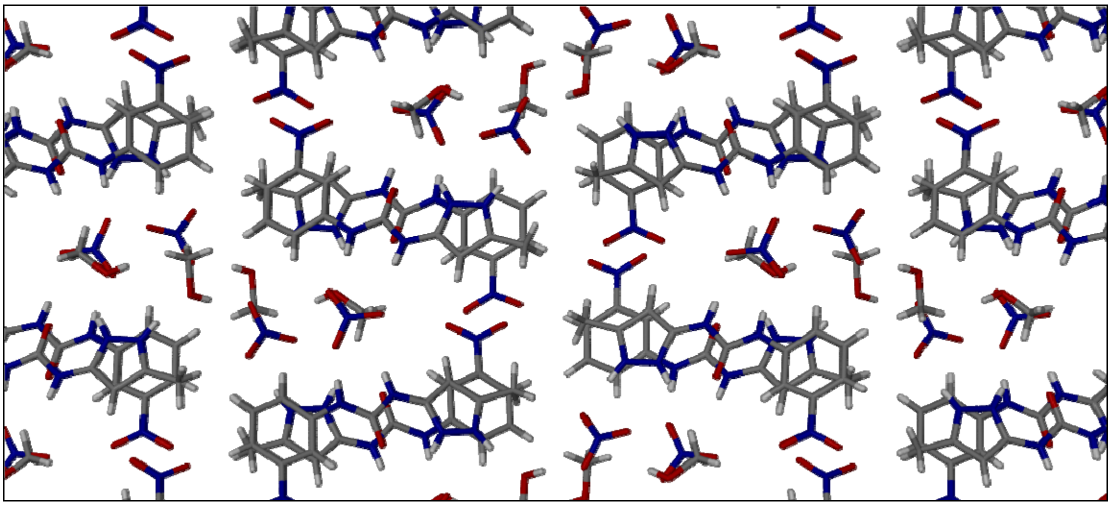

Figure 3.57. Overall crystal packing of (**3.10H$^+$**)(NO_3^-)·MeOH. Hydrogen bonds are not shown for clarity.

The crystal structure determined for 2[(**3.10H$^+$**)(Cl^-)]·MeOH·H_2O (Figure 3.58), from the crystallization of **3.10** from a HCl acidified solution in MeOH, shows similarities in the anion binding to the structure of (**3.10H$^+$**)NO_3^-·MeOH. Once again the **3.10H$^+$** molecules are planar with the pyrazole protonated, RMS deviations of 0.0533 Å (C1 containing molecule) and 0.0995 Å (C12 containing molecule). The intra-molecular hydrogen bonds between the pyrazole and the carbonyl of the urea and the carbonyl group of the urea and the CH on the nitrophenyl group aid planarization. As with the nitrate structure, there is a chloride chelated between the two urea groups of **3.10H$^+$**. The $R_2^1(6)$ hydrogen bonding by both ureas is symmetrical. The N1–H1N group of the pyrazole hydrogen bonds to the second chloride. The other pyrazole group has hydrogen bonds to the MeOH and water molecules. The MeOH hydrogen bonds to the chelated Cl1. As seen with the other structures containing a protonated **3.10**, the **3.10H$^+$** in this chloride structure pack one on top of each other, but as with the nitrate structure, in an alternating motif. This results in the now familiar stacks of **3.10H$^+$** with anion and solvent in between, and, as a result of the smaller size of the Cl^-, the “channel” between four stacks is shifted resulting in a kinked column (Figure 3.59).

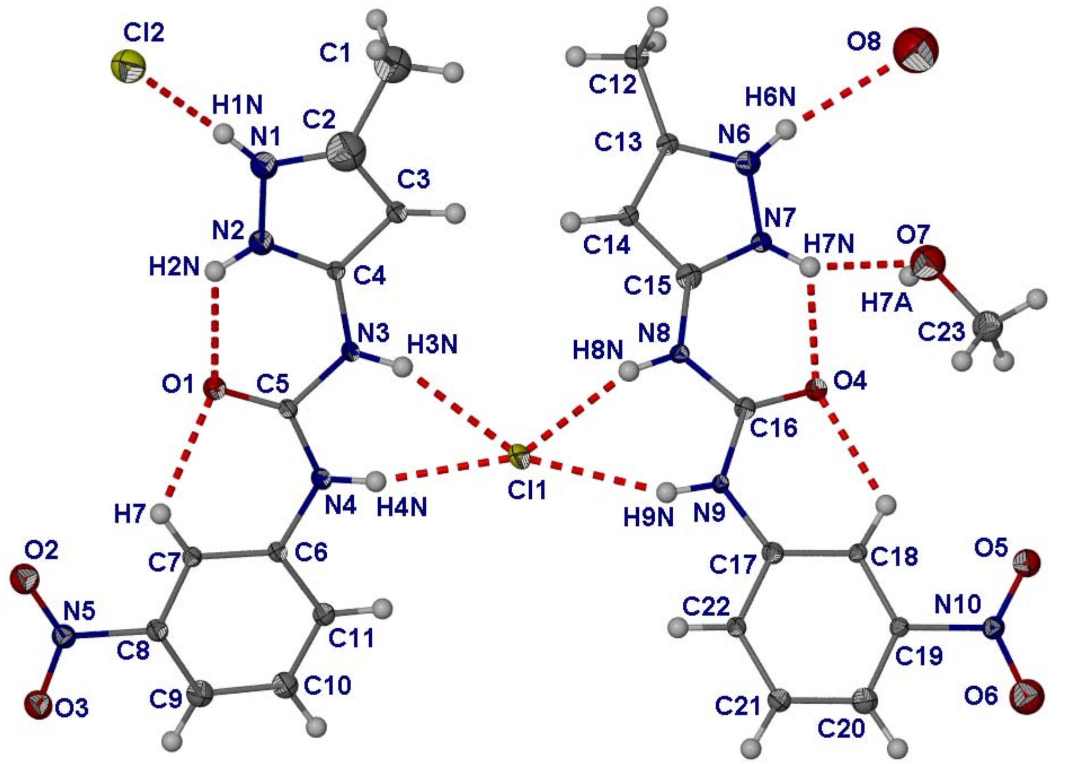

Figure 3.58. Molecular structure of 2[(**3.10H$^+$**)(Cl$^-$)]·MeOH·H_2O. Atoms are shown as ellipsoids at 20% probability. Selected hydrogen bonds for intra-molecular hydrogen bond: N2···O1 = 2.716(19) Å; ∠ N2–H2N···O1 = 121.0^o, C7···O1 = 2.906(18) Å; ∠ C7–H7···O1 = 123.2^o, N7···O4 = 2.657(17) Å; ∠ N7–H7N···O4 = 118.5^o and C18···O4 = 2.805(18) Å; ∠ C18–H18···O4 = 119.9^o. Selected hydrogen bonds for Cl1: N3···Cl1 = 3.258(16) Å; ∠ N3–H3N··· Cl1 = 159.0^o, N4··· Cl1 = 3.230(16) Å; ∠ N4–H4N··· Cl1 = 165.4^o, N8··· Cl1 = 3.172(16) Å; ∠ N8–H8N··· Cl1 = 160.9^o and N9··· Cl1 = 3.281(15) Å; ∠ N9–H9N··· Cl1 = 156.9^o. Selected hydrogen bonds for Cl2 and methanol: N1···Cl1 = 2.956(18) Å; ∠ N1–H1N··· Cl1 = 174.1^o, N6···O8 = 3.330(16) Å; ∠ N6–H6N··· O8 = 163.3^o, N7···O7 = 2.775(15) Å; ∠ N7–H7N··· O7 = 145.2^o and Cl1, O7···Cl1^i = 3.009(16) Å; ∠ O7–H7A··· Cl1^i = 156.6^o (*i* = 1-x, 2-y, 1-z).

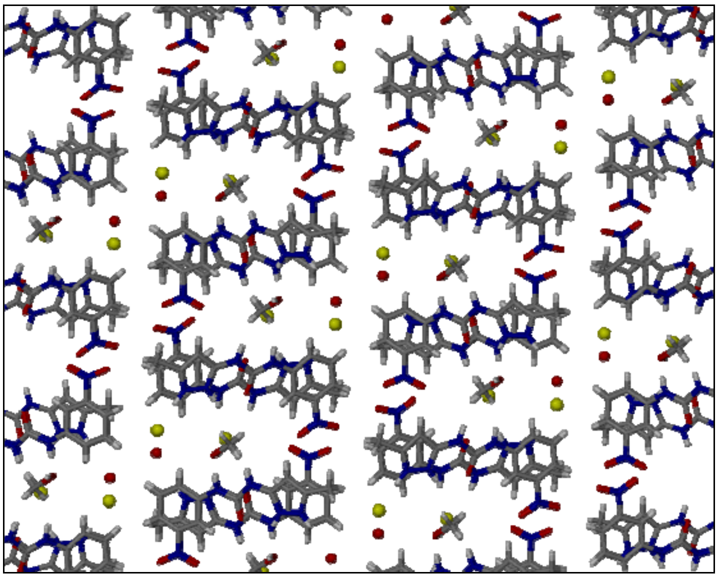

Figure 3.59. Overall packing of 2(**3.10H$^+$**) 2Cl$^-$ MeOH H_2O. Atoms are shown in capped stick representation except for the Cl$^-$ and water oxygen which are shown as small spheres.

The PXRD patterns of the precipitate from the **3.10** acidified water solutions for both HCl and HNO_3 do not correspond to the two single crystal structures due to these crystal structures containing MeOH (Figures 3.60 and 3.61).

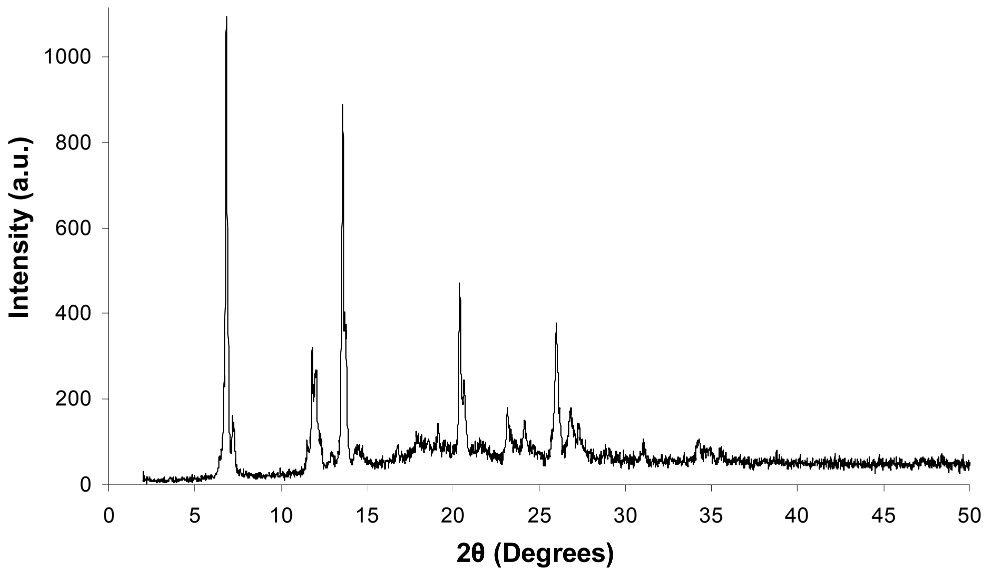

Figure 3.60. PXRD pattern for dried **3.10** gel acidified with HNO_3.

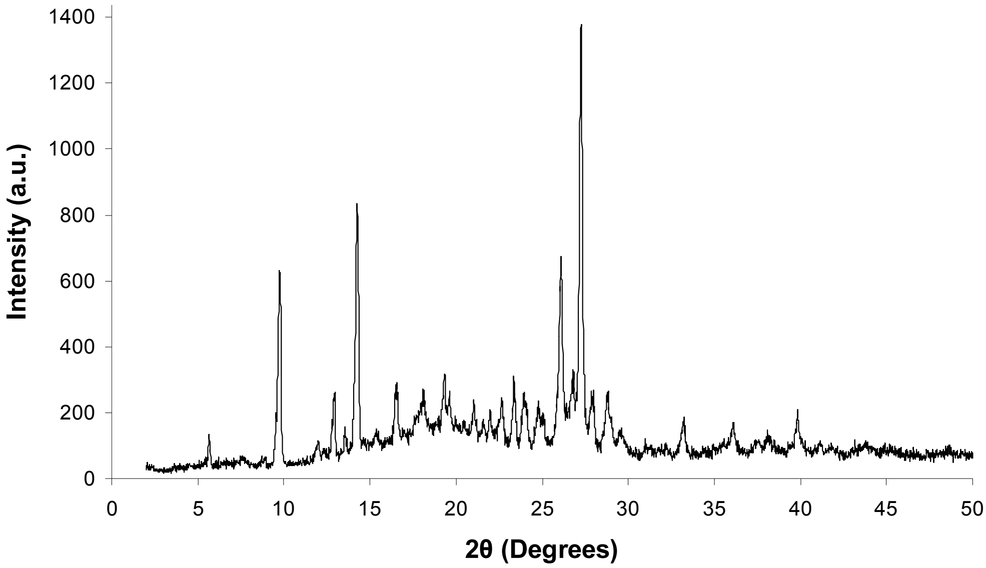

Figure 3.61. PXRD pattern for dried **3.10** gel acidified with HCl.

3.6.6 Anion tuning of gels formed by 1-(3-methyl-1*H*-pyrazol-5-yl)-3-(3-nitrophenyl)urea

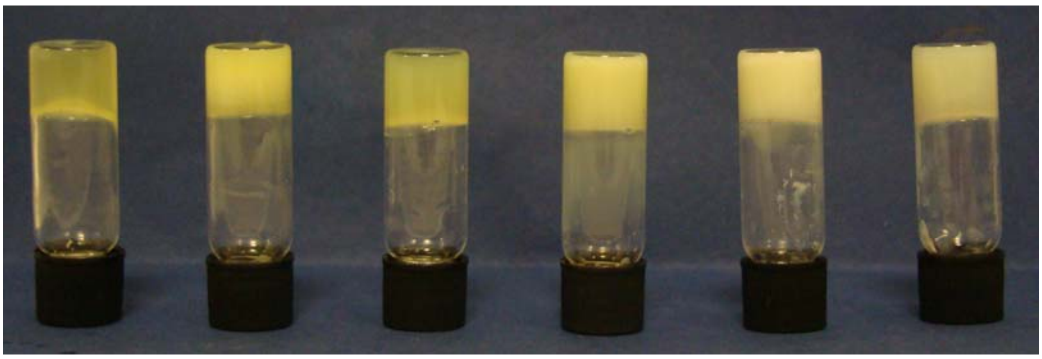

Figure 3.62. Photograph of gels of **3.10** at 1% by weight in water acidified with, from left to right, $EtPO_3H_2$; $MePO_3H_2$, H_3PO_4; H_2SO_4; HPF_6 and HBF_4. The samples for the acids H_3PO_4; H_2SO_4; HPF_6 and HBF_4 are the same as those shown in Figure 3.31.

A large number of salts of organic anions and cations with inorganic counter ions as well as purely organic salts have been discovered to gel a wide variety of solvents.[40,193,197-205] The anion characteristics play a large part in the gelation ability of these compounds. There have been, however, surprisingly few studies performed that look directly at the influence of the anion in LMWG salts, often because a simple change in the anion results in a complete loss of gel character.[40,193,197-205] With the two organic acid based gels and the four inorganic acid based gels that have been described above, a study of the effect of the anion on the rheological characteristics of the **3.10** gels was undertaken (Figure 3.62 and 3.63). The comparison of the gels at 1% by weight with the six acids, and therefore anions, shows that the G' value for each of the anions follows the trend H_2SO_4 > $MePO_3H_2$ > H_3PO_4 ~ HBF_4 ~ HPF_6 > $EtPO_3H_2$ (Figure 3.60). The "yield stress" shows the more detailed trend of H_2SO_4 > $MePO_3H_2$ > HPF_6 > H_3PO_4 > HBF_4 > $EtPO_3H_2$.

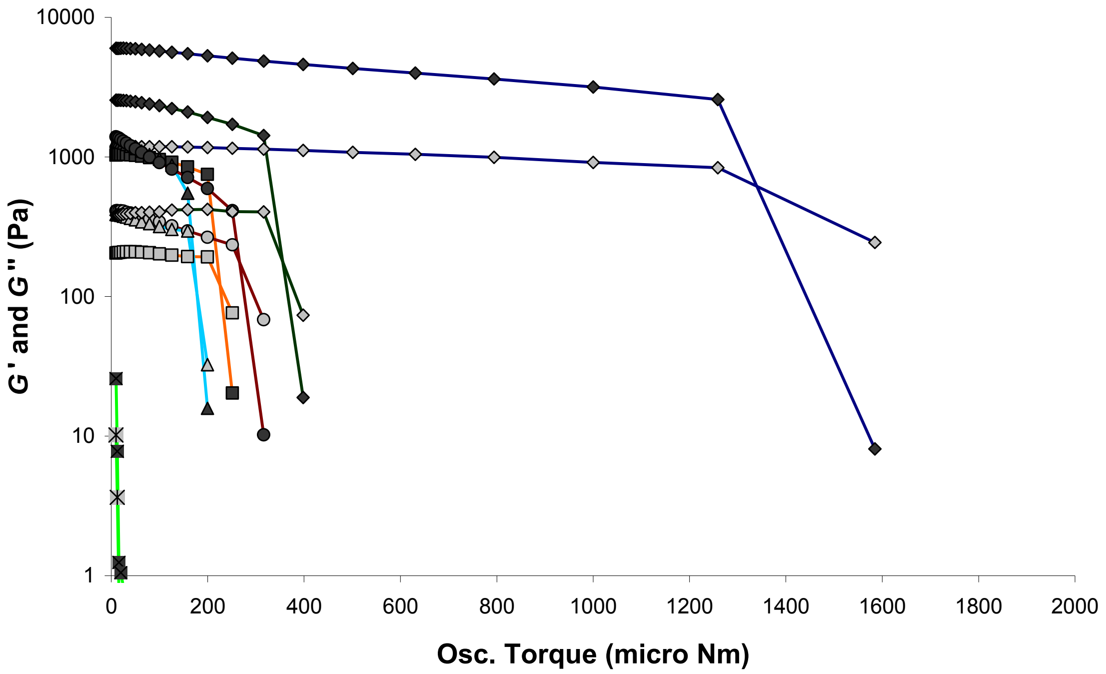

Figure 3.63. Anion tuning of the rheometric characterisations of **3.10** gels shown by stress sweep rheometry of the hydrogels of **3.10** at 1% by weight acidified with H_2SO_4 (Blue ◇), H_3PO_4[3] (Orange □), $MePO_3H_2$ (Green ◇), HBF_4 (Light blue △), HPF_6 (Brown ○) and $EtPO_3H_2$ (Light green □).

It is of interest to compare this series of the anion tuning of the **3.10** gels with the classical Hofmeister series.[46,206,207] The Hofmeister series ranks the anions used in this study in the order from kosmotropic (strongly hydrated anions) to chaotropic (weakly hydrated anions) as: $SO_4^{2-} \sim MePO_3^{2-} \sim HPO_4^{2-} > EtPO_3^{2-} > Cl^- > NO_3^- > PF_6^- > BF_4^-$, kosmotropic meaning salting-out anions and chaotropic meaning salting-in anions. When the kosmotropic anions, from the acids H_2SO_4, $MePO_3H_2$, H_3PO_4, $EtPO_3H_2$, were used, gel formation was seen, with the SO_4^{2-} and $MePO_3^{2-}$ based gels being the strongest. The chaotropic anions NO_3^-, PF_6^- and BF_4^- also formed gels; however, these gels had different morphologies to the kosmotropic anion based gels. The hydration of the anions, therefore, possibly plays a role in the morphology of the gel. In addition, crystallisation, determined by the identity of the anion, also appears to play an important part in the tunability of the **3.10** hydrogels. The crystallinity of a substance is partly determined by its solubility and lattice energy. As shown by the precipitation of the NO_3^- and $EtPO_3^{2-}$ gels, the induced crystallisation of (**3.10H**$^+$)$_2$(SO_4^{2-})·7H_2O from the SO_4^{2-} gels and crystals of (**3.10H**$^+$)(BF_4^-) from the HBF_4 gels, the crystalline solids are more thermodynamically stable than the gels (a meta-stable state). The chelation of the NO_3^- and Cl^- anions by the urea groups, as seen in the structures (**3.10H**$^+$)(NO_3^-)·MeOH and 2[(**3.10H**$^+$)(Cl^-)]·MeOH·H_2O, is noteworthy.[207] This direct hydrogen bonding interaction between the cation and anion may provide the driving force for crystallisation and, therefore, lack of stable gel formation. The non-planar character of the **3.10H**$^+$ cation within the structure (**3.10H**$^+$)(BF_4^-)·H_2O is also to be noted. This need to have a non-planar conformation for the **3.10H**$^+$ cation within the crystal form allows for the formation of the meta-stable gel. It, therefore, appears that the position of the anions in the Hofmeister series plays an important role in the tuning of the gel properties. On top of these effect is super-imposed the crystallisation tendencies of the compounds, determined by the identity of the anion and its interactions (hydrogen bonding) with the **3.10H**$^+$ cation.

In summary compound **3.10** was found to form hydrogels in the pH range of 1 to 2, thus making compound **3.10** a hydrogelator with pH tunable gelation ability.[25,42,149-168] Rheological characterisation, in conjunction with TEM and SEM imaging, of the H_2SO_4 acidified gels indicated a cellular solid gel material that consists of load bearing struts interconnected via crosslinks or junction points which deform by bending.[173,180,182,183] The anion tuning of the gel characteristics was accomplished by changing the identity of the anion by changing the acid used to adjust the pH of the water solutions. Gel formation was changed to crystallisation by the use of chloride or nitrate resulting in the ability to precipitate a gel by the addition of salts containing these anions. Characterisation of the crystalline salts of **3.10** indicates that the assembly of the gel is encouraged by the 1D stacking of the planar **3.10H**$^+$ driven by hydrophobic effects.[51] The anion-induced change from gel to precipitate appears to be due to the ability of **3.10H**$^+$ to coordinate through multiple hydrogen bonds to the anion.[169,170] The smaller NO_3^- and Cl^- ions are coordinated between two molecules by the urea groups as shown by the (**3.10H**$^+$)(NO_3^-)·MeOH and 2[(**3.10H**$^+$)(Cl^-)]·MeOH·H_2O crystal structures. The rheological anion tuning of gels of **3.10** was studied, and the gels found to vary in strength according to the identity of the anion. The identity of the anion determines the rheological strength of the gels and following order, according to the acid, was found $H_2SO_4 > MePO_3H_2 > HPF_6 > H_3PO_4 > HBF_4 > EtPO_3H_2$.

3.7 Conclusion

The synthesis of urea and thiourea derivatised pyrazoles was not as straightforward as it at first appeared, i.e. reacting the isocyanate or isothiocyanate with the aminopyrazole did not always lead to a desired urea or thiourea. The reaction of *t*-butyl isothiocyanate with 3-amino-5-methylpyrazole in refluxing $CHCl_3$ was performed, and, in agreement with literature results, the derived thiourea compound **3.3** was isolated.[7,48,53-55] The reaction of isocyanates with 3-amino-5-methylpyrazole resulted in the formation of carboxamides, compounds **3.1** and **3.2**, for example.[7,47,48] This problem was circumvented by BOC-protection of the pyrazole ring allowing for the urea functionalisation of the amine group to yield the desired urea functionalised pyrazole compounds. The propensity of the thiourea and urea groups to form an intra-molecular hydrogen bond to the pyrazole moiety, and therefore, be in an *anti* conformation was revealed in the determination of the crystal structures of these compounds. The inability to form one-dimensional aggregates, through the unidirectional hydrogen bonding of urea tapes, was prevented by the formation of the intra-molecular hydrogen bond. The compounds were all crystalline in nature and did not form gels.

The induced opening of the urea group from the *anti* conformation to the *syn* conformation was tested as a means to induce the gel formation by the pyrazole urea compounds. Metal complexes of compounds **3.10** and **3.11a** were found not to form gels even though the urea group was induced to open into the *syn* conformation. Complexes of **3.10** show how the urea-derivatised pyrazole acts as a bidentate ligand with copper and zinc, coordinating through the carbonyl group of the urea and the Lewis basic pyrazolyl N-donor group next to the urea moiety. The bidentate coordination is similar to that found for amide-derivatised pyrazole.[68,72]

The anion binding by **3.3** does not appear to cause the breaking of the intra-molecular hydrogen bond between the thiourea group and the Lewis basic pyrazolyl N-donor group. This was confirmed by the elucidation of the host guest complex between **3.3** and $MeCO_2^-$ in the crystal of (**3.3**)(TBA^+)($MeCO_2^-$)·H_2O. The structure shows the intra-molecular hydrogen bond to still be present.

Protonation of compound **3.10** resulted in the formation of hydrogels in the pH range of 1 to 2, thus making compound **3.10** a hydrogelator with pH tunable gelation ability.[25,42,149-168] Rheological characterization, in conjunction with TEM and SEM imaging, of the H_2SO_4 acidified gels indicated a cellular solid gel material that consisted of load bearing struts interconnected via crosslinks or junction points which deform by bending.[173,180,182,183] In addition, SEM and TEM imaging revealed a morpholigical difference between the gels with anions BF_4^- and PF_6^-, to the gels synthesized with oxygen containing anions; SO_4^{2-}, HPO_4^{2-}, $EtPO_3^{2-}$ and $MePO_3^{2-}$. The anion tuning of the **3.10** gel characteristics was accomplished by varying the identity of the anion by changing the acid used to adjust the pH of the water solutions. Gel formation changed to crystallisation when Cl^- or NO_3^- was introduced. This resulted in the ability to precipitate a gel by the addition of salt containing these anions. The smaller NO_3^- and Cl^- are coordinated between two molecules by the urea groups in the solid state, as shown by the crystal structures of (**3.10H**$^+$)(NO_3^-)·MeOH and 2[(**3.10H**$^+$)(Cl^-)]·MeOH·H_2O. Characterisation of the crystalline salts of **3.10** indicated that the assembly of the gel was encouraged by the 1D stacking of the planar **3.10H**$^+$ driven by hydrophobic effects and π-

π stacking.[51] The anion induced change from gel to precipitate appears to be due to the ability of **3.10H**$^+$ to coordinate through multiple hydrogen bonds to the anion. These hydrogen bond patterns, in combination with other factors, including lattice energy, nucleation and the thermodynamics of the systems, led to higher stability of the crystalline states over the gel states.[169,170] The crystal structures (**3.10H**$^+$)(BF_4^-)·H_2O and (**3.10H**$^+$)$_2$(SO_4^{2-})·7H_2O reveal a slight change in conformation of the **3.10H**$^+$ cation, and the level of hydration, respectively. In addition to the anion tuning from gel to crystal states, the anion tuning of the rheological characteristics of gels of **3.10** was accomplished.[40,193,197-205] The gels of **3.10** were found by rheology to have the order, in relation to "strength", of, according to the acid:

$$H_2SO_4 > MePO_3H_2 > HPF_6 > H_3PO_4 > HBF_4 > EtPO_3H_2$$

Neither the Hofmeister series and/or level of hydration of the anions were found to conclusively explain the order of strength of the **3.10** gels. The change in morphology of the gels, from the oxygen containing anions to BF_4^- and PF_6^-, may explain the inconsistency, as the structures are seen to be different due to the hydrogen bond propensity of these anions, as shown by the crystal structure (**3.10H**$^+$)(BF_4^-)·H_2O. Additionally, the crystallisation abilities of the salts are super-imposed onto the gelation of this series of anion containing gels. The tuning of the gel characteristics of gels of **3.10** is summarized in Table 3.4. This study, overall, shows that LMWG salts can be tuned in terms of gel rheology characteristics, and overall gel formation, by simply varying the identity of the anion.

Table 3.4. Summary of the anion-based tuning of gel characteristics of compound **3.10**.

Acid	HBF_4	HPF_6	HCl	HNO_3	H_3PO_4	H_2SO_4	$MePO_4H_2$	$EtPO_4H_2$
Gelation pH range	1 – 2.0	1 – 1.7	n/a	1 – 2.5	1 – 2.1	1 – 2.0	1 – 2.0	1 – 2.0
CGC[a]	0.30	0.20	n/a	Unstable	0.11	0.12	0.13	0.18
Appearance	Opaque Cream Gel	Opaque Cream Gel	Light Cream Precipitate	Unstable Opaque Cream-Yellow Gel	Clear to Opaque Yellow Gel	Clear to Opaque Yellow Gel	Opaque Cream Gel	Clear, Yellow Weak Gel
Morphology	Particulate	Particulate	Crystalline	Fibre to Crystalline	Sponge-like	Sponge-like	Sponge-like	Sponge-like
Crystal structures	(**3.10H**$^+$)(BF_4^-)·H_2O	n/a	2[(**3.10H**$^+$)(Cl^-)]·MeOH·H_2O	(**3.10H**$^+$)(NO_3^-)·MeOH	n/a	(**3.10H**$^+$)$_2$(SO_4^{2-})·7H_2O	n/a	n/a
Hydration of anion[b]	Monohydrate	n/a	None	None	n/a	Heptahydrate	n/a	n/a
Hofmeister series[c]	8	7	5	6	3	1	2	4

Rheological Strength[d]	5	3	n/a	n/a	4	1	2	6

a) %, Critical Gel Concnetration (CGC) in weight percentage. b) Hydration determined from crystal structures. c) Order of 1 to 8 being from kosmotropic (strongly hydrated anions) to chaotropic (weakly hydrated anions). d) 1 being the strongest and 6 being the weakest, according to rheological properties like *G′* value and “yield stress”.

3.8 References

(1) Halcrow, M. A. *Dalton Trans.* **2009**, 2059-2073.
(2) Trofimenko, S. *Chem. Rev.* **1972**, *72*, 497-509.
(3) Trofimenko, S. *Prog. Inorganic Chem.* **1986**, *34*, 115-210.
(4) Mani, F. *Coord. Chem. Rev.* **1992**, *120*, 325-359.
(5) Mukherjee, R. *Coord. Chem. Rev.* **2000**, *203*, 151-218.
(6) Sadimenko, A. P.; Basson, S. S. *Coord. Chem. Rev.* **1996**, *147*, 247-297.
(7) Anwar, H. F.; Elnagdi, M. H. *Arkivoc* **2009**, 198-250.
(8) Ward, M. D.; McCleverty, J. A.; Jeffery, J. C. *Coord. Chem. Rev.* **2001**, *222*, 251-272.
(9) Pettinari, C.; Pettinari, R. *Coord. Chem. Rev.* **2005**, *249*, 525-543.
(10) Pettinari, C.; Pettinari, R. *Coord. Chem. Rev.* **2005**, *249*, 663-691.
(11) Halcrow, M. A. *Coord. Chem. Rev.* **2005**, *249*, 2880-2908.
(12) Pérez, J.; Riera, L. *Chem. Commun.* **2008**, 533-543.
(13) Pérez, J.; Riera, L. *Chem. Soc. Rev.* **2008**, *37*, 2658-2667.
(14) Jones, L. F.; Kilner, C. A.; Halcrow, M. A. In *10th International Conference on Molecule-Based Magnets (ICMM 2006)*; Sp. Iss. SI ed.; Pergamon-Elsevier Science Ltd: Victoria, CANADA, 2006; Vol. 26, p 1977-1983.
(15) Liu, X. M.; Kilner, C. A.; Halcrow, M. A. *Chem. Commun.* **2002**, 704-705.
(16) Renard, S. L.; Franken, A.; Kilner, C. A.; Kennedy, J. D.; Halcrow, M. A. *New J. Chem.* **2002**, *26*, 1634-1637.
(17) Renard, S. L.; Sylvestre, I.; Barrett, S. A.; Kilner, C. A.; Halcrow, M. A. *Inorg. Chem.* **2006**, *45*, 8711-8718.
(18) Nieto, S.; Perez, J.; Riera, L.; Riera, V.; Miguel, D. *Chem. Eur. J.* **2006**, *12*, 2244-2251.
(19) Arroyo, M.; Miguel, D.; Villafane, F.; Nieto, S.; Perez, J.; Riera, L. *Inorg. Chem.* **2006**, *45*, 7018-7026.
(20) Kishimura, A.; Yamashita, T.; Aida, T. *J. Am. Chem. Soc.* **2005**, *127*, 179-183.
(21) Fages, F. *Angew. Chem. Int. Ed.* **2006**, *45*, 1680-1682.
(22) Piepenbrock, M. O. M.; Lloyd, G. O.; Clarke, N.; Steed, J. W. *Chem. Rev.* **2009**, in press.
(23) Applegarth, L.; Clark, N.; Richardson, A. C.; Parker, A. D. M.; Radosavljevic-Evans, I.; Goeta, A. E.; Howard, J. A. K.; Steed, J. W. *Chem. Commun.* **2005**, 5423-5425.
(24) Piepenbrock, M.-O. M.; Clarke, N.; Steed, J. W. *Langmuir* **2009**, *25*, 8451-8456.
(25) Kumar, D. K.; Jose, D. A.; Das, A.; Dastidar, P. *Chem. Commun.* **2005**, 4059-4061.
(26) Kumar, D. K.; Jose, D. A.; Dastidar, P.; Das, A. *Chem. Mat.* **2004**, *16*, 2332-2335.
(27) Hafkamp, R. J. H.; Kokke, B. P. A.; Danke, I. M.; Geurts, H. P. M.; Rowan, A. E.; Feiters, M. C.; Nolte, R. J. M. *Chem. Commun.* **1997**, 545-546.
(28) Xing, B. G.; Choi, M. F.; Xu, B. *Chem. Commun.* **2002**, 362-363.
(29) Xing, B. G.; Choi, M. F.; Xu, B. *Chem. Eur. J.* **2002**, *8*, 5028-5032.
(30) Liu, Y. R.; He, L. S.; Zhang, J. Y.; Wang, X. B.; Su, C. Y. *Chem. Mater.* **2009**, *21*, 557-563.
(31) Liu, Q. T.; Wang, Y. L.; Li, W.; Wu, L. X. *Langmuir* **2007**, *23*, 8217-8223.
(32) Kim, H. J.; Zin, W. C.; Lee, M. *J. Am. Chem. Soc.* **2004**, *126*, 7009-7014.
(33) Kim, H. J.; Jung, E. Y.; Jin, L. Y.; Lee, M. *Macromolecules* **2008**, *41*, 6066-6072.
(34) Kawano, S. I.; Fujita, N.; van Bommel, K. J. C.; Shinkai, S. *Chem. Lett.* **2003**, *32*, 12-13.
(35) Westcott, A.; Sumby, C. J.; Walshaw, R. D.; Hardie, M. J. *New J. Chem.* **2009**, *33*, 902-912.
(36) Miravet, J. F.; Escuder, B. *Chem. Commun.* **2005**, 5796-5798.
(37) Arai, S.; Imazu, K.; Kusuda, S.; Yoshihama, I.; Tonegawa, M.; Nishimura, Y.; Kitahara, K.; Oishi, S.; Takemura, T. *Chem. Lett.* **2006**, *35*, 634-635.
(38) Smith, P. J.; Reddington, M. V.; Wilcox, C. S. *Tetrahedron Lett.* **1992**, *33*, 6085-6088.
(39) Nishizawa, S.; Buhlmann, P.; Iwao, M.; Umezawa, Y. *Tetrahedron Lett.* **1995**, *36*, 6483-6486.
(40) Fages, F.; Vögtle, F.; Žinić, M. *Top. Curr. Chem.* **2005**, *256*, 77-131.
(41) Yamanaka, M.; Nakagawa, T.; Aoyama, R.; Nakamura, T. *Tetrahedron* **2008**, *64*, 11558–11567.
(42) Estroff, L. A.; Hamilton, A. D. *Angew. Chem. Int. Ed.* **2000**, *39*, 3447-3450.
(43) van Esch, J.; Schoonbeek, F.; de Loos, M.; Kooijman, H.; Spek, A. L.; Kellogg, R. M.; Feringa, B. L. *Chem. Eur. J.* **1999**, *5*, 937-950.

(44) de Loos, M.; van Esch, J.; Kellogg, R. M.; Feringa, B. L. *Angew. Chem. Int. Ed.* **2001**, *40*, 613-616.
(45) Maeda, H. *Chem. Eur. J.* **2008**, *14*, 11274-11282.
(46) Lloyd, G. O.; Steed, J. W. *Nat. Chem.* **2009**, *1*, 437-442.
(47) Graubaum, H. *J. Prakt. Chem.-Chem. Ztg.* **1993**, *335*, 585-588.
(48) Pask, C. M.; Camm, K. D.; Kilner, C. A.; Halcrow, M. A. *Tetrahedron Lett.* **2006**, *47*, 2531-2534.
(49) Vogel, A.; Troxler, F. *Helv. Chim. Acta* **1975**, *58*, 761-771.
(50) Kaftory, M.; Botoshansky, M.; Sheinin, Y. *Cryst. Growth Des.* **2005**, *5*, 2242-2247.
(51) Dastidar, P. *Chem. Soc. Rev.* **2008**, *37*, 2699-2715.
(52) de Loos, M.; Feringa, B. L.; van Esch, J. H. *Eur. J. Org. Chem.* **2005**, 3615-3631.
(53) Elghandour, A. H. H.; Ramiz, M. M. M.; Ibrahim, M. K. A.; Elmoghayar, M. R. H. *Org. Prep. Proced. Int.* **1989**, *21*, 479-484.
(54) Vicentini, C. B.; Mares, D.; Tartari, A.; Manfrini, M.; Forlani, G. *J. Agric. Food Chem.* **2004**, *52*, 1898-1906.
(55) Insuasty, H.; Estrada, M.; Cortes, E.; Quiroga, J.; Insusasty, B.; Abonia, R.; Nogueras, M.; Cobo, J. *Tetrahedron Lett.* **2006**, *47*, 5441-5443.
(56) Lenthall, J. T.; Anderson, K. M.; Smith, S. J.; Steed, J. W. *Cryst. Growth Des.* **2007**, *7*, 1858-1862.
(57) Kelman, D. R.; Claborn, K. A.; Kaminsky, W.; Goldberg, K. I.; West, D. X. *J. Mol. Struct.* **2002**, *642*, 119-127.
(58) Kelman, D. R.; Claborn, K. A.; Kaminsky, W.; Goldberg, K. I.; Li, D. T.; West, D. X. *J. Mol. Struct.* **2003**, *654*, 145-152.
(59) Kelman, D. R.; Szczepura, L. F.; Goldberg, K. I.; Kaminsky, W.; Hermetet, A. K.; Ackerman, L. J.; Swearingen, J. K.; West, D. X. *J. Mol. Struct.* **2002**, *610*, 143-150.
(60) Valdes-Martinez, J.; Hernandez-Ortega, S.; Hermetet, A. K.; Ackerman, L. J.; Presto, C. A.; Swearingen, J. K.; Kelman, D. R.; Goldberg, K. I.; Kaminsky, W.; West, D. X. *J. Chem. Crystallogr.* **2002**, *32*, 431-438.
(61) Kaminsky, W.; Kelman, D. R.; Giesen, J. M.; Goldberg, K. I.; Claborn, K. A.; Szczepura, L. F.; West, D. X. *J. Mol. Struct.* **2002**, *616*, 79-89.
(62) Giesen, J. M.; Claborn, K. A.; Goldberg, K. I.; Kaminsky, W.; West, D. X. *J. Mol. Struct.* **2002**, *613*, 223-233.
(63) Hermetet, A. K.; Ackerman, L. J.; Swearingen, J. K.; Presto, C. A.; Kelman, D. R.; Giesen, J. M.; Goldberg, K. I.; Kaminsky, W.; West, D. X. *J. Chem. Crystallogr.* **2002**, *32*, 17-25.
(64) Hermetet, A. K.; Ackerman, L. J.; Eilts, K. K.; Johnson, T. K.; Swearingen, J. K.; Giesen, J. M.; Goldberg, K. I.; Kaminsky, W.; West, D. X. *J. Mol. Struct.* **2002**, *605*, 241-247.
(65) Kaminsky, W.; Goldberg, K. I.; West, D. X. *J. Mol. Struct.* **2002**, *605*, 9-15.
(66) Szczepura, L. F.; Kelman, D. R.; Hermetet, A. K.; Ackerman, L. J.; Goldberg, K. I.; Claborn, K. A.; Kaminsky, W.; West, D. X. *J. Mol. Struct.* **2002**, *608*, 245-251.
(67) Valdes-Martinez, J.; Hernandez-Ortega, S.; Espinosa-Perez, G.; Presto, C. A.; Hermetet, A. K.; Haslow, K. D.; Ackerman, L. J.; Szczepura, L. F.; Goldberg, K. I.; Kaminsky, W.; West, D. X. *J. Mol. Struct.* **2002**, *608*, 77-87.
(68) Lu, Y. S.; Kraatz, H. B. *Inorg. Chim. Acta* **2004**, *357*, 159-166.
(69) Bagley, M. C.; Davis, T.; Dix, M. C.; Widdowson, C. S.; Kipling, D. *Org. Biomol. Chem.* **2006**, *4*, 4158-4164.
(70) Orsini, P.; Traquandi, G.; Sansonna, P.; Pevarello, P. *Tetrahedron Lett.* **2005**, *46*, 933-935.
(71) Pevarello, P.; Brasca, M. G.; Amici, R.; Orsini, P.; Traquandi, G.; Corti, L.; Piutti, C.; Sansonna, P.; Villa, M.; Pierce, B. S.; Pulici, M.; Giordano, P.; Martina, K.; Fritzen, E. L.; Nugent, R. A.; Casale, E.; Cameron, A.; Ciomei, M.; Roletto, F.; Isacchi, A.; Fogliatto, G.; Pesenti, E.; Pastori, W.; Marsiglio, A.; Leach, K. L.; Clare, P. M.; Fiorentini, F.; Varasi, M.; Vulpetti, A.; Warpehoski, M. A. *J. Med. Chem.* **2004**, *47*, 3367-3380.
(72) Lu, Y. S.; Kraatz, H. B. *Inorg. Chem. Commun.* **2003**, *6*, 666-669.
(73) Liu, Y. N.; Orlowski, G.; Schatte, G.; Kraatz, H. B. *Inorg. Chim. Acta* **2005**, *358*, 1151-1161.
(74) Rzepecki, P.; Hochdorffer, K.; Schaller, T.; Zienau, J.; Harms, K.; Ochsenfeld, C.; Xie, X.; Schrader, T. *J. Am. Chem. Soc.* **2008**, *130*, 586-591.
(75) Seelen, W.; Schafer, M.; Ernst, A. *Tetrahedron Lett.* **2003**, *44*, 4491-4493.
(76) Steed, J. W. *CrystEngComm* **2003**, 169-179.

(77) Corbin, P. S.; Zimmerman, S. C.; Thiessen, P. A.; Hawryluk, N. A.; Murray, T. J. *J. Am. Chem. Soc.* **2001**, *123*, 10475-10488.
(78) Tiliakos, M.; Cordopatis, P.; Terzis, A.; Raptopoulou, C. P.; Perlepes, S. P.; Manessi-Zoupa, E. *Polyhedron* **2001**, *20*, 2203-2214.
(79) Fares, V.; Flamini, A.; Pasetto, P. *J. Chem. Soc. Perkin Trans. 1* **2000**, 4520-4525.
(80) Corbin, P. S.; Zimmerman, S. C. *J. Am. Chem. Soc.* **2000**, *122*, 3779-3780.
(81) Sheldrick, G. M. In *SHELXL-97* University of Göttingen, 1997.
(82) Nangia, A. *Acc. Chem. Res.* **2008**, *41*, 595-604.
(83) Dunitz, J. D.; Bernstein, J. *Acc. Chem. Res.* **1995**, *28*, 193-200.
(84) Rodriguez-Spong, B.; Price, C. P.; Jayasankar, A.; Matzger, A. J.; Rodriguez-Hornedo, N. *Adv. Drug Deliv. Rev.* **2004**, *56*, 241-274.
(85) Bernstein, J. *Chem. Commun.* **2005**, 5007-5012.
(86) Byrne, P.; Turner, D. R.; Lloyd, G. O.; Clarke, N.; Steed, J. W. *Cryst. Growth Des.* **2008**, *8*, 3335-3344.
(87) Smithson, R. J.; Kilner, C. A.; Brough, A. R.; Halcrow, M. A. *Polyhedron* **2003**, *22*, 725-733.
(88) Bushuev, M. B.; Virovets, A. V.; Garcia, Y.; Gieck, C.; Sheludyakova, L. A.; Ikorskii, V. N.; Tremel, W.; Gutlich, P.; Lavrenova, L. G. *Polyhedron* **2002**, *21*, 797-804.
(89) Cingi, M. B.; Lanfranchi, M.; Lanfredi, A. M. M.; Ferrer, S.; Haasnoot, J. G.; Reedijk, J. *Inorg. Chim. Acta* **1993**, *209*, 219-223.
(90) Piepenbrock, M. O. M.; Anderson, K. M.; Sansam, B. C. R.; Clarke, N.; Steed, J. W. *CrystEngComm* **2009**, *11*, 118-121.
(91) Kyriakidou, F.; Panagiotopoulos, A.; Perlepes, S. P.; ManessiZoupa, E.; Raptopoulou, C. P.; Terzis, A. *Polyhedron* **1996**, *15*, 1031-1034.
(92) Armstrong, C. M.; Bernhardt, P. V.; Chin, P.; Richardson, D. R. *Eur. J. Inorg. Chem.* **2003**, 1145-1156.
(93) Dawe, L. N.; Abedin, T. S. M.; Kelly, T. L.; Thompson, L. K.; Miller, D. O.; Zhao, L.; Wilson, C.; Leech, M. A.; Howard, J. A. K. *J. Mater. Chem.* **2006**, *16*, 2645-2659.
(94) Dey, S. K.; Thompson, L. K.; Dawe, L. N. *Chem. Commun.* **2006**, 4967-4969.
(95) Milway, V. A.; Abedin, S. M. T.; Niel, V.; Kelly, T. L.; Dawe, L. N.; Dey, S. K.; Thompson, D. W.; Miller, D. O.; Alam, M. S.; Muller, P.; Thompson, L. K. *Dalton Trans.* **2006**, 2835-2851.
(96) Das, S.; Maloor, S. A.; Pal, S. *Cryst. Growth Des.* **2006**, *6*, 2103-2108.
(97) Onions, S. T.; Frankin, A. M.; Horton, P. N.; Hursthouse, M. B.; Matthews, C. J. *Chem. Commun.* **2003**, 2864-2865.
(98) Onions, S. T.; Heath, S. L.; Price, D. J.; Harrington, R. W.; Clegg, W.; Matthews, C. J. *Angew. Chem. Int. Ed.* **2004**, *43*, 1814-1817.
(99) Matthews, C. J.; Onions, S. T.; Morata, G.; Salvia, M. B.; Elsegood, M. R. J.; Price, D. J. *Chem. Commun.* **2003**, 320-321.
(100) Dey, S. K.; Bag, B.; Malik, K. M. A.; El Fallah, M. S.; Ribas, J.; Mitra, S. *Inorg. Chem.* **2003**, *42*, 4029-4035.
(101) Wang, X. B.; Vittal, J. J. *Inorg. Chem.* **2003**, *42*, 5135-5142.
(102) Colacio, E.; Ghazi, M.; Kivekas, R.; Moreno, J. M. *Inorg. Chem.* **2000**, *39*, 2882-2890.
(103) Brook, D. J. R.; Fornell, S.; Stevens, J. E.; Noll, B.; Koch, T. H.; Eisfeld, W. *Inorg. Chem.* **2000**, *39*, 562-567.
(104) Vankoningsbruggen, P. J.; Haasnoot, J. G.; Degraaff, R. A. G.; Reedijk, J. *Inorg. Chim. Acta* **1995**, *234*, 87-94.
(105) Ali, M. A.; Mirza, A. H.; Ravoof, T.; Bernhardt, P. V. *Polyhedron* **2004**, *23*, 2031-2036.
(106) Thompson, L. K.; Matthews, C. J.; Zhao, L.; Xu, Z. Q.; Miller, D. O.; Wilson, C.; Leech, M. A.; Howard, J. A. K.; Heath, S. L.; Whittaker, A. G.; Winpenny, R. E. P. *J. Solid State Chem.* **2001**, *159*, 308-320.
(107) Sangeetha, N. R.; Pal, S. *Polyhedron* **2000**, *19*, 1593-1600.
(108) Majumder, A.; Rosair, G. M.; Mallick, A.; Chattopadhyay, N.; Mitra, S. *Polyhedron* **2006**, *25*, 1753-1762.
(109) Filipovic, N. R.; Bacchi, A.; Lazic, M.; Pelizzi, G.; Radulovic, S.; Sladic, D. M.; Todorovic, T. R.; Andelkovic, K. K. *Inorg. Chem. Commun.* **2008**, *11*, 47-50.
(110) Epstein, D. M.; Choudhary, S.; Churchill, M. R.; Keil, K. M.; Eliseev, A. V.; Morrow, J. R. *Inorg. Chem.* **2001**, *40*, 1591-1596.

(111) Basu, T.; Sparkes, H. A.; Bhunia, M. K.; Mondal, R. *Cryst. Growth Des.* **2009**, *9*, 3488-3496.
(112) O'Brien, A. Y.; Hitzbleck, J.; Torvisco, A.; Deacon, G. B.; Ruhlandt-Senge, K. *Eur. J. Inorg. Chem.* **2008**, 172-182.
(113) Omary, M. A.; Elbjeirami, O.; Gamage, C. S. P.; Sherman, K. M.; Dias, H. V. R. *Inorg. Chem.* **2009**, *48*, 1784-1786.
(114) Saeed, I.; Katao, S.; Nomura, K. *Inorg. Chem.* **2009**, *48*, 5011-5020.
(115) Kaden, T. A. *Coord. Chem. Rev.* **1998**, *192*, 371-389.
(116) Gust, K. R.; Knox, J. E.; Heeg, M. J.; Schlegel, H. B.; Winter, C. H. *Eur. J. Inorg. Chem.* **2002**, 2327-2334.
(117) Gust, K. R.; Knox, J. E.; Heeg, M. J.; Schlegel, H. B.; Winter, C. H. *Angew. Chem. Int. Ed.* **2002**, *41*, 1591-1594.
(118) Addison, A. W.; Burke, P. J. *J. Heterocycl. Chem.* **1981**, *18*, 803-805.
(119) Deacon, G. B.; Delbridge, E. E.; Forsyth, C. M.; Junk, P. C.; Skelton, B. W.; White, A. H. *Aust. J. Chem.* **1999**, *52*, 733-739.
(120) Mosch-Zanetti, N. C.; Kratzner, R.; Lehmann, C.; Schneider, T. R.; Uson, I. *Eur. J. Inorg. Chem.* **2000**, 13-16.
(121) Beaini, S.; Deacon, G. B.; Delbridge, E. E.; Junk, P. C.; Skelton, B. W.; White, A. H. *Eur. J. Inorg. Chem.* **2008**, 4586-4596.
(122) Beaini, S.; Deacon, G. B.; Erven, A. P.; Junk, P. C.; Turner, D. R. *Chem.-Asian J.* **2007**, *2*, 539-550.
(123) Deacon, G. B.; Forsyth, C. M.; Gitlits, A.; Harika, R.; Junk, P. C.; Skelton, B. W.; White, A. H. *Angew. Chem. Int. Ed.* **2002**, *41*, 3249-3251.
(124) Deacon, G. B.; Delbridge, E. E.; Evans, D. J.; Harika, R.; Junk, P. C.; Skelton, B. W.; White, A. H. *Chem. Eur. J.* **2004**, *10*, 1193-1204.
(125) Krummenacher, I.; Fernandez, I.; Ruegger, H.; Weigend, F.; Breher, F. *Dalton Trans.* **2009**, 5335-5347.
(126) Deacon, G. B.; Fallon, G. D.; Forsyth, C. M.; Harris, S. C.; Junk, P. C.; Skelton, B. W.; White, A. H. *Dalton Trans.* **2006**, 802-812.
(127) Cole, M. L.; Junk, P. C. *New J. Chem.* **2005**, *29*, 135-140.
(128) Dagorne, S.; Atwood, D. A. *Chem. Rev.* **2008**, *108*, 4037-4071.
(129) Alcantara-Garcia, J.; Jancik, V.; Barroso, J.; Hidalgo-Bonilla, S.; Cea-Olivares, R.; Toscano, R. A.; Moya-Cabrera, M. *Inorg. Chem.* **2009**, *48*, 5874-5883.
(130) Sheldrick, G. M. *Acta Crystallogr. Sect. A* **2008**, *64*, 112-122.
(131) *CSD, version 1.11, May 2009 update*; Cambridge Crsytallographic Data Centre.
(132) Yu, Z. K.; Wittbrodt, J. M.; Xia, A. B.; Heeg, M. J.; Schlegel, H. B.; Winter, C. H. *Organometallics* **2001**, *20*, 4301-4303.
(133) Zheng, W. J.; Mosch-Zanetti, N. C.; Roesky, H. W.; Noltemeyer, M.; Hewitt, M.; Schmidt, H. G.; Schneider, T. R. *Angew. Chem. Int. Ed.* **2000**, *39*, 4276-4279.
(134) Zheng, W. J.; Roesky, H. W.; Noltemeyer, M. *Organometallics* **2001**, *20*, 1033-1035.
(135) Uhl, W. *Coord. Chem. Rev.* **1997**, *163*, 1-32.
(136) Uhl, W.; Vester, A.; Fenske, D.; Baum, G. *J. Organomet. Chem.* **1994**, *464*, 23-34.
(137) Wong, W. K.; Zhang, L.; Xue, F.; Mak, T. C. W. *J. Chem. Soc., Dalton Trans.* **1999**, 3053-3062.
(138) Ecker, A.; Koppe, R.; Uffing, C.; Schnockel, H. *Z. Anorg. Allg. Chem.* **1998**, *624*, 817-822.
(139) Westerhausen, M.; Birg, C.; Noth, H.; Knizek, J.; Seifert, T. *Eur. J. Inorg. Chem.* **1999**, 2209-2214.
(140) Britnell, D.; Drew, M. G. B.; Fowles, G. W. A.; Rice, D. A. *Inorg. Nucl. Chem Lett.* **1973**, *9*, 415-417.
(141) Deacon, G. B.; Junk, P. C.; Moxey, G. J. *Z. Anorg. Allg. Chem.* **2008**, *634*, 2789-2792.
(142) Anderson, K. M.; Probert, M. R.; Whiteley, C. N.; Rowland, A. M.; Goeta, A. E.; Steed, J. W. *Cryst. Growth Des.* **2009**, *9*, 1082-1087.
(143) Anderson, K. M.; Goeta, A. E.; Steed, J. W. *Cryst. Growth Des.* **2008**, *8*, 2517-2524.
(144) Anderson, K. M.; Steed, J. W. *CrystEngComm* **2007**, *9*, 328-330.
(145) Desiraju, G. R. *CrystEngComm* **2007**, *9*, 91-92.
(146) Frassineti, C.; Ghelli, S.; Gans, P.; Sabatini, A.; Moruzzi, M. S.; Vacca, A. *Anal. Biochem.* **1995**, *231*, 374-382.
(147) Gans, P.; HypNMR 2006, University of Leeds: Leeds, 2006.

(148) Beer, P. D.; Drew, M. G. B.; Smith, D. K. *J. Organomet. Chem.* **1997**, *543*, 259-261.
(149) Blow, D. M.; Rich, A. *J. Am. Chem. Soc.* **1960**, *82*, 3566-3571.
(150) Müller, W. M.; Müller, U.; Mieden-Gundert, G.; Vögtle, F.; Lescanne, M.; Heuzé, K.; D'Aléo, A.; Fages, F. *Eur. J. Org. Chem.* **2002**, 2891-2893.
(151) Yang, Z. M.; Gu, H. W.; Zhang, Y.; Wang, L.; Xu, B. *Chem. Commun.* **2004**, 208-209.
(152) Suzuki, M.; Yumoto, M.; Shirai, H.; Hanabusa, K. *Org. Biomol. Chem.* **2005**, *3*, 3073-3078.
(153) Lee, D. C.; McGrath, K. K.; Jang, K. *Chem. Commun.* **2008**, 3636-3638.
(154) Rodríguez-Llansola, F.; Escuder, B.; Miravet, J. F. *Org. Biomol. Chem.* **2009**, *7*, 3091-3094.
(155) Panda, J. J.; Mishra, A.; Basu, A.; Chauhan, V. S. *Biomacromolecules* **2008**, *9*, 2244-2250.
(156) Tsekova, D. S.; Escuder, B.; Miravet, J. F. *Cryst. Growth Des.* **2008**, *8*, 11–13.
(157) Kim, T. H.; Seo, J.; Lee, S. J.; Lee, S. S.; Kim, J.; Jung, J. H. *Chem. Mat.* **2007**, *19*, 5815-5817.
(158) Chung, J. W.; An, B. K.; Park, S. Y. *Chem. Mat.* **2008**, *20*, 6750-6755.
(159) Hwang, I.; Jeon, W. S.; Kim, H. J.; Kim, D.; Kim, H.; Selvapalam, N.; Fujita, N.; Shinkai, S.; Kim, K. *Angew. Chem. Int. Ed.* **2007**, *46*, 210-213.
(160) Velázquez, D. G.; Díaz, D. D.; Ravelo, A. G.; Tellado, J. J. M. *J. Am. Chem. Soc.* **2008**, *130*, 7967-7973.
(161) Komatsu, H.; Matsumoto, S.; Tamaru, S.; Kaneko, K.; Ikeda, M.; Hamachi, I. *J. Am. Chem. Soc.* **2009**, *131*, 5580-5585.
(162) Srivastava, A.; Ghorai, S.; Bhattacharjya, A.; Bhattacharya, S. *J. Org. Chem.* **2005**, *70*, 6574-6582.
(163) Shome, A.; Debnath, S.; Das, P. K. *Langmuir* **2008**, *24*, 4280-4288.
(164) Kar, T.; Debnath, S.; Das, D.; Shome, A.; Das, P. K. *Langmuir* **2009**, *25*, 8639-8648.
(165) Kiyonaka, S.; Zhou, S. L.; Hamachi, I. *Supramol. Chem.* **2003**, *15*, 521-528.
(166) Zhou, S. L.; Matsumoto, S.; Tian, H. D.; Yamane, H.; Ojida, A.; Kiyonaka, S.; Hamachi, I. *Chem. Eur. J.* **2005**, *11*, 1130-1136.
(167) van Bommel, K. J. C.; van der Pol, C.; Muizebelt, I.; Friggeri, A.; Heeres, A.; Meetsma, A.; Feringa, B. L.; van Esch, J. *Angew. Chem., Int. Ed.* **2004**, *43*, 1663-1667.
(168) Kiyonaka, S.; Shinkai, S.; Hamachi, H. *Chem. Eur. J.* **2003**, *9*, 976-983.
(169) Roubeau, O.; Colin, A.; Schmitt, W.; Clérac, R. *Angew. Chem. Int. Ed.* **2004**, *43*, 3283-3286.
(170) Wang, Y. J.; Tang, L. M.; Yu, J. *Cryst. Growth Des.* **2008**, *8*, 884-889.
(171) Hanabusa, K.; Hiratsuka, K.; Kimura, M.; Shirai, H. *Chem. Mat.* **1999**, *11*, 649-655.
(172) Cravotto, G.; Cintas, P. *Chem. Soc. Rev.* **2009**, *38*, 2684-2697.
(173) Terech, P.; Pasquier, D.; Bordas, V.; Rossat, C. *Langmuir* **2000**, *16*, 4485-4494.
(174) Li, J. L.; Liu, X. Y.; Wang, R. Y.; Xiong, J. Y. *J. Phys. Chem. B* **2005**, *109*, 24231-24235.
(175) Brinksma, J.; Feringa, B. L.; Kellogg, R. M.; Vreeker, R.; van Esch, J. *Langmuir* **2000**, *16*, 9249-9255.
(176) Terech, P.; Friol, S. *Tetrahedron* **2007**, *63*, 7366-7374.
(177) Menger, F. M.; Caran, K. L. *J. Am. Chem. Soc.* **2000**, *122*, 11679-11691.
(178) Terech, P.; Rossat, C.; Volino, F. *J. Coll. Interface Sci.* **2000**, *227*, 363-370.
(179) Larson, R. G. *The Structure and Rheology of Complex Fluids*; Oxford University Press: Oxford, 1999.
(180) Sangeetha, N. M.; Bhat, S.; Choudhury, A. R.; Maitra, U.; Terech, P. *J. Phys. Chem. B* **2004**, *108*, 16056-16063.
(181) Shih, W. H.; Shih, W. Y.; Kim, S. I.; Liu, J.; Aksay, I. A. *Phys. Rev. A* **1990**, *42*, 4772-4779.
(182) Gibson, L. J.; Ashby, M. F. *Proc. Roy. Soc. London Ser. A* **1982**, *382*, 43-59.
(183) Buxton, G. A.; Clarke, N. *Phys. Rev. Lett.* **2007**, *98*, 23-26.
(184) Ahn, C. C.; Krivanek, O. L. *EELS Atlas*; Gatan Inc.: Warendale, USA, 1983.
(185) Wang, J. Z.; Loh, K. P.; Wang, Z.; Yan, Y. L.; Zhong, Y. L.; Xu, Q. H.; Ho, P. C. *Angew. Chem. Int. Ed.* **2009**, *48*, 6282-6285.
(186) Wang, Y. L.; Li, W.; Wu, L. *Langmuir* **2009**, *25*, 13194-13200.
(187) Bag, S.; Trikalitis, P. N.; Chupas, P. J.; Armatas, G. S.; Kanatzidis, M. G. *Science* **2007**, *317*, 490-493.
(188) Desiraju, G. R. *CrystEngComm* **2003**, *5*, 466-467.
(189) Dunitz, J. D. *CrystEngComm* **2003**, *5*, 506-506.
(190) Aakeroy, C. B.; Salmon, D. J. *CrystEngComm* **2005**, *7*, 439-448.
(191) Zaworotko, M. J. *Cryst. Growth Des.* **2007**, *7*, 4-9.

(192) Bond, A. D. *CrystEngComm* **2007**, *9*, 833-834.
(193) Estroff, L. A.; Hamilton, A. D. *Chem. Rev.* **2004**, *104*, 1201-1217.
(194) Moffat, J. R.; Smith, D. K. *Chem. Commun.* **2008**, 2248-2250.
(195) Turner, D. R.; Spencer, E. C.; Howard, J. A. K.; Tocher, D. A.; Steed, J. W. *Chem. Commun.* **2004**, 1352-1353.
(196) Bernstein, J.; Davis, R. E.; Shimoni, L.; Chang, N.-L. *Angew. Chem. Int. Ed. Engl.* **1995**, *34*, 1555-1573.
(197) Hirst, A. R.; Escuder, B.; Miravet, J. F.; Smith, D. K. *Angew. Chem. Int. Ed.* **2008**, *47*, 8002-8018.
(198) Terech, P.; Weiss, R. G. *Chem. Rev.* **1997**, *97*, 3133-3159.
(199) Ishi-i, T.; Shinkai, S. In *Supermolecular Dye Chemistry*; Springer-Verlag Berlin: Berlin, 2005; Vol. 258, p 119-160.
(200) van Esch, J. H.; Feringa, B. L. *Angew. Chem. Int. Ed.* **2000**, *39*, 2263-2266.
(201) Sangeetha, N. M.; Maitra, U. *Chem. Soc. Rev.* **2005**, *34*, 821-836.
(202) Weiss, R. G.; Terech, P. *Molecular Gels: Materials with Self-Assembled Fibrillar Networks*; Kluwer Academic Publishers: Dordrecht, 2005.
(203) Henstock, H. *J. Am. Chem. Soc.* **1939**, *61*, 670–673.
(204) Abdallah, D. J.; Weiss, R. G. *Chem. Mater.* **2000**, *12*, 406-413.
(205) Trivedi, D. R.; Dastidar, P. *Cryst. Growth Des.* **2006**, *6*, 2114-2121.
(206) Eds. Kanz, W. L. N., P.; Ninham, B. W. *Curr. Opin. Colloid Interface Sci.* **2004**, *9*, 1-197.
(207) Becker, T.; Goh, C. Y.; Jones, F.; McIldowie, M. J.; Mocerino, M.; Ogden, M. I. *Chem. Commun.* **2008**, 3900-3902.

Chapter 4

Future Work

4.1 Chiral bisurea LMWGs

A full characterisation of the rheological properties and morphologies of the gels of the chiral bisurea LMWGs was not carried out when the solvent or solvent mixtures were varied. It would be of interest to determine the changes that occur when moving from apolar to polar solvents, if any. This is especially true when it comes to elucidating the mechanism behind the thixotropic character of gels formed by **2.2**.[1] Connected to this is the use of environmental SEM imaging of the gels. As shown, the TEM, SEM and cryo-SEM techniques give different points of view of the gel morphology. The non-drying conditions, in which the imaging is performed within the environmental SEM technique, should lead to a more representative image of the gel morphology. Characterisation of the behaviour of the molecules prior to nucleation and gel formation was not performed and would be desirable. Studies utilising small and wide angle x-ray or neutron scattering, static light scattering, NMR and vapour pressure osmometry experiments on the chiral bisurea compounds, would provide insights into the behaviour of the compounds prior to gel formation.[2] A key experimental technique not utilised in this study was circular dichroism.[3-5] Due to the chirality of the compounds, useful structural information of the gel could be highlighted by using this technique.

Crystal growth within the gel milieu of a LMWG was attempted within the study. From the results found and presented within this thesis, it can be concluded that there is great room for further studies to be performed using a greater range of LWMGs, solvents and crystal forming compounds. One obvious study that could easily be done, and that has high scientific interest, is the crystallisation of calcium carbonate (bio-mineralisation) within LMWGs.[6,7]

The drug delivery studies could be extended to other drugs and other LMWGs other than compound **2.1a**. Further experiments are certainly needed to elucidate the potential of the gels to control drug release both *in vivo* and *in vitro*. The initial investigations described in this thesis revealed an intriguing mechanism of drug release, and this could be further studied by utilising diffusion probing methods such as NMR-DOSY experiments and neutron scattering.

4.2 Pyrazole LMWGs

The coordination chemistry of the pyrazole ureas was investigated with moderate success. Further studies utilising softer metals like Hg and Ag could have been done, especially considering that the mixtures of compound **3.10** and Ag salts formed gel-like precipitates (partial gels). The synthesis of pyrazole urea analogues to the gel forming pyridyl ureas was unsuccessfully attempted within this study, but could be yet be made to succeed. Very little synthetic variation was made to the gel-forming pyrazole ureas utilised in this study. Simple modifications, such as the position of the nitro group on the phenyl group, indeed, even the full removal of the group, could lead to further understanding of the aggregation phenomena of the gel forming compound **3.10**.

Complete x-ray diffraction characterisation of all the different crystalline **3.10H$^+$** materials produced would be advantageous, in order to give a complete understanding of why these compounds showed anion-dependent rheologies and morphologies. The difficulty of producing single crystals could be circumvented by solving the structures from powder x-ray diffraction data.[8] The visually determined colour differences between the gels of **3.10H$^+$** could easily be quantified using solid-state reflection UV spectroscopy. This would give structural details of the **3.10H$^+$** molecules within the gel fibres, especially, if the UV results are coupled with theoretical calculations. The gelation of water by the salts of **3.10H$^+$** reveals that this pyrazole urea class of compounds can, indeed, form gels. The extension of the gel formation within other solvents was only briefly explored and is, therefore, a study that could be expanded.

References

1. Lescanne, M.; Grondin, P.; d'Aléo, A.; Fages F.; Pozzo, J.-L.; Mondain Monval, O.; Reinheimer, P.; Colin, A. *Langmuir* **2004**, *20*, 3032-3041.

2. Liu, X. Y. In *Low Molecular Mass Gelators: Design, Self-Assembly, Function*; Springer-Verlag Berlin: Berlin, 2005; Vol. 256, p 1-37.
3. Smith, D. K. *Chem. Soc. Rev.* **2009**, *38*, 684-694.
4. Brizard, A.; Oda, R.; Huc, I. In *Low Molecular Mass Gelators: Design, Self-Assembly, Function*; Springer-Verlag Berlin: Berlin, 2005; Vol. 256, p 167-218.
5. Palmans, A. R. A.; Meijer, E. W. *Angew. Chem., Int. Ed.* **2007**, *46*, 8948-8968.
6. Dey, A.; de With G.; Sommerdijk, N. A. J. M. *Chem. Soc. Rev.* **2010**, *39*, 397-409.
7. Petrova, R. I.; Patel, R. Swift, J. A. *Cryst. Growth Des.* **2006**, *6*, 2709-2715.
8. Anderson, K. M.; Day, G. M.; Paterson M. J.; Byrne, P.; Clarke, N; Steed, J. W. *Angew. Chem. Int. Ed.* **2008**, *47*, 1058-1062.

List of publications from this work

M. O. M. Piepenbrock, **Gareth O. Lloyd**, Nigel Clarke, Jonathan W. Steed, Gelation is crucially dependent on functional group orientation and may be tuned by anion binding, *Chem. Commun.*, **2008**, 2644-2645.

Gareth O. Lloyd and Jonathan W. Steed, Anion-tuning of supramolecular gel properties, *Nature Chem.*, **2009**, *1*, 437-442.

M. O. M. Piepenbrock, **Gareth O. Lloyd**, Nigel Clarke, Jonathan W. Steed, Metal- and Anion-Binding Supramolecular Gels, *Chem. Rev.*, **2010**, in press.

Gareth O. Lloyd, Jacinta Bakker, Leonard J. Barbour, Glen B. Deacon, Jonathan W. Steed and Peter C. Junk, Redox Transmetallation/Ligand Exchange Reactions with Aluminium and 3,5-Di-*tert*-butylpyrazole, Chem*. An Asian J.*, **2010**, submitted.

Appendix A - Equipment Experimental

NMR

^{1}H and ^{13}C NMR spectra were run at room temperature using one of the following machines, Bruker Avance-400 spectrometer, Varian Mercury-400 spectrometer and Varian Inova-500 spectrometer operating at 400 MHz, 400 MHz and 500 MHz, respectively (Durham) or Bruker AM300 spectrometer operating at 300 MHz (Monash) for ^{1}H NMR. Chemical shifts are reported in parts per million (δ) relative to the residual protic solvent as an internal reference. Coupling constants (*J*) are reported in Hertz (Hz). ^{27}Al chemical shifts reported as parts per million (δ) relative to an external standard ($Al(NO_3)_3$, 0.67 M (aq), ^{27}Al $\delta = 0.0$).

NMR Titrations

^{1}H NMR titration experiments were carried out at room temperature using either a Varian Inova-500 spectrometer operating at 500 MHz or Varian Mercury-400 spectrometer operating at 400 MHz (Durham). All chemical shifts are reported in ppm relative to the residual protic solvent as an internal reference. A solution of the host species of known concentration, typically 0.02 M, was made up in an NMR tube using the appropriate deuterated solvent (0.5 ml). Solutions of the anions, as TBA^+ salts, were made up in volumetric flasks (2 ml) with a concentration five times greater than that of the host. The guest solution was typically added in 10 μl aliquots, representing 0.1 equivalents of the guest with respect to the host. Larger aliquots were used in some cases where no inflection of the trace was evident. Spectra were recorded after each addition and the trace followed. Results were analysed using the curve-fitting program HypNMR,[1,2] simultaneously fitting as many peaks as could be accurately followed throughout the experiment.

Elemental Analysis

Samples were run using an Exeter Analytical E-440 Elemental Analyser (Durham). Elemental analyses on compounds **3.13** and **3.14** were performed by The Campbell Microanalytical Laboratory, Chemistry Department, University of Otago, Dunedin, New

Zealand.

Mass Spectrometry

Compounds dissolved in an appropriate solvent were run using either a Thermoquest Trace machine or Thermo-Finnigan LTQ FT machine (Durham) running in positive or negative electrospray (ES) mode.

FT-IR

Fourier transform infrared spectra were recorded with a Perkin Elmer Spectrum 100 ATR instrument. For each spectrum of solid samples, 64 scans were conducted over a spectral range of 4000 to 600 cm^{-1} with a resolution of 4 cm^{-1}. The analyses were carried out with the Spectrum Express 1.01 software. FT-IR spectra for compounds **3.13** and **3.14** were obtained as nujol mulls with a Perkin Elmer 1600 FTIR instrument (Monash). Peak intensity described as strong (s), medium (m) or weak (w).

SEM

Samples were partially dried under room temperature and atmosphere, and then fully dried under high vacuum on a piece of silicon wafer. They were then coated with a thin layer of platinum of 3 – 5 nm using a 308UHR Ultra High Resolution Coating System. Samples were imaged using a S-5200 UHR FE-SEM Hitachi Scientific instrument. (Durham)

TEM

Samples were deposited onto a holey carbon grid and were immediately examined in a JEOL 2100F FEG TEM (Durham) operating at 200 kV. EELS spectra and EFTEM mapping were carried out using a Gatan GIF Tridiem (the energy resolution of the EELS spectra is approximately 1 eV).

Fluorescence

Samples were scanned in 1 ml glass vials using a Jobin-Yvon Horiba Fluorolog 3-222 Tau-3 Spectrofluorimeter with a front facing illumination method and were corrected for the spectral response of the machine (Durham).

Powder X-ray Diffraction

Samples were processed through a 100 μm microsieve and run on silica blank disks. Samples were run on a Bruker D500 (Durham).

Single Crystal Crystallography

Suitable single crystals were mounted using either silicon grease or perflouropolyether on a thin glass fibre. Crystallographic measurements were carried out using a Bruker SMART 6K (6000 CCD) (Durham) or a Bruker ApexII diffractometer (Monash) or Nonius Kappa CCD diffractometer (Monash). The instruments were equipped with a graphite monochromatic Mo-Kα radiation (γ = 0.71073). The standard data collection temperature was 120 K, maintained using an open flow N_2 Oxford Cryostream device. Integration was carried out using SAINT software. Data sets were corrected for Lorentz and polarization effects and for the effects of absorption. Structures were solved using direct methods in SHELXS-97[3] and developed using conventional alternating cycles of least-squares refinement with SHELXL-97[4] and difference Fourier synthesis with the aid of the graphical interface program X-Seed.[5,6] All non-hydrogen atoms were treated as anisotropic. In all cases hydrogen atoms were fixed in idealised positions and allowed to ride on the parent atom to which they were attached. Hydrogen atom thermal parameters were tied to those of the parent atom. Where possible N-H and O-H hydrogen atoms were located experimentally and their position and displacement parameters refined or their position parameters constrained to ideal distances from their parent atoms. Molecular graphics were produced using the program POV-ray.[7]

Rheometry

Rheology experiments were performed using a TA Instruments Advanced Rheometer 2000 (Durham). A cylindrical cup geometry was used for experiments run on gel samples of compounds **1.1a** and **1.2**. A parallel plate geometry (40 mm diameter) was used for experiments run on gel samples of compound **3.10**. All experiments were run at 20 ^{o}C. Frequency sweep measurements were performed over a range of 1 to 100 Hz with a constant ocs. torque value of 100 Nm. Stress sweep measurements were performed over an osc. torque range of 1 Nm to 20000 Nm with a constant frequency of 1 Hz. Time or temperature sweep measurements were performed at a constant ocs. torque value of 100 Nm and constant frequency value of 1 Hz.

A typical measurement performed by the rheometer was done by rotating the head group (the parallel plate or cylinder) at a specified rotation (frequency in Hz) and specified torque (in Nm). The torque was converted into "stress" (expressed in Pa) by taking into account the contact surface area between the sample and the instrument. Results in this work are presented as the instrument parameter. Osc. torque (Nm) was chosen rather than the "stress" (Pa) parameter, as the "stress" is dependent on the geometry used and the contact area between the sample and the instrument. Comparison of the data from plotting sample variables like G' and G'' against osc. torque or "stress" reveal no differences in the trends seen for all the gel samples tested.[8-10]

A typical experiment with the cylindrical cup geometry involved the following. A 10 ml gel sample in a sealed 15 ml screw cap vial was dissolved by heating (care must be taken when heating sealed vessels due to the build up of pressure). The head cylinder was lowered to a gap distance of 500 μm. The solution was transferred via a preheated syringe to the rheometer. The sample was allowed to equilibrate at a pre-determined temperature and the experiment was performed.

A typical experiment with the parallel plates involved removing the pre-formed gel with a small spatula and placing it uniformly on the stationary plate covering the entire contact surface area between the two plates. The rotating plate was lowered to a gap distance of 1 mm. Frequency and stress sweep measurements were then performed.

There are two errors to take into account in all measurements. The errors on the output parameters of the machine are considerably smaller than experimental errors produced from volume and weight measurements, due to high accuracy of the instrument. However, as each measurement is performed at a specific frequency and specific torque, if a transition of interest happens to occur between two specific measurements the accuracy of this point of interest can only be determined by how close the two measurements are. The average of the two measurements is taken as the value for the transition of interest and the systematic errors shown in figures as the standard deviation of the average between the two measurements. The second error is due to the accuracy of producing samples of gels that are identical (a random error). No two gels are identical. It was found that gels of a LMWG in a specific solvent at the same concentration varied in their exact rheological characteristics. Nucleation plays a very important role in the formation of LMW gels.[11-13] To prevent error due to variation in nucleation due to different numbers of nuclei all vials used were cleared of dust by blowing high pressured gas through the vial before samples were prepared. The dryness of the organic solvents was also found to affect gel formation so all solvents used were dried over molecular sieves. The injection or adding of gel samples to the rheometer was also found to affect the measurements. Samples were therefore added using spatulas, with samples taken of equivalent size, or injected at similar rates and consistent directions. Even with all these precautions results were found to vary. Where possible this type of error was shown by running more than one sample but it was found that the errors in sample measurements did not prevent identification of trends within this work. Adding anions directly to preformed gels resulted in large errors in measurements, therefore, all anion experiments were on gels that had been formed after the anion was added.

Appendix B - Synthesis and analytical data

Compound 2.1a

1-[(1*S*)-1-Phenylethyl]-3-[2-({[(1*S*)-1-phenylethyl]carbamoyl}amino)ethyl] urea

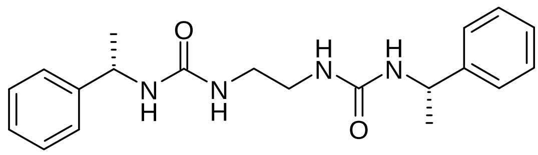

2.1a

Synthesis: (*S*)-1-Phenylethyl isocyanate (2.10 g, 13.6 mmol,) was added to dry $CHCl_3$ (150 mL) in a three necked round bottom flask fitted with a condenser and flowing N_2. To this solution was added ethylene diamine (0.408 g, 0.450 mL, 6.8 mmol) dropwise. The reaction mixture was refluxed for 24 hours under N_2. A white precipitate formed which was filtered off using a Büchner funnel.

Yield: 1.96 g; 81%; 5.5 mmol

^{1}H NMR: (400 MHz, d_6-DMSO, δ/ppm, *J*/Hz) 1.30 (6H, doublet, J = 7.1, -CH_3) 2.92-3.01 (4H, multiplet, -CH_2-) 4.67-4.74 (2H, multiplet, -CH-) 5.82-5.86 (2H, broad multiplet, -NH-CH_2) 6.42 (2H, doublet, J = 8.1, -CH-NH-) 7.15-7.30 (10H, multiplet, Ar. C-H)

^{13}C NMR: (100 MHz, d_6-DMSO, δ/ppm) 14.05; 23.30; 48.56; 125.75; 126.35; 128.13; 145.76; 157.37

Mass Spectra: ES$^+$ m/z = 355.3 [44%] $C_{20}H_{26}N_4O_2 + H^+$

m/z = 377.2 [100%] $C_{20}H_{26}N_4O_2 + Na^+$

Elemental analysis: Calc. C 67.8% H 7.38% N 15.8%

Exp. C 66.9% H 7.32% N 15.6%

Melting point: 216 +/- 1 °C

FT-IR: (ν, cm^{-1}) 3321 (m), 2970 (w), 2930 (w), 2866 (w), 1620 (s), 1571 (s), 1526 (m).

Crystal data for **2.1a:** $C_{20}H_{26}N_4O_2$, M = 354.45, colourless needle, 0.40 × 0.11 × 0.10 mm^3, monoclinic, space group $P2_1$ (No. 4), a = 12.1914(14), b = 4.6342(6), c = 17.341(2) Å, β = 107.849(5)°, V = 932.57(19) Å^3, Z = 2, D_c = 1.262 g/cm^3, F_{000} = 380, Smart-6K, MoKα radiation, λ = 0.71073 Å, T = 120(2)K, $2\theta_{max}$ = 56.5º, 7921 reflections collected, 4407 unique (R_{int} = 0.2294). Final *GooF* = 0.896, *R1* = 0.0972, *wR2* = 0.2219, *R* indices based on 2170 reflections with I >2sigma(I) (refinement on F^2), 235 parameters, 1 restraint. Lp and absorption corrections applied, μ = 0.084 mm^{-1}.

Compounds 2.1b -2.1g

1-((S)-1-Phenyl-ethyl)-3-{4-[3-((S)-1-phenyl-ethyl)-ureido]-alkyl}-ureas

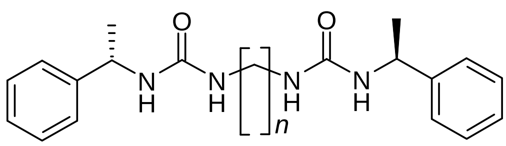

2.1a - g with *n* = 2 - 8

Synthesis and analytical work performed by Dr. M. O. M. Piepenbrock; X-ray crystallography performed by author.

Synthesis: In a typical synthesis a solution of (*S*)-(-)-*α*-methylbenzyl isocyanate (0.90 g, 6.1 mmol) in dry $CHCl_3$ (100 mL) was added dropwise to a stirred solution of the appropriate α-ω-diaminoalkane (3.0 mmol) under reflux. After complete addition the reaction was allowed to reflux under an inert N_2 atmosphere for up to 24h. The resulting precipitate formed was collected by filtration and washed with $CHCl_3$ (3 × 10 mL). The resulting white powders were obtained in good yields (75-82%).

See supplementary data of the paper, M. O. M. Piepenbrock, Gareth O. Lloyd, Nigel Clarke, Jonathan W. Steed, Gelation is crucially dependent on functional group orientation and may be tuned by anion binding, *Chem. Commun.*, **2008**, 2644-2645, for analytical data for compounds **2.1b-2.1g**.

Crystal data for **2.1c** (form I): $C_{22}H_{30}N_4O_2$, M = 382.50, colourless needle, 0.35 × 0.21 × 0.16 mm^3, monoclinic, space group $C2$ (No. 5), a = 35.285(15), b = 4.651(2), c = 12.784(5) Å, β = 97.518(7)°, V = 2079.7(15) Å^3, Z = 4, D_c = 1.222 g/cm^3, F_{000} = 824, Smart-6K, MoKα radiation, λ = 0.71073 Å, T = 120(2)K, $2\theta_{max}$ = 56.4º, 12725 reflections collected, 5076 unique (R_{int} = 0.0619). Final $GooF$ = 1.152, $R1$ = 0.0761, $wR2$ = 0.1907, R indices based on 4339 reflections with I >2sigma(I) (refinement on F^2), 253 parameters, 1 restraint. Lp and absorption corrections applied, μ = 0.080 mm^{-1}.

Crystal data for **2.1c** (form II): $C_{22}H_{30}N_4O_2$, M = 382.50, colourless needle, 0.21 × 0.07 × 0.05 mm^3, monoclinic, space group $P2_1$ (No. 4), a = 4.5914(1), b = 19.6481(4), c = 11.2393(3) Å, β = 90.8720(10)°, V = 1013.81(4) Å^3, Z = 2, D_c = 1.253 g/cm^3, F_{000} = 412, Smart-6K, MoKα radiation, λ = 0.71073 Å, T = 120(2)K, $2\theta_{max}$ = 61.0º, 18937 reflections collected, 3189 unique (R_{int} = 0.0399). Final $GooF$ = 1.104, $R1$ = 0.0376, $wR2$ = 0.0886, R indices based on 2763 reflections with I >2sigma(I) (refinement on F^2), 253 parameters, 1 restraint. Lp and absorption corrections applied, μ = 0.082 mm^{-1}.

Crystal data for **2.1d**: $C_{23}H_{32}N_4O_2$, M = 396.53, colourless needle, 0.49 × 0.24 × 0.10 mm^3, monoclinic, space group $P2_1$ (No. 4), a = 12.317(2), b = 4.6108(8), c = 19.488(3) Å, β = 107.519(4)°, V = 1055.4(3) Å^3, Z = 2, D_c = 1.248 g/cm^3, F_{000} = 428, Smart-6K, MoKα radiation, λ = 0.71073 Å, T = 120(2)K, $2\theta_{max}$ = 55.1º, 7923 reflections collected, 4625 unique (R_{int} = 0.0499). Final $GooF$ = 1.018, $R1$ = 0.0624, $wR2$ = 0.1354, R indices based on 3061 reflections with I >2sigma(I) (refinement on F^2), 262 parameters, 1 restraint. Lp and absorption corrections applied, μ = 0.081 mm^{-1}.

Crystal data for **2.1f**: $C_{25}H_{36}N_4O_2$, M = 424.58, colourless needle, 0.50 × 0.23 × 0.08 mm^3, monoclinic, space group $P2_1$ (No. 4), a = 12.275(4), b = 4.6302(15), c = 20.791(7) Å, β = 102.108(9)°, V = 1155.4(7) Å^3, Z = 2, D_c = 1.220 g/cm^3, F_{000} = 460, Smart-6K, MoKα radiation, λ = 0.71073 Å, T = 120(2)K, $2\theta_{max}$ = 54.0º, 12691 reflections collected, 4874 unique (R_{int} = 0.1213). Final $GooF$ = 0.988, $R1$ = 0.0592, $wR2$ = 0.1468, R indices based on 4077 reflections with I >2sigma(I) (refinement on F^2), 280 parameters, 1 restraint. Lp and absorption corrections applied, $\mu = 0.078$ mm^{-1}.

Compound 2.2

1-[(1*R*)-1-(1-Naphthyl)ethyl]-3-[2-({[(1*R*)-1-(1-naphthyl)ethyl]carbamoyl}amino) ethyl]urea

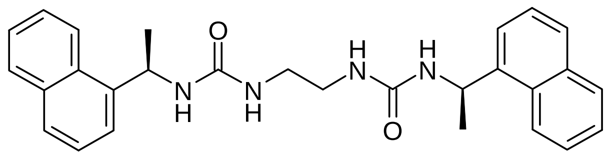

2.2

Synthesis: (*R*)-1-(1-Naphthyl) isocyanate (1.00 g, 5.08 mmol) was added to dry $CHCl_3$ (150 mL) in a three necked round bottom flask fitted with a condenser and flowing N_2. To this solution was added ethylene diamine (0.152 g, 0.170 mL, 2.54 mmol) dropwise. The reaction mixture was refluxed for 24 hours under N_2. A white precipitate formed and was filtered off using a Buchner funnel.

Yield: 0.95 g; 82%; 2.1 mmol

^{1}H NMR: (400 MHz, d_6-DMSO, δ/ppm, *J*/Hz) 1.44 (6H, doublet, J = 6.8, -CH_3) 2.96-3.08 (4H, multiplet, -CH_2-) 5.51-5.58 (2H, multiplet, -CH-) 5.87 (2H, broad, -NH-CH_2) 6.57 (2H, doublet, J = 8.1, -CH-NH-) 7.44-7.56 (8H, multiplet, J = 7.3; 7.6; 8.1, Ar. C-H) 7.79 (2H, doublet, J = 7.6, Ar. C-H) 7.92 (2H, doublet, J = 7.3, Ar. C-H) 8.12 (2H, doublet, J = 8.1, Ar. C-H)

^{13}C NMR: (100 MHz, d_6-DMSO, δ/ppm) 14.05; 22.45; 44.64; 121.98; 123.23; 125.42; 125.46; 126.00; 126.97; 128.54; 130.31; 133.37; 141.31; 157.30

Elemental analysis: Calc. C 74.0% H 6.65% N 12.3%

Exp. C 73.6% H 6.64% N 12.1%

Melting point: 243 +/- 1 ^{o}C

Mass Spectra: ES$^+$ m/z = 455 [78%] $C_{28}H_{30}N_4O_2 + H^+$

$m/z = 477$ (100%) $C_{28}H_{30}N_4O_2 + Na^+$

$m/z = 931$ (52%) $2C_{28}H_{30}N_4O_2 + Na^+$

FT-IR: (ν, cm^{-1}) 3315 (m), 2972.4 (w), 2938 (w), 2868 (w), 1614 (m), 1569 (s), 1509 (m).

Compound 2.3

2-(3-{2-[3-((1*S*)-1-Methoxycarbonyl-2-methyl-propyl)-ureido]-ethyl}-ureido)-(1*S*)-3-methyl-butyric acid methyl ester

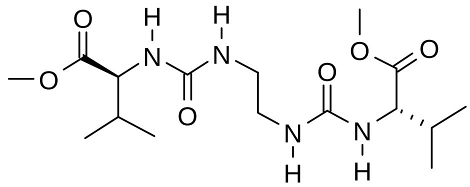

2.3

Synthesis: Methyl (*S*)-2-isocyanato-3-methylbutyrate (0.500 g, 3.18 mmol) was added to dry $CHCl_3$ (150 mL) in a three necked round bottom flask fitted with a condenser and flowing N_2. To this solution was added ethylene diamine (0.096 g, 0.110 mL, 1.54 mmol) dropwise. Reflux for 24 hours under N_2. Solvent was removed using a rotary evaporator to give an oil which crystallized on standing. Crude product was purified by recrystallisation from MeCN.

Yield: 0.26 g; 43%, 0.69 mmol

^{1}H NMR: (400 MHz, d_3-MeCN, δ/ppm, *J*/Hz) 0.88 (6H, doublet, *J* = 6.9, *tert*-CH-C**H**$_3$) 0.91 (6H, doublet, *J* = 6.9, *tert*-CH-C**H**$_3$) 1.99-2.09 (2H, multiplet, *J* = 5.6; 6.9; -C**H**-(CH$_3$)$_2$) 3.13 (4H, multilpet, -CH$_2$-) 3.66 (6H, singlet, -O-CH$_3$) 4.15 (2H, doublet of doublets, *J* = 8.5; 5.6, -CH-NH) 5.33 (2H, broad, urea-N**H**-CH$_2$-) 5.39 (2H, doublet, *J* = 8.5, urea-N**H**-CH-)

^{13}C NMR: (100 MHz, d_6-DMSO, δ/ppm) 17.00; 18.13; 30.38; 40.47; 51.02; 58.09; 157.91; 173.13

Elemental analysis: Calc. C 51.3% H 8.08% N 15.0%

Exp. C 51.6% H 8.13% N 14.6%

Melting point: 190 +/- 2 °C

Mass Spectra: ES$^+$ m/z = 375 [100%] $C_{16}H_{30}N_4O_6 + H^+$

m/z = 397 (95%) $C_{16}H_{30}N_4O_6 + Na^+$

m/z = 771 (45%) $2C_{16}H_{30}N_4O_6 + Na^+$

FT-IR: (v, cm^{-1}) 3327 (s), 3299 (s), 2659 (m), 2942 (m), 2976 (w), 1718 (s), 1663 (s).

Crystal data for **2.3:** $C_{16}H_{30}N_4O_6$, M = 374.44, colourless blocks, 0.24 × 0.20 × 0.17 mm^3, monoclinic, space group $P2_1$ (No. 4), a = 9.138(11), b = 10.858(13), c = 11.209(12) Å, β = 106.57(3)°, V = 1066(2) Å^3, Z = 2, D_c = 1.167 g/cm^3, F_{000} = 404, Smart-6K, MoKα radiation, λ = 0.71073 Å, T = 250(2)K, $2\theta_{max}$ = 56.5°, 11442 reflections collected, 5093 unique (R_{int} = 0.0300). Final $GooF$ = 0.989, $R1$ = 0.0528, $wR2$ = 0.1383, R indices based on 3345 reflections with I >2sigma(I) (refinement on F^2), 235 parameters, 1 restraint. Lp and absorption corrections applied, μ = 0.089 mm^{-1}.

Compound 3.1

N-1,4-Di(5-methyl-3-amino-1*H*-pyrazol-1-carboxamidyl)butane

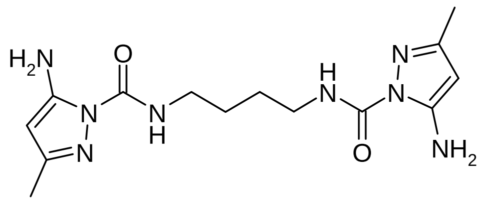

3.1

Synthesis: 3-Amino-5-methylpyrazole (1.25 g, 12.8 mmol) was added to dry $CHCl_3$ (100 mL) in a three necked round bottom flask fitted with a condenser and flowing N_2. To this solution was added 1,4-diisocyanatobutane (0.847 g, 0.810 mL, 6.4 mmol) dropwise. Reflux for 24 hours under N_2. Solvent was removed using a rotary evaporator to give crystalline material.

Yield: 2.08 g; 97%, 6.2 mmol

^{1}H NMR: (400 MHz, $CDCl_3$, δ/ppm, *J*/Hz) 1.65-1.71 (4H, multiplet, $-CH_2-$) 2.11 (6H, singlet, $-CH_3$) 3.30-3.40 (4H, multiplet, N-CH_2-) 5.20 (2H, singlet, =CH-) 5.38 (4H, broad singlet, $-NH_2$) 7.10 (2H, singlet, -NH-)

^{13}C NMR: (100 MHz, d_6-DMSO, δ/ppm) 13.7, 26.7, 38.7, 87.7, 150.1, 150.6, 152.6

Elemental analysis: Calc. C 50.3% H 6.63% N 33.5%

Exp. C 49.4% H 6.54% N 32.7%

Melting point: 158 +/- 2 °C

Mass Spectra: ES^+ m/z = 335 [100%] $C_{14}H_{22}N_8O_2 + H^+$

m/z = 357 [24%] $C_{14}H_{22}N_8O_2 + Na^+$

FT-IR: (ν, cm^{-1}) 3450 (m), 3383 (m), 3340 (m), 2985 (w), 2945 (m), 2928 (w), 2862 (w), 1705 (s), 1693 (s), 1615 (s), 1548 (m), 1523 (s).

Crystal data for **3.1**: $C_{14}H_{22}N_8O_2$, M = 334.40, colourless needles, 0.15 × 0.12 × 0.07 mm^3, monoclinic, space group $P2_1/c$ (No. 14), a = 8.4926(15), b = 8.8024(14), c = 11.241(2) Å, β = 92.522(6)°, V = 839.5(2) Å^3, Z = 2, D_c = 1.323 g/cm^3, F_{000} = 356, Smart-6K, MoKα radiation, λ = 0.71073 Å, T = 116(2)K, $2\theta_{max}$ = 54.0º, 3603 reflections collected, 1830 unique (R_{int} = 0.0596). Final *GooF* = 0.970, *R1* = 0.0518, *wR2* = 0.1331, R indices based on 1259 reflections with I >2sigma(I) (refinement on F^2), 110 parameters, 0 restraints. Lp and absorption corrections applied, μ = 0.094 mm^{-1}.

Crystal data for **3.1.CHCl$_3$**: $C_{16}H_{24}Cl_6N_8O_2$, M = 573.13, colourless block, 0.21 × 0.18 × 0.16 mm^3, monoclinic, space group $P2_1/c$ (No. 14), a = 14.0047(6), b = 7.9376(3), c = 11.8478(5) Å, β = 107.107(2)°, V = 1258.78(9) Å^3, Z = 2, D_c = 1.512 g/cm^3, F_{000} = 588, Smart-6K, MoKα radiation, λ = 0.71073 Å, T = 123(2)K, $2\theta_{max}$ = 56.0º, 10086 reflections collected, 3041 unique (R_{int} = 0.0346). Final *GooF* = 1.029, *R1* = 0.0587, *wR2* = 0.1514, R indices based on 2165 reflections with I >2sigma(I) (refinement on F^2), 146 parameters, 0 restraints. Lp and absorption corrections applied, μ = 0.713 mm^{-1}.

Compound 3.2

5-Amino-*N*-*p*-tolyl-1*H*-pyrazole-1-carboxamide

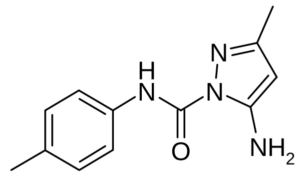

3.2

Synthesis: 3-Amino-5-methylpyrazole (1.00 g, 10.3 mmol) was added to 100 mL dry $CHCl_3$ in a three necked round bottom flask fitted with a condenser and flowing N_2. To this solution was added *p*-tolyl isocyanate (1.37 g, 1.300 ml, 10.3 mmol). Reflux for 24 hours under N_2. Solvent was removed using a rotary evaporator to give crystalline solid.

Yield: 2.06 g; 87%, 8.96 mmol

^{1}H NMR: (400 MHz, $CDCl_3$, δ/ppm, *J*/Hz) 2.17 (3H, singlet, -CH_3 (pyr)) 2.33 (3H, singlet, -CH_3 (tolyl)) 5.26 (1H, singlet, =CH-) 5.44 (2H, broad, -NH_2) 7.16 (2H, doublet, J = 8.4, -CH=(tolyl)) 7.44 (2H, doublet, J = 8.4, -CH=(tolyl)) 8.97 (1H, singlet, -NH-)
^{13}C NMR: (100 MHz, d_6-DMSO, δ/ppm) 12.7, 19.3, 99.6, 117.9, 128.2, 130.2, 137.0, 141.7, 149.1, 151.7

Elemental analysis: Calc. C 62.6% H 6.13% N 24.3%
Exp. C 62.5% H 6.07% N 24.0%

Melting point: 172 +/- 2 °C

Mass Spectra: ES$^+$ m/z = 231 [100%] $C_{12}H_{14}N_4O + H^+$
m/z = 253 [92%] $C_{12}H_{14}N_4O + Na^+$
m/z = 483 [45%] $2C_{12}H_{14}N_4O + Na^+$

FT-IR: (ν, cm^{-1}) 3284 (w), 2989 (s), 2977 (s), 2907 (m), 1709 (m), 1673 (m), 1611 (w), 1507 (s).

Crystal data for **3.2**: $C_{12}H_{14}N_4O$, M = 230.27, colourless block, 0.41 × 0.14 × 0.08 mm^3, orthorhombic, space group *Pbca* (No. 61), a = 13.1977(5), b = 8.5124(3), c = 20.9749(8) Å, V = 2356.41(15) Å^3, Z = 8, D_c = 1.298 g/cm^3, F_{000} = 976, Smart-6K, MoKα radiation, λ = 0.71073 Å, T = 120(2)K, $2\theta_{max}$ = 56.0°, 33994 reflections collected, 2842 unique (R_{int} = 0.0666). Final *GooF* = 1.029, *R1* = 0.0499, *wR2* = 0.1255, *R* indices based on 2083 reflections with I >2sigma(I) (refinement on F^2), 162 parameters, 2 restraints. Lp and absorption corrections applied, μ = 0.087 mm^{-1}.

Compound 3.3

1-*tert*-Butyl-3-(3-methyl-1*H*-pyrazol-5-yl)thiourea

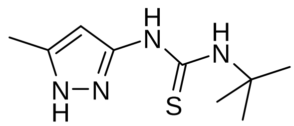

3.3

Synthesis: 3-Amino-5-methylpyrazole (0.766 g, 7.9 mmol) was added to 100 mL dry CH_2Cl_2 in a three necked round bottom flask fitted with a condenser and flowing N_2. To this solution was added *t*-butyl isothiocyanate (0.908 g, 1.00 mL, 7.9 mmol) dropwise. Reflux for 24 hours under N_2. Solvent was removed using a rotary evaporator to give oil. Crude product was purified by recrystallisation from $CHCl_3$ to form a crystalline solvate that lost the solvent to give the pure compound upon exposure to the atmosphere.

Yield: 1.23 g; 74%, 5.86 mmol

^{1}H NMR: (400 MHz, $CDCl_3$, δ/ppm, *J*/Hz) 1.57 (9H, singlet, methyl *t*-butyl) 2.27 (3H, singlet, $-CH_3$) 5.53 (1H, singlet, =CH-) 7.87 (1H, singlet, -NH-) 9.20 (1H, broad singlet, -NH-N=) 9.80 (1H, singlet -NH-)

^{13}C NMR: (100 MHz, d_6-DMSO, δ/ppm) 10.31; 28.38; 52.83; 93.03); 138.92; 150.05; 175.89

Elemental analysis: Calc. C 50.9% H 7.60% N 26.4%

Exp. C 50.7% H 7.60% N 26.3%

Melting point: 186 +/- 1 ^oC

Mass Spectra: ES^- *m*/*z* = 211.3 [50%] $C_9H_{16}N_4S - H^+$

m/*z* = 256.9 (100%) $C_9H_{16}N_4S + Cl^-$

m/*z* = 422.4 [5%] $2(C_9H_{16}N_4S) - H^+$

m/*z* = 458.3 (3%) $2(C_9H_{16}N_4S) + Cl^-$

FT-IR: (v, cm^{-1}) 3231 (m), 3190 (m), 3145 (w), 3072 (m), 2984 (w), 2966 (m), 2932 (w), 2874 (w), 1593 (s), 1547 (s), 1486 (s).

Crystal data for **3.3:** $C_9H_{16}N_4S$, M = 212.32, colourless block, 0.28 × 0.16 × 0.13 mm^3, monoclinic, space group $P2_1/n$ (No. 14), a = 9.9582(2), b = 10.3379(2), c = 12.2352(3) Å, β = 108.2790(10)°, V = 1196.02(4) Å^3, Z = 4, D_c = 1.179 g/cm^3, F_{000} = 456, Smart-6K, MoKα radiation, λ = 0.71073 Å, T = 120(2)K, $2\theta_{max}$ = 61.0º, 11608 reflections collected, 3632 unique (R_{int} = 0.0373). Final *GooF* = 1.028, *R1* = 0.0499, *wR2* = 0.1359, *R* indices based on 2620 reflections with I >2sigma(I) (refinement on F^2), 127 parameters, 0 restraints. Lp and absorption corrections applied, μ = 0.242 mm^{-1}.

Crystal data for **3.3.CHCl$_3$:** $C_{20}H_{26}Cl_6N_8S_2$, M = 655.31, colourless block, 0.21 × 0.21 × 0.17 mm^3, monoclinic, space group $P2_1/c$ (No. 14), a = 20.5918(7), b = 12.7948(4), c = 12.6182(4) Å, β = 102.5780(10)°, V = 3244.70(18) Å^3, Z = 4, D_c = 1.341 g/cm^3, F_{000} = 1344, Smart-6K, MoKα radiation, λ = 0.71073 Å, T = 120(2)K, $2\theta_{max}$ = 56.0º, 19739 reflections collected, 7834 unique (R_{int} = 0.0676). Final *GooF* = 0.966, *R1* = 0.0516, *wR2* = 0.1403, *R* indices based on 5257 reflections with I >2sigma(I) (refinement on F^2), 325 parameters, 0 restraints. Lp and absorption corrections applied, μ = 0.682 mm^{-1}.

Compound 3.4

tert-Butyl 5-amino-1*H*-pyrazole-1-carboxylate

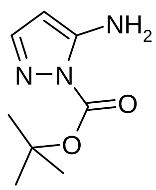

3.4

Synthesis: 3-Aminopyrazole (1.00 g, 12.0 mmol) is added to dry $CHCl_3$ (100 mL) in a three necked round bottom flask fitted with a condenser and bubbler. To this solution was added di-*tert*-butylpyrocarbonate (2.63 g, 12.0 mmol). Solution was stirred for 24 hours. Solvent was removed using a rotary evaporator to give oil. Recrystallised from $CHCl_3$ to give pure crystalline material.

Yield: 1.52 g; 69%, 8.30 mmol

^{1}H NMR: (400MHz, $CDCl_3$, δ/ppm, *J*/Hz) 1.62 (9H, singlet, -$(CH_3)_3$) 5.25 (1H, singlet, =CH-) 5.26 (2H, broad singlet, -NH_2) 7.24 (1H, singlet, -CH=)
^{13}C NMR: (100 MHz, $CDCl_3$, δ/ppm) 28.2, 85.2, 88.7, 99.3, 143.6, 150.4,
Elemental analysis: Calc. C 52.5% H 7.15% N 22.9%
Exp. C 52.0% H 7.20% N 22.9%
Melting point: 117 +/- 2 °C
Mass Spectra: ES$^+$ m/z = 84 [45%] $C_3H_5N_3 + H^+$
m/z = 447 (8%) $C_8H_{13}N_3O_2 + H^+$
FT-IR: (v, cm^{-1}) 3443 (m), 3286 (w), 3165 (w), 3116 (w), 2982 (m), 2940 (w), 2907 (w), 1710 (s), 1619 (s).

Crystal data for **3.4**: $C_8H_{13}N_3O_2$, M = 183.21, colourless prism, 0.28 × 0.24 × 0.20 mm^3, monoclinic, space group $P2_1/c$ (No. 14), a = 10.0050(19), b = 8.4249(16), c = 12.184(2) Å, β = 108.487(6)°, V = 974.0(3) Å^3, Z = 4, D_c = 1.249 g/cm^3, F_{000} = 392, Smart-6K, MoKα radiation, λ = 0.71073 Å, T = 100(2)K, $2\theta_{max}$ = 61.6°, 8496 reflections collected, 2989 unique (R_{int} = 0.0626). Final *GooF* = 1.011, *R1* = 0.0531, *wR2* = 0.1233, *R* indices based on 1714 reflections with I >2sigma(I) (refinement on F^2), 126 parameters, 2 restraints. Lp and absorption corrections applied, μ = 0.092 mm^{-1}.

Compound 3.5
tert-Butyl 5-amino-3-methyl-1*H*-pyrazole-1-carboxylate

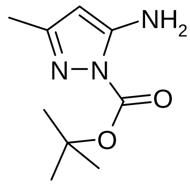

3.5

Synthesis: 3-Amino-5-methylpyrazole (2.00 g, 20.3 mmol) was added to dry $CHCl_3$ (100 mL) in a three necked round bottom flask fitted with a condenser and bubbler. To this solution was added di-*tert*-butylpyrocarbonate (4.49 g, 20.3 mmol). Solution was stirred for 24 hours. Solvent was removed using a rotary evaporator to give oil that crystallized upon standing.

Yield: 3.83 g; 96%, 19.4 mmol

^{1}H NMR: (400 MHz, $CDCl_3$, δ/ppm, *J*/Hz) 1.60 (9H, singlet, -$(CH_3)_3$) 2.12 (3H, singlet, -CH_3) 5.18 (1H, singlet, =CH-) 5.35 (2H, broad singlet, -NH_2)
^{13}C NMR: (100 MHz, $CDCl_3$, δ/ppm) 14.4, 28.0, 84.9, 89.3, 92.0, 150.7, 153.2
Elemental analysis: Calc. C 54.8% H 7.67% N 21.3%
Exp. C 54.3% H 7.61% N 20.9%
Melting point: 120 +/- 2 ^{o}C
Mass Spectra: ES$^+$ m/z = 198 [100%] $C_9H_{15}N_3O_2 + H^+$
m/z = 220 [5%] $C_9H_{15}N_3O_2 + Na^+$
m/z = 395 [33%] $2C_9H_{15}N_3O_2 + H^+$
FT-IR: (v, cm^{-1}) 3441 (m), 3358, (w), 3285 (w), 3212 (w), 3161 (w), 3120 (w), 2982 (m), 2933 (w), 1710 (s), 1619 (s), 1553 (m).

Crystal data for **3.5**: $C_9H_{15}N_3O_2$, M = 197.24, colourless prism, 0.24 × 0.19 × 0.13 mm^3, monoclinic, space group $P2_1/c$ (No. 14), a = 9.8180(3), b = 9.6472(3), c = 11.6088(4) Å, β = 106.9080(10)°, V = 1052.01(6) Å^3, Z = 4, D_c = 1.245 g/cm^3, F_{000} = 424, Smart-6K, MoKα radiation, λ = 0.71073 Å, T = 120(2)K, $2\theta_{max}$ = 61.0º, 9721 reflections collected, 3199 unique (R_{int} = 0.0403). Final $GooF$ = 1.024, $R1$ = 0.0479, $wR2$ = 0.1228, R indices based on 2223 reflections with I >2sigma(I) (refinement on F^2), 135 parameters, 4 restraints. Lp and absorption corrections applied, $\mu = 0.090$ mm^{-1}.

Compound 3.6

tert-Butyl 5-amino-3-phenyl-1*H*-pyrazole-1-carboxylate

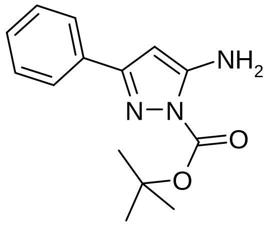

3.6

Synthesis: 3-Amino-5-phenylpyrazole (2.00 g, 12.6 mmol) was added to dry $CHCl_3$ (100 mL) in a three necked round bottom flask fitted with a condenser and bubbler. To this solution was added di-*tert*-butylpyrocarbonate (2.74 g, 12.6 mmol). Solution was stirred for 24 hours. Solvent was removed using a rotary evaporator to give pure crystalline material.

Yield: 3.14 g; 96%, 12.1 mmol

^{1}H NMR: (400 MHz, $CDCl_3$, δ/ppm, *J*/Hz) 1.68 (9H, singlet, -$(CH_3)_3$) 5.35 (2H, broad singlet, -NH_2) 5.75 (1H, singet, =CH-) 7.34 (1H, triplet, J = 8.0, -CH=(phenyl)) 7.38 (2H, triplet, J = 8.0, -CH=(phenyl)) 7.81 (2H, doublet, J = 8.0, -CH=(phenyl))

^{13}C NMR: (100 MHz, $CDCl_3$, δ/ppm) 27.0, 84.2, 85.5, 125.3, 127.4, 127.8, 131.4, 149.7, 150.0, 153.0

Elemental analysis: Calc. C 64.9% H 6.61% N 16.2%

Exp. C 64.2% H 6.60% N 15.9%

Melting point: 138 +/- 2 °C

Mass Spectra: ES$^+$ m/z = 160 [100%] $C_9H_9N_3 + H^+$

m/z = 260 (12%) $C_{14}H_{17}N_3O_2 + H^+$

FT-IR: (ν, cm^{-1}) 3481 (m), 3387 (w), 3289 (M), 3223 (w), 3182 (w), 2981 (m), 2936 (w), 2902 (w), 1746 (s), 1614 (s), 1567 (s), 1519 (w).

Crystal data for **3.6**: $C_{14}H_{17}N_3O_2$, M = 259.31, colourless block, 0.28 × 0.26 × 0.25 mm^3, monoclinic, space group $P2_1/n$ (No. 14), a = 6.2704(4), b = 13.1872(8), c = 16.6178(10) Å, β = 99.116(2)°, V = 1356.75(14) Å^3, Z = 4, D_c = 1.269 g/cm^3, F_{000} = 552, Smart-6K, MoKα radiation, λ = 0.71073 Å, T = 120(2)K, $2\theta_{max}$ = 61.0º, 24229 reflections collected, 4127 unique (R_{int} = 0.0440). Final $GooF$ = 1.026, $R1$ = 0.0440, $wR2$ = 0.1191, R indices based on 3371 reflections with I >2sigma(I) (refinement on F^2), 180 parameters, 0 restraints. Lp and absorption corrections applied, μ = 0.087 mm^{-1}.

Compound 3.7

tert-Butyl 3-methyl-5-(3-(naphthalen-1-yl)ureido)-1H-pyrazole-1-carboxylate

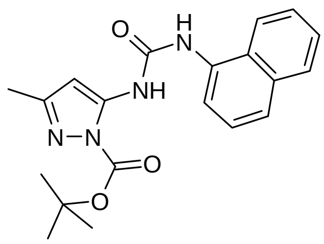

3.7

Synthesis: Compound **3.5** (1.22 g, 6.20 mmol) was added to dry $CHCl_3$ (100 mL) in a three necked round bottom flask fitted with a condenser and flowing N_2. To this solution was added 1-naphthylisocyanate (1.05 g, 0.890 ml. 6.20 mmol). Refluxed under N_2 for 24 hours. Precipitate formed which was filtered and was found to be pure.

Yield: 1.16 g; 51%, 3.18 mmol

^{1}H NMR: (400 MHz, $CDCl_3$, δ/ppm, J/Hz) 1.47 (9H, singlet, -$(CH_3)_3$) 2.17 (3H, singlet, -CH_3) 6.53 (1H, singlet, =CH-) 7.44-7.50 (3H, multiplet, -CH=) 7.69-7.71 (1H, multiplet, -CH=) 7.73-7.75 (1H, multiplet, -CH=) 7.85-7.88 (1H, multiplet, -CH=) 8.03-8.08 (1H, multiplet, -CH=) 8.20 (1H, broad singlet, -NH-) 9.76 (1H, singlet, -NH-)

^{13}**C NMR:** (100 MHz, d_6-DMSO, δ/ppm) 10.6, 27.6, 84.8, 96.1, 116.8, 117.4, 122.1, 123.9, 125.4, 125.7, 126.1, 128.5, 133.6, 144.2, 151.1, 151.2, 152.0

Elemental analysis: Calc. C 65.6% H 6.05% N 15.3%

Exp. C 66.6% H 5.93% N 14.7%

Melting point: Decomposition 220 ^{o}C

Mass Spectra: ES^{+} m/z = 366 [30%] $C_{20}H_{22}N_4O_3 + Na^+$

m/z = 755 [100%] $2C_{20}H_{22}N_4O_3 + Na^+$

FT-IR: (v, cm^{-1}) 3305 (w), 3280 (w), 3235 (w), 3161 (w), 3046 (w), 2982 (w), 2935 (w), 1747 (w), 1724 (m), 1704 (m), 1667 (m), 1635 (w), 1535 (s).

Compound 3.8

tert-Butyl 3-methyl-5-(3-p-tolylureido)-1*H*-pyrazole-1-carboxylate

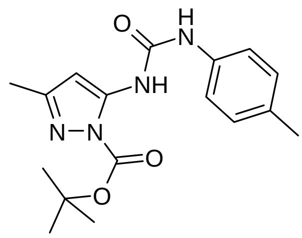

3.8

Synthesis: Compound **3.5** (1.50 g, 7.60 mmol) was added to dry $CHCl_3$ (100 mL) in a three necked round bottom flask fitted with a condenser and flowing N_2. To this solution was added *p*-tolyl isocyanate (1.01 g, 0.960 ml, 7.60 mmol). Refluxed under N_2 for 24 hours. Solvent was removed using a rotary evaporator to give an oil. Oil was recrystallised from MeOH to give pure crystalline material.

Yield: 0.93 g; 37%, 2.82 mmol

^{1}**H NMR:** (400 MHz, $CDCl_3$, δ/ppm, J/Hz) 1.52 (9H, singlet, -$(CH_3)_3$) 2.21 (3H, singlet, -CH_3 (pyrazole)) 2.30 (3H, singlet, -CH_3 (tolyl)) 6.54 (1H, singlet, =CH-) 7.11 (2H, doublet, , J = 10.0, -CH=) 7.30 (2H, doublet, , J = 10.0, -CH=) 7.94 (1H, broad singlet, -NH-) 9.63 (1H, singlet, -NH-)

^{13}C NMR: (100 MHz, d_6-DMSO, δ/ppm) 11.8, 20.1, 28.5, 83.2, 98.7, 118.3, 121.9, 128.4, 131.2, 136.7, 148.8, 151.6, 152.9

Elemental analysis: Calc. C 61.8% H 6.71% N 17.0%

Exp. C 61.4% H 6.79% N 16.6%

Melting point: 184 +/- 2 ^{o}C

Mass Spectra: ES$^+$ *m/z* = 330.9 [85%] $C_{17}H_{22}N_4O_3 + H^+$

m/z = 353.0 (50%) $C_{17}H_{22}N_4O_3 + Na^+$

m/z = 660.1 [35%] $2(C_{17}H_{22}N_4O_3) + H^+$

m/z = 683.0 (100%) $2(C_{17}H_{22}N_4O_3) + Na^+$

Crystal data for **3.8**: $C_{17}H_{22}N_4O_3$, M = 330.39, colourless needle, 0.25 × 0.21 × 0.19 mm^3, monoclinic, space group $P2_1/c$ (No. 14), a = 11.4293(8), b = 16.9788(11), c = 18.1269(11) Å, β = 90.217(3)°, V = 3517.6(4) Å^3, Z = 8, D_c = 1.248 g/cm^3, F_{000} = 1408, Smart-6K, MoKα radiation, λ = 0.71073 Å, T = 120(2)K, $2\theta_{max}$ = 61.1º, 37755 reflections collected, 10755 unique (R_{int} = 0.0587). Final *GooF* = 1.022, *R1* = 0.0540, *wR2* = 0.1287, *R* indices based on 6500 reflections with I >2sigma(I) (refinement on F^2), 437 parameters, 0 restraints. Lp and absorption corrections applied, μ = 0.088 mm^{-1}.

Compound 3.9

tert-Butyl 3-methyl-5-(3-(3-nitrophenyl)ureido)-1*H*-pyrazole-1-carboxylate

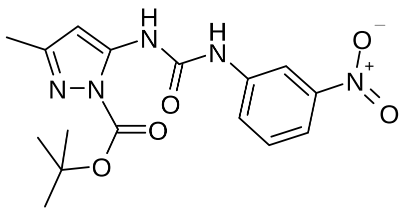

3.9

Synthesis: Compound **3.5** (1.50 g, 7.60 mmol) was added to dry $CHCl_3$ (100 mL) in a three necked round bottom flask fitted with a condenser and flowing N_2. To this solution was added 3-nitrophenylisocyanate (1.25 g, 0.960 ml, 7.60 mmol). Refluxed under N_2 for 24 hours. Solvent was removed using a rotary evaporator to give pure yellow precipitate.

Yield: 2.61 g; 96%, 7.27 mmol

^{1}H NMR: (400 MHz, d_6-DMSO, δ/ppm, *J*/Hz) 1.58 (9H, singlet, -$(CH_3)_3$) 2.13 (3H, singlet, -CH_3) 6.48 (1H, singlet, =CH-) 7.56 (1H, triplet, *J* = 8.4, -CH=) 7.70 (1H, doublet of doublets of doublets, *J* = 8.4, 1.0, 2.2, -CH=) 7.83 (1H, doublet of doublets of doublets, *J* = 8.4, 1.0, 2.2, -CH=) 8.53 (1H, triplet, *J* = 2.2, -CH=) 9.72 (1H, singlet, -NH-) 10.50 (1H, singlet, -NH-)

^{13}C NMR: (100 MHz, d_6-DMSO, δ/ppm) 13.8, 27.6, 85.1, 94.0, 96.1, 112.0, 116.7, 124.2, 130.1, 140.6, 141.8, 148.1, 150.1, 151.8

Elemental analysis: Calc. C 53.2% H 5.30% N 19.4%
Exp. C 53.0% H 5.54% N 17.8%

Melting Point: 176 +/-1 ^{o}C

Mass Spectra: ES$^-$ *m/z* = 360.2 [51%] $C_{11}H_{11}N_5O_3$ - H^+
m/z = 405.9 (80%) $C_{11}H_{11}N_5O_3$ + Cl^-
m/z = 720.7 [25%] 2($C_{11}H_{11}N_5O_3$) - H^+
m/z = 566.2 (12%) 2($C_{11}H_{11}N_5O_3$) + Cl^-

FT-IR: (*v*, cm^{-1}) 3342 (w), 3272 (m), 3141 (w), 3092 (w), 3034 (w), 2989 (w), 2940 (w), 1694 (m), 1661 (m), 1608 (m), 1586 (w), 1564 (m).

Compound 3.10

1-(3-Methyl-1*H*-pyrazol-5-yl)-3-(3-nitrophenyl)urea

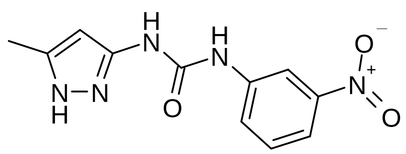

3.10

Synthesis: Compound **3.9** (2.50 g, 9.65mmol) was added to acetic acid (25 ml) in a round bottom flask fitted with a condenser. Refluxed for 24 hours. Upon cooling a solid formed which was filtered off. The solid was washed with water (2 x 25 ml) and saturated sodium carbonate solution (2 x 25 ml) to give crude product. The filtered solvent was dried by removing the solvent using a rotary evaporator to give fine yellow solid. This solid product was washed with water (2 x 25 ml) and saturated sodium carbonate solution (2 x 25 ml) to give crude product. The product was recrystallisation from MeCN if found to be not analytically pure.

Yield: 2.31 g; 92%, 8.92 mmol

^{1}H NMR: (400 MHz, d_3-MeCN, δ/ppm, J/Hz) 2.23 (3H, singlet, -CH_3) 5.85 (1H, singlet, =CH-) 7.46 (1H, triplet, J = 8.0, -CH=) 7.71 (1H, doublet of doublets of doublets, J = 8.0, 0.9, 2.2, -CH=) 7.81 (1H, doublet of doublets of doublets, J = 8.0, 0.9, 2.2, -CH=) 8.13 (1H, broad singlet, -NH- (pyrazole)) 8.55 (1H, triplet, J = 2.2, -CH=) 10.10 (1H, broad singlet, -NH-) 10.45 (1H, broad singlet -NH-)

^{13}C NMR: (100 MHz, d_6-DMSO, δ/ppm) 10.8, 94.0, 112.0, 116.1, 124.2, 130.0, 141.2, 148.11, 152.0

Elemental analysis: Calc. C 50.6% H 4.24% N 26.8%
Exp. C 50.4% H 4.25% N 26.2%

Melting Point: 180 +/-1 ^oC

Mass Spectra: ES$^-$ m/z = 260.2 [53%] $C_{11}H_{11}N_5O_3$ - H^+
m/z = 306.0 (100%) $C_{11}H_{11}N_5O_3$ + Cl^-
m/z = 520.8 [25%] 2($C_{11}H_{11}N_5O_3$) - H^+
m/z = 566.2 (12%) 2($C_{11}H_{11}N_5O_3$) + Cl^-

FT-IR: (ν, cm^{-1}) 3346 (m), 3042 (m), 3010 (w), 2936 (w), 1707 (s), 1611 (m), 1583 (m), 1544 (s), 1523 (s).

Crystal data for **3.10**: $C_{22}H_{22}N_{10}O_6$, M = 522.50, yellow prism, 0.21 × 0.18 × 0.10 mm^3, monoclinic, space group $P2_1/n$ (No. 14), a = 10.4699(10), b = 5.4899(5), c = 20.581(2) Å, β = 103.507(4)°, V = 1150.26(19) Å^3, Z = 2, D_c = 1.509 g/cm^3, F_{000} = 544, Smart-6K, MoKα radiation, λ = 0.71073 Å, T = 120(2)K, $2\theta_{max}$ = 61.0°, 10993 reflections collected, 3450 unique (R_{int} = 0.0388). Final $GooF$ = 1.031, $R1$ = 0.0486, $wR2$ = 0.1254, R indices based on 2428 reflections with I >2sigma(I) (refinement on F^2), 173 parameters, 0 restraints. Lp and absorption corrections applied, $\mu = 0.114$ mm^{-1}.

Compound 3.11a

1-(1-(*p*-Tolylcarbamoyl)-5-methyl-1*H*-pyrazol-3-yl)-3-*p*-tolylurea

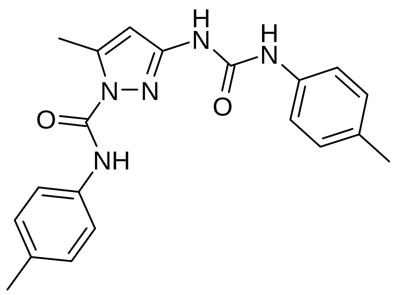

3.11a

Synthesis: 3-amino-5-methylpyrazole (1.00 g, 10.3 mmol) was added to dry $CHCl_3$ (100 mL) in a three necked round bottom flask fitted with a condenser and flowing N_2. To this solution was added *p*- tolyl isocyanate (2.74 g, 2.60 ml, 20.6 mmol) dropwise. The solution was refluxed for 24 hours under N_2. The solvent was removed using a rotary evaporator to give a crystalline solid of a mixture of isomers. Compound **3.11a** was isolated by crystallisation from hot $CHCl_3$ and the crystalline material filtered hot. Solid was washed with hot $CHCl_3$ (15 ml).

Yield: 0.79 g; 33%, 0.34 mmol

^{1}H NMR: (400 MHz, d_6-DMSO, δ/ppm, *J*/Hz) 2.22 (3H, singlet, $-CH_3$) 2.51 (3H, singlet, $-CH_3$) 3.32 (3H, singlet, $-CH_3$) 6.44 (1H, singlet, =CH-) 7.08 (2H, doublet, J = 6.4; -CH=(tolyl)) 7.14 (2H, doublet, J = 7.2; -CH=(tolyl)) 7.34 (2H, doublet, J = 6.4; -CH=(tolyl)) 7.53 (2H, doublet, J = 7.2; -CH=(tolyl)) 8.99 (1H, singlet, -NH-) 9.12 (1H, singlet, -NH-) 9.81 (1H, singlet, -NH-)

^{13}C NMR: (100 MHz, d_6-DMSO, δ/ppm) 13.8, 20.3, 20.4, 101.4, 118.4, 121.2, 129.0, 129.1, 131.2, 133.0, 134.5, 136.5, 143.2, 148.4, 148.6, 151.7

Elemental analysis: Calc. C 65.9% H 5.93% N 19.2%

Exp. C 66.1% H 5.82% N 19.3%

Melting point: 158 +/- 2 ^oC

Mass Spectra: ES^+ m/z = 231 [100%] $C_{20}H_{21}N_5O_2 - C_8H_7N_4O_1 + H^+$

m/z = 364 [34%] $C_{20}H_{21}N_5O_2 + H^+$

m/z = 386 [78%] $C_{20}H_{21}N_5O_2 + Na^+$

m/z = 749 [45%] $2C_{20}H_{21}N_5O_2 + Na^+$

FT-IR: (ν, cm^{-1}) 3382 (m), 3283 (m), 3136, w), 3037 (W), 2977 (w), 2923 (w), 2866 (w), 1732 (m), 1648 (m), 1594 (m).

Crystal data for **3.11a** (form I): $C_{20}H_{21}N_5O_2$, M = 363.42, colourless needle, 0.31 × 0.14 × 0.06 mm^3, triclinic, space group P-1 (No. 2), a = 5.8615(2), b = 11.0671(4), c = 14.0882(5) Å, α = 91.1250(10), β = 98.7050(10), γ = 97.0080(10)°, V = 895.95(5) $Å^3$, Z = 2, D_c = 1.347 g/cm^3, F_{000} = 384, Smart-6K, MoKα radiation, λ = 0.71073 Å, T = 120(2)K, $2\theta_{max}$ = 61.0º, 16676 reflections collected, 5478 unique (R_{int} = 0.0371). Final $GooF$ = 1.031, $R1$ = 0.0541, $wR2$ = 0.1468, R indices based on 3835 reflections with I >2sigma(I) (refinement on F^2), 244 parameters, 0 restraints. Lp and absorption corrections applied, μ = 0.091 mm^{-1}.

Crystal data for **3.11a** (form II): $C_{20}H_{21}N_5O_2$, M = 363.42, colourless needle, 0.27 × 0.16 × 0.09 mm^3, triclinic, space group P-1 (No. 2), a = 4.5914(16), b = 7.115(2), c = 28.028(10) Å, α = 93.378(7), β = 92.584(7), γ = 104.976(7)°, V = 881.3(5) $Å^3$, Z = 2, D_c = 1.370 g/cm^3, F_{000} = 384, Smart-6K, MoKα radiation, λ = 0.71073 Å, T = 120(2)K, $2\theta_{max}$ = 50.0º, 7025 reflections collected, 3086 unique (R_{int} = 0.0601). Final $GooF$ = 1.136, $R1$ = 0.1765, $wR2$ = 0.4279, R indices based on 2257 reflections with I >2sigma(I) (refinement on F^2), 244 parameters, 0 restraints. Lp and absorption corrections applied, μ = 0.092 mm^{-1}.

Metal complexes of **3.10** and **3.11a**

Crystal data for $[Zn_2Cl_2(\mu\text{-}Cl)_2(\kappa\text{-}N,O\text{-}\mathbf{3.10})_2]$: $C_{11}H_{11}Cl_2N_5O_3Zn$, M = 397.52, yellow prism, 0.31 × 0.15 × 0.13 mm^3, monoclinic, space group $C2/c$ (No. 15), a = 27.907(3), b = 7.9249(8), c = 14.6409(14) Å, β = 113.679(4)°, V = 2965.3(5) Å^3, Z = 8, D_c = 1.781 g/cm^3, F_{000} = 1600, Smart-6K, MoKα radiation, λ = 0.71073 Å, T = 120(2)K, $2\theta_{max}$ = 50.0º, 7266 reflections collected, 2479 unique (R_{int} = 0.0586). Final $GooF$ = 1.380, $R1$ = 0.0894, $wR2$ = 0.2203, R indices based on 2034 reflections with I >2sigma(I) (refinement on F^2), 200 parameters, 0 restraints. Lp and absorption corrections applied, μ = 2.035 mm^{-1}.

Crystal data for $[CuBr(\kappa\text{-}N,O\text{-}\mathbf{3.10})_2]Br\cdot 2H_2O$: $C_{22}H_{26}Br_2CuN_{10}O_8$, M = 781.89, green block, 0.29 × 0.28 × 0.24 mm^3, monoclinic, space group $P2_1/c$ (No. 14), a = 15.0983(6), b = 14.3747(5), c = 14.4724(5) Å, β = 111.9580(10)°, V = 2913.14(18) Å^3, Z = 4, D_c = 1.783 g/cm^3, F_{000} = 1564, Smart-6K, MoKα radiation, λ = 0.71073 Å, T = 120(2)K, $2\theta_{max}$ = 61.1º, 52510 reflections collected, 8905 unique (R_{int} = 0.0625). Final $GooF$ = 1.011, $R1$ = 0.0358, $wR2$ = 0.0771, R indices based on 6131 reflections with I >2sigma(I) (refinement on F^2), 406 parameters, 6 restraints. Lp and absorption corrections applied, μ = 3.557 mm^{-1}.

Crystal data for $[Cu(\kappa\text{-}N,O\text{-}\mathbf{3.10})_2(MeOH)_2]\cdot 2BF_4$: $C_{24}H_{30}B_2CuF_8N_{10}O_8$, M = 823.74, ocean blue plate, 0.29 × 0.27 × 0.24 mm^3, triclinic, space group P-1 (No. 2), a = 6.9003(4), b = 9.9005(7), c = 12.6217(8) Å, α = 76.351(2), β = 83.346(2), γ = 74.686(2)°, V = 806.85(9) Å^3, Z = 1, D_c = 1.695 g/cm^3, F_{000} = 419, Smart-6K, MoKα radiation, λ = 0.71073 Å, T = 120(2)K, $2\theta_{max}$ = 61.0º, 12758 reflections collected, 4904 unique (R_{int} = 0.0378). Final $GooF$ = 1.100, $R1$ = 0.0447, $wR2$ = 0.1312, R indices based on 4271 reflections with I >2sigma(I) (refinement on F^2), 244 parameters, 0 restraints. Lp and absorption corrections applied, μ = 0.788 mm^{-1}.

Crystal data for $[\{Cu(\mu\text{-}\kappa\text{-}O,O,N,N\text{-}\mathbf{3.11a})(MeOH)\}_6](MeCO_2)_6\cdot 6MeOH$: $C_{24}H_{31}CuN_5O_6$, M = 549.08, blue prism, 0.13 × 0.11 × 0.05 mm^3, trigonal, space group R-3 (No. 148), a = b = 31.7325(8), c = 13.6585(7) Å, V = 11910.8(7) Å^3, Z = 18, D_c =

1.378 g/cm^3, F_{000} = 5166, Smart-6K, MoKα radiation, λ = 0.71073 Å, T = 120(2)K, 2θ_{max} = 50.0°, 22616 reflections collected, 4635 unique (R_{int} = 0.1729). Final *GooF* = 0.860, *R1* = 0.0518, *wR2* = 0.1021, *R* indices based on 1988 reflections with I >2sigma(I) (refinement on F^2), 334 parameters, 3 restraints. Lp and absorption corrections applied, μ = 0.872 mm^{-1}.

Mass Spectra: ES$^+$ *m*/*z* = 364 [10%] ($C_{20}H_{21}N_5O_2$) + H^+
m/*z* = 386 [38%] ($C_{20}H_{21}N_5O_2$) + Na^+
m/*z* = 457 [100%] ($C_{21}H_{24}CuN_5O_3$) = (Cu + **3.11**$^-$ + MeOH)
m/*z* = 788 [95%] $C_{40}H_{40}CuN_{10}O_4$ + H^+ = (Cu + 2**3.11**$^-$ + H^+)
m/*z* = 1574 [12%] 6($C_{23}H_{27}CuN_5O_5$) + 2Na^+

Crystal data for *mer*-[Cd(κ-*O,N,N*-**3.11a**)$_2$]: $C_{42}H_{50}CdN_{10}O_7$, M = 917.30, colourless block, 0.11 × 0.07 × 0.04 mm^3, monoclinic, space group $P2_1$ (No. 4), a = 12.329(7), b = 12.877(7), c = 14.883(6) Å, β = 91.625(18)°, V = 2362(2) Å^3, Z = 2, D_c = 1.290 g/cm^3, F_{000} = 948, Smart-6K, MoKα radiation, λ = 0.71073 Å, T = 120(2)K, 2θ_{max} = 50.0°, 13385 reflections collected, 8275 unique (R_{int} = 0.0586). Final *GooF* = 1.032, *R1* = 0.0719, *wR2* = 0.1676, *R* indices based on 6012 reflections with I >2sigma(I) (refinement on F^2), 567 parameters, 3 restraints. Lp and absorption corrections applied, μ = 0.518 mm^{-1}. Absolute structure parameter = 0.02(5).

Compound 3.13

Synthesis: The product **3.13** was air- and moisture-sensitive. All manipulations were carried out under purified nitrogen using standard Schlenk techniques. Aluminium foil (cut into small strips) (0.500 g, 18.5 mmol), 3,5-Di-*t*-butylpyrazole (0.911 g, 5.0 mmol), dipentaflourophenylmercury (1.377 g, 2.5 mmol) and 2 drops of elemental mercury were added to a 150 ml Schlenk flask. The Schlenk flask was kept under dynamic vacuum for three hours to ensure dryness. THF (50 ml) was added and the Schlenk flask was then placed in a sonic bath for 24 hours. The liquid solvent was filtered into another Schlenk flask using a cannula. This filtered liquid was reduced until precipitation began. The solution was reheated to dissolve precipitate and was placed in a fridge upon which crystallisation of the product occured.

Yield: 0.71 g; 60%, 1.0 mmol

^{1}H NMR: (400 MHz, d_8-THF, δ/ppm, J/Hz)) 1.15 (singlet, 54H, (-CH_3)$_3$) 1.72-1.75 (multiplet, 8H, -CH2-) 3.56-3.59 (multiplet, 8H, -CH2-) 5.91 (singlet, 3H, -CH-)
^{27}Al NMR: (78 MHz, d_8-THF, δ/ppm) 23.8 and 67.3
Elemental analysis: Calc. C 69.5% H 10.38% N 11.9%
Exp. C 67.0% H 9.72% N 15.0%
Mass Spectra: ES$^+$ m/z = 385 [100%] $C_{33}H_{57}N_6Al - C_{11}H_{19}N_2^-$
m/z = 564 [46%] $C_{33}H_{57}N_6Al + H^+$
FT-IR: (v, cm^{-1}) 2955 (s) 2924 (s) 2845 (s) 1511 (m) 1462 (s) 1375 (s) 1309 (w) 1257 (s) 1232 (w) 1204 (w) 1075 (s) 992 (w) 960 (w) 915 (w) 796 (w) 723 (s)

Crystal data for **1.13**: $C_{41}H_{73}AlN_6O_2$, M = 709.03, colourless rectangular prism, 0.39 × 0.36 × 0.31 mm^3, monoclinic, space group $P2_1/c$ (No. 14), a = 11.934(7), b = 19.011(10), c = 19.148(12) Å, β = 101.095(15)°, V = 4263(4) Å^3, Z = 4, D_c = 1.105 g/cm^3, F_{000} = 1560, Nonius Kappa CCD, MoKα radiation, λ = 0.71073 Å, T = 123(2)K, $2\theta_{max}$ = 53.0º, 31846 reflections collected, 8799 unique (R_{int} = 0.0467). Final $GooF$ = 1.029, $R1$ = 0.0548, $wR2$ = 0.1237, R indices based on 6473 reflections with I >2sigma(I) (refinement on F^2), 497 parameters, 34 restraints. Lp and absorption corrections applied, μ = 0.087 mm^{-1}.

Compound 3.14

Synthesis: The products **3.14** and **3.12** were air- and moisture-sensitive. All manipulations were carried out under purified nitrogen using standard Schlenk techniques. Aluminium foil (cut into small strips) (0.650 g, 24.0 mmol), 3,5-Di-*t*-butylpyrazole (0.514 g, 2.5 mmol), dipentaflourophenylmercury (0.800 g, 1.25 mmol) and 2 drops of elemental mercury were added to a 150 ml Schlenk flask. The Schlenk flask was kept under dynamic vacuum for three hours to ensure dryness. DME (50 ml) was added and the Schlenk flask was then placed in a sonic bath for 24 hours. The liquid was filtered into another Schlenk flask using a cannula. This filtered liquid was reduced until precipitation began. The solution was reheated to dissolve the precipitate and was placed in a fridge upon which compound **3.14** crystallised. The liquid was again filtered off into another Schlenk flask using a cannula to give **3.14**. This new filtered liquid was reduced to the point that precipitation began again. Reheating of the solution to dissolve the precipitate and standing at room temperature over night resultd in isolation of **3.12**. The liquid was once again filtered off into another Schlenk flask using a cannula to give **3.12**. This liquid was reduced to dryness resulting in isolation of unreacted 3,5-di-*t*-butylpyrazole.

Yield: Compound **3.14** 0.29 g; 23%, 0.28 mmol
Compound **3.12** 0.52 g; 37%, 0.93 mmol

^{1}H NMR: (400 MHz, C_6D_6, δ/ppm, *J*/Hz) 1.22 (singlet, 54H, $(-CH_3)_3$) 3.10-3.15 (multiplet, 8H, -CH2-) 3.30-36 (multiplet, 9H, -CH2-) 5.98 (singlet, 3H, -CH-)
^{19}F NMR: (282 MHz, C_6D_6, δ/ppm) -166.7 -154.4 -162.5
^{27}Al NMR: (78 MHz, C_6D_6, δ/ppm) 77.9
Elemental analysis: Calc. C 57.6% H 6.44% N 8.4%
Exp. C 57.4% H 7.46% N 8.4%
Mass Spectra: ES^+ m/z = 225 [100%] $C_7H_3OF_5Al$
m/z = 821 [18%] $C_{48}H_{64}Al_2F_{10}N_6O_2$-$C_{11}H_{10}N_2$
FT-IR: (ν, cm^{-1}) 2934 (s) 2848 (s) 1635 (m) 1507 (m) 1456 (s) 1380 (m) 1365 (m) 1303 (w) 1268 (w) 1252 (w) 1227 (w) 1205 (w) 1125 (w) 1069 (m) 962 (m) 804 (m) 799 (m) 722 (w) 666 (w)

Crystal data for **3.14**: $C_{50}H_{69}Al_2F_{10}N_6O_3$, M = 1046.07, colourless block, 0.40 × 0.38 × 0.25 mm^3, triclinic, space group P-1 (No. 2), a = 10.618(2), b = 12.964(3), c = 20.759(4) Å, α = 73.27(3), β = 76.49(3), γ = 87.32(3)°, V = 2660.1(9) Å^3, Z = 2, D_c = 1.306 g/cm^3, F_{000} = 1102, Nonius Kappa CCD, MoKα radiation, λ = 0.71073 Å, T = 123(2)K, $2\theta_{max}$ =

52.0º, 32892 reflections collected, 10390 unique (R_{int} = 0.0796). Final *GooF* = 1.036, *R1* = 0.0697, *wR2* = 0.1778, *R* indices based on 5682 reflections with I >2sigma(I) (refinement on F^2), 695 parameters, 0 restraints. Lp and absorption corrections applied, μ = 0.136 mm^{-1}.

Crystal data for **3.12**: $C_{33}H_{57}N_6Al_1$, M = 564.83, colourless prism, 0.45 × 0.21 × 0.18 mm3, triclinic, space group P-1 (No. 2), *a* = 10.4999(5), *b* = 19.4670(10), *c* = 33.9263(18) Å, α = 91.127(3), β = 92.024(2), γ = 97.265(2)°, V = 6872.6(6) Å3, Z = 8, Dc = 1.092 g/cm3, F000 = 2480, Nonius Kappa CCD, MoKα radiation, λ = 0.71073 Å, T = 123(2)K, $2\theta_{max}$ = 55.0º, 142018 reflections collected, 31492 unique (R_{int} = 0.0448). Final GooF = 1.107, R1 = 0.0781, *w*R2 = 0.1757, *R* indices based on 24910 reflections with I >2sigma(I) (refinement on F^2), 1442 parameters, 0 restraints. Lp and absorption corrections applied, μ = 0.089 mm-1.

Salts of **3.10** – Crystallographic data

Crystal data for (**3.10H**$^+$)$_2$(SO_4^{2-})·7H_2O: $C_{22}H_{38}N_{10}O_{17}S$, *M* = 746.68, light yellow needle, 0.38 × 0.28 × 0.24 mm^3, monoclinic, space group $P2_1/c$ (No. 14), *a* = 8.60190(10), *b* = 16.2504(2), *c* = 23.2724(3) Å, β = 91.1000(10)°, *V* = 3252.52(7) $Å^3$, *Z* = 4, D_c = 1.525 g/cm^3, F_{000} = 1568, Smart-6K, MoKα radiation, λ = 0.71073 Å, *T* = 120(2)K, $2\theta_{max}$ = 61.0º, 33366 reflections collected, 9934 unique (R_{int} = 0.0401). Final *GooF* = 1.053, *R1* = 0.0523, *wR2* = 0.1414, *R* indices based on 7653 reflections with I >2sigma(I) (refinement on F^2), 503 parameters, 14 restraints. Lp and absorption corrections applied, μ = 0.192 mm^{-1}.

Crystal data for (**3.10H**$^+$**)**(BF_4^-)·H_2O: $C_{11}H_{14}BF_4N_5O_4$, *M* = 367.08, light yellow block needle, 0.31 × 0.21 × 0.13 mm^3, triclinic, space group *P*-1 (No. 2), *a* = 7.7509(4), *b* = 8.2203(5), *c* = 13.2848(7) Å, α = 94.481(2), β = 104.643(2), γ = 110.579(2)°, *V* = 753.54(7) $Å^3$, *Z* = 2, D_c = 1.618 g/cm^3, F_{000} = 376, Smart-6K, MoKα radiation, λ = 0.71073 Å, *T* = 120(2)K, $2\theta_{max}$ = 61.1º, 12989 reflections collected, 4594 unique (R_{int} =

0.0481). Final *GooF* = 1.025, *R1* = 0.0585, *wR2* = 0.1402, *R* indices based on 2963 reflections with I >2sigma(I) (refinement on F^2), 235 parameters, 2 restraints. Lp and absorption corrections applied, μ = 0.153 mm^{-1}.

Crystal data for (**3.10H**$^+$)(BF_4^-)·**3.10**: $C_{22}H_{23}BF_4N_{10}O_6$, M = 610.31, yellow prism, 0.16 × 0.09 × 0.06 mm^3, triclinic, space group P-1 (No. 2), a = 7.5596(4), b = 12.6366(6), c = 13.7797(6) Å, α = 100.6610(10), β = 94.926(2), γ = 96.370(2)°, V = 1277.98(11) Å^3, Z = 2, D_c = 1.586 g/cm^3, F_{000} = 628, Smart-6K, MoKα radiation, λ = 0.71073 Å, T = 120(2)K, $2\theta_{max}$ = 56.0°, 17616 reflections collected, 6149 unique (R_{int} = 0.0494). Final *GooF* = 1.011, *R1* = 0.0587, *wR2* = 0.1474, *R* indices based on 3877 reflections with I >2sigma(I) (refinement on F^2), 390 parameters, 0 restraints. Lp and absorption corrections applied, μ = 0.136 mm^{-1}.

Crystal data for (**3.10H**$^+$)(NO_3^-)·MeOH: $C_{24}H_{32}N_{12}O_{14}$, M = 712.62, yellow plates, 0.28 × 0.24 × 0.21 mm^3, monoclinic, space group $P2_1/c$ (No. 14), a = 7.6261(3), b = 25.9299(11), c = 16.0689(7) Å, β = 98.908(2)°, V = 3139.2(2) Å^3, Z = 4, D_c = 1.508 g/cm^3, F_{000} = 1488, Smart-6K, MoKα radiation, λ = 0.71073 Å, T = 120(2)K, $2\theta_{max}$ = 61.1°, 30666 reflections collected, 9546 unique (R_{int} = 0.0692). Final *GooF* = 1.008, *R1* = 0.0613, *wR2* = 0.1458, *R* indices based on 5157 reflections with I >2sigma(I) (refinement on F^2), 457 parameters, 0 restraints. Lp and absorption corrections applied, μ = 0.126 mm^{-1}.

Crystal data for 2[(**3.10H**$^+$)(Cl^-)]·MeOH·H_2O: $C_{23}H_{30}Cl_2N_{10}O_8$, M = 643.45, yellow needle, 0.25 × 0.08 × 0.02 mm^3, triclinic, space group P-1 (No. 2), a = 7.557(8), b = 14.027(16), c = 15.689(17) Å, α = 70.74(2), β = 77.71(2), γ = 87.03(2)°, V = 1534(3) Å^3, Z = 2, D_c = 1.393 g/cm^3, F_{000} = 668, Smart-6K, MoKα radiation, λ = 0.71073 Å, T = 120(2)K, $2\theta_{max}$ = 50.0°, 15248 reflections collected, 5366 unique (R_{int} = 0.2267). Final *GooF* = 1.812, *R1* = 0.2848, *wR2* = 0.5981, *R* indices based on 2474 reflections with I >2sigma(I) (refinement on F^2), 383 parameters, 280 restraints. Lp and absorption corrections applied, μ = 0.273 mm^{-1}.

References

(1) Frassineti, C.; Ghelli, S.; Gans, P.; Sabatini, A.; Moruzzi, M. S.; Vacca, A. *Anal. Biochem.* **1995**, *231*, 374-382.
(2) Gans, P.; HypNMR 2006, University of Leeds: Leeds, 2006.
(3) Sheldrick, G. M. In *SHELXS-97* University of Göttingen, 1997.
(4) Sheldrick, G. M. In *SHELXL-97* University of Göttingen, 1997.
(5) Barbour, L. J. *J. Supramol. Chem.* **2001**, *1*, 189-191.
(6) Atwood, J. L.; Barbour, L. J. *Cryst. Growth Des.* **2003**, *3*, 3-8.
(7) Persistance of Vision Raytrcer Pty. L.: 2004.
(8) Terech, P.; Rossat, C.; Volino, F. *J. Coll. Interface Sci.* **2000**, *227*, 363-370.
(9) Menger, F. M.; Caran, K. L. *J. Am. Chem. Soc.* **2000**, *122*, 11679-11691.
(10) Terech, P.; Friol, S. *Tetrahedron* **2007**, *63*, 7366-7374.
(11) Liu, X. Y. In *Low Molecular Mass Gelators: Design, Self-Assembly, Function*; Springer-Verlag Berlin: Berlin, 2005; Vol. 256, p 1-37.
(12) Wang, R. Y.; Liu, X. Y.; Xiong, J. Y.; Li, J. L. *J. Phys. Chem. B* **2006**, *110*, 7275-7280.
(13) Li, J. L.; Liu, X. Y.; Wang, R. Y.; Xiong, J. Y. *J. Phys. Chem. B* **2005**, *109*, 24231-24235.

CD – X-ray crystallography files